

2009

# Development of a Versatile Section Analysis Tool (VSAT) for use in structural design with a seismic emphasis

Jared C. Levings  
*Iowa State University*

Follow this and additional works at: <https://lib.dr.iastate.edu/etd>

 Part of the [Civil and Environmental Engineering Commons](#)

## Recommended Citation

Levings, Jared C., "Development of a Versatile Section Analysis Tool (VSAT) for use in structural design with a seismic emphasis" (2009). *Graduate Theses and Dissertations*. 11089.  
<https://lib.dr.iastate.edu/etd/11089>

This Thesis is brought to you for free and open access by the Iowa State University Capstones, Theses and Dissertations at Iowa State University Digital Repository. It has been accepted for inclusion in Graduate Theses and Dissertations by an authorized administrator of Iowa State University Digital Repository. For more information, please contact [digirep@iastate.edu](mailto:digirep@iastate.edu).

**Development of a Versatile Section Analysis Tool (VSAT) for use in structural design  
with a seismic emphasis**

by

**Jared Christopher Levings**

A thesis submitted to the graduate faculty  
in partial fulfillment of the requirements for the degree of  
**MASTER OF SCIENCE**

Major: Civil Engineering (Structural Engineering)

Program of Study Committee:  
Sri Sritharan, Major Professor  
LaDon Jones  
Jon Rouse

Iowa State University

Ames, Iowa

2009

## TABLE OF CONTENTS

LIST OF TABLES .....	vi
LIST OF FIGURES .....	vii
LIST OF NOTATION .....	xi
ACKNOWLEDGEMENTS .....	xvii
ABSTRACT .....	xviii
Chapter 1: INTRODUCTION.....	1
1.1 Historical Background .....	1
1.2 Seismic Design.....	1
1.2.1 Capacity Design Philosophy.....	2
1.2.2 Behavior of Plastic Hinges .....	3
1.2.3 Moment-Curvature Approach.....	6
1.3 Current Section Analysis Tools .....	7
1.3.1 Geometry and Defaults .....	7
1.3.2 Reinforcement Model.....	8
1.3.3 Concrete Model.....	8
1.3.4 Temperature Effects.....	10
1.3.5 Soil Confinement Effects.....	11
1.4 Scope of Research.....	12
1.5 Report Layout .....	13
Chapter 2: LITERATURE REVIEW.....	14
2.1 Introduction.....	14
2.2 Behavior of Concrete .....	14
2.2.1 Stress-Strain Behavior of Concrete .....	14
2.2.2 Temperature Effects.....	17
2.3 Behavior of UHPC.....	21
2.4 Behavior of Mild Steel Reinforcement.....	22
2.4.1 Stress-Strain Behavior of Mild Steel.....	23
2.4.2 Temperature Effects.....	24
2.5 Behavior of Prestressing Steel .....	26
2.5.1 Menegotto and Pinto.....	26
2.5.2 Devalapura and Tadros .....	27
2.6 Analytical Models.....	27
2.6.1 King's Program (King et al., 1986).....	28
2.6.2 LPILE (Ensoft, Inc., 2005).....	29
2.6.3 OpenSees (Mazzoni et al., 2009).....	29
2.6.4 XTRACT (TRC/Imbsen Software Systems, 2009) .....	30
Chapter 3: Behavior of A706 Mild Steel Reinforcement under Cold Temperatures .....	31
3.1 Introduction.....	31

3.2	Background .....	32
3.3	Past Studies .....	32
3.4	Experimental Study.....	34
3.4.1	<i>Sample Preparation</i> .....	34
3.4.2	<i>Test Setup</i> .....	36
3.4.3	<i>Monotonic Testing</i> .....	37
3.5	Test Matrix.....	38
3.6	Test Results and Discussion.....	39
3.6.1	<i>Effects of Temperature</i> .....	40
3.6.2	<i>Effects of Bar Size</i> .....	43
3.6.3	<i>Effects of Strain Rate</i> .....	45
3.6.4	<i>Summary of Previous Research Comparison</i> .....	48
3.7	Modeling.....	49
3.8	Recommendations and Conclusions .....	50
Chapter 4: VSAT – An ANALYTICAL PROGRAM.....		52
4.1	Introduction.....	52
4.1.1	<i>Background</i> .....	52
4.1.2	<i>Capabilities</i> .....	52
4.1.3	<i>Disclaimer</i> .....	53
4.2	Theoretical Procedures.....	54
4.2.1	<i>Introduction</i> .....	54
4.2.1.1	<i>Overview</i> .....	54
4.2.1.2	<i>Sign Convention</i> .....	54
4.2.2	<i>Section Details</i> .....	54
4.2.3	<i>Concrete Properties</i> .....	56
4.2.3.1	<i>Normal Strength Confined Concrete</i> .....	57
4.2.3.2	<i>Normal Strength Unconfined Concrete</i> .....	62
4.2.3.3	<i>Variable Confinement Model for Normal Concrete</i> .....	63
4.2.3.4	<i>Tensile Strength of Normal Strength Concrete</i> .....	66
4.2.3.5	<i>Normal Strength Maximum Concrete Strain</i> .....	66
4.2.3.6	<i>Ultra-High Performance Concrete</i> .....	67
4.2.4	<i>Mild Steel Reinforcement Properties</i> .....	68
4.2.4.1	<i>Simplified Model</i> .....	69
4.2.4.2	<i>Sophisticated Model</i> .....	70
4.2.4.3	<i>Bar Sizes</i> .....	71
4.2.5	<i>Prestressing Steel Properties</i> .....	71
4.2.5.1	<i>Menegotto and Pinto Model</i> .....	72
4.2.5.2	<i>Devalapura and Tadros Model</i> .....	73
4.2.5.3	<i>Prestressing Steel Properties</i> .....	76
4.2.6	<i>Soil Effects</i> .....	78
4.2.6.1	<i>Confined Core Concrete</i> .....	78
4.2.6.2	<i>Confined Cover Concrete</i> .....	79
4.2.7	<i>Steel Shell Effects</i> .....	79
4.2.7.1	<i>Confined Cover Concrete</i> .....	80

4.2.7.2	<i>Confined Core Concrete</i> .....	81
4.2.8	<i>Temperature Effects</i> .....	81
4.2.8.1	<i>Concrete</i> .....	82
4.2.8.2	<i>Mild Steel Reinforcement</i> .....	83
4.2.8.3	<i>Prestressing Steel</i> .....	84
4.2.8.4	<i>Soil</i> .....	84
4.2.9	<i>Analysis</i> .....	84
4.2.9.1	<i>Section Segmentation</i> .....	85
4.2.9.2	<i>Forces in Concrete</i> .....	86
4.2.9.3	<i>Reinforcing Steel in Rectangular Sections</i> .....	88
4.2.9.4	<i>Circular Section Reinforcing Steel</i> .....	89
4.2.9.5	<i>Rectangular Section with Circular Reinforcing Steel</i> .....	91
4.2.9.6	<i>Octagonal Section with Circular Reinforcing Steel</i> .....	91
4.2.9.7	<i>H-Shaped Section</i> .....	92
4.2.9.8	<i>Forces in Mild Steel Reinforcement</i> .....	92
4.2.9.9	<i>Forces in Prestressing Steel</i> .....	93
4.2.9.10	<i>Determination of the Neutral Axis Depth</i> .....	94
4.2.9.11	<i>Calculation of Moment Capacity</i> .....	96
4.2.9.12	<i>Calculation of Moment-Curvature Response</i> .....	96
4.2.9.13	<i>Conditions for Stopping Analysis</i> .....	98
Chapter 5:	EXAMPLE PROBLEMS AND VALIDATION .....	99
5.1	Introduction .....	99
5.2	Circular Concrete Section .....	99
5.2.1	<i>Comparison of VSAT to King's Program</i> .....	99
5.3	Rectangular Concrete Section .....	101
5.3.1	<i>Comparison of VSAT to King's Program</i> .....	101
5.4	Circular Section with Different Concrete Models .....	102
5.5	H-Shaped UHPC Section .....	103
5.5.1	<i>Comparison of VSAT to Vande Voort et al. (2008)</i> .....	104
5.6	Rectangular Concrete Section with Circular Prestressing Steel Configuration....	105
5.6.1	<i>Comparison of VSAT to Vande Voort et al. (2008)</i> .....	105
5.7	Effects of Temperature .....	107
Chapter 6:	SUMMARY, CONCLUSIONS AND RECOMMENDATIONS .....	109
6.1	Introduction .....	109
6.2	Summary .....	109
6.2.1	<i>VSAT</i> .....	110
6.3	Conclusions .....	111
6.3.1	<i>Temperature Effects on A706 Mild Steel</i> .....	111
6.3.2	<i>VSAT</i> .....	112
6.4	Recommendations .....	113
6.4.1	<i>Temperature Effects</i> .....	113
6.4.2	<i>Additional Material Properties</i> .....	114
6.4.3	<i>VSAT</i> .....	115

REFERENCES .....	116
APPENDIX A: A706 MILD STEEL ADDITIONAL GRAPHS .....	120
APPENDIX B: VSAT USER MANUAL.....	126
B.1 Introduction.....	126
B.2 Title Page and Section Type .....	127
B.3 Section Parameters.....	129
B.4 Circular Section Geometry .....	131
B.5 Rectangular Section Geometry and Circular Core.....	134
B.6 Rectangular Section Geometry and Rectangular Core .....	136
B.7 Octagonal Section Geometry .....	138
B.8 H-Shaped Section Geometry.....	140
B.9 External Soil Pressure .....	142
B.10 Defining Properties of Concrete.....	143
B.11 Defining Properties of Mild Steel Reinforcement.....	152
B.12 Defining Properties of Prestressing Steel Reinforcement .....	157
B.13 Analysis Parameters .....	172
B.14 Saving and Viewing Output .....	174
B.15 Opening a Saved Input File .....	175

## LIST OF TABLES

Table 2-1: Advantages and Disadvantages of Concrete Material Models .....	21
Table 3-1: Monotonic Test Matrix for the Effects of Temperature and Section Size on A706 Mild Steel.....	38
Table 3-2: Monotonic Test Matrix for the Effects of Strain Rate on A706 Mild Steel .....	39
Table 4-1: Default VSAT Steel Properties .....	70
Table 4-2: ASTM Standard Bar Information .....	71
Table 4-3: Coefficients Recommended for Defining the Stress-Strain Behavior of Prestressing Steel by Naaman (1985) .....	73
Table 4-4: Coefficients Recommended for Defining the Stress-Strain Behavior of Prestressing Steel by Devalapura and Tadros (1992) .....	75
Table 4-5: Strand Prestressing Steel Properties.....	76
Table 4-6: Wire and Bar Prestressing Steel Properties .....	77

## LIST OF FIGURES

Figure 1-1:	1971 San Fernando Earthquake Damage, (a) Confinement Failure (b) Shear Failure within Plastic Hinge (Priestley et al., 1996).....	3
Figure 1-2:	Flexural Design Method Based on the Equivalent Stress Block (ACI, 2008) ....	4
Figure 1-3:	Comparison between Actual and Idealized Moment-Curvature Responses of a Concrete Section.....	7
Figure 2-1:	Confined and Unconfined Concrete Model by Mander et al. (1988b).....	15
Figure 2-2:	Comparison of Concrete Model Proposed by Mander et al. and Hose et al. ....	16
Figure 2-3:	Compressive Strength Increases due to Low Temperatures as Digitized from Sehnal et al. (1983).....	18
Figure 2-4:	Increase in (a) Compressive Strength, (b) Elastic Modulus, and (c) Tensile Strength with Decreasing Temperature as Digitized from Lee et al. (1988).....	19
Figure 2-5:	Comparison of Van Der Veen and Reinhardt's (1989) Experimental Data to Equations Presented by Rostásy and Goto and Miura that Define the Increase in Concrete Strength as a Function of Temperature and Moisture Content .....	20
Figure 2-6:	UHPC Stress-Strain Behavior as Presented by Vande Voort et al. (2008) .....	22
Figure 2-7:	Stress-Strain Behavior of Milled and Unmilled A706 Mild Steel Reinforcement Samples at a Strain Rate of 0.01/s that Experienced Thawing During Testing (Sloan, 2005).....	25
Figure 2-8:	Yield and Ultimate Strength Increases vs. Temperature of A706 Mild Steel Reinforcement as Reported by Sloan (2005) .....	26
Figure 3-1:	Outer and Inner Surfaces of Aluminum Sleeves Before and After Testing .....	35
Figure 3-2:	Test Setup .....	37
Figure 3-3:	Idealized Mild Steel Reinforcement Stress-Strain Curve.....	40
Figure 3-4:	Effects of Cold Temperature on the Yield Strength of A706 Mild Steel Reinforcement Established from Monotonic Testing .....	41
Figure 3-5:	Effects of Cold Temperature on the Ultimate Strength of A706 Mild Steel Reinforcement Established from Monotonic Testing .....	43
Figure 3-6:	Comparison between Yield Strength Increases of #6 and #8 A706 Mild Steel Reinforcing Bars Subjected to Monotonic Loading and Low Temperatures....	44
Figure 3-7:	Comparison between Ultimate Strength Increases of #6 and #8 A706 Mild Steel Reinforcing Bars Subjected to Monotonic Loading and Low Temperatures .....	44
Figure 3-8:	Effects of Strain Rate on the Yield Strength of A706 Mild Steel at Cold Temperatures .....	45
Figure 3-9:	Effects of Strain Rate on the Yield Plateau Length of A706 Mild Steel at Cold Temperatures .....	46
Figure 3-10:	Dissipation of Yield Plateau Length Due to Strain Rate of a Milled #8 A706 Mild Steel Bar at -4°F (-20°C) .....	47
Figure 3-11:	Effects of Strain Rate on the Ultimate Strength of A706 Mild Steel at Cold Temperatures .....	48
Figure 3-12:	(a) Yield Strength and (b) Ultimate Strength Increases of Milled Bars.....	48



Figure 3-13: Comparison of A706 Temperature Effects to A572, CSA G30.16, and the NCSU Assumption .....	49
Figure 4-1: Section Shapes Currently Available in VSAT .....	56
Figure 4-2: Concrete Compressive Stress-Strain Model as Proposed by Mander et al. (1988b) .....	60
Figure 4-3: A Plan View of Sections Showing the Effective Cores that are Confined by Transverse Reinforcement.....	61
Figure 4-4: Cross-Sectional Views along the Member Length Showing the Effective Cores that are Confined by Transverse Reinforcement.....	61
Figure 4-5: Incremental Step for Determining the Stress-Strain Behavior of Concrete by Hose et al. (2001) .....	65
Figure 4-6: Comparison of Concrete Model Proposed by Mander et al. and Hose et al. ....	65
Figure 4-7: Stress-Strain Model Used for UHPC in VSAT .....	68
Figure 4-8: Stress-Strain Behavior of A706 Mild Steel Reinforcement .....	69
Figure 4-9: Menegotto and Pinto Model for Defining the Stress-Strain Curve of Prestressing Steel.....	73
Figure 4-10: Devalapura and Tadros Model for Defining the Stress-Strain Curve of Prestressing Steel.....	75
Figure 4-11: Comparison between Expected and Assumed Soil Confining Pressure used in VSAT .....	79
Figure 4-12: Dimensions of a Circular Section with an Exterior Steel Shell .....	81
Figure 4-13: Example of Zone, Strip, and Material Segmentation .....	86
Figure 4-14: Determining the Strain for Strip $i$ and a Given Curvature .....	87
Figure 4-15: Steel Distribution for Rectangular Sections .....	88
Figure 4-16: Segmentation of a Rectangular Section and Smearing of Longitudinal Steel Reinforcement .....	89
Figure 4-17: Segmentation of a Circular Section and Smearing of Longitudinal Steel Reinforcement .....	90
Figure 4-18: Circular Steel Shell Segmentation and Location.....	91
Figure 4-19: Section Segmentation of a H-Shape Section and Defining the Location of Prestressing Steel and Cross Section Width Changes .....	92
Figure 4-20: Moment-Curvature Response Segmentation and Conditions .....	97
Figure 5-1: Details of the Circular Section Example .....	100
Figure 5-2: Moment-Curvature Comparison for the Example Circular Section in Figure 5-1 .....	100
Figure 5-3: Details of the Rectangular Section Example.....	101
Figure 5-4: Moment-Curvature Comparison for the Rectangular Section Example in Figure 5-3 .....	102
Figure 5-5: Moment-Curvature Comparison of Different VSAT Concrete Models.....	103
Figure 5-6: Example H-Shape Section Details .....	104
Figure 5-7: Moment-Curvature Comparison of Example H-Shaped Section .....	104
Figure 5-8: Example Prestressed Section Details .....	106
Figure 5-9: Moment-Curvature Comparison to OpenSees .....	106
Figure 5-10: Temperature Effects on Moment-Curvature Response .....	108
Figure A-1: Modulus of Elasticity vs. Temperature at 0.001896 in./in./min.....	120

Figure A-2: Modulus of Elasticity vs. Strain Rate.....	121
Figure A-3: Yield Plateau Length vs. Temperature at 0.001897 in./in./min. ....	121
Figure A-4: Ultimate Strain vs. Temperature at 0.275 in./in./min. ....	122
Figure A-5: Ultimate Strain vs. Strain Rate.....	122
Figure A-6: Strain-Hardening Equation Validation at 20°C.....	123
Figure A-7: Strain-Hardening Equation Validation at 5°C.....	123
Figure A-8: Strain-Hardening Equation Validation at -1°C .....	124
Figure A-9: Strain-Hardening Equation Validation at -20°C .....	124
Figure A-10: Strain-Hardening Equation Validation at -40°C .....	125
Figure B-1: Definition of User Information in VSAT.....	127
Figure B-2: Definition of Section Parameters in VSAT.....	129
Figure B-3: Defining Details of a Circular Section in VSAT.....	131
Figure B-4: Defining Details of a Rectangular Section and Circular Core .....	134
Figure B-5: Defining Details of a Rectangular Section and Rectangular Core .....	136
Figure B-6: Defining Details of an Octagonal Section.....	138
Figure B-7: Defining Details of a H-Shape Section .....	140
Figure B-8: Defining an External Soil Pressure for Confinement of a Section.....	142
Figure B-9: Defining Material Properties of Concrete without Temperature Effects .....	143
Figure B-10: Defining the Properties of Concrete with Temperature Effects .....	145
Figure B-11: Defining the Properties of Concrete with Variable Confinement .....	146
Figure B-12: Defining the Transverse Mild Steel Reinforcement Properties for Concrete with Variable Confinement.....	147
Figure B-13: Defining the Properties of UHPC.....	150
Figure B-14: Defining Mild Steel Reinforcement Properties without Temperature Effects.....	152
Figure B-15: Defining Mild Steel Reinforcement Properties with Temperature Effects .....	154
Figure B-16: Defining Prestressing Strand Properties.....	157
Figure B-17: Defining the Stress-Strain Model for Prestressing Strands.....	158
Figure B-18: Defining the Menegotto and Pinto (1973) Stress-Strain Model for Prestressing Strands.....	159
Figure B-19: Defining the Simplified Devalapura and Tadros (1992) Model for Prestressing Strands.....	160
Figure B-20: Defining the Sophisticated Devalapura and Tadros Model for Prestressing Strands .....	161
Figure B-21: Defining Prestressing Bar Properties .....	162
Figure B-22: Defining the Stress-Strain Model for Prestressing Bars.....	163
Figure B-23: Defining the Menegotto and Pinto Stress-Strain Model for Prestressing Bars.....	163
Figure B-24: Defining the Simplified Devalapura and Tadros Model for Prestressing Bars.....	164
Figure B-25: Defining the Sophisticated Devalapura and Tadros Model for Prestressing Bars.....	165
Figure B-26: Defining Prestressing Wire Properties .....	167
Figure B-27: Defining the Stress-Strain Model for Prestressing Wires .....	168

Figure B-28: Defining the Menegotto and Pinto Stress-Strain Model for Prestressing	
Wires .....	168
Figure B-29: Defining the Simplified Devalapura and Tadros Model for Prestressing	
Wires .....	169
Figure B-30: Defining the Sophisticated Devalapura and Tadros Model for Prestressing	
Wires .....	170
Figure B-31: Defining the Analysis Parameters in VSAT.....	172
Figure B-32: Saving VSAT Analysis Results.....	174
Figure B-33: Opening a Saved VSAT Input File.....	175

## LIST OF NOTATION

$A_{cor,compi}$	Area of core concrete in compression zone for strip i
$A_{cor,teni}$	Area of core concrete in tension zone for strip i
$A_{cov,compi}$	Area of cover concrete in compression zone for strip i
$A_{cov,teni}$	Area of cover concrete in tension zone for strip i
$A_{p,comp}$	Area of prestressing steel in compression zone
$A_{perc,long}$	Percent of steel shell area contributing to flexural action
$A_{p,ten}$	Area of prestressing steel in tension zone
$Arc_{shell}$	Arc length of circular steel shell located at the centerline of steel
$arm_i$	Distance from strip i to the neutral axis, i.e. $(c - y_{ci})$
$A_s$	Total area of longitudinal mild steel reinforcement
$A_{s,comp}$	Area of mild steel in compression zone
$A_{shell}$	Total cross-sectional area of steel shell
$A_{shell,long}$	Area of steel shell contributing to flexural action
$A_{shell,trans}$	Area of steel shell contributing to confining action
$A_{s,ten}$	Area of mild steel reinforcement in tension zone
$A_{sh}$	Area of transverse mild steel reinforcement
$A_{s,strip}$	Area of steel present within strip i of the section
$A_{sx}$	Area of longitudinal steel parallel to the axis of bending
$A_{sy}$	Area of longitudinal steel perpendicular to the axis of bending
$b_c$	Width of rectangular core concrete measured from centerline to centerline of transverse reinforcement
$c$	Neutral axis depth from the extreme compression fibers of the section
$C_c$	Concrete resultant compressive force
$cover$	Cover distance measured from the extreme compression fiber to longitudinal reinforcing bars
$C_p$	Prestress resultant compressive force
$C_s$	Mild steel resultant compressive force

$D$	Gross section diameter
$d_b$	Diameter of mild steel reinforcing bar
$d_c$	Depth of rectangular core concrete measured from centerline to centerline of transverse reinforcement
$d_s$	Diameter of circular core concrete measured from centerline to centerline of transverse reinforcement
$d_t$	Diameter of concrete for a circular section with a steel shell
$E_c$	Young's modulus of elasticity for concrete
$E_{c,cold}$	Young's modulus of elasticity for concrete at a specific cold temperature
$E_s$	Young's modulus of elasticity for mild steel reinforcement
$E_{sec}$	Secant stiffness of concrete defined as $f'_{cc}/\epsilon'_{cc}$
$E_p$	Young's modulus of elasticity for prestressing steel
$f_c$	Stress of concrete in compression
$f'_c$	Unconfined compressive strength of concrete
$f'_{cc}$	Compressive strength of confined concrete
$f'_{c,cold}$	Unconfined compressive strength of concrete at a specific cold temperature
$f_{cor,compi}$	Stress of core concrete in compression zone for strip i
$f_{cor,teni}$	Stress of core concrete in tension zone for strip i
$f_{cov,compi}$	Stress of cover concrete in compression zone for strip i
$f_{cov,teni}$	Stress of core concrete in tension zone for strip i
$f_{c,ten}$	Stress of UHPC in tension (ksi)
$f_l$	Lateral confining pressure
$f_{l,shell}$	Lateral confining pressure from a steel shell
$f_{l,soil}$	Lateral confining pressure from soil
$f'_l$	Effective lateral confining pressure
$f'_{l,core}$	Effective lateral confining pressure for core concrete
$f'_{l,cover}$	Effective lateral confining pressure for cover concrete
$f_{p,comp}$	Stress of prestressing steel in the compression zone
$f_{p,ten}$	Stress of prestressing steel in the tension zone

$f_{py}$	Yield strength of prestressing steel
$f_{pu}$	Ultimate tensile strength of prestressing steel
$f_s$	Stress of mild steel reinforcement
$f_{s,comp}$	Stress of mild steel reinforcement in compression zone
$f_{so}$	The stress at the intersection of the two linear portions of the prestressing steel curve
$f_{s,ten}$	Stress of mild steel reinforcement in tension zone
$f_{su}$	Ultimate strength of mild steel reinforcement
$f'_t$	Tensile strength of concrete
$f'_{te}$	Elastic tensile strength of UHPC (ksi)
$f'_{t,max}$	Maximum tensile strength of UHPC (ksi)
$f_x$	Arbitrary stress along the strain hardening curve of mild steel reinforcement
$f_y$	Yield strength of longitudinal mild steel reinforcement
$f_{yh}$	Yield strength of transverse reinforcement
$k_e$	Concrete confinement effectiveness coefficient
$k_{e,shell}$	Concrete confinement effectiveness for a steel shell
$k_{e,soil}$	Concrete confinement effectiveness for soil
$m$	Constant used in VSAT to determine the strain hardening curve of mild steel reinforcement (refer to Eq. 2.39 for details)
$M$	Moment resistance at a specific curvature
$N_{bars}$	Number of longitudinal bars in a concrete section
$p$	Constant used in VSAT to determine the strain hardening curve of mild steel reinforcement (refer to Eq. 2.35 for details)
$P$	Resultant internal force perpendicular to the section
$P_{applied}$	Externally applied axial load perpendicular to the section
$R$	Constant used in VSAT to determine the strength of confined concrete
$r$	Radius from the center of section to the centerline of the main reinforcing steel
$r_c$	Ratio between $E_c$ and the difference of $E_c$ and $E_{sec}$ , i.e. $(E_c/E_c - E_{sec})$

$r_s$	Difference between ultimate strain and strain hardening strain for mild steel reinforcement, i.e. $(\varepsilon_{su} - \varepsilon_{sh})$
$s$	Centerline to centerline spacing between transverse reinforcement
$s'$	Clear spacing between transverse reinforcement
$t$	Temperature of material in °C
$T_c$	Resultant concrete tensile force for a specific curvature
$T_p$	Resultant prestress tensile force for a specific curvature
$T_s$	Resultant mild steel tensile force for a specific curvature
$\omega$	Percent of water, by weight, in concrete
$W$	Average center to center spacing between longitudinal reinforcement
$W'$	Average clear spacing between longitudinal reinforcement
$x$	Ratio between $\varepsilon_c$ and $\varepsilon'_{cc}$ , i.e. $(\varepsilon_c / \varepsilon'_{cc})$
$X$	A positive constant used in VSAT for the determination of $f'_t$
$X_{long}$	Percent of total steel shell area contributing to flexural action
$y_{ci}$	Distance from compressive strip i to the center of the section
$y_i$	Distance from extreme compression fiber to strip i
$y_{pi}$	Distance from the top of the H-shaped section to the center of prestressing bar
$y_{ti}$	Distance from tensile strip i to the center of the section
$\Delta\varepsilon_1$	Concrete strain step change for Hose et al. (2001) concrete model
$\Delta\varepsilon_d$	Transverse dilation strain change for Hose et al. (2001) concrete model
$\varepsilon_1$	Beginning concrete strain for Hose et al. (2001) concrete model
$\varepsilon_c$	Concrete compressive strain
$\varepsilon'_{cc}$	Concrete compressive strain corresponding to $f'_{cc}$
$\varepsilon'_{co}$	Concrete compressive strain corresponding to $f'_c$
$\varepsilon_{c,ten}$	Ultimate tensile concrete strain corresponding to $f'_t$
$\varepsilon_{cu}$	Ultimate compression strain of confined concrete
$\varepsilon_d$	Beginning transverse dilation strain for Hose et al. (2001) concrete model
$\varepsilon_{d,new}$	New transverse dilation strain for Hose et al. (2001) concrete model
$\varepsilon_i$	Strain in strip i

$\varepsilon_{py}$	Yield strain of prestressing steel corresponding to $f_{py}$
$\varepsilon_{ps}$	Prestressing steel strain
$\varepsilon_{pu}$	Ultimate strain of prestressing steel corresponding to $f_{pu}$
$\varepsilon_{spall}$	Concrete strain corresponding to spalling of cover concrete
$\varepsilon_s$	Strain in mild steel reinforcement
$\varepsilon_{sh}$	Strain in mild steel reinforcement at the onset of the strain hardening curve
$\varepsilon_{su}$	Steel strain corresponding to the ultimate strength of longitudinal mild steel reinforcement
$\varepsilon_{su,comp}$	Allowable maximum compressive strain in mild steel reinforcement, i.e. $(\varepsilon_{su} - \varepsilon_{su,ten})$
$\varepsilon_{su,ten}$	Allowable maximum tensile strain in mild steel reinforcement
$\varepsilon_t$	Tensile strain in UHPC
$\varepsilon_x$	An arbitrary strain along the strain hardening curve of mild steel reinforcement corresponding to $f_x$
$\varepsilon_y$	Yield strain of mild steel reinforcement corresponding to $f_y$
$\eta$	Constant to accurately model hoop strain for Hose et al. concrete model
$J$	Constant to accurately model hoop strain for Hose et al. concrete model
$\mu_e$	Elastic portion of tangent Poisson's ratio for Hose et al. concrete model
$\mu_t$	Total tangent Poisson's ratio for Hose et al. concrete model
$\mu_{tn}$	Non-elastic portion of tangent Poisson's ratio for Hose et al. concrete model
$\sigma'$	Difference between unconfined and confined beginning stress for Hose et al. concrete model
$\sigma_h$	Transverse hoop stress for Hose et al. concrete model
$\varphi$	Section curvature
$\rho_{cc}$	Volumetric ratio of longitudinal reinforcement to core concrete
$\rho_{cc,core}$	Volumetric ratio of longitudinal reinforcement to core concrete when soil or a steel shell exists
$\rho_{cc,cover}$	Volumetric ratio of longitudinal reinforcement to a gross concrete section when soil or a steel shell exists



$\rho_l$	Volumetric ratio of longitudinal reinforcement to gross cross section
$\rho_s$	Volumetric ratio of transverse reinforcement to core concrete
$\rho_{s,core}$	Volumetric ratio of transverse reinforcement to concrete core when soil or a steel shell exists
$\rho_{s,cover}$	Volumetric ratio of transverse reinforcement to gross concrete section when soil or a steel shell exists
$\rho_x$	Volumetric ratio of transverse reinforcement in the x-direction to core concrete of a rectangular section
$\rho_y$	Volumetric ratio of transverse reinforcement in the y-direction to core concrete of a rectangular section

## ACKNOWLEDGEMENTS

The research for this project was completed due to the interest and financial support from the Alaska Department of Transportation and Public Facilities (ADOT&PF), Alaska University Transportation Center (AUTC), and the Department of Civil, Construction and Environmental Engineering (CCEE) at Iowa State University in Ames, Iowa.

The author would like to thank Dr. Sri Sritharan for the opportunity to take part in this project and for the ongoing guidance and professional expertise he provided that aided in the completion of the project.

The author would also like to thank Dr. LaDon Jones for his knowledge of Visual Basic 6.0 and guidance he provided during the development stages of the Versatile Section Analysis Tool (VSAT) program. It is also appreciated that Dr. LaDon Jones and Dr. Jon Rouse were willing to serve on the committee for this thesis project.

Finally, the author would like to thank Aaron Shelman for his contribution of information for the development of the soil and concrete behavior in cold temperatures.

## ABSTRACT

The design of structural members subjected to seismic activity has progressed in recent years but does not yet include the effects of cold temperatures. In areas such as Alaska, the Midwest, East Coast, and even in some parts of the West Coast, this approach introduces a real deficiency as it is likely that an earthquake will occur during winter months. The current research program was initiated to address this deficiency by developing a section analysis tool program capable of defining the moment-curvature response in either warm or low temperatures. As part of this investigation, the stress-strain behavior of A706 Grade 60 mild steel reinforcement was studied under low temperatures (20°C to -40°C) to ensure that the effects of temperature is accurately accounted for in the newly developed analysis tool. In addition to mild steel, the effects of cold temperatures on the behavior of soil, unconfined concrete, and confined concrete are currently being examined by other researchers at Iowa State University.

The Versatile Section Analysis Tool (VSAT) was developed to reduce the general limitations found in other programs. Amongst these limitations are limited available material models, lack of commonly used section shapes, and the exclusion of soil and low temperature effects. VSAT was constructed with many different features to provide versatility in how the user wishes to establish material properties for a particular analysis. VSAT includes the following features: permitting different cross-sections, defining normal strength or UHPC material properties, defining simplistic or sophisticated mild steel or prestressing steel material properties, allowing the addition of soil pressure, including a steel shell circular section, and accounting for low temperature effects on material behavior.

The testing of mild steel reinforcement at low temperatures showed a quadratic increase in the yield and ultimate strengths of 5.1 and 6.3 percent, respectively, when lowering specimen temperatures from 20°C to -40°C. It was also found that the modulus of elasticity, ultimate strain, and strain hardening strain were insignificantly affected under the same conditions. Assumptions for the behavioral changes of concrete under low temperatures to be used in VSAT have been compiled from previous research until current testing can be

completed. These assumptions will then be replaced with experimental data collected by this project's partner researcher, Aaron Shelman.

As portions of VSAT were completed, the program was continually verified to be functioning correctly. First, previously known material models were verified to coincide with those presented in this thesis by hand and within the newly developed program. Second, as shown in the verification section of this thesis, non-prestressed rectangular and circular sections were compared with King's Program to ensure accuracy. UHPC H-shaped sections were also examined based upon the work and experimentation of Vande Voort et al. (2008). Unique features, where a comparison is impossible (i.e. temperature effects on the stress-strain behavior of mild steel reinforcement), have been carefully added to VSAT. The effects of these features have been checked, by hand, to ensure that the program is functioning properly.

The development of VSAT has been successfully initiated and the results for particular sections have proven to be comparable with previously created section analysis programs. Further expansion of the program is possible as additional desired features become apparent. Due to time constraints and the scope of this project, any addition features and continual testing of the program was left for a successor to complete.

## Chapter 1: INTRODUCTION

### 1.1 Historical Background

A bridge, by definition, is “a structure built to span a valley, road, railroad track, river, body of water, or any other physical obstacle, for the purpose of providing passage over that obstacle” (Bridge, 2009). The first bridges were produced by nature and may have been as simplistic as a log fallen over a river. Since this time, bridges have been made from various materials such as stone, lumber, rope, steel, and concrete. Today, through the advancements in technology and knowledge, bridge designers have developed new methods of design and utilized advanced materials (i.e. ultra-high performance concrete) to attain longer spans, withstand heavier loads, and maintain an artistic appeal that may, or may not, have been demanded by the consumer. This quest for additional knowledge, particularly in structural behavior and construction materials, has increased the efficiency of design and will continue to do so as further knowledge is attained.

Bridges are comprised of a substructure and a superstructure. The substructure includes columns and foundations while the superstructure contains all other elements of the bridge. A bridge normally contains one of two different types of foundations, a deep foundation or a shallow foundation. Due to most of today’s bridges spanning over unstable soils (e.g. soil near a body of water) or site constraints (e.g. property lines), the substructure frequently utilizes deep foundations for support because it’s usually a simpler and more cost effective solution. Regardless of the system used, each structural member must be designed to withstand significant lateral loading in seismically active regions.

### 1.2 Seismic Design

The design of bridges is an ever-changing field in structural engineering that is based upon the knowledge ascertained over the years. Specifically, seismic engineering has become of great importance due to structural failures occurring in past and recent seismic events. A few of these major earthquakes throughout U.S. history are the New Madrid Series during the winter of 1811-1812, the Fort Tejon earthquake of 1857, the Owens Valley earthquake of 1872, the San Francisco earthquake of 1906, the 1940 El Centro earthquake,

the Loma Prieta Earthquake of 1989, an earthquake occurring in the Gulf of Mexico in 2006, and the Andean Islands earthquake of 2008 (U.S. Geological Survey, 2009).

The New Madrid earthquakes in the winter of 1811-1812 consisted of three earthquakes exceeding a magnitude 8 on the Richter scale with thousands of aftershocks (Sritharan et al., 2007), caused large areas of earth to sink, new lakes to form, and the Mississippi River to change course, leading to devastating effects upon the surrounding buildings in the central United States (Stover and Coffman, 2009). Further understanding of earthquakes, their ground excitations (accelerations), and their effects on structures were attained during the 1940 El Centro and subsequent earthquakes where important ground excitation data could be recovered.

For decades, a force-based design approach has been used in seismic design. In the 1980s, prior brittle failures of columns, connections, and piers led engineers to realize there were issues in their current force-based approach. The underestimation of design loads, use of an elastic design method, and no concept for energy dissipation were amongst some of these challenges (Priestley et al., 1996). A new design philosophy needed to be conceived and adopted.

### ***1.2.1 Capacity Design Philosophy***

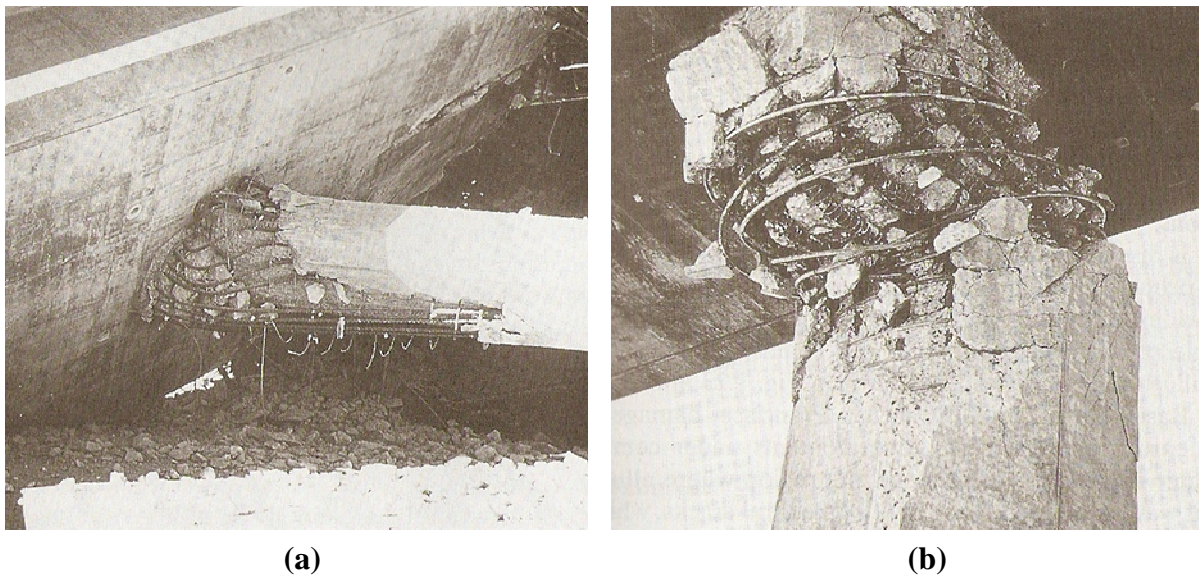
In high seismic regions of the United States, such as California and Alaska, structures are now designed to ensure satisfactory performance by following the capacity design philosophy. This seismic design philosophy, as stated by Priestley et al. (1996), may be stated as follows:

- under design-level earthquakes, the structure shall be allowed to respond inelastically through flexural yielding;
- plastic hinge locations should be preselected and carefully detailed to ensure that the structure can undergo an adequate ductile response; and
- undesirable inelastic mechanisms, such as shear failure and anchorage failure, are prohibited by providing a suitable strength margin between nonductile failure modes and the dependable ductile mode of deformation through the formation of inelastic plastic hinges.

This philosophy chooses plastic hinge locations in structural members that are designed to allow for plastic deformation during a seismic event while maintaining structural integrity. Upon the conclusion of the event, trained engineering inspectors should assess the damage and determine if the structure requires repairing or replacing before reopening for public use.

### 1.2.2 Behavior of Plastic Hinges

The predetermined placement of plastic hinges is vital in seismic design. Plastic hinges are designed and detailed to dissipate energy by responding inelastically during a seismic event without experiencing significant strength degradation (Priestley et al., 1996). The locations are determined by establishing the critical section of the flexural members. These plastic hinges can be positioned in a structure to allow for a bridge superstructure to perform elastically or to provide redundancy in buildings in order to protect human life during a seismic event. If designed properly, the catastrophic failures depicted in Figure 1-1 and the collapse of the entire structure can be prevented.

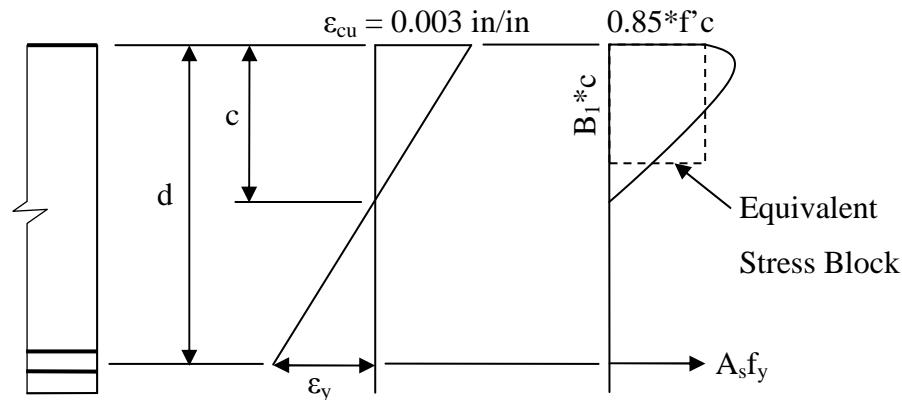


**Figure 1-1: 1971 San Fernando Earthquake Damage, (a) Confinement Failure (b) Shear Failure within Plastic Hinge (Priestley et al., 1996)**

Flexural members need to be designed in such a way that they meet the displacement or displacement ductility requirements at the ultimate limit state as specified in the code of practice (i.e. ACI or AASHTO). To attain this displacement ductility, the preselected hinges undergo deformation during the design seismic event. They should also be designed so that

undesirable failure modes, such as shear and buckling, do not dictate the member's performance during the structure's design life (Priestley et al., 1996).

The current procedure to design for the ultimate limit state is presented by the ACI-08 code and/or the AASHTO LRFD Bridge Design Specifications with interim revisions (ACI, 2008; AASHTO LRFD Bridge Design Specifications, 2007). Both sources, ACI-08 Chapter 21 and AASHTO Section 5.7.2.2, use the equivalent stress block method to determine the flexural capacity of a flexural member and provide provisions on transverse reinforcement near the ends of these members to incorporate ductility. The equivalent stress block method, as shown in Figure 1-2, recreated from ACI-08 Section 10.2, assumes that the non-uniform concrete compressive stress contour provides a total force that can be represented as a stress block with dimensions  $0.85*f'_c$  by  $B_1*c$ . All mild steel within the section is assumed to be at yield,  $f_y$ , or at the nominal flexural capacity,  $f_{ps}$ , in prestressed sections (ACI-08 Section 18.7.1 and AASHTO Section 5.7.3.1). From these assumptions, one can determine the ultimate flexural capacity of the section. The AASHTO code allows for the  $0.85*f'_c$  concrete strength to be modified for sections if experimentation can prove the new value accurate and dependable (AASHTO LRFD Bridge Design Specifications, 2007).



**Figure 1-2: Flexural Design Method Based on the Equivalent Stress Block (ACI, 2008)**

The equivalent stress block method has some limitations and disadvantages. This method tends to be conservative (Priestley et al., 1996), leading to more costly sections. The underestimation of flexural strength may lead to additional funds being spent on retrofitting existing structures where a more precise method of analysis may deem the section adequate. The equivalent stress block method cannot accurately depict the true flexural capacity of the



section because the resultant compressive force location is not known. An inaccuracy in the section's flexural resistance may cause undesirable failures, such as shear failure, to occur because the demand is too high. Finally, the designer has no control over the ductility of the system because it cannot be determined with the information provided.

In Section 8.4 of the newest AASHTO Design guide, AASHTO Guide Specifications for LRFD Seismic Bridge Design, a moment-curvature approach for designing sections is provided (AASHTO Guide Specifications for LRFD Seismic Bridge Design, 2009). This approach is more consistent to the Capacity Design Philosophy and also contains information on material models that can be used in lieu of material test data. This design guide was created in response to the vulnerability of columns with inadequate transverse reinforcement and anchorage of longitudinal reinforcement found in the 1989 Loma Prieta and 1998 Northridge earthquakes (AASHTO Guide Specifications for LRFD Seismic Bridge Design, 2009). Unfortunately, only mild steel and prestressing steel reinforcement models are given. Furthermore, utilizing this material information may lead to errors in the moment-curvature response if the data used in the field isn't properly represented (e.g. a full definition of the strain hardening region of mild steel reinforcement is not defined in this document).

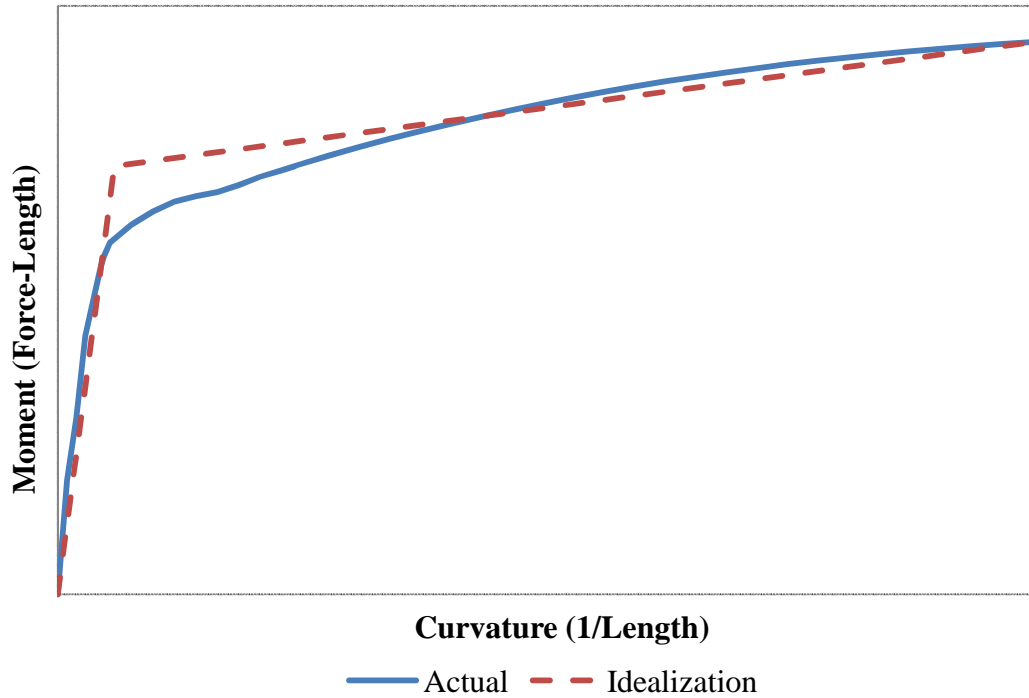
Upon the completion of designing for the ultimate limit state, the service limit state should be checked. After an event, no remedial action should be required. This means that no crushing of concrete, extensive cracks that require injection grouting, or spalling of the concrete should form under service and/or minor earthquake loading. Currently, this is satisfied in code by extra provisions such as crack control reinforcement spacing or deflection check requirements.

To better estimate the actual behavior and capacity of flexural members for ultimate and service limit states while maintaining the most cost effective section, a moment-curvature approach can be used. The stresses are more refined to more accurately predict moment capacities and an idealized displacement capacity can be found. This is not possible with the LRFD method because ductility is empirically integrated into equations.

### ***1.2.3 Moment-Curvature Approach***

Section geometry, loading, and material models are required to generate a moment-curvature response such as that shown in Figure 1-3. Upon obtaining this moment vs. curvature relationship, the first-yield and ultimate limit states can be used to idealize the curve and the approximate ductility of the section can be established. If the limit state requirements are not attained or the ductility is deemed unsatisfactory for the predicted seismic loading, the geometry and reinforcement details of the section need be altered. Then the entire process is repeated for the revised section.

To generate a moment-curvature graph, the section must first be discretized into pieces. The accuracy of the data found is inversely proportional to the size of the pieces used. For a given rotation or curvature value and neutral axis depth, the strains, stresses, forces, and moments of each individual material and piece are found. The summation of these forces and moments are the total axial and flexural resistance of the section. Next, a tedious iterative process is performed in order to find equilibrium between the applied axial load and the axial resistance. Once completed, the corresponding flexural resistance for the particular curvature is correct. The entire process is then repeated for all points along the moment-curvature graph until the ultimate condition is reached. If the resulting moment-curvature response doesn't meet the designer's requirements, the section is modified and the entire moment-curvature graph must be recalculated. Utilizing computer software is both beneficial and common design practice when generating the appropriate moment-curvature graph(s) in a relatively short period of time. In addition, utilizing a computer analysis tool avoids the accumulation of errors associated with hand calculations.



**Figure 1-3: Comparison between Actual and Idealized Moment-Curvature Responses of a Concrete Section**

### 1.3 Current Section Analysis Tools

There are many section analysis tools that are available for use. A few of these programs are: King's Program (King et al., 1986), LPile (Ensoft, Inc., 2005), OpenSees (Mazzoni et al., 2009), and XTRACT (TRC/Imbsen Software Systems, 2009). They are all capable of attaining a moment-curvature response given the necessary input. Generally, however, these programs lack features and/or versatility that are both beneficial and crucial to the determination to better estimate the moment capacity of a section. These shortcomings will be discussed below starting with geometry and defaults, reinforcement models, concrete models, temperature parameters, and soil parameters.

#### 1.3.1 Geometry and Defaults

A software program used to aid in design needs to be easy to operate. For a moment-curvature software, it is desirable to incorporate preset section shapes, standard reinforcement sizes and areas throughout the program. To the author's knowledge OpenSees

allows for circular, rectangular and triangular sections with no standard reinforcement sizes (Mazzoni et al., 2009); King's Program allows for circular and rectangular sections with no standard reinforcement sizes (King et al., 1986); LPILE allows for several different sections with reinforcement sizes (Ensoft, Inc., 2005); and Xtract uses circular and rectangular sections with no standard reinforcement sizes (TRC/Imbsen Software Systems, 2009). In addition, finding a program that can analyze concrete sections with an exterior circular steel shell, octagonal or a H-shaped section with appropriate features is difficult. It is important that a moment-curvature analysis program is capable of handling numerous sections while providing predetermined standard reinforcement sizes for functionality and to ease the work required of the user, respectively.

### ***1.3.2 Reinforcement Model***

In order to generate all possible sections in design, prestressing and mild steel reinforcement need be available. To the author's knowledge OpenSees has both mild and prestressing steel reinforcement (Mazzoni et al., 2009), King's Program has no prestressing reinforcement (King et al., 1986), Xtract allows for any material model available within the Xtract Library (TRC/Imbsen Software Systems, 2009), and LPILE has both prestressing and mild steel reinforcement (Ensoft, Inc., 2005). Of the programs including mild steel, the stress-strain curve is defined by an elastic, perfectly plastic, and parabolic strain-hardening region. Unfortunately, these programs do not allow for the strain-hardening portion of the curve to be altered because more information would be required. This limitation, such as that experienced in King's Program (King et al., 1986), leads to errors in the program's generated output. Since the necessary information to account for these errors is not always known, the reinforcement models should have the option of being defined with a sophisticated or simplistic material model.

### ***1.3.3 Concrete Model***

As previously stated in Section 1.2, the stress-strain behavior of each individual material present within the section must be captured to attain an accurate moment-curvature response. Structural design software programs generally utilize one relatively simple method for

defining material behavior, forcing the user to use what is available. Mander's model, or a simpler model, is typically used for defining the stress-strain curve of both confined and unconfined concrete. In simpler models the strain at which the maximum stress occurs, the transverse reinforcement stress, and the ultimate strain are preset parameters that cannot be altered. Incorrectly represented material properties lead to errors within the output generated.

First, when the maximum stress of concrete increases,  $f'_{cc}$ , so should the strain at which it occurs,  $\epsilon'_{cc}$ . This is apparent in the equations presented by Mander et al. (1988b) but may be fixed by the available software or concrete model used. This will alter all confined stresses at their particular strains.

Second, models such as those provided by Mander et al. (1988b) assume that the transverse reinforcement is always at yield. The stress of the transverse reinforcement directly affects the confined concrete stress calculated due to equilibrium requirements within the section. For this reason, an overestimation of the confined concrete stress occurs at low strains where the transverse reinforcement has not yet reached its yield strength and an underestimation of the confined concrete stress occurs at higher strains where the transverse reinforcement should be in the strain hardening region of the stress-strain curve. Recent developments by Hose et al. (2001) help alleviate this problem by accounting for the variation in transverse steel stress, adjusting the concrete stresses for each strain.

Unfortunately, this model is not available in previously created programs.

Finally, the ultimate strain of concrete should not be a constant because it is dependent upon the confining steel and the confined concrete maximum strength (Priestley et al., 1996). This problem could be avoided if programs provided an option for a user defined ultimate confined concrete strain.

Since each of the previously mentioned parameters plays a key role in attaining an accurate concrete stress-strain curve, they need to be available for alteration. If not, these errors will be imbedded within the moment-curvature response that may lead to an over-conservative or under-conservative final design.

### ***1.3.4 Temperature Effects***

Although the development of design has greatly progressed, little research has yet been done on the design of these same structures subjected to seasonal freezing. This is a major deficiency in the seismic engineering field as some of the largest earthquakes (e.g., 1811-1812 New Madrid Series and the 1964 Great Alaska Earthquake) have occurred during winter months.

It has been shown through experimental testing by Sehnal et al. (1983), Lee et al. (1988), and Van Der Veen and Reinhardt (1989) on concrete and by Filiatrault and Holleran (2001), Bruneau's et al. (1997), and Sloan (2005) on various reinforcement types that cold temperature alters the behavior of materials. Logically, these changes should affect the moment-curvature response of the designed section and the performance of the structural member.

The previous statement was evident in research conducted by Suleiman et al. (2006), where seasonally frozen conditions cause considerable changes in the response of structures with the same section design. As part of their testing, two identical cast-in-drilled-hole shafts were tested, one in warm and one in cold conditions. Suleiman et al. observed that the frozen shaft experienced a higher effective elastic stiffness, an increase in lateral load resistance, an upward shift of the maximum moment location, and a reduced length in the plastic region when compared to the warm shaft (Suleiman et al., 2006). They attributed these performance changes to a 0.76m deep frozen soil layer near the ground surface. In addition to the behavioral changes associated with cold weather conditions, some regions of the United States (e.g., Alaska) further complicate the issue by adding an exterior steel shell to circular sections. To the author's knowledge, no available moment-curvature analysis program is capable of handling this particular section.

As presented above, the effects of cold temperature upon the moment-curvature response must be included in the design process to ensure an adequately designed section for a seismic event occurring during winter months. This task requires the use of an analysis tool that is capable of altering steel and concrete properties as a function of temperature, something not currently available to a designer.

### 1.3.5 Soil Confinement Effects

Plastic hinges can be designed to form in above-ground (i.e. columns) and in-ground (i.e. foundation shafts) locations and should be analyzed separately due to the presence of soil. Soil pressure can have an extreme impact on the moment-curvature response of a section. In a study conducted by Budek et al. (2004) on scaled cast-in-drilled-hole piles with and without artificially added soil pressure, it was found that soil confinement can play a significant role in the pile shaft response. This study found that adding a confining pressure caused an increase in the confinement effectiveness, ductility capacity, and plastic hinge length.

The soil confinement activated during displacement will alter all concrete stresses while also inhibiting the spalling of concrete, altering the entire moment-curvature response. This should be accounted for in the moment-curvature analysis of sections. This was illustrated in work conducted by Sritharan et al. (2007) where soil pressure was idealized as artificially adding a secondary reinforcement layer on the outside of the tested sections. The appropriate confinement pressure was determined iteratively. The section was analyzed first without soil confinement with a moment-curvature analysis tool. This information was then used in LPile to determine the confinement pressure exerted by the compression-only soil springs upon the section at various depths. The soil confinement pressure was next represented as an equivalent transverse reinforcement layer on the exterior of the original section. The moment-curvature data gathered from this modified section was used for subsequent iterations.

The aforementioned iterative method requires an additional step from LPile to the section analysis tool, creating the equivalent transverse reinforcement layer. Some of the programs available today, such as King's Program (King et al., 1986) and Xtract (TRC/Imbsen Software Systems, 2009), do not allow for the presence of soil pressure to be captured via any method. For those programs allowing a secondary confinement layer, it must be ensured that the effects of both the secondary and primary transverse reinforcement are captured correctly to adequately define the confined concrete stress-strain curve.

#### 1.4 Scope of Research

The preceding sections have demonstrated a significant lack of features that need be available in the existing moment-curvature analysis tools for the design of structural elements. Designers may be unwillingly and unknowingly imbedding errors into their analyses due to material definition limitations and restrictions.

If a seismic event were to occur in the United States during the winter, as history has documented occurrences, systems will react to altered soil pressure and material behavior. If the column/foundation was designed only to maintain a warm weather seismic event, the capacity may be significantly reduced and the plastic hinge(s) may form in a different location(s) due to an upward shift in the maximum moment location. These alterations may lead to a brittle failure and, ultimately, a collapse because the excess demand is dissipated through undesirable failure modes. Had a section analysis tool capable of handling these types of conditions been used, such a failure may have been avoided.

The main focus of this thesis is to develop a section analysis tool, Versatile Section Analysis Tool (VSAT), which will aid in the design of columns/piles with the inclusion of the following options:

1. Analyze reinforced concrete sections in warm and cold weather conditions
2. Analyze prestressed concrete sections in warm weather conditions
3. Include concrete sections experiencing a secondary confining pressure through soil pressure and/or exterior steel shell
4. Include prestressed concrete sections in combination with ultra-high performance concrete
5. Automate rebar and prestress reinforcement sizes and areas
6. Include different material behavior models with appropriate options
7. Define default parameters for the material models

In addition, to aid in the designing of a section analysis tool, a comprehensive testing on A706 mild steel reinforcement was conducted. The effects of temperature and strain rate on the Young's modulus, yield stress and strain, strain hardening region, and ultimate stress and strain of the material were examined.



## 1.5 Report Layout

The remainder of this thesis discusses, in detail, the procedures of the aforementioned project. Chapter 2 includes a literature review of the current available material behavior with advantages, disadvantages, available models and reasoning for choosing the models used in VSAT. Chapter 3 describes the comprehensive testing on A706 mild steel and its behavior changes due to temperature and strain rate. Chapter 4 presents a theoretical manual, discusses all equations and models that were used in the development of VSAT with appropriate accreditation. Chapter 5 is comprised of example problems that both validates the capability of the program while also showing the importance of including such parameters as temperature and soil pressure. Finally, Chapter 6 provides the conclusions and recommendations determined upon the completion of this project.

## Chapter 2: LITERATURE REVIEW

### 2.1 Introduction

This chapter presents a review of literature relevant to the development of VSAT introduced in Chapter 1, as well as, that required for the completion of this thesis. This includes chosen material models for concrete, UHPC, mild steel reinforcement and prestressing steel, and their advantages and disadvantages. Since VSAT is designed to include the ability to examine cold temperature effects on the moment-curvature response of concrete sections, the findings of temperature effects on material behavior is also discussed. In addition, a summary of capabilities of existing moment-curvature programs are presented, which also clearly shows the benefits of features included in the development of VSAT.

Note that the amount of detail in this chapter is limited to avoid repetition within this document. The development of the theoretical procedures for VSAT further discusses the material models in Chapter 4.

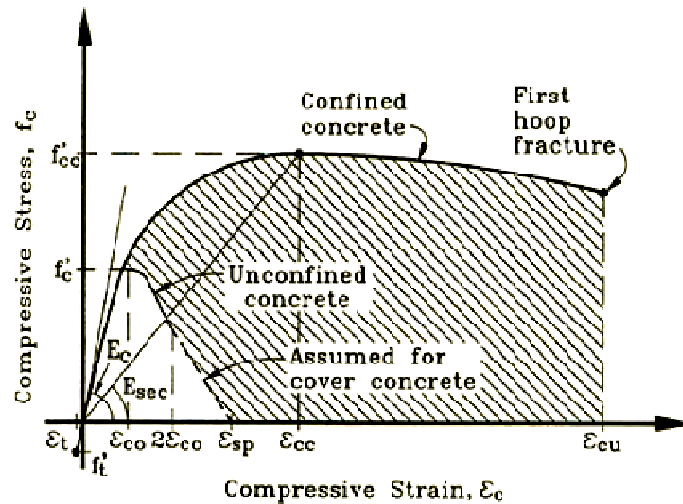
### 2.2 Behavior of Concrete

Two models capable of defining the stress-strain behavior of both unconfined and confined concrete were examined in this study. In addition, three models suggested for defining the effects of cold temperature on the behavior of concrete are discussed.

#### 2.2.1 *Stress-Strain Behavior of Concrete*

Confined concrete contains longitudinal and transverse reinforcement, which provides a confining pressure around the “core”. This pressure causes an increase in the strength and strain capacity of the concrete. Unconfined concrete contains no reinforcement and, for the purposes of structural members, encases the confined core concrete. This “cover” is used to prevent the corrosion of reinforcement while providing an aesthetic aspect. At a specific strain, referred to as the spalling strain, the cover concrete crushes and subsequently spalls off, no longer contributing to the moment resistance of the section. Typically, the model presented by Mander et al. (1988b), or a more simplistic model, is used to define the stress-strain behavior of concrete.

The concrete model presented by Mander et al. (1988b) can define both confined and unconfined concrete with a single stress equation given the required parameters. This model, which is defined in Section 4.2.3, is depicted graphically in Figure 2-1. The model was established from a series of nearly full-scale column tests with varying longitudinal and transverse steel ratios (Mander et al., 1988a and 1988b). These columns had circular, rectangular or square cross sections and were subjected to either slow or fast (dynamic) strain rates with either monotonic or cyclic loading.

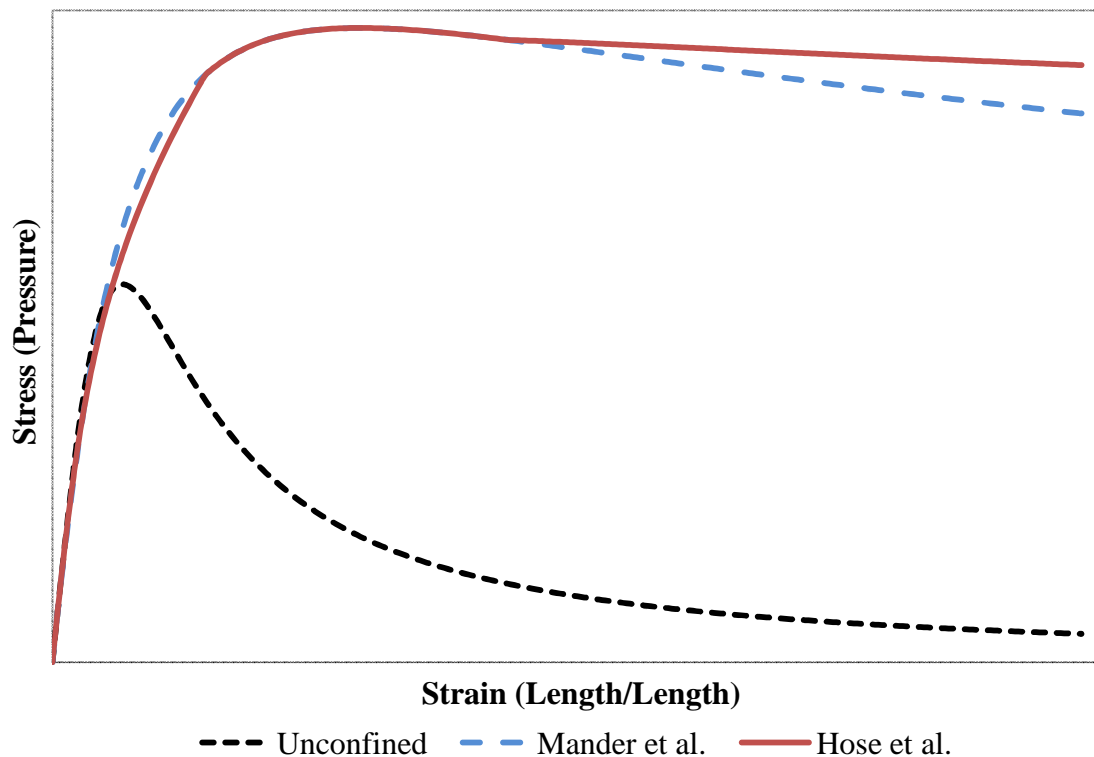


**Figure 2-1: Confined and Unconfined Concrete Model by Mander et al. (1988b)**

The model was developed assuming the transverse steel is at a constant yield stress. It also automatically develops critical parameters shown in Figure 2-1 (e.g. elastic modulus ( $E_c$ ), confined concrete stress ( $f'_{cc}$ ), spalling strain ( $\epsilon'_{sp}$ ), and ultimate strain ( $\epsilon'_{cu}$ )) to lessen the extent of knowledge required from the user. This particular model was selected because it is widely used in design when confined concrete is significant, which is made apparent by other programs using the same material model (e.g. King's Program and XTRACT). This model also has parameters that were used in VSAT as user defined, allowing the user to have more control over the stress-strain behavior of concrete. The features used in this model are advantageous but the simplifications can provide the overestimation and underestimation of confined concrete stresses at particular strains. Another model was selected that can account for variable transverse reinforcement stress to correct this issue.

Hose et al. (2001) investigated the effects of variable confining (transverse) steel stress and its effects on concrete strength to refine the work conducted by Mander et al. The model was developed to analyze highway structures in California that were constructed prior to 1990 with A615 steel instead of A706 as it required today (Hose et al., 2001). The concern was whether or not retrofitting or replacement was necessary for these structures and analysis design models current at the time assumed too high of a transverse strain capacity. It was shown through Hose et al.'s model that these structures had adequate transverse confinement and that the strains stayed well below the known strain capacity levels.

Because Mander et al. assumed that the transverse steel is always at a constant yield stress, the actual strength of concrete at the beginning of the stress-strain curve was overestimated as shown in Figure 2-2. With the inclusion of strain hardening, as accounted for in VSAT, the model also underestimates the stress-strain behavior upon reaching the onset of the strain hardening region within the transverse steel.



**Figure 2-2: Comparison of Concrete Model Proposed by Mander et al. and Hose et al.**

Hose et al. (2001) modified the model presented by Mander et al. by replacing the constant transverse reinforcement constant yield stress with a variable one. This, in turn, modifies the confining pressure and the stress for a particular strain as shown in Figure 2-2.

In order to quantify the stress of concrete at a particular strain, the dilation of concrete must be known which also requires the dilation and stress of the transverse reinforcement to be found. Using experimental data, Hose et al. (2001) developed equations based upon an incremental strain process to determine the stress of the transverse reinforcement for a given concrete strain (see Section Figure 4-5). This was combined with the model presented by Mander et al. to make a modified stress-strain concrete model. Through constants  $\eta$  and  $J$ , Hose et al. made this model versatile. The designer can opt to change these values, which alter the concrete and steel performance and thus the stress-strain behavior, if they possess adequate experimental data showing that these new values are reliable.

This model was selected due to its features discussed above that further allow the user to modify the stress-strain behavior of confined concrete. The more sophisticated model requires more data from the user on the stress-strain behavior of the transverse reinforcement, but should provide a more adequate moment-curvature response for the section of interest.

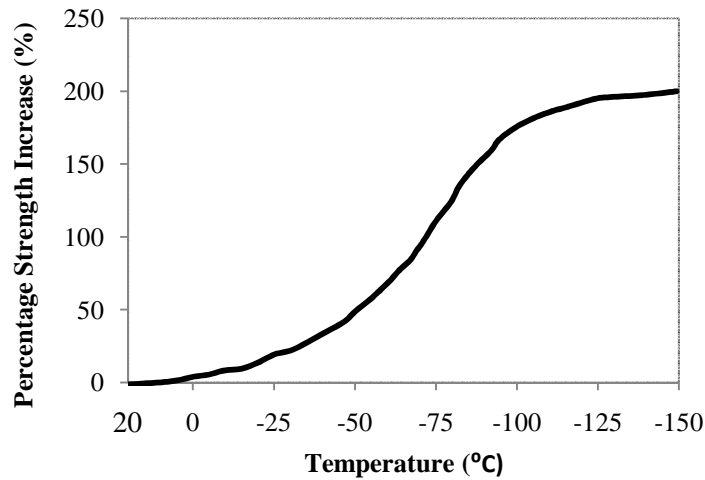
### 2.2.2 Temperature Effects

According to Lee et al. (1988) and Van Der Veen and Reinhardt (1989), the main component attributing to the change in behavior of concrete due to temperature is the presence and percentage of water. This means above  $0^{\circ}\text{C}$ , concrete experiences little or no changes in its behavior because the water has not experienced any significant behavioral changes. After the temperature of concrete drops below  $0^{\circ}\text{C}$ , the water freezes, which alters the Young's Modulus ( $E_c$ ), ultimate tensile strength ( $f_t'$ ), ultimate compressive strength ( $f_c$ ), and Poisson's Ratio ( $\nu$ ) of concrete.

Research conducted by Wiedemann (1982), Sehnal et al. (1983), Lee et al. (1988), and Van Der Veen and Reinhardt (1989) will be examined in this section. These particular projects were selected due to their extent of information but are limited to the range of temperatures relevant to this study ( $20^{\circ}\text{C}$  to  $-40^{\circ}\text{C}$ ). In a parallel study, a series of tests on confined and unconfined concrete is currently under way at Iowa State University. Upon the

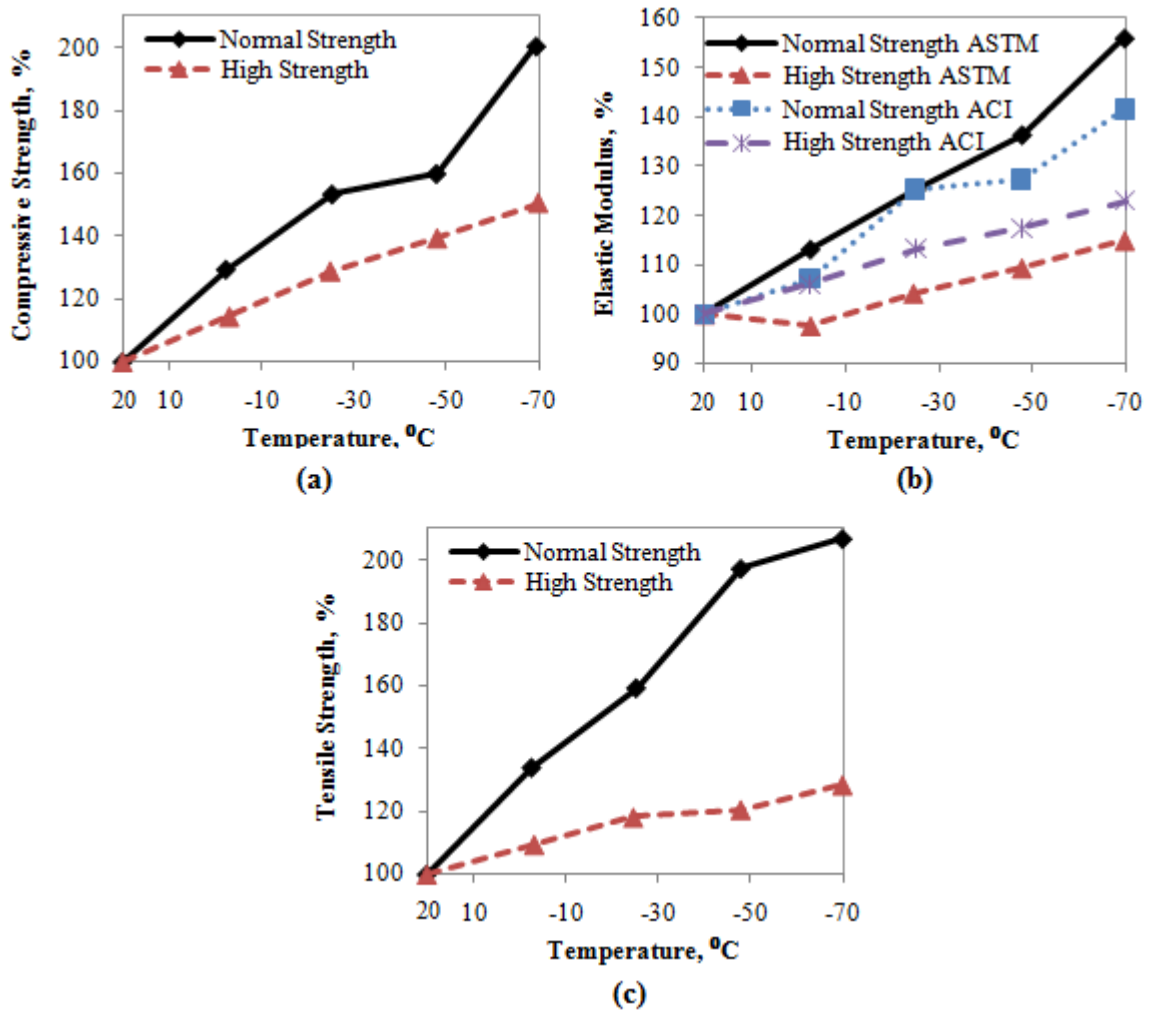
completion of testing, the effects of temperature on the stress-strain behavior of concrete will be modified, as needed, in VSAT. Until then, the following testing results will be used to quantify the effects of temperature on the behavior of concrete.

Sehna et al. (1983) conducted testing on a single mix of 100mm (3.94in) concrete cubes to examine the effects of temperature upon the compressive strength of concrete. As shown in Figure 2-3, the temperature range used for this testing is far larger than that desired for VSAT (20°C to -40°C). This testing, however, does provide guidance and a means to compare what compressive strength increase should be experienced for the temperature range in consideration for the development of the section analysis tool.



**Figure 2-3: Compressive Strength Increases due to Low Temperatures as Digitized from Sehna et al. (1983)**

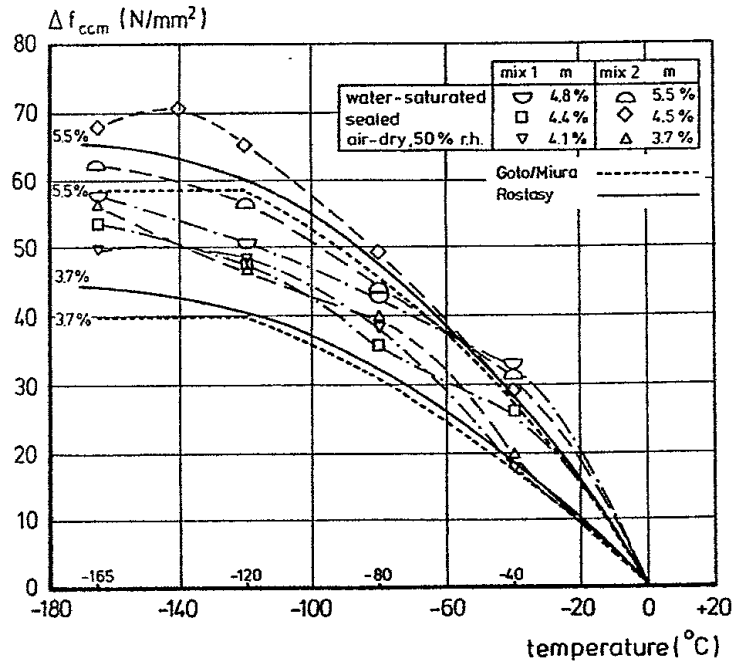
Lee et al. (1988) conducted testing on concrete cylinders to determine the compressive strength, splitting tensile strength, and the modulus of elasticity of high- and low-strength concrete at low temperatures. As shown in Figure 2-4, all three characteristics tend to increase linearly when temperature decreases. At least 21 specimens per temperature were used for compressive strength and Young's modulus to ensure that an accurate average could be taken. This data set, however, only included tests at 20°C, -10°C, -30°C, -50°C, and -70°C making it impossible to define the compressive strength increase and other parameters between 20°C and 0°C and 0°C and -10°C, where the concrete is said to first begin exhibiting behavioral changes.



**Figure 2-4: Increase in (a) Compressive Strength, (b) Elastic Modulus, and (c) Tensile Strength with Decreasing Temperature as Digitized from Lee et al. (1988)**

Finally, Van Der Veen and Reinhardt (1989) conducted testing on concrete cylinders with varying moisture contents of 3.7% to 5.5% (by weight). They confirmed, in general, the conclusions made by Weidemann in 1982 that the compressive strength of concrete increases as temperature decreases and is more affected in samples with higher moisture contents. As shown in Figure 2-5, they also compared their experimental data with equations provided by Rostásy and Goto (1978) and Miura (1984) that were developed to predict the increase in compressive strength as a function of temperature and moisture content. Note, as with the previous testing, the range of interest is a small portion of their experimental curve. They only performed testing at 20°C, -40°C, -80°C, -120°C and -165°C, making it impossible to

accurately capture increases as a function of temperature for the range of interest for this project.



**Figure 2-5: Comparison of Van Der Veen and Reinhardt's (1989) Experimental Data to Equations Presented by Rostásy and Goto and Miura that Define the Increase in Concrete Strength as a Function of Temperature and Moisture Content**

Due to the limitations of the testing by Weidemann (1982), Sehnal et al. (1983), Lee et al. (1988), and Van Der Veen and Reinhardt (1989), all models were compiled into Table 2-1 to determine which would be used to define the effects of temperature on the behavior of concrete until the research at Iowa State University could be completed. The asterisks, “\*”, found on the table indicate which models were used for the determination of Eqs. 4.64 through 4.67 in Chapter 4. As shown, the modulus effects were taken from Lee et al. (1988), and the compressive and tensile strength increases were taken from Van Der Veen and Reinhardt (1989). Sehnal et al.'s graph was not used because water content was deemed important. Weidemann's work was excluded from this table due to the information being not readily available except for the comments cited through Van Der Veen and Reinhardt's work.



**Table 2-1: Advantages and Disadvantages of Concrete Material Models**

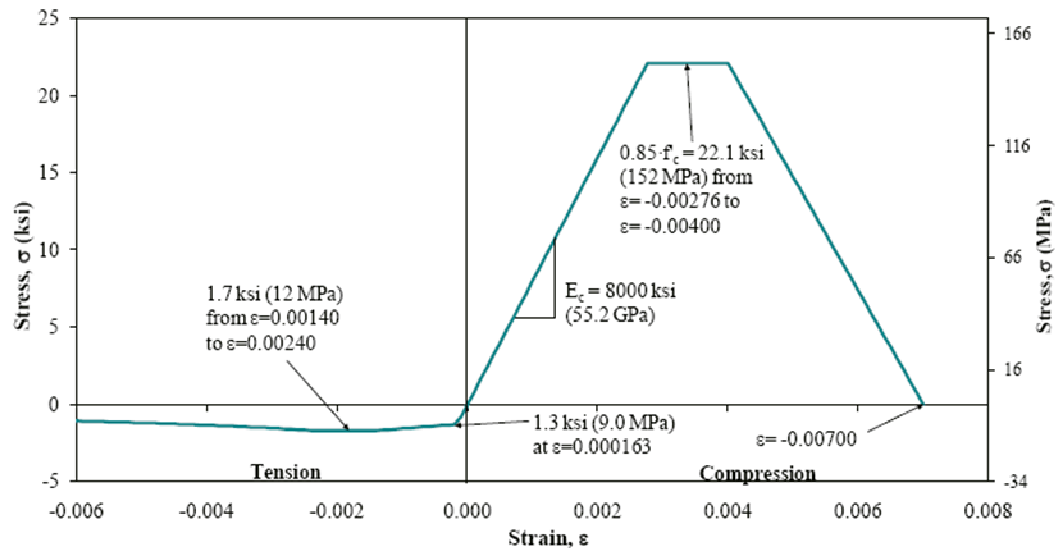
<b>Model</b>	<b>Advantages</b>	<b>Disadvantages</b>
<b>Temperature Effects on Concrete Models</b>		
Lee et al.	Contains Information of Target Temperature Range Compressive Strength, Modulus*, and Tensile Influences Provided	Independent of Water Content No Influence Equations Given
Sehna et al.	Contains Information of Target Temperature Range Compressive Strength Influence Provided	Equation Hard to Establish from Data Given Only Compressive Strength Influences Provided Independent of Water Content
Van Der Veen and Reinhardt	Study Depends on Water Content Confirms Provided Equation by Rostásy Compressive Strength and Tensile Influences Provided*	No Modulus Influence Provided

Note: “\*” indicates which models were used for the creation of the analysis program

### 2.3 Behavior of UHPC

The compression behavior of ultra-high performance concrete (UHPC) is different than that of normal concrete. A tri-linear relationship, which was developed by Gowripalan and Gilbert in 2000 with recommended values by Vande Voort et al. (2008), is used to define the compressive stress-strain behavior as shown by Figure 2-6 (see Section 4.2.3.6). The compressive stress-strain model was based upon actual compression tests conducted by Acker and Behloul in 2004 on UHPC cylinders (Vande Voort et al., 2008).

The tension behavior of UHPC developed by Vande Voort et al. (2008) was based upon tests conducted by Bristow and Sritharan. As shown in Figure 2-6, this portion of the model consists of a linear segment equal to the elastic modulus of the material, a segment with decreased stiffness, and a horizontal straight line, and an exponentially decreasing stiffness. Vande Voort et al. (2008) developed an excel program supplemented by field tests of UHPC H-shaped piles for the determination of their moment-curvature response. The development of the H-shaped section in VSAT followed the work conducted by Vande Voort et al. to ensure that the program was functioning properly for this section type.



**Figure 2-6: UHPC Stress-Strain Behavior as Presented by Vande Voort et al. (2008)**

The combined UHPC model was selected as it was a current project being conducted at Iowa State University at the beginning of the VSAT development and the theoretical response was validated through field tests. It is important to note that this particular model doesn't distinguish between tensile and compressive strains and that the required stresses must be in ksi units. Finally, this material is only applicable to warm temperature conditions as no temperature-variant testing has been completed to date. As such, VSAT will only allow room temperature material properties to be defined.

#### 2.4 Behavior of Mild Steel Reinforcement

The stress-strain behavior of mild steel reinforcement currently used in design practice can be expressed theoretically with three portions: an elastic portion, a yield plateau portion, and a strain hardening portion. Due to the models for mild steel reinforcement being fully described in Chapter 4, only the advantages and disadvantages of each material model will be discussed. Similarly, due to the complementary research conducted to examine the temperature effects on the behavior of mild steel, only the advantages and disadvantages of past models will be examined.

### 2.4.1 Stress-Strain Behavior of Mild Steel

The first mild steel reinforcement model as presented by King et al. (1986) was selected for its simplicity and can be found Section 4.2.4. From this model, one can define an entire stress-strain curve without a complete set of experimental data. It is possible to also exclude, or include, the effects of strain hardening by altering the strain hardening and ultimate strength parameters accordingly.

Due to the required input and the assumptions of the model, the strain hardening region of the curve cannot be altered and may be inadequate for some analyses. This problem, however, cannot be resolved because only two points along the curve are used to define the model: the onset of strain hardening point and the ultimate point. For the purposes of a simplified model to be used in VSAT, the model presented by King et al. is sufficient. An additional model is required to more accurately represent the strain hardening portion of the mild steel reinforcement curve when sufficient data is known.

The second model as presented by Dodd and Restrepo-Posada (1995) was selected for a more sophisticated mild steel reinforcement model and is presented in Section 4.2.4.2. This model has capabilities similar to that of King et al. but requires an additional data point, an arbitrary point along the strain hardening curve. The inclusion of this point allows one to alter the strain hardening region of the curve, by means of a quadratic function, to reflect the actual stress-strain behavior of the material.

Due to the structure of the equations used, one cannot define an elastic, perfectly plastic stress-strain model because the  $p$ -term becomes undefined. This challenge, however, is only easily resolved by hand as one can exclude the equation containing strain hardening effects or Eq. 2.8.

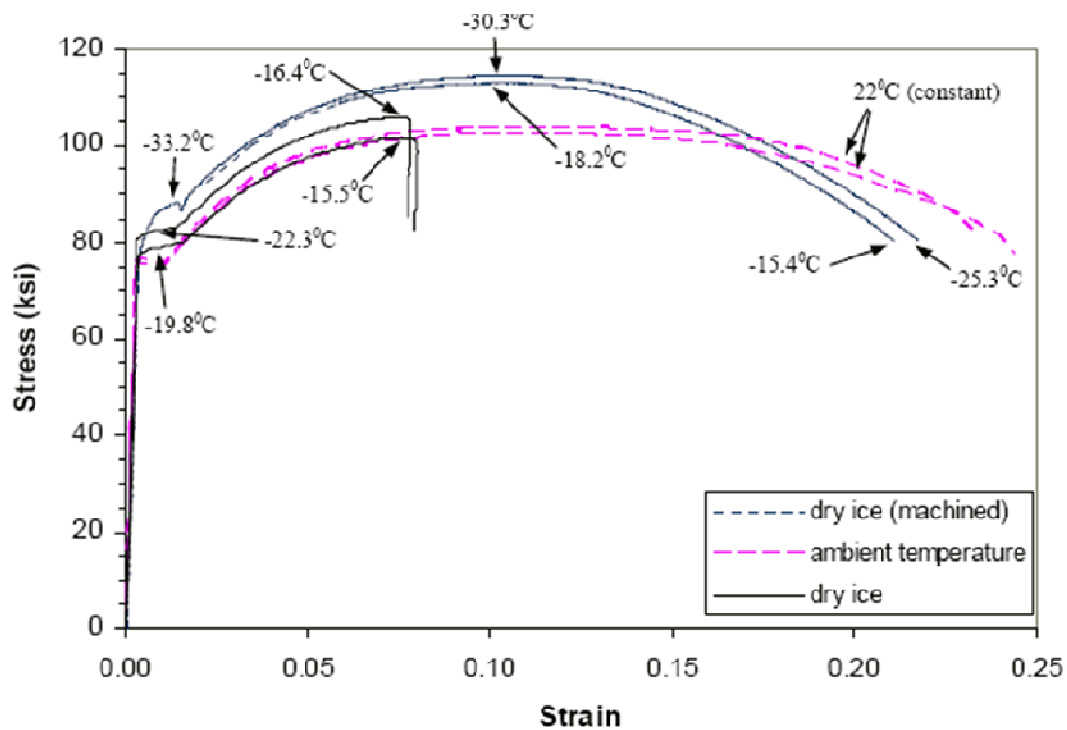
Current analysis tools generally use a simplified steel model where the strain hardening region of the curve cannot be altered. Furthermore, these programs require that the designer use the particular model chosen for that program. The inability to change critical parameters in the stress-strain behavior of mild steel can and will have an impact on the moment-curvature response of the section. Because the moment-curvature approach is used to attain a more accurate moment capacity and to quantify ductility, these features need be alterable.

### 2.4.2 Temperature Effects

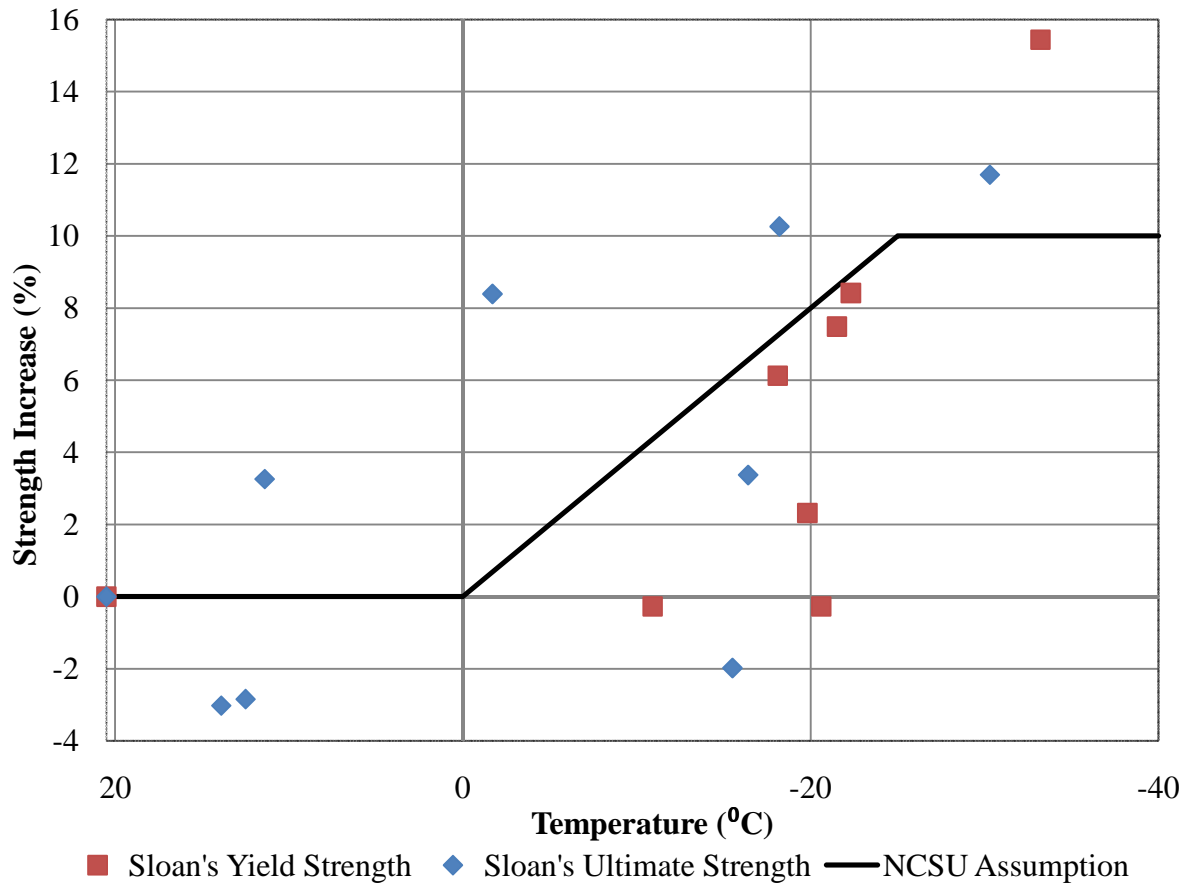
Bruneau et al. (1997) conducted testing on ASTM A572 Grade 50 steel to examine the behavioral changes due to decreased temperatures. Filiatrault and Holleran (2001) conducted similar tests on CSA G30.16 reinforcing steel with a nominal yield strength of 400MPa (58 ksi) and a reference temperature of 20°C. Both sets of data provided a basic understanding of the effects of temperature on the behavior of mild steel reinforcement. Unfortunately, because A706 mild steel was not utilized for the tests, a requirement of reinforcement in seismic regions (ACI, 2008) and no effects on the strain hardening portion of the curve was presented, these models could not be applied for use in VSAT.

Sloan (2005) examined the effects of temperature on A706 mild steel reinforcement. From his data, strength increases of 8% and 12% for yield and ultimate strength, respectively, were found around -22°F (-30°C) that should have been applicable in VSAT. There were, however, challenges that were experienced for his experimentation due to using dry ice to cool the samples rather than an environmental chamber. First, a thermocouple was attached to the exterior of each sample during cooling and the sample was tested upon reaching the desired temperature (Sloan, 2005). It is believed this method may have caused the temperature inside the sample to be different than the reported value. Second, the samples were removed from the dry ice for testing. This same method was considered by Iowa State University by pre-freezing the samples, but within minutes the authors of this thesis found the samples had increased in temperature 10-20°C before testing due to heat transfer. Sloan (2005) stated in his thesis that the warming of the samples made it difficult to correctly quantify the cold temperature stresses during testing; the rate of testing became a factor (see Figure 2-7). Next, failure of specimens were experienced near the grips due to rapid warming, likely due to heat transfer (Sloan, 2005). Milled samples were then used toward the end of testing to resolve this phenomenon. As shown in Figure 2-7, Sloan's milled samples experienced higher stresses than the unmilled samples, it is believed that there is a discrepancy between the ASTM nominal area and the actual area of a deformed reinforcing bar. Finally, the target temperature for Sloan's work was -22°F (-30°C) and contained a high scatter. This target temperature coincided with additional testing he would perform not pertinent to this thesis, but also created a data gap between the temperatures of

68°F (20°C) and -22°F (-30°C). To better understand and illustrate Sloan's findings, Figure 2-8 was established from the experimental data provided in his paper (Sloan, 2005) and an assumption made by the North Carolina State University (NCSU) has been added. This assumption was based upon two different material types, A706 by Sloan and CSA G30.16 by Filiatrault and Holleran (Montejo et al., 2008). As shown, no trend for either the ultimate or yield strength increases as a function of temperature could be established for the temperature range of interest for this thesis. Note that the assumption made from NCSU doesn't seem to be reflective of A706 mild steel reinforcement.



**Figure 2-7: Stress-Strain Behavior of Milled and Unmilled A706 Mild Steel Reinforcement Samples at a Strain Rate of 0.01/s that Experienced Thawing During Testing (Sloan, 2005)**



**Figure 2-8: Yield and Ultimate Strength Increases vs. Temperature of A706 Mild Steel Reinforcement as Reported by Sloan (2005)**

## 2.5 Behavior of Prestressing Steel

The stress-strain behavior of prestressing steel currently used in the field can be expressed theoretically by a bilinear curve with a curved transition. Due to the models for prestressing steel being fully described in Chapter 4, only the advantages and disadvantages of each material model will be discussed.

### 2.5.1 Menegotto and Pinto

The model by Menegotto and Pinto, as presented by Naaman and Harajli (1985) was selected because the entire stress-strain behavior of prestressing steel can be expressed by a single equation which is presented in Eq. 4.48. Three coefficients K, N, and Q make this

model extremely versatile. Changing these coefficients allow the user to modify all portions of the curve including the elastic or first linear portion, the transition portion, and the secondary linear portion. This model was also selected because recommended values were presented with the equation by Naaman and Harajli (1985). The model is capable of defining a curve with a large transitional area and one with a very small transitional area but cannot create a bi-linear curve due to the formulation method of the equations.

### **2.5.2 Devalapura and Tadros**

The model by Devalapura and Tadros (1992), as presented by the PCI Journal, was selected because the entire stress-strain behavior of prestressing steel can also be expressed by a single equation which is presented in Eq. 4.50. This model was selected, in addition to Menegotto and Pinto, to provide an alternative model with a completely different set of recommended values (Devalapura and Tadros, 1992) while maintaining its versatility. Four coefficients A, B, C, and D allow the user to modify all portions of the curve including the elastic or first linear portion, the transition portion, and the secondary linear portion. The model is capable of defining a curve with a large transitional area and one with a very small transitional area but cannot create a bi-linear curve due to the formulation method of the equations.

## **2.6 Analytical Models**

The following section provides the capabilities and inabilities of the following computer section analysis programs: King's Program (King et al., 1986), LPile (Ensoft, Inc., 2005), OpenSees (Mazzoni et al., 2009), and XTRACT (TRC/Imbsen Software Systems, 2009). These are some programs that can currently be used for the development of a moment-curvature. Note that only the features relevant to establishing a moment-curvature response are discussed below and are to the author's best knowledge having reviewed the features of each program.

### 2.6.1 King's Program (King et al., 1986)

King's Program is capable of the following:

- Assist in initial section design
- Analyze sections containing confined concrete, unconfined concrete, and mild steel reinforcement
- Analyze cross sections using the following methods:
  - Uniaxial bending of rectangular sections using the ACI stress block
  - Biaxial bending of rectangular sections using the ACI stress block
  - Circular sections using the ACI stress block
  - Uniaxial bending of rectangular sections using the Mander model
  - Circular sections using the Mander model

King's Program has some deficiencies that would be advantageous in an analytical model. First, the program can only be run in DOS mode. This means that there are no graphics depicting what the program is asking for other than the user manual which, at times, also lacks sufficient information. This is very important in the design, since a misinterpretation can lead to inaccurate results and possibly failure of the structure after being built. Second, the program requires the size and area of rebar be entered by hand. This can become cumbersome and result in an error if one uses an area that is not representative of those used in the field. Third, the parameters used to define the stress-strain behavior of concrete and mild steel are fixed. This creates a problem because the materials used in design have changed since the creation of this program and may still change in the future. Furthermore, this program does not provide the generated stress-strain curves used for the analysis to verify that the materials were correctly defined. Fourth, the ultimate strain capacity of concrete cannot be altered by the user when more accurate data is available. Finally, the program does not account for the presence of temperature or soil and their effects upon the stress-strain behavior of the materials presented above.



### 2.6.2 *LPile (Ensoft, Inc., 2005)*

LPile is capable of the following:

- Analyze sections containing confined concrete, unconfined concrete, mild steel, and prestressing steel
- Provides standard reinforcement sizes and areas
- Analyze several different cross sections such as circular, rectangular and circular containing an exterior steel shell

LPile also is incapable of handling a few features that would be advantageous in an analytical model. First, the program has material models that are fixed or limited. For concrete, the user may only specify a compressive strength,  $f'_c$ , for concrete. The maximum compressive strength is reduced in LPile is then  $0.85*f'_c$  rather than increasing in strength as with confined concrete. This means a simplistic concrete stress-strain profile is used for the entire section regardless if it is confined or unconfined. It also fixes the ultimate strain of concrete to 0.0038 that usually is dependent on the confinement and concrete parameters. For mild steel, only an elastic perfectly plastic material can be used rather than allowing the user to include strain hardening effects. For prestressing steel, only the total force, prestress losses, and two grade types can be defined. Altering the stress-strain behavior is not possible. Second, the material thickness for discretizing the section, which directly affects the accuracy of the output, is set at 0.79in (20mm) and cannot be altered. Third, every value for the section must be inputted into LPile except for mild steel areas and sizes. This becomes cumbersome and requires additional knowledge (e.g. calculating the modulus of elasticity for concrete or the moment of inertia of the section after entering the section geometry) to complete an analysis. Finally, the program does not account for the presence of temperature or soil and their effects upon the stress-strain behavior of the materials presented above.

### 2.6.3 *OpenSees (Mazzoni et al., 2009)*

OpenSees is capable of the following:

- Provides a library of materials that include confined concrete, unconfined concrete, bilinear and non-bilinear prestressing steel, and mild steel
- Provides tensile concrete strength

- Analyze the circular, rectangular, and triangular fiber cross sections

OpenSees also is incapable of handling a few features that would be advantageous in an analytical model. First, the program requires the size and area of rebar be entered by hand. As stated previously, this can be tedious and result in human error. Second, the strain hardening region cannot always be correctly defined because a tangent from the onset of the strain hardening region is used rather than a point along the curve. Finally, the program does not account for the presence of temperature or soil and their effects upon the stress-strain behavior of the materials presented above.

#### **2.6.4 XTRACT (TRC/Imbsen Software Systems, 2009)**

XTRACT is capable of the following:

- Provides a library of materials that include confined concrete, unconfined concrete, bilinear steel with parabolic strain hardening, and prestressing steel
- Create user defined materials
- Provides an interactive template library to define and analyze circular and rectangular cross sections quickly
- Discretize arbitrary cross sections

XTRACT also is incapable of handling a few features that would be advantageous in an analytical model. First, the program requires the size and area of rebar be entered by hand. Again, this can be tedious and result in human error. Second, the material properties provided only give one model type (e.g. Menegotto and Pinto model for defining prestressing), otherwise requiring the user to define their own stress-strain material model. Versatility should be provided to allow for multiple materials to be developed while not requiring full knowledge of a method to define the material's stress-strain behavior. Finally, the program does not account for the presence of temperature or soil and their effects upon the stress-strain behavior of the materials presented above.

## **Chapter 3: BEHAVIOR OF A706 MILD STEEL REINFORCEMENT UNDER COLD TEMPERATURES**

### **3.1 Introduction**

Over 400,000 bridges or 2/3 of all the bridges in the United States experience seasonal freezing as temperatures vary between 68<sup>0</sup>F (20<sup>0</sup>C) and -40<sup>0</sup>F (-40<sup>0</sup>C). In addition, approximately fifty percent of the 66,000 bridges located in active seismic regions also experience seasonal freezing (Sritharan and Shelman, 2008). The effects of cold temperature, though applicable in all structures, become more significant in seismic design where the moment-curvature response and ductility are desired. Unfortunately, our knowledge of these effects is limited and, therefore, is rarely implemented in routine design methods. To improve existing design and more accurately predict bridge performance, the temperature-variant behavior of the utilized materials must be known.

History lacks a systematic study on the behavioral changes that low temperatures have on ASTM A706 Grade 60 reinforcing steel. To fulfill this need while satisfying current code provisions, only this material will be examined. Utilizing quasi-static loading and temperatures varying from 68<sup>0</sup> F (20<sup>0</sup>C) to -40<sup>0</sup> F (-40<sup>0</sup>C), Iowa State University studied the effects of cold temperature on the stress-strain behavior of this material for the Alaska University Transportation Center (AUTC) and the Alaska Department of Transportation and Public Facilities (Alaska DOT & PF).

The following sections examine the effects of temperature on the yield strength and corresponding strain, modulus of elasticity, stress and strain at the onset of strain hardening, and the ultimate strength and corresponding strain of ASTM A706 Grade 60 mild steel reinforcement. Furthermore, two different bar sizes and three different strain rates were used for this study to determine whether bar size or strain rate affects any of the aforementioned properties. A background of A706 mild steel, past studies, a testing plan and matrix, results, comments, and conclusions will be discussed in this chapter.

### 3.2 Background

The first version of ASTM A706 was published by ASTM international in 1974. It was created in response to the engineering requirements for deformed reinforcing bars with a controlled tensile strength for earthquake-resistant structures and for its weldability (Gustafson, 2007). As stated in Note 1 of ASTM A615, “welding of the material in this specification should be approached with caution since no specific provisions have been included to enhance its weldability” (ASTM Standard A615, 2009). In 1990, the Concrete Reinforcing Steel Institute (CRSI) published Report No. 34, "ASTM A706 Reinforcing Bars- Technical Information with Commentary on Usage and Availability" to respond to questions regarding A706 mild steel reinforcement from engineers, architects, and constructors for A706 (Concrete Reinforcing Steel Institute, 1990).

It was the California Department of Transportation (Caltrans) that first required the use of A706 reinforcement in virtually all concrete structures except for minor structures (Gustafson, 2007). From 1995 to the present time, several Departments of Transportation (DOT's) followed in the footsteps of Caltrans. Some of these, which also are leading seismic states of the country, include: the Illinois DOT, Alaska DOT Public Facility, and Washington DOT (Gustafson, 2007). Today, Section 21.1.5.2 of the ACI 318-08 code states that all “Deformed reinforcement resisting earthquake-induced flexural and axial forces...shall comply with ASTM A706” (ACI, 2008).

### 3.3 Past Studies

Previous studies by Bruneau et al. (1997), Filiatrault and Holleran (2001a and 2001b), and Sloan (2005) have been conducted on the effects of low temperature on various steel reinforcement types. Regardless if these test samples were A706 or not, which most aren't, they are mentioned because they offered insight on possible strength increases that could be experienced which was utilized to determine test sample preparation methods for this document. The material properties of ASTM A706 Grade 60 reinforcing steel to be established from the proposed testing will then be compared to this research.

Bruneau's et al. (1997) summarized the results of cold temperature testing on ASTM A572 Grade 50 steel conducted by the Bethlehem Steel Corporation. The Bethlehem Steel

Corporation found the yield and ultimate strengths increased in a quadratic fashion by 9 percent and 5 percent, respectively, when decreasing from 20°C to -40°C. It was also reported that the modulus and ultimate strain were unaffected by the cold. Further information regarding the sample shape, size, testing temperatures and temperature control method was unavailable.

In a report by Filiatrault and Holleran (2001a and 2001b), the authors discuss research conducted on CSA G30.16 reinforcing steel with a nominal yield strength of 58ksi (400MPa) at 68°F (20°C), -4°F (-20°C), and -40°F (-40°C) and different strain rates. The research examined the stress-strain response of milled 0.591in (15mm) deformed bar samples, all from a single bar, under different temperatures and loading rates. A temperature-controlled chamber was installed around the samples to maintain a constant temperature during each test. Upon test completion, the researchers concluded that the Young's modulus and the ultimate tensile strain of CSA G30.16 reinforcing were unaffected by temperature, but the yield and ultimate tensile strengths increased linearly by 20 percent and 10 percent, respectively, when temperatures were decreased from 20°C to -40°C (Filiatrault and Holleran, 2001a and 2001b). Their data suggests that the yield and ultimate strength changes associated with altering the strain rate may also be dependent upon the temperature of the specimen. This is justified by the strength vs. strain rate graphs, where increasing the strain rate at each temperature causes a higher increase in strength for cold specimens than warm specimens.

Sloan (2005) conducted testing on A706 mild steel reinforcement at 71.6°F (22°C) and the temperature of dry ice as a part of his research to examine the effects of low temperatures on the performance of reinforced concrete members. Upon examining his data, an estimated increase of 8% in yield strength and 12% in ultimate strength was found by the authors of this paper around -22°F (-30°C) but no trend could be established. Unfortunately, some challenges arose due to using dry ice to cool the test samples rather than an environmental chamber. First, a thermocouple was attached to the exterior of each sample during cooling and the sample was tested upon reaching the desired temperature (Sloan, 2005). It is believed this method may have caused the temperature inside the sample to be different than the reported value. Second, the samples were removed from the dry ice for testing. This

same method was considered by Iowa State University by pre-freezing the samples, but within minutes the authors of this thesis found the samples had increased in temperature 10-20°C before testing due to heat transfer. Sloan (2005) stated that the warming of the samples made it difficult to correctly quantify the cold temperature stresses during testing; the rate of testing was a factor. Finally, failure of specimens was experienced near the grips due to rapid warming, likely due to heat transfer (Sloan, 2005). Milled samples were then used toward the end of testing to resolve this phenomenon. Upon observing that Sloan's milled samples experienced higher stresses than the unmilled samples, it is believed that there is a discrepancy between the ASTM nominal area and the actual area of a reinforcing bar.

In all cases, regardless of material type, the effects of temperature on strain hardening were not provided and temperature increments for the given range were large. Additional testing with a reliable cooling method is required to determine which data set, if any, is applicable to the ASTM A706 Grade 60 reinforcing steel used in the U.S. today.

### **3.4 Experimental Study**

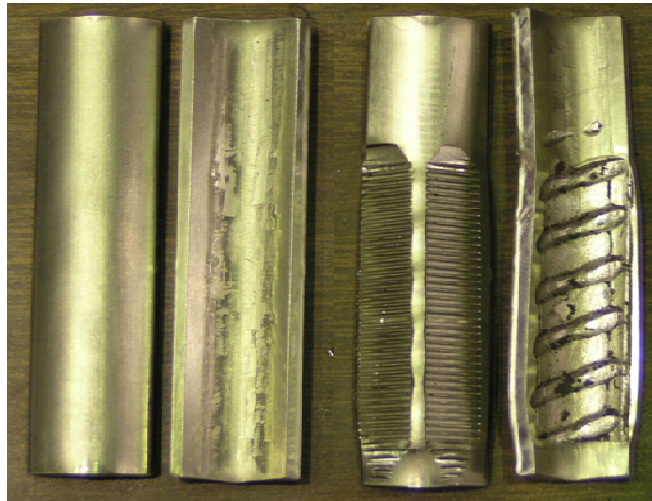
Presented in this section are details of the experimental study undertaken to quantify the stress-strain response of A706 reinforcing steel at low temperatures and a summary of those results. The testing performed followed the guidelines presented by ASTM E8 as testing conditions permitted (ASTM Standard E8, 2004 (2006)). The subsequent sections will discuss the test preparation, setup, and types of tests performed along with some challenges that arose, or were experienced, during this study.

#### **3.4.1 Sample Preparation**

#6 and #8 deformed bars ordered from a steel manufacturing company were used instead of a test coupon to ensure that the material composition and performance be the reflective of that used in the field. From these bars, specimens were cut into approximately 3 foot lengths. These lengths were required for the environmental chamber to fit in the MTS machine during testing. Each bar segment was separated, marked, and tested at each predetermined temperature to avoid introducing other variables into the test data. Each segment, as shown in Figure 3-2, was then milled at its center to a cylindrical cross-section for a specified gauge

length. This was done for three reasons. First, this enabled the exact cross-sectional area of the specimen, utilized in calculating stress, to be determined. Second, the reduced area forced the failure to occur within the milled region. Finally, during initial sample testing, the authors of this document found a discrepancy between the ASTM nominal area and the actual bar provided by steel manufacturers, the actual bar area was smaller than that reported by ASTM. This discrepancy was compensated by a higher strength in steel resulting in the same force-strain curve as a bar with an ASTM nominal area. As only the milled stress-strain data and stress-dependent parameters (i.e. elastic modulus) are presented in this document, the area discrepancy must be measured.

Deformed reinforcing bars cannot be gripped directly for testing. The ribs located on the bar, normally used to enhance the transfer of forces in the field, cause stress concentrations in the grips if gripped directly. This increase in stress can lead to the failure of the testing apparatus and occurred during the initial stages of testing on A706. This problem can be resolved by two methods that were used for this study. First, four aluminum half-pipe sleeves, as shown in Figure 3-1, can be placed on the ends of each bar at the point of gripping. Upon gripping, these sleeves form to the bar, allowing for a constant transverse stress to be attained during each test. Second, the ends of each bar can be milled to a cylindrical cross-section to avoid the stress concentration from forming. The first of these methods were used on the #6 bars and the latter on #8 bars. This was necessary due to size constraints of the testing apparatus.



**Figure 3-1: Outer and Inner Surfaces of Aluminum Sleeves Before and After Testing**

### 3.4.2 Test Setup

All specimens were tested in an environmental chamber that was designed to fit a 110 kip capacity uniaxial Materials Testing Systems (MTS) fatigue machine as shown in Figure 3-2. The environmental chamber ensured that the specimens would be subjected to the chosen representative temperatures. A “dummy” bar with a hole drilled at its centerline housed a thermocouple and was inserted into the chamber for the side as shown in Figure 3-2. Another thermocouple was placed in the chamber to verify that the environmental temperature readout was accurate during testing. Upon reaching the desired stable temperature, the testing of each specimen was initiated. During each test the temperature was monitored to ensure no significant change in temperature occurred that would render the test useless.

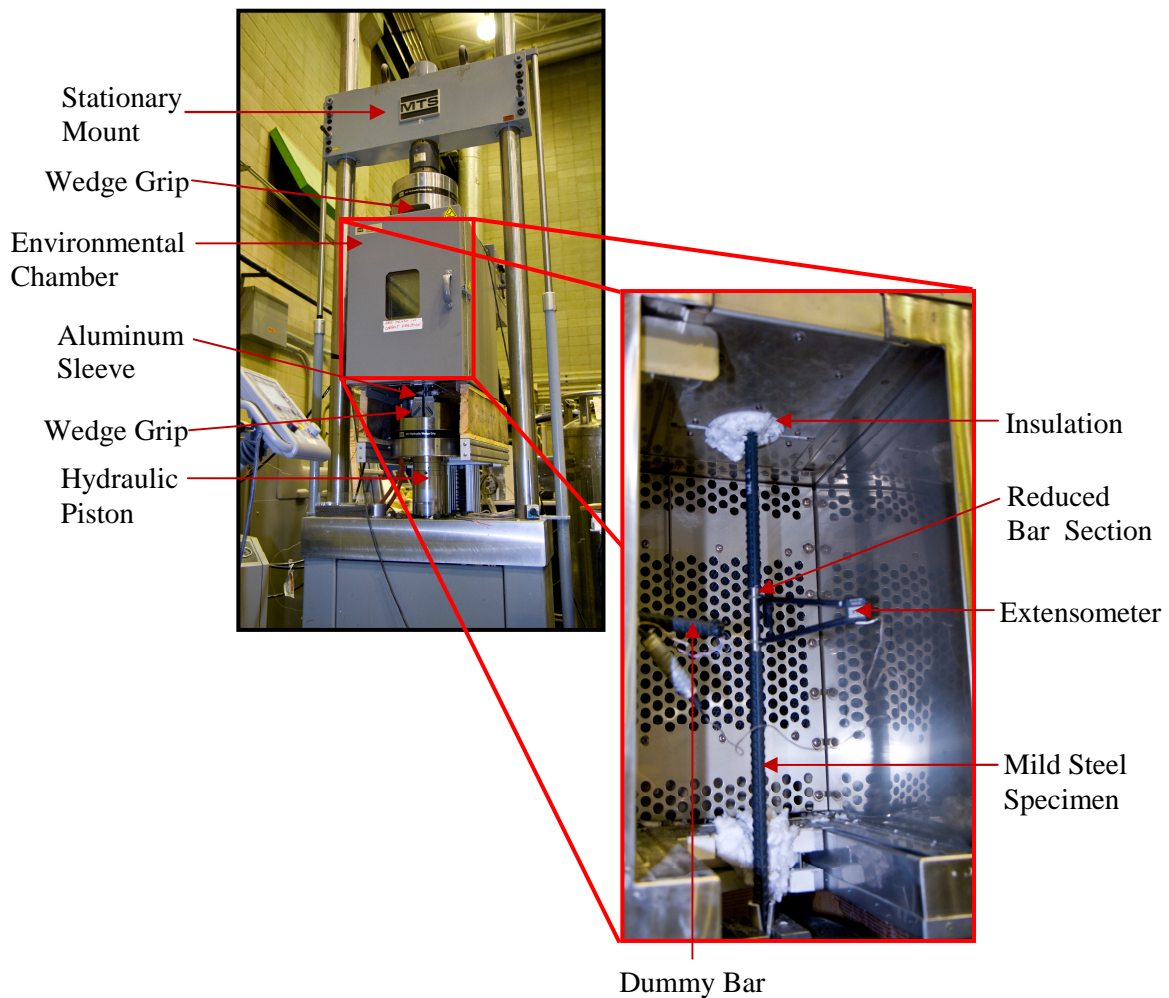
The main gauge used for monitoring strains was an extensometer that was rated to function at the required temperatures. It was placed on the milled section of the specimen by direct contact to capture the strains for the exact milled area instead of the nominal area reported by ASTM (See Figure 3-2). The tensile stresses induced on the specimen were determined by a load cell that measured the applied axial load during testing. These values were then divided by the reduced cross sectional area of the specimen. Data recorded from each test was used to develop a stress-strain curve as a function of temperature to be used in the moment-curvature analysis of columns and foundation shafts.

Cooling of the steel samples in the environmental chamber proposed a problem. When conducting a trial test to determine how long the sample would take to cool, it was found that if the temperature in the chamber was set to the desired testing temperature it could take an excess of 2-3 hours before the sample was ready for testing. To lessen this time burden, the chamber was set at a temperature 10-15°C colder than desired at the beginning of each test. This reduced the time necessary for a sample to reach the desired temperature to about 30 minutes. Upon reaching the desired temperature in the specimen, the temperature discrepancy was lowered until the desired testing temperature in both the sample and the chamber coincided.



### 3.4.3 Monotonic Testing

The monotonic testing, with the setup shown in Figure 3-2, utilized two different, yet constant, strain rates per test. Both strain rates corresponded to the middle rate as specified by ASTM E8. The first strain rate, 0.001896 inch per inch per minute (in./in./min.), was used to determine the yield strength of the sample up to a strain of 0.01. This strain corresponded to the onset of the strain hardening region of the stress-strain curve. Upon reaching 1% strain, a faster rate, 0.275 in./in./min., was used until the test was over at 18% strain. This second strain rate was applied until 18% strain was reached and aided in the determination of the ultimate strength of the specimen. Additional testing was conducted at constant strain rates of 0.003, 0.03, and 0.3 in./in./min. throughout the entire test to determine if strain rate affects the materials stress-strain behavior.



**Figure 3-2: Test Setup**

### 3.5 Test Matrix

All testing was performed on ASTM A706 Grade 60 deformed steel reinforcement. A summary of the study is presented in Table 3-1 and Table 3-2. As seen in Table 3-1, the first portion of the study utilized two different bar sizes that were subjected to monotonic testing, a #8 bar and a #6 bar, and were tested at five temperatures: 68°F (20°C), 41°F (5°C), 30.2°F (-1°C), -4°F (-20°C), and -40°F (-40°C). These bar sizes were chosen as they are commonly used in design and are capable of being tested in the provided MTS Machine. Larger specimens would require a higher load capacity machine. Eight tests, with three samples per test (28 samples), were used to determine the behavioral changes of the material under low temperatures and the effects of section size. As depicted in Table 3-2, the second portion of the study consisted of testing #8 bars, tested at 30.2°F (-1°C) and -4°F (-20°C), that were used to examine the effects of strain rate on the stress-strain behavior of the material. Six tests, with a minimum of two samples per test (6 samples), were used.

**Table 3-1: Monotonic Test Matrix for the Effects of Temperature and Section Size on A706 Mild Steel**

Number of Tests (Samples)	Temperature	Bar Size	Loading Rate(s)	Purpose
1 (3 Samples)	-40°C	#8	0.001896/0.2750	Determine the Effects of Temperature
1 (3 Samples)	-20°C	#8	0.001896/0.2750	
1 (3 Samples)	-1°C	#8	0.001896/0.2750	
1 (3 Samples)	5°C	#8	0.001896/0.2750	
1 (3 Samples)	20°C	#8	0.001896/0.2750	
1 (3 Samples)	-40°C	#6	0.001896/0.2750	Determine the Effects of Temperature and Section Size
1 (3 Samples)	-20°C	#6	0.001896/0.2750	
1 (3 Samples)	-1°C	#6	0.001896/0.2750	
1 (3 Samples)	5°C	#6	0.001896/0.2750	
1 (3 Samples)	20°C	#6	0.001896/0.2750	

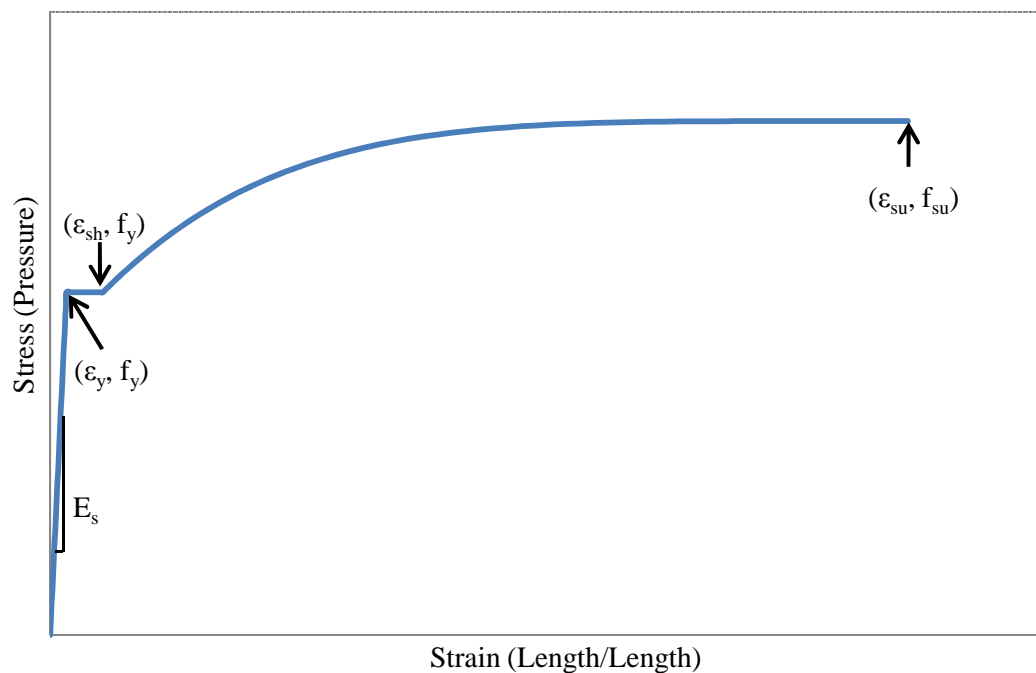
**Table 3-2: Monotonic Test Matrix for the Effects of Strain Rate on A706 Mild Steel**

Number of Tests (Samples)	Temperature	Bar Size	Loading Rate(s)	Purpose
1 (2 Samples)	-20°C	#8	0.003	Determine the Effects of Strain Rate
1 (2 Samples)	-1°C	#8	0.003	
1 (2 Samples)	-20°C	#8	0.03	Determine the Effects of Strain Rate
1 (2 Samples)	-1°C	#8	0.03	
1 (2 Samples)	-20°C	#8	0.3	Determine the Effects of Strain Rate
1 (2 Samples)	-1°C	#8	0.3	

### 3.6 Test Results and Discussion

This section is devoted to the experimental results that were attained during the aforementioned test matrix along with a discussion of these results. A summary of the effects of temperature on the modulus of elasticity,  $E_s$ ; yield strength and strain,  $f_y$  and  $\epsilon_y$ ; onset of the strain hardening,  $\epsilon_{sh}$ ; and ultimate strength and strain,  $f_{su}$  and  $\epsilon_{su}$ , of A706 mild steel will be discussed followed by the effects of strain rate and bar size. A graphical idealization of the stress-strain behavior of mild steel reinforcement with these key points has been provided in Figure 3-3. Note that the behavioral changes mentioned below are present even before the specimen temperature has reached 0°C.

All reported information in this section is based upon the milled cross-sectional area. To make proper adjustments to stress-dependent values, such as the elastic modulus and the stress-strain relationship, it was found that the unmilled area of the experimental rebar was 4.279% smaller than the ASTM area for the #8 rebar and 2.299% smaller for the #6 rebar. Note that this does not affect the strength increases reported as they are based upon percent increase and not stress increase.



**Figure 3-3: Idealized Mild Steel Reinforcement Stress-Strain Curve**

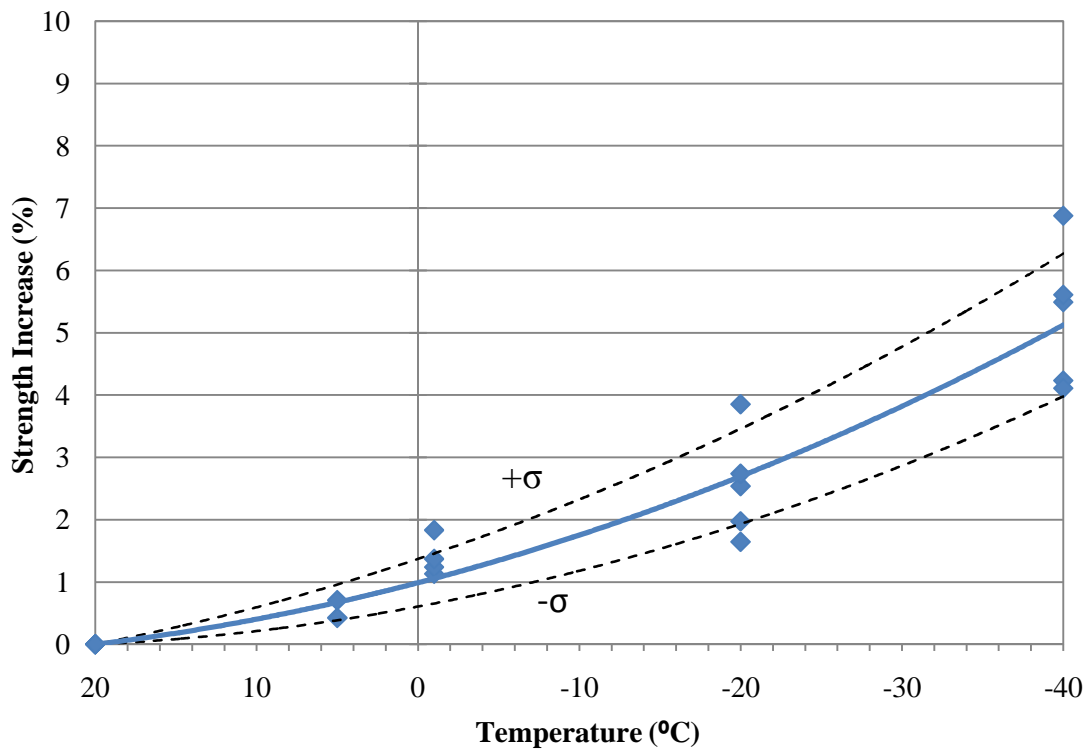
### 3.6.1 Effects of Temperature

The modulus of elasticity,  $E_s$ , was found using the best fit slope between zero stress and the yield stress. From the testing performed, it was found that varying the temperature caused no significant change in the modulus. This coincides with the conclusions of the past studies mentioned in this document. A graphical representation of this data may be found in Appendix A.

The yield strength,  $f_y$ , was attained by applying a best fit horizontal line to the yield plateau within the stress-strain curve of the material. Specimens experienced a 5.1 percent increase in yield strength as the temperature decreased from 68°F (20°C) to -40°F (-40°C). The data varies in a quadratic fashion, as depicted in Figure 3-4, best described by the equation below that corresponds to the best fit trendline of the data set. A standard deviation equation,  $\pm\sigma$ , has been provided for those who wish to examine the ramifications of using the minimum or maximum yield strength increases rather than the best fit for the effects temperature.

- % Increase =  $0.0009(T)^2 - 0.0674(T) + 0.9880$  with T in °C
- $\pm \sigma = \pm (0.0191(T) - 0.3820)$

The data variation is similar in contour to A572 reported by Bruneau et al. but conflicts with the linear variation of CSA G30.16 suggested by Filiatrault and Holleran. In addition, the magnitude to which the yield strength of A706 is affected by all temperatures examined is less than that observed for these two materials. Lastly, the yield strength increase experienced at -22°F (-30°C), or about 3%, is considerably less than that reported by Sloan but the scatter of the data collected is considerably less than that found in his research. Note that the assumption made by NCSU based on Sloan's and Filiatrault and Holleran's work is not reflected in this study and an increase in the yield strength is apparent even before reaching 32°F (0°C).



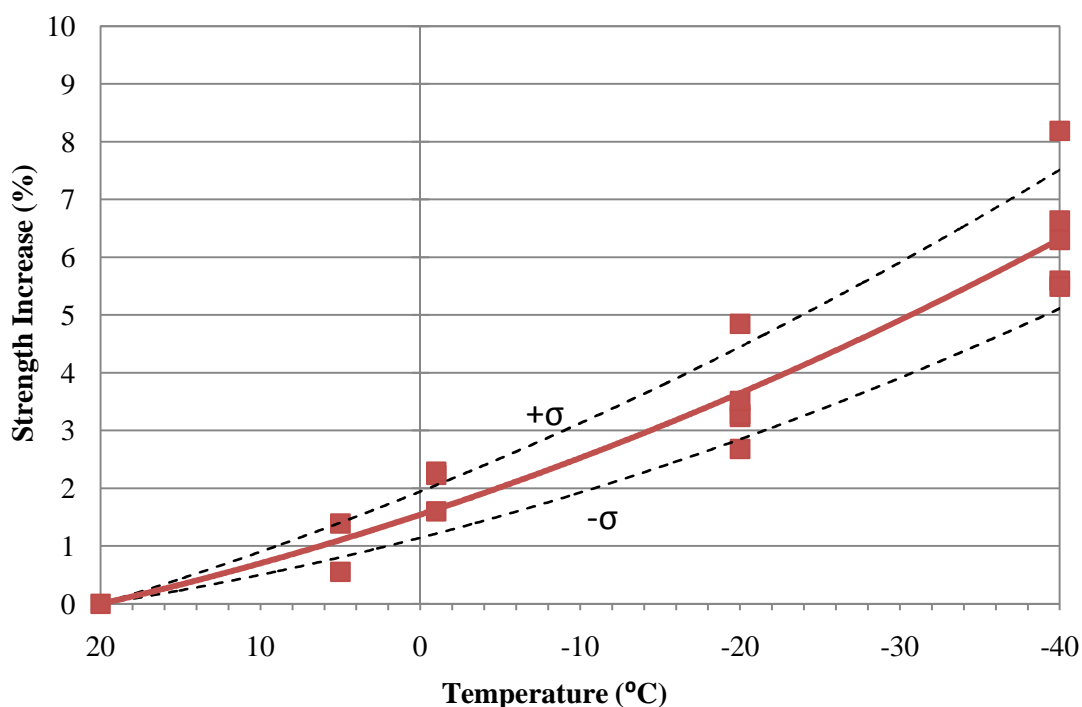
**Figure 3-4: Effects of Cold Temperature on the Yield Strength of A706 Mild Steel Reinforcement Established from Monotonic Testing**

The yield strain,  $\varepsilon_y$ , was calculated by dividing the yield strength by the modulus for each specimen (i.e.,  $\varepsilon_y = f_y / E$ ) and the strain hardening strain,  $\varepsilon_{sh}$ , was defined as the strain at which the specimen begins to steadily increase in strength after yielding (see Figure 3-3). The yield plateau length can then be defined as the difference between the strain hardening strain and the calculated yield strain (i.e.,  $\varepsilon_{sh} - \varepsilon_y$ ). No considerable change occurred in this parameter as the temperature decreased. See Appendix A for the graphical representation of yield plateau length vs. temperature data.

The ultimate strength,  $f_{su}$ , was defined as the maximum stress occurring during each test. The strain corresponding to this stress is then defined as the ultimate strain,  $\varepsilon_{su}$  (see Figure 3-3). Specimens experienced a 6.3 percent increase in ultimate strength as the temperature decreased from 68°F (20°C) to -40°F (-40°C). The data varies in a quadratic fashion, as depicted in Figure 3-5, best described by the equation below that corresponds to the best fit trendline of the data set. Similar to the yield strength increase equation, a standard deviation equation,  $\pm\sigma$ , has been provided for those who wish to examine the ramifications of using the minimum or maximum ultimate strength increases rather than the best fit for the effects temperature.

- % Increase =  $0.0007(T)^2 - 0.0912(T) + 1.5440$  with T in °C
- $\pm\sigma = \pm(0.0200(T) - 0.4000)$

The data variation is similar in contour to A572 reported by Bruneau et al. but conflicts with the linear variation of CSA G30.16 suggested by Filiatrault and Holleran. In addition, the magnitude to which the ultimate strength of A706 is affected by all temperatures examined is less than that observed for CSA G30.16, but more than that observed for A572. Lastly, the ultimate strength increase experienced at -22°F (-30°C), or about 5%, is considerably less than that reported by Sloan but, similar to the yield strength, the scatter of data collected is considerably less than that found in his research. Note that the assumption made by NCSU based on Sloan's and Filiatrault and Holleran's work is not reflected in this study and an increase in the ultimate strength is apparent even before reaching 32°F (0°C).

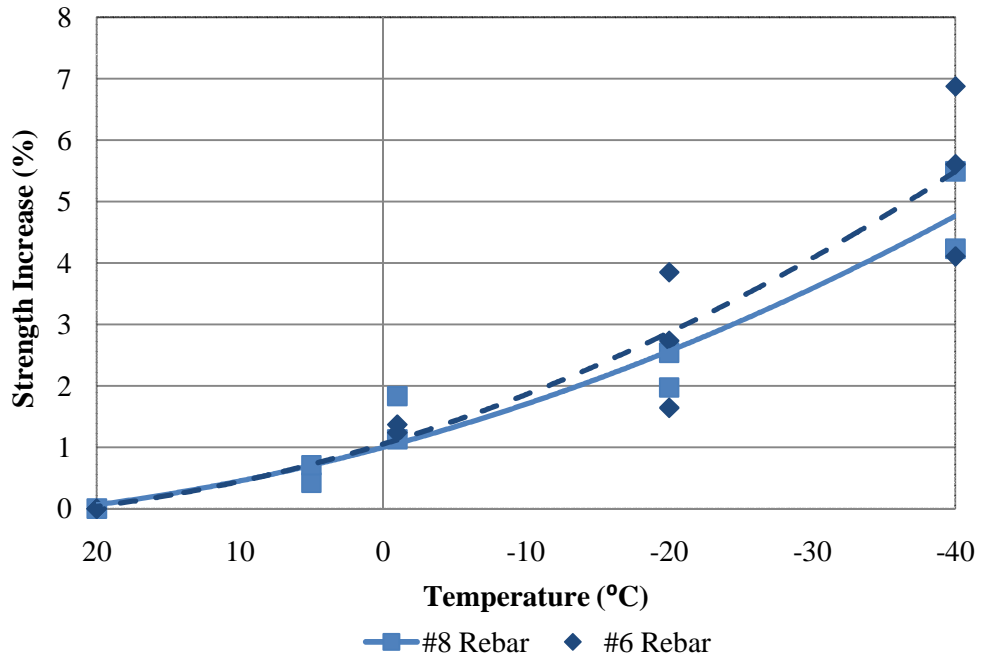


**Figure 3-5: Effects of Cold Temperature on the Ultimate Strength of A706 Mild Steel Reinforcement Established from Monotonic Testing**

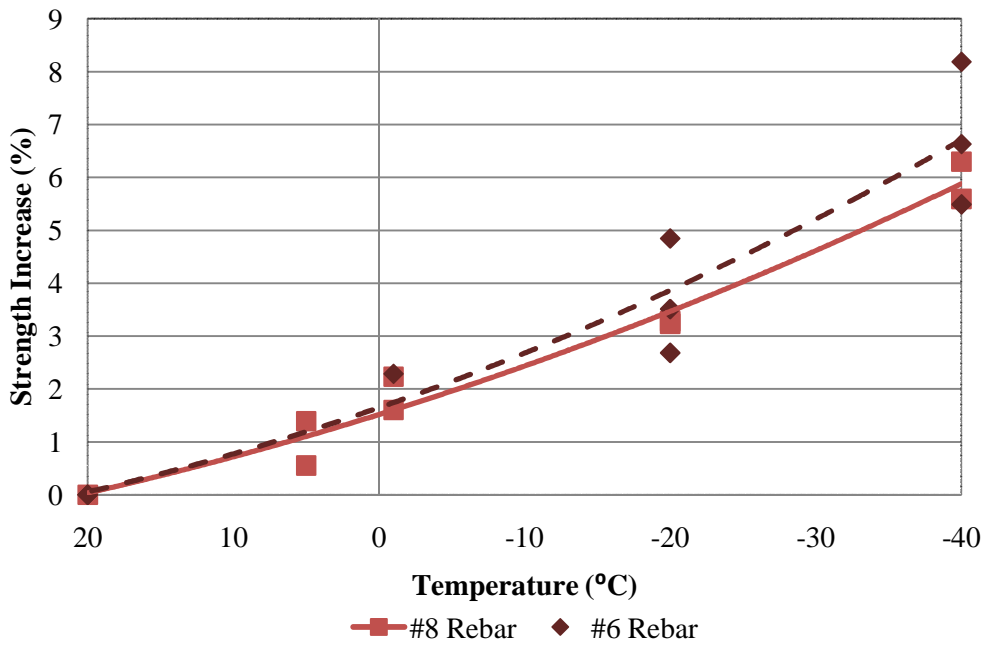
The ultimate strain,  $\epsilon_{su}$ , was defined as the strain corresponding to the maximum stress attained in each (see Figure 3-3). For all temperatures, the scatter of the data revealed no considerable change to the ultimate strain as the temperature decreased with an average value of 0.1158 in./in. The constant ultimate strain observation is consistent with those reported by the previous studies mentioned in this chapter. A graphical representation of this data can be found in Appendix A.

### 3.6.2 Effects of Bar Size

The increases in yield and ultimate strength presented in the previous section ignore the effects of bar size by combining the #6 and #8 milled bars data. The test matrix included both of these bar sizes to look at the effects upon the previously mentioned parameters of interest. As depicted in Figure 3-6 and Figure 3-7, both the yield and ultimate strength seem to be a function of bar size but there is insufficient data to fully support this observation. For this reason, the information presented in Section 3.6.1 includes both bar sizes.



**Figure 3-6: Comparison between Yield Strength Increases of #6 and #8 A706 Mild Steel Reinforcing Bars Subjected to Monotonic Loading and Low Temperatures**



**Figure 3-7: Comparison between Ultimate Strength Increases of #6 and #8 A706 Mild Steel Reinforcing Bars Subjected to Monotonic Loading and Low Temperatures**



### 3.6.3 Effects of Strain Rate

From the testing performed, it was observed that varying the strain rate from 0.003 to 0.3 in./in./min. caused no significant change in the modulus. This is apparent in the graphical representation of data as presented in Appendix A, where the scatter contains a nearly horizontal linear line for a best fit trendline.

As depicted in Figure 3-8, increasing the strain rate from 0.003 to 0.3 in./in./min. caused an increase of around 2 ksi (3%) in the yield strength of the milled #8 rebar specimens. The scatter to this data set was minimal for each of the two temperatures, 30.2°F (-1°C) and -4°F (-20°C), and the best fit trendlines corresponding to the yield strength increase of this data set were logarithmic functions, which are provided in the figure. The magnitudes of the strength increases seem to be dependent on temperature which is shown by an increased slope of the best fit lines when comparing the two temperatures. This is consistent with the findings of Filiatrault and Holleran. Because samples were tested at only two temperatures, further testing would be required to quantify this observation.

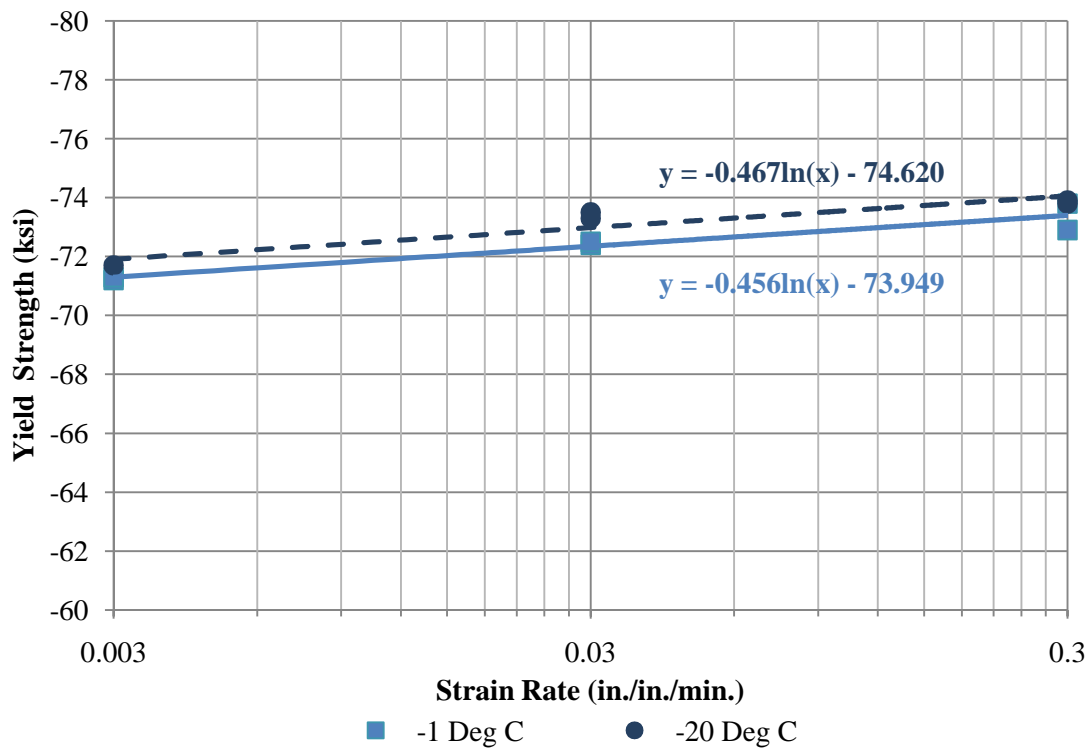
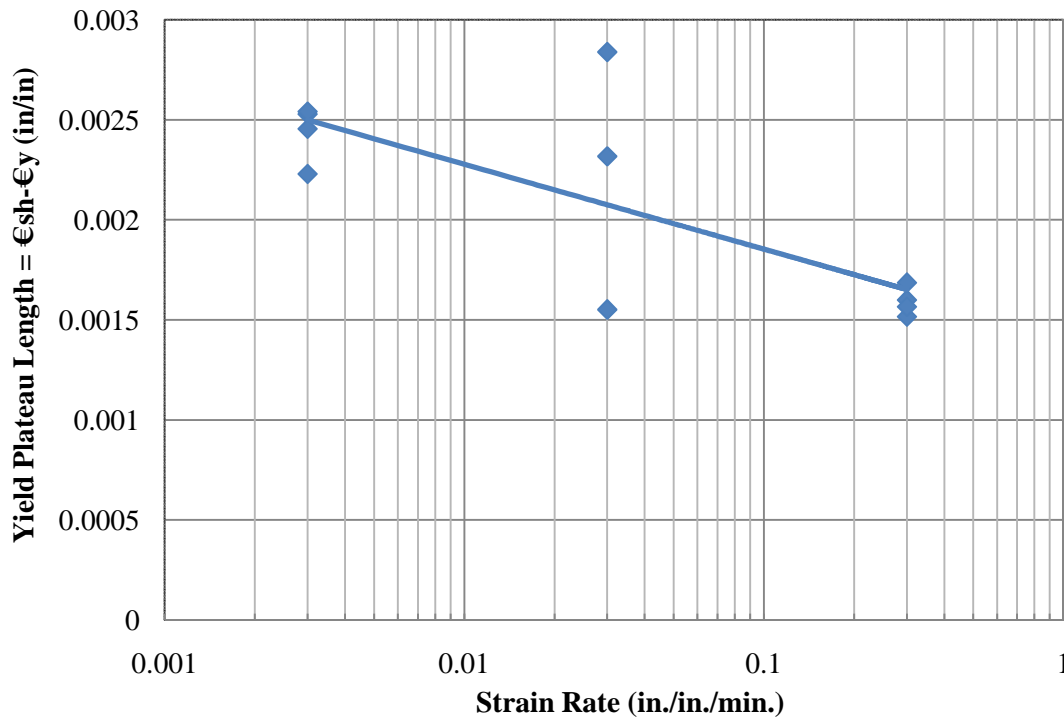
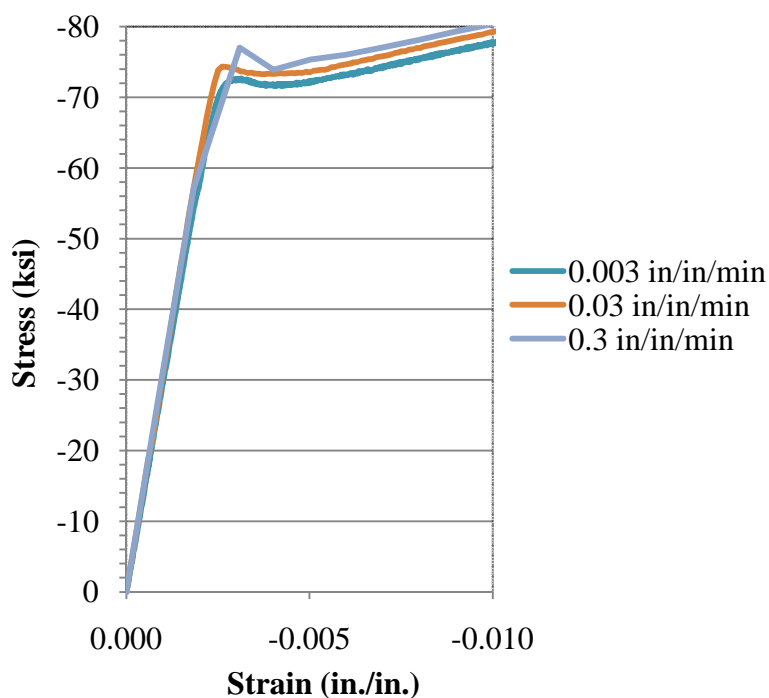


Figure 3-8: Effects of Strain Rate on the Yield Strength of A706 Mild Steel at Cold Temperatures

The effects of strain rate upon the yield plateau length were examined collectively and are expressed in Figure 3-9. Under the strain rate and temperature conditions mentioned previously, the yield plateau length dissipated an average 0.0084 in./in. (34.7%) as the strain rate was increased from 0.003 to 0.3 in./in./min. (see Figure 3-9). The scatter for this portion of the study was heightened because of this dissipation. At the highest strain rate of 0.3 in./in./min., it was necessary to define  $\epsilon_{sh}$  as the minimum stress after the elastic portion of the curve was stabled because yield plateau length had completely dissipated. A graphical representation of this effect is illustrated in Figure 3-10 for clarification where a best fit logarithmic trendline has been added.

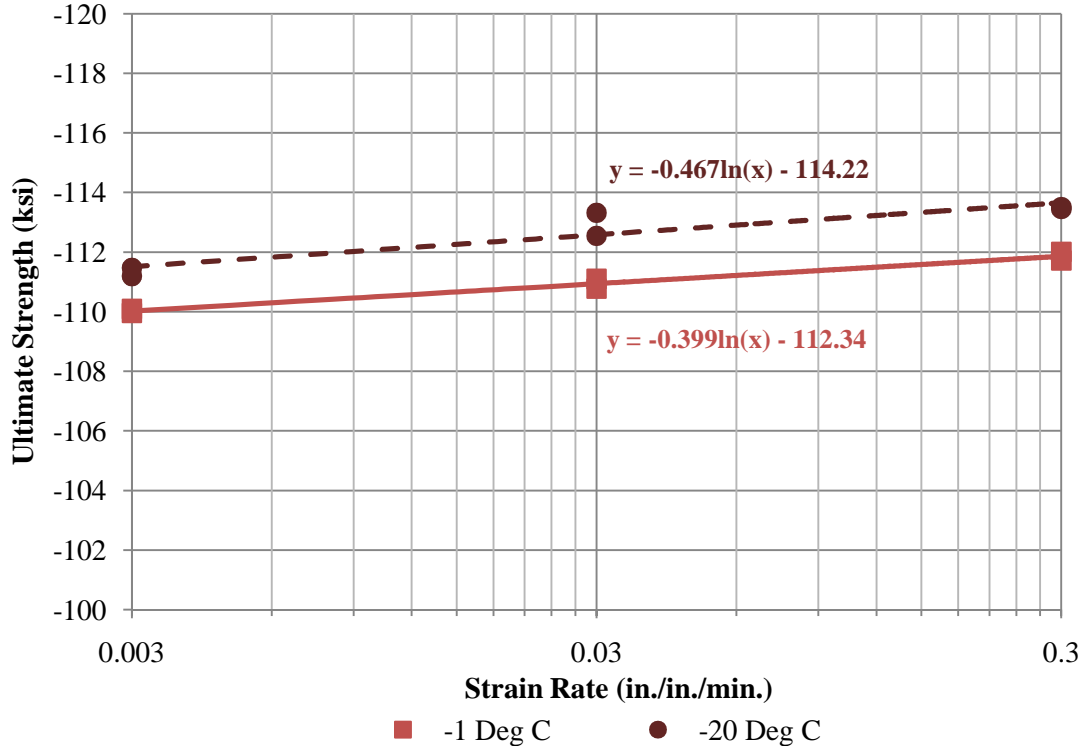


**Figure 3-9: Effects of Strain Rate on the Yield Plateau Length of A706 Mild Steel at Cold Temperatures**



**Figure 3-10: Dissipation of Yield Plateau Length Due to Strain Rate of a Milled #8 A706 Mild Steel Bar at -4°F (-20°C)**

As depicted in Figure 3-11, increasing the strain rate from 0.003 to 0.3 in./in./min. caused an increase of around 2 ksi (1.67%) in the yield strength of the milled #8 rebar specimens. The scatter to this data set was minimal for each of the two temperatures, 30.2°F (-1°C) and -4°F (-20°C), and the best fit trendlines corresponding to the ultimate strength increase of this data set were logarithmic functions, which are provided in the figure. The magnitudes of the strength increases, similar to the yield strength, seem to be dependent on temperature which is shown by an increased slope of the best fit lines when comparing the two temperatures. Again, this is consistent with the findings of Filiatrault and Holleran and because samples were tested at only two temperatures, further testing would be required to quantify this observation.



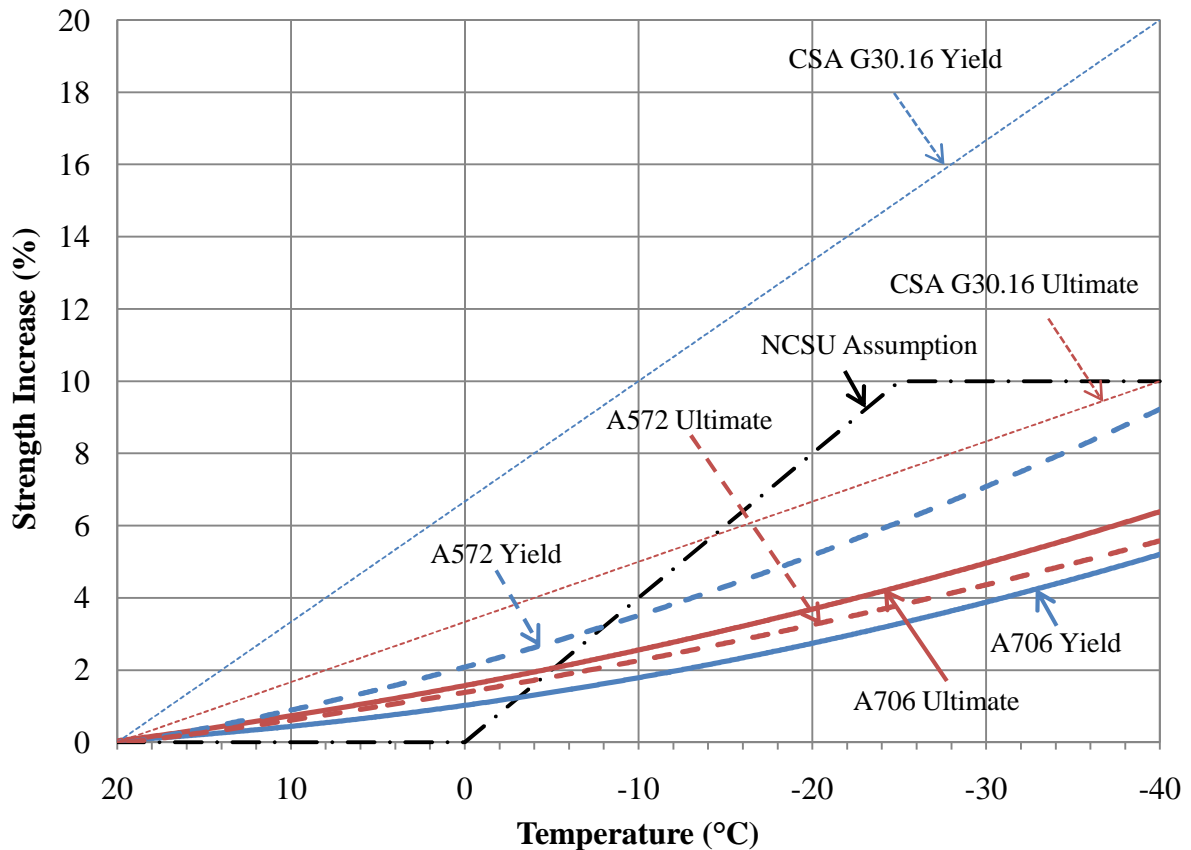
**Figure 3-11: Effects of Strain Rate on the Ultimate Strength of A706 Mild Steel at Cold Temperatures**

Similar to the elastic modulus, it was observed that that varying the strain rate caused no significant change in the ultimate strain rate. This is apparent in the graphical representation of data as presented in Appendix A, where the scatter contains a nearly horizontal linear line for a best fit trendline.

#### 3.6.4 Summary of Previous Research Comparison

Figure 3-13 illustrates an accumulation of the experimental increases of A706 mild steel reinforcement and the previous research mentioned in this report excluding work done by Sloan as no trend could be established from his data. As stated previously, the variation in both the yield strength and ultimate strength of A706 mild steel vary quadratically which is dissimilar to the information presented by Filiatrault and Holleran (Filiatrault and Holleran, 2001a and 2001b). The magnitudes of temperature increases are generally lower than previous research with the impact on ultimate strength greater than yield strength, opposite to the trends reported in previous research. Note that the impact of temperature on A706 for

this report is considerably lower than the average 8% for yield and 12% for ultimate from Sloan's research and the divergence from the NSCU assumption. As Figure 3-13 illustrates, the material behavior of A706 mild steel reinforcement is different than those materials previously studied.



**Figure 3-13: Comparison of A706 Temperature Effects to A572, CSA G30.16, and the NCSU Assumption**

### 3.7 Modeling

In order to completely model the stress-strain curve of A706 accurately, an additional arbitrary point along the strain hardening curve,  $(f_x, \epsilon_x)$ , is needed. A strain of 0.03 in./in. was examined for this study. From the stress-strain parameters discussed above, an estimation of the increase in strength for 0.03 in./in. strain was made from the already defined yield and ultimate strength increases. Using the mild steel material model presented by Dodd and Restrepo-Posada (1995) that defines the elastic, perfectly plastic, and strain

hardening behavior of the stress-strain curve similar to Figure 3-3, the following equation was established:

- $\% \text{ Increase}_{0.03 \text{ in/in}} = (\% \text{ Increase}_{\text{yield}} + \% \text{ Increase}_{\text{ult}}) / 3$  with T in °C

This equation reflects the best fit of other possible linear combinations of the yield and ultimate strength increases. This was chosen over analyzing another strength increase graph at 0.03 in./in. for simplicity during design and deemed acceptable for A706 mild steel reinforcement.

### 3.8 Recommendations and Conclusions

This chapter has presented an investigation on the effects of cold temperature, bar size, and strain rate on the behavioral changes of ASTM A706 Grade 60 mild steel reinforcement for the purposes of designing structures that undergo seasonal freezing. The following section provides recommendations and conclusions for A706 mild steel as a result from this study.

- The material behavior is altered even before reaching -32°F (0°C). This is complementary to previous research on other materials but dissimilar to the assumption made by NCSU for the material.
- There is a discrepancy between the cross-sectional area of the actual reinforcing bar and the ASTM nominal. The bars are, on average, 2.3 percent smaller 4.3 percent smaller than that reported by ASTM for a #6 bar and a #8 bar, respectively.
- The modulus of elasticity is insignificantly affected by temperature and strain rate. It is therefore recommended that the modulus be assumed constant with a value, adjusted for the ASTM nominal bar areas, of 29,864 ksi (205,905 MPa) for all temperatures and strain rates.
- An increase in the yield and ultimate strengths of 5.1 and 6.3 percent were experienced, respectively, when lowering the temperature from 20°C to -40°C.

These increases varied quadratically instead of linearly as suggested by Filiatrault

and Holleran. The recommended equations used for the definition of these increases coincide with those defined in Section 3.6.1. If a linear representation of these increases is desired, the following equations are acceptable between the temperatures of 68°F (20°C) and -4°F (-20°C):

$$\circ \quad \% \text{ Yield Increase} = -0.063(T) + 1.260 \quad \text{with } T \text{ in } ^\circ\text{C}$$

$$\circ \quad \% \text{ Ultimate Increase} = -0.088(T) + 1.760 \quad \text{with } T \text{ in } ^\circ\text{C}$$

- The magnitude of temperature increases for the yield and ultimate strength of A706 mild steel are generally lower than previous research on other materials, particularly the average 8% increase in yield strength and 12% increase in ultimate strength at 30°C observed in Sloan's research.
- The impact of temperature on the ultimate strength with an overall increase of 3% is greater than that on the yield strength, 1.67%, and is opposite to previous research conducted on other materials.
- Although a complete conclusion on the effects of bar size cannot be made, it is apparent that bar size does affect the magnitudes at which the increase in yield and ultimate strength occur along with the stress-strain curve. This should be fully researched for validation.
- The yield plateau generally dissipates as the strain rate increases and completely disappears upon reaching a strain rate of 0.3 in./in./min. A total dissipation of 0.0084 in/in (34.7%) is experienced in the yield plateau length when varying the strain rate from 0.003 in./in./min. to 0.3 in./in./min. This dissipation seems to be dependent upon temperature but should be researched fully for validation.
- For modeling purposes, an additional point along the strain hardening curve is desirable. The recommended equation for the increases of this point, 0.03 in./in., corresponds to that defined in Section 0.

## Chapter 4: VSAT – AN ANALYTICAL PROGRAM

### 4.1 Introduction

#### 4.1.1 Background

A Versatile Section Analysis Tool (VSAT) was created to aid in structural design of concrete columns, foundation shafts, and piles. The intention of VSAT was to create an analysis tool capable of providing moment-curvature responses of common sections with advanced features. The amount of hand calculations required from the user is minimized in VSAT while complimenting it with visual aids during the section analysis. This minimizes errors during section and material definitions that could otherwise lead to catastrophic repercussions. This chapter describes the internal processes of VSAT via this theoretical chapter.

#### 4.1.2 Capabilities

In order to effectively capture the moment-curvature response of typical sections used in design, VSAT was constructed with many different features. These features include: 1) permitting different cross-sections; 2) allowing both normal strength and ultra-high performance concrete (UHPC) material behavior; 3) enabling mild steel and prestress reinforcing steel; 4) allowing the confining effects of soil pressure; 5) including a steel shell circular section; and 6) accounting for low temperature effects on concrete and steel behavior. After allowing for the selection of appropriate features, VSAT will define the moment-curvature response of the chosen section.

The geometry of the cross-section is a major contributor to the moment-curvature response; therefore, different sections must be defined. VSAT accommodates four different types of section: circular, rectangular, octagonal and H-shaped. These sections can be subjected to a compressive or tensile external axial load and prestress forces during the entire analysis. Sections may be hollow or solid to model the sections commonly used in design practice. After defining the geometry, zones are created within VSAT and they are assigned to a specific stress-strain behavior.



Normal strength concrete and UHPC models exist in VSAT to allow a user to accurately define the behavior of concrete with a limited number of variables. Both maximum tensile and compressive strengths are modeled in VSAT to allow for a more accurate depiction of how concrete strength contributes to the section's performance in tensile and compressive axial load states.

In addition to the concrete models, mild steel and prestressing steel that are used as longitudinal reinforcing bars are defined with standard ASTM diameters and areas. This lessens the input required by the user during the analysis definition stage. The user may, however, opt to enter other values for bar longitudinal reinforcement sizes as well as the reinforcement's effectiveness to confine concrete as deemed necessary.

Soil behavior and/or an exterior steel shell alter(s) the section's performance during loading. VSAT models these effects as a secondary confining pressure that confines all concrete within the section and inhibits the section from spalling cover concrete during loading.

Low temperatures alter material behavior and are thus included in VSAT. The user may enter both an analysis temperature and a temperature at which the material properties are known to eliminate further experimentation that would otherwise be required to account for the effects of a temperature difference. By defining each testing material temperature separately, the user need not conduct testing of each material at the same temperature to use in VSAT. These changes in behavior can greatly affect the section's performance depending on the range over which the temperature is changed.

#### **4.1.3 Disclaimer**

VSAT is in its beta version and this current version is intended strictly for educational purposes only until it has been fully developed and checked for errors. It may, therefore, not yet be utilized for commercial applications. Any information determined by VSAT must be evaluated and deemed "accurate" by the user before being used in design. The author of VSAT assumes no responsibility for the output provided by the program and/or any problems or failures that may arise from analysis results. If a problem arises during the usage of VSAT or more knowledge is required, contact those currently supporting the program.

## 4.2 Theoretical Procedures

### 4.2.1 Introduction

#### 4.2.1.1 Overview

The theoretical section was created to aid in understanding of the inner-workings of VSAT. Various topics in this chapter include: 1) stress-strain behavior of concrete, mild steel, and prestressing steel; 2) the effects of soil and/or an exterior steel shell on concrete behavior; 3) the effects of low temperatures on material behavior; and 4) analytical procedures to determine the section's moment-curvature response. These topics are separately presented below to portray all possible combinations that VSAT is capable of handling during an analysis.

#### 4.2.1.2 Sign Convention

The following sign conventions are used in this chapter and in VSAT:

- Compression forces are positive.
- Tension forces are negative.

### 4.2.2 Section Details

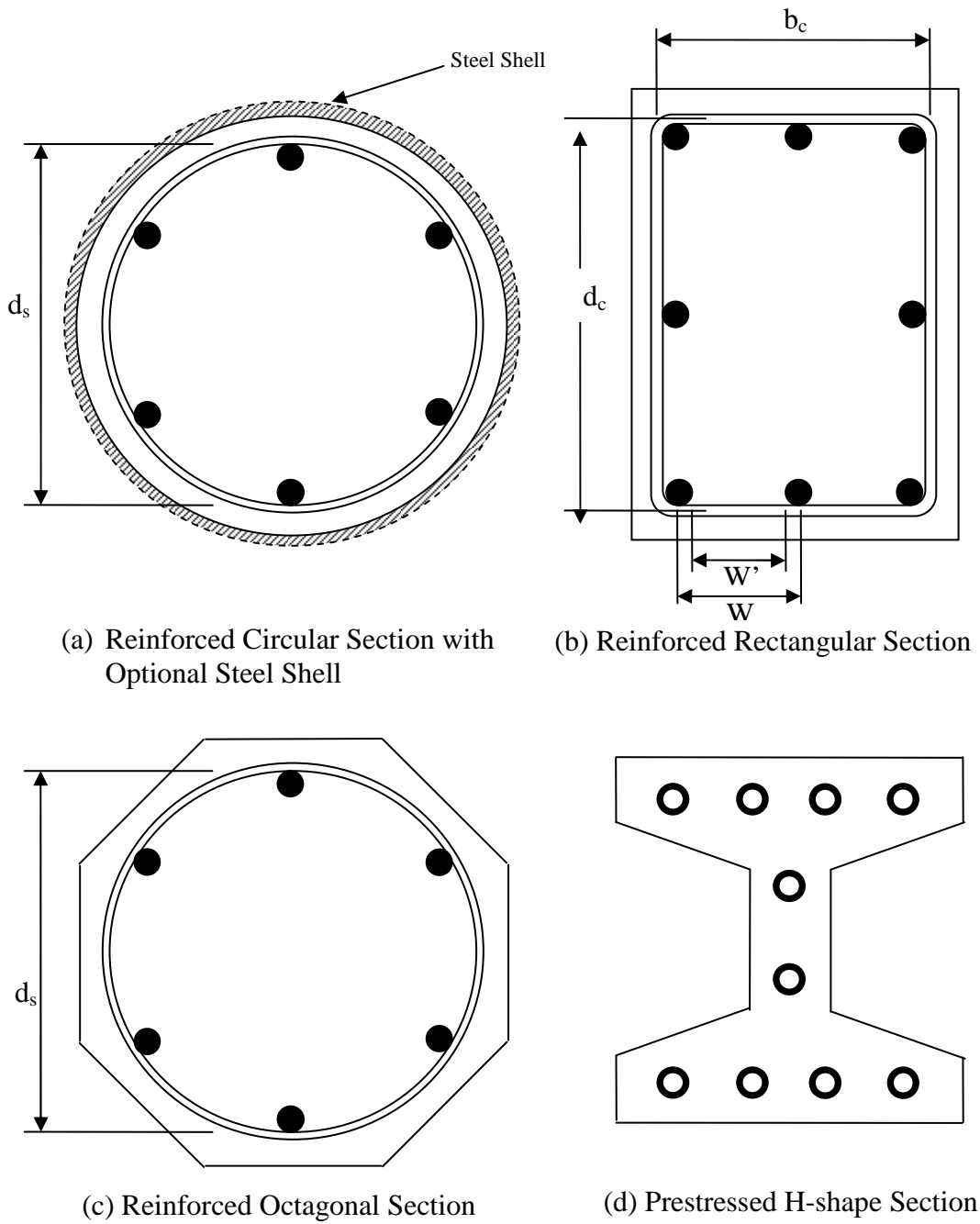
The first step in conducting an analysis with VSAT is to define the section details. These details include: 1) section shape; 2) longitudinal and transverse reinforcement quantities; and 3) external actions.

The section's shape is defined by the gross section geometry. VSAT supports circular sections, with or without an exterior steel shell; rectangular sections; octagonal sections; and H-shaped sections (see Figure 4-1). Upon choosing a geometric shape, one may opt for the section to be hollow instead of solid. Note that the H-shaped section is required to be only a solid section.

The transverse reinforcement style refers to the confining reinforcement that may be ties, hoops, or a spiral as shown in Figure 4-4. The addition of this steel provides a confining pressure,  $f_l'$ , which creates a confined (core) concrete region. This region has an increased strength and a different stress-strain behavior than the unconfined concrete typically present

in the cover. A circular transverse reinforcement style may be chosen for either a circular, rectangular, or octagonal section, while a rectangular transverse reinforcement may only be chosen for rectangular sections. If the section is hollow, the transverse reinforcement style must follow that of the hole within the section (i.e., a section with a circular hole must have a circular transverse reinforcement). The H-shaped section does not account for transverse reinforcement as this was developed for a special application, which is detailed in Section 4.2.3.6.

External actions may include an applied axial load, an applied soil pressure, and temperature effects. To maintain equilibrium during an analysis, the applied axial load must always be balanced by the equivalent internal forces developed in the material strips in that section. These strips are a segmentation process necessary to conduct the analysis, which are further discussed in Section 4.2.9.1. The soil pressure and temperatures are used to alter the material behavior used in the analysis. To determine the extent to which the material properties are altered, both the temperature at which data is available for the material and the analysis temperature are required.



**Figure 4-1: Section Shapes Currently Available in VSAT**

#### 4.2.3 Concrete Properties

The following sections will present information for two different concrete models available in VSAT: normal strength concrete and UHPC. The necessary information for

defining the confined, unconfined, tensile and ultimate compressive strength of normal strength concrete will presented, followed by the behavior of UHPC.

#### 4.2.3.1 Normal Strength Confined Concrete

Normal strength confined core concrete exhibits an increase in compressive strength and compressive strain capacity due to the confining pressure that may be provided by the addition of transverse reinforcement, steel shell, or external pressure to the section. An analytical model proposed by Mander et al. (1988b) was the first model chosen to define the confined behavior of normal concrete. As provided below, this model calculates the confined-compressive stress in concrete,  $f_c$ , for a given concrete strain between 0 and  $\varepsilon_{cu}$ , where  $\varepsilon_{cu}$  is the ultimate strain capacity of confined concrete (see Figure 4-2). As shown by the figure, it is advantageous to use this model because the entire curve can be defined with one equation:

$$f_c = \frac{f'_{cc} x r_c}{r - 1 + x r_c} \quad \text{Eq. (4.1)}$$

$$f'_l = k_e f_l = 0.5 k_e \rho_s f_{yh} \quad \text{Eq. (4.2)}$$

$$E_c = 57,000 \sqrt{f'_c} \quad \text{Eq. (4.3)}$$

$$f'_{cc} = f'_c \left( 2.254 \sqrt{1 + \frac{7.94 f'_l}{f'_c}} - \frac{2 f'_l}{f'_c} - 1.254 \right) \quad \text{Eq. (4.4)}$$

$$\varepsilon'_{cc} = \varepsilon'_{co} \left\{ R \left( \frac{f'_{cc}}{f'_c} - 1 \right) + 1 \right\} \quad \text{Eq. (4.5)}$$

$$R = 5 \text{ (a recommended average)} \quad \text{Eq. (4.6)}$$

$$E_{sec} = \frac{f'_{cc}}{\varepsilon'_{cc}} \quad \text{Eq. (4.7)}$$

$$r_c = \frac{E_c}{E_c - E_{sec}} \quad \text{Eq. (4.8)}$$

$$x = \frac{\varepsilon_c}{\varepsilon'_{cc}} \quad \text{Eq. (4.9)}$$

where  $f_l$  = Lateral confining pressure

$k_e$  = Concrete confinement effective coefficient

$\varepsilon'_{co}$  = Concrete compressive strain corresponding to  $f'_c$

As recommended by Mander et al. (1988b), VSAT's default strain at which the maximum unconfined concrete stress is reached,  $\varepsilon'_{co}$ , is 0.002, but this may be altered by the user to account for the increase in  $\varepsilon'_{co}$  as the unconfined concrete cylinder strength,  $f'_c$ , increases.

To determine the effective lateral confining pressure,  $f'_l$ , the effectiveness of the section,  $k_e$ , is required. As presented by Figure 4-3 and Figure 4-4, the value of  $k_e$  is an indication of how well the longitudinal and transverse reinforcement confines the core concrete. Notice in Figure 4-3 the degree at which the unconfined concrete penetrates into the core concrete region. The determination of  $k_e$  for circular and rectangular cross sections was provided by King et al. (1986) and was extended by the author to include octagonal sections, which contain a core identical to that of a circular section, in VSAT. VSAT further restricted  $k_e$  to lie between 0 and 1.0 to simulate zero or full-section effectiveness, respectively. A value of less than zero would indicate that the section has less strength than unconfined concrete and a value greater than one would indicate that more than the full section is effective, both of these values, thus, have no physical meaning. The effective confinement coefficient,  $k_e$ , for circular core sections (includes octagonal section) may be found from the following equations as presented by Mander et al. (1988b):

$$k_e = \frac{\left(1 - 0.5 \frac{s'}{d_s}\right)^2}{1 - \rho_l} \quad \text{for circular hoops} \quad \text{Eq. (4.10)}$$

$$k_e = \frac{1 - 0.5 \frac{s'}{d_s}}{1 - \rho_{cc}} \quad \text{for spirals} \quad \text{Eq. (4.11)}$$

$$\rho_s = \frac{4A_{sh}}{sd_s} \quad \text{Eq. (4.12)}$$

$$\rho_{cc} = \frac{4A_s}{\pi d_s^2} \quad \text{Eq. (4.13)}$$

where  $s$  = Centerline to centerline spacing between transverse reinforcement

$s'$  = Clear spacing between transverse reinforcement

$d_s$  = Diameter of circular core concrete measured from the centerline to centerline of transverse reinforcement

$A_{sh}$  = Area of transverse mild steel reinforcement

The effective confinement coefficient,  $k_e$ , for rectangular core sections may be found from the following equations as presented by Mander et al. (1988b) and King et al. (1986):

$$k_e = \left\{ 1 - \frac{N_{bars}(W')^2}{6b_c d_c} \right\} \left\{ \frac{\left(1 - 0.5 \frac{s'}{b_c}\right) \left(1 - 0.5 \frac{s'}{d_c}\right)}{1 - \rho_l} \right\} \quad \text{Eq. (4.14)}$$

$$\rho_s = \rho_x + \rho_y = \frac{A_{sx}}{b_c d_{cs}} + \frac{A_{sy}}{b_c d_{cs}} \quad \text{Eq. (4.15)}$$

$$\rho_{cc} = \frac{A_s}{b_c d_c} \quad \text{Eq. (4.16)}$$

where  $N_{bars}$  = number of longitudinal bars

$W'$  = average clear distance between longitudinal bars

$A_s$  = Total area of longitudinal mild steel reinforcement

$b_c$  = Width of rectangular core concrete measured from centerline to centerline of transverse reinforcement

$d_c$  = Depth of rectangular core concrete measured from centerline to centerline of transverse reinforcement

$A_{sx}$  = Area of longitudinal mild steel parallel to the axis of bending

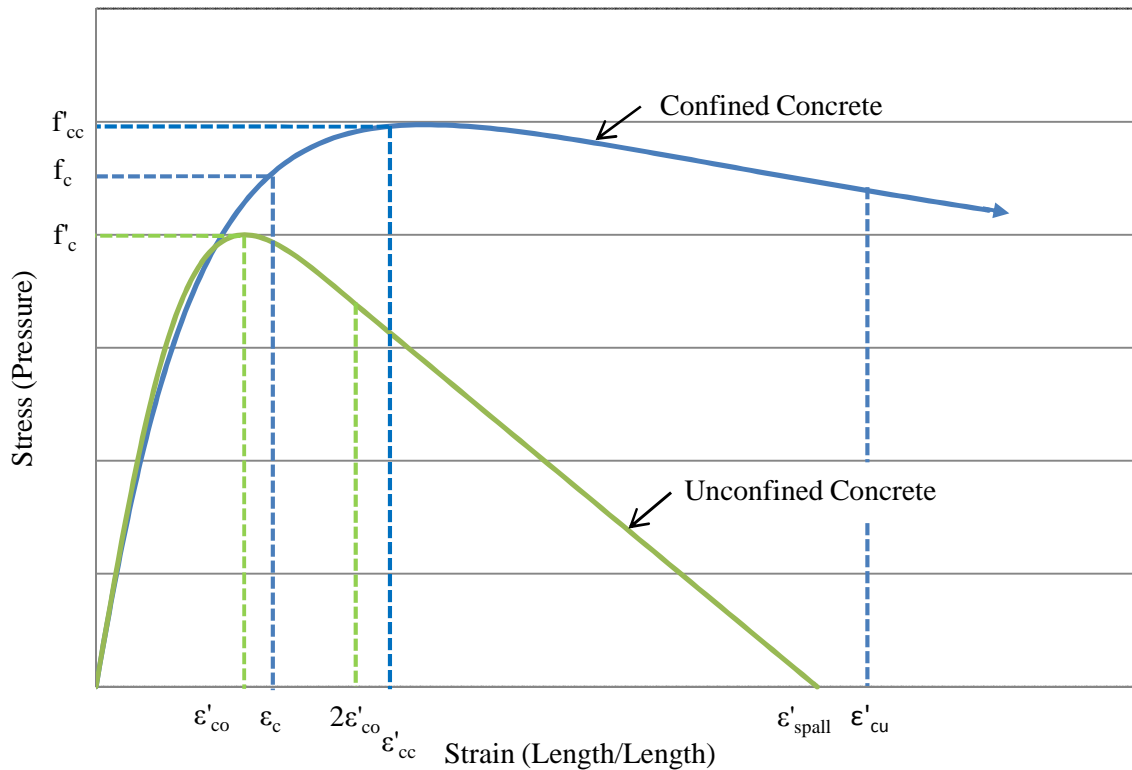
$A_{sy}$  = Area of longitudinal mild steel perpendicular to the axis of bending

As shown in Eqs. 4.14 through 4.16, the determination of  $k_e$  for rectangular sections has the potential to be problematic. For example, if a rectangular section were to have more reinforcement in one direction or unevenly spaced longitudinal bars, an error between the section's true effectiveness and the theoretical effectiveness would exist. To overcome this issue, VSAT makes the following assumptions for all sections as applicable:

1. transverse reinforcement is evenly spaced and longitudinal reinforcement is evenly spaced per direction (i.e., parallel and perpendicular to the axis of bending);

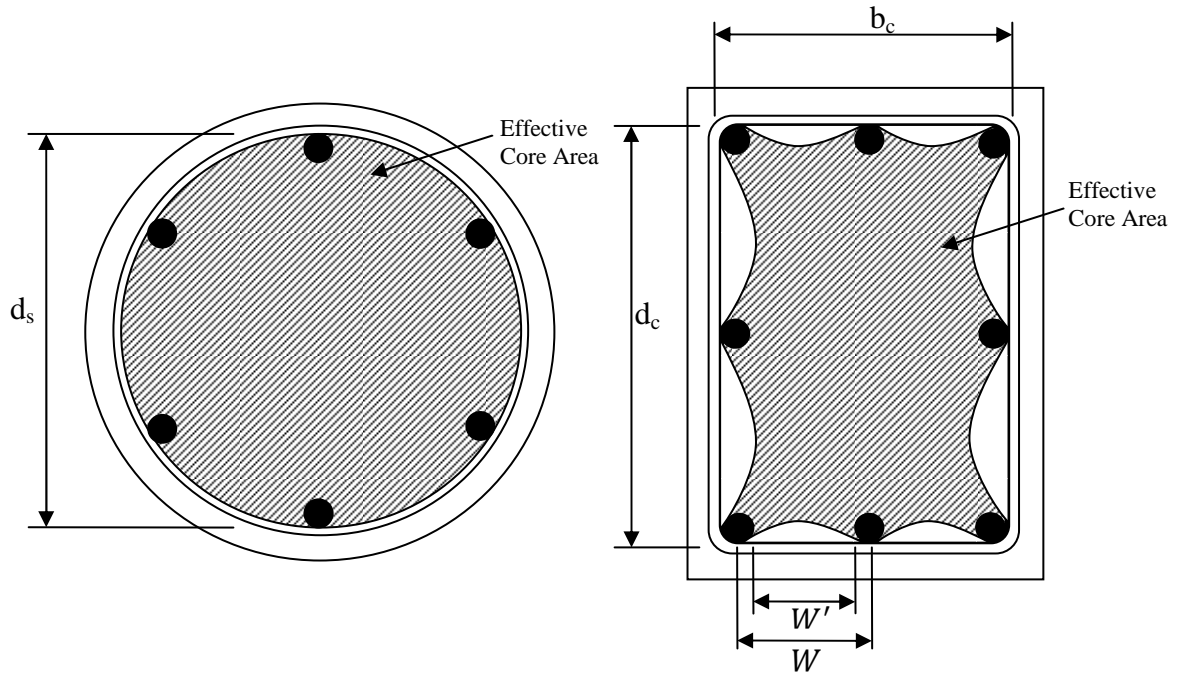
2. prestressing bars are ignored in the calculation of  $k_e$  when mild steel longitudinal reinforcement exists;
3. an average value of  $\rho_s$  is used for all sides of the section; and
4. an average value of  $\rho_s$  is used.

Assumption 1 allows an analysis to be conducted when the final placement of reinforcement is unknown and also lessens the input required from the user. Assumption 2 is justified by realizing that mild steel reinforcement usually has a considerably larger area than that of prestressing steel. Finally, assumptions 3 and 4 eliminate the chance of calculating a value  $\rho_s$  that is misrepresentative of the section. If the user wishes to bypass these assumptions, the user may opt to use their own means of calculating  $\rho_s$  and enter an appropriate value directly into VSAT.

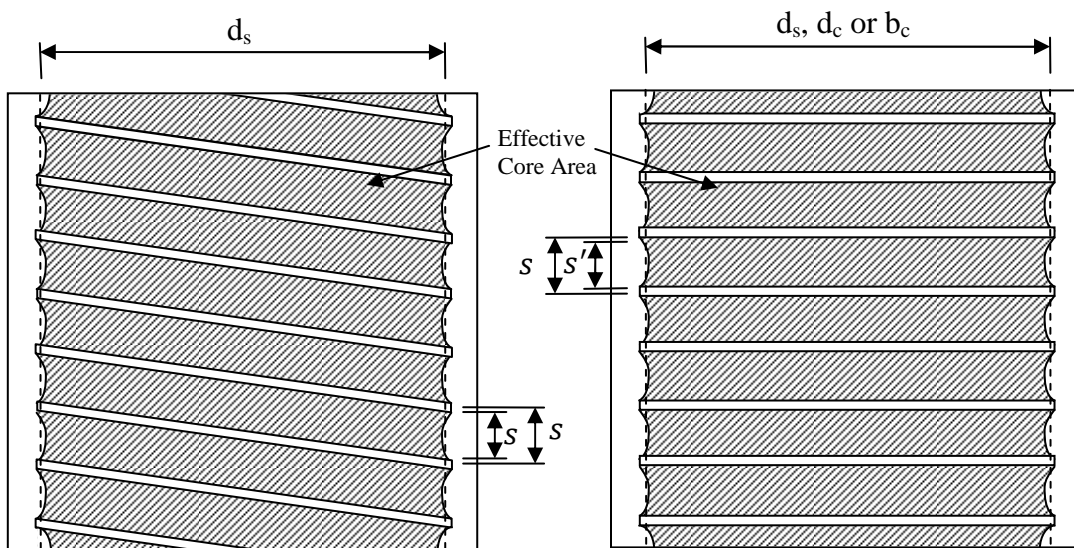


**Figure 4-2: Concrete Compressive Stress-Strain Model as Proposed by Mander et al. (1988b)**





**Figure 4-3: A Plan View of Sections Showing the Effective Cores that are Confined by Transverse Reinforcement**



**Figure 4-4: Cross-Sectional Views along the Member Length Showing the Effective Cores that are Confined by Transverse Reinforcement**

#### 4.2.3.2 Normal Strength Unconfined Concrete

Unconfined concrete, usually present in the cover region of a concrete section, will follow the stress-strain curve in Figure 4-2. This curve is defined by the procedure described in Section 4.2.3.1 with the confining stress,  $f_l'$ , equal to zero. Eqs. 4.4, 4.5, 4.7 and 4.9 are thus reduced to:

$$f'_{cc} = f'_c \quad \text{Eq. (4.17)}$$

$$\varepsilon'_{cc} = \varepsilon'_{co} \quad \text{Eq. (4.18)}$$

$$E_{sec} = \frac{f'_c}{\varepsilon'_{co}} \quad \text{Eq. (4.19)}$$

$$x = \frac{\varepsilon_c}{\varepsilon'_{co}} \quad \text{Eq. (4.20)}$$

In VSAT, these equations are applicable to unconfined concrete until the strain has reached  $2\varepsilon'_{co}$ , upon which the curve becomes linear until reaching the spalling strain,  $\varepsilon'_{spall}$ . The linear portion of the stress-strain curve is determined by using the slope between  $1.7\varepsilon'_{co}$  and  $2\varepsilon'_{co}$  until the stress reaches zero. Any part of the unconfined concrete exceeding the spalling strain will sustain zero stress and, therefore, no longer contributes to the moment resistance of the section. The numerical representation of the resulting stress-strain curve can be expressed by Eqs. 4.21 to 4.23.

$$f_c = \frac{f'_c r x}{r-1+x^r} \quad \text{for } \varepsilon_c \leq 2\varepsilon'_{co} \quad \text{Eq. (4.21)}$$

$$f_c = f_{2\varepsilon'_{co}} + \frac{f_{2\varepsilon'_{co}} - f_{1.7\varepsilon'_{co}}}{2\varepsilon'_{co} - 1.7\varepsilon'_{co}} (\varepsilon_c - 2\varepsilon'_{co}) \quad \text{for } 2\varepsilon'_{co} \leq \varepsilon_c < \varepsilon'_{spall} \quad \text{Eq. (4.22)}$$

$$f_c = 0 \quad \text{for } \varepsilon_c > \varepsilon'_{spall} \quad \text{Eq. (4.23)}$$

If desired by the user, the value of  $\varepsilon'_{spall}$  may be redefined in VSAT. Upon altering  $\varepsilon'_{spall}$ , the slope of Eq. 4.22 is redefined from  $2\varepsilon'_{co}$  to the chosen value of  $\varepsilon'_{spall}$ . The remaining equations, Eqs. 4.21 and 4.23, are unaltered.

#### 4.2.3.3 Variable Confinement Model for Normal Concrete

Hose et al. (2001) investigated the effects of variable confining stress and its effects on concrete strength. This is because the real confining steel stress varies with strain but the model provided by Mander et al. assumes this confining stress to be constant, equivalent to the yield strength of the material. This assumption overestimated and the actual confining pressure over a certain strain range and underestimated the confining pressure over a different strain range. Because Mander et al. assumed that the transverse steel is always at a constant stress, the actual strength of concrete at the beginning of the stress-strain curve was slightly overestimated.

When concrete is loaded axially the concrete expands or dilates. This dilation can be expressed in terms of a hoop strain. From this hoop strain a new  $f'_l$  and  $f_c$  can be calculated. The following equations adjust for this error while all other equations presented by Mander et al. (i.e., Eqs. 4.1 and 4.3 through 4.16) remain the same (See Figure 4-5 and Figure 4-6).

$$\Delta\varepsilon_d = \Delta\varepsilon_1 * \mu_t \quad \text{Eq. (4.24)}$$

$$\mu_t = \mu_{tn} + \mu_e \quad \text{Eq. (4.25)}$$

$$\mu_{tn} = \sum \frac{\sigma'}{2f_l} \quad \text{Eq. (4.26)}$$

$$\Sigma = \left( \frac{1}{1 + \frac{1}{\eta\varepsilon_1 + J}} \right) \quad \text{Eq. (4.27)}$$

$$\varepsilon_{d,new} = \varepsilon_d + \Delta\varepsilon_d \quad \text{Eq. (4.28)}$$

$$f'_l = k_e f_l = 0.5k_e \rho_s \sigma_h \quad \text{Eq. (4.29)}$$

Where  $\Delta\varepsilon_d$  = Change in dilation strain of the transverse hoop reinforcement

$\Delta\varepsilon_1$  = Concrete strain step change

$\mu_e$  = Elastic portion of tangent Poisson's ratio

$\sigma'$  = Difference between unconfined and confined beginning stress

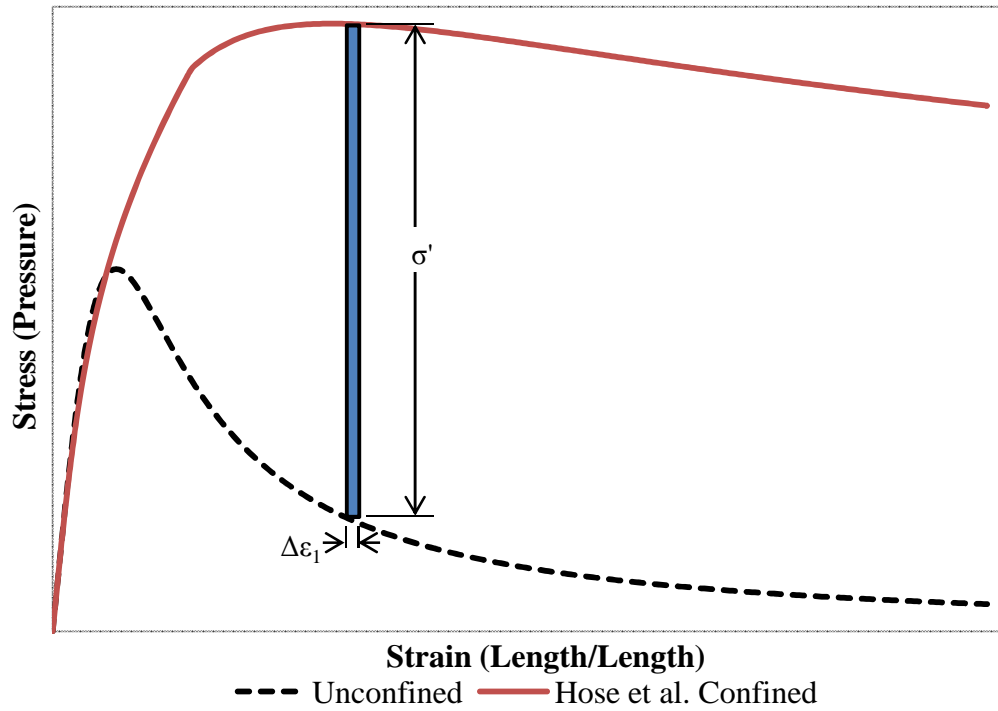
$\eta, J$  = Constants to accurately model hoop strain

$\varepsilon_d$  = Beginning transverse dilation strain

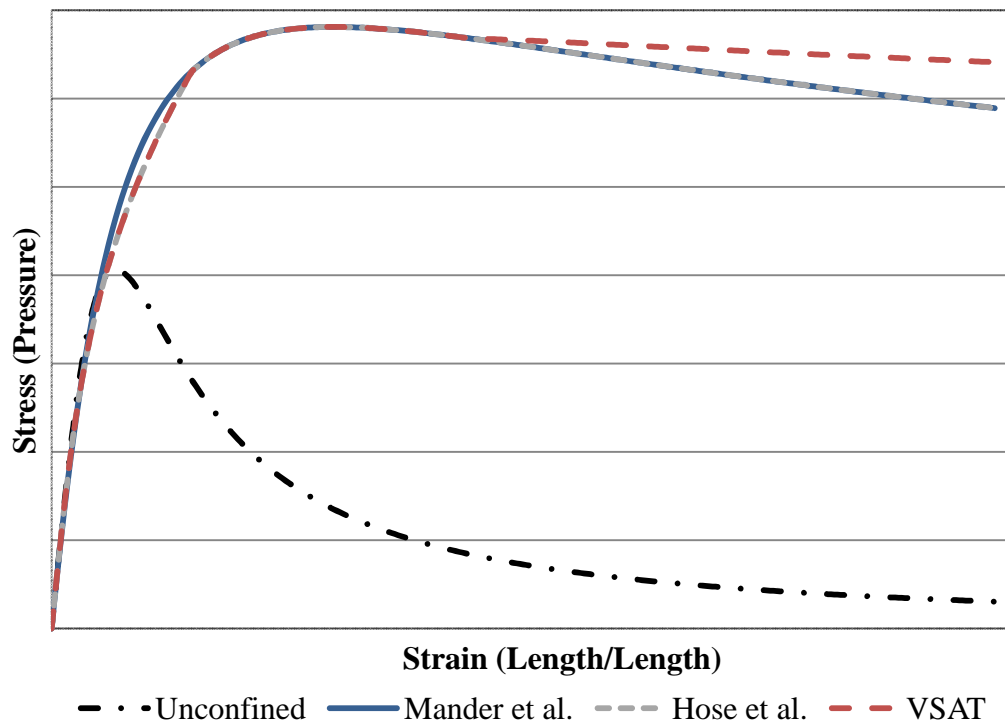
$$\sigma_h = \text{Transverse hoop stress of } \varepsilon_{d,new}$$

To begin the process of developing the stress-strain curve, a strain step of  $\Delta\varepsilon_l$  is taken to the first strain value of  $\varepsilon_l$ . Next, the total tangent Poisson's ratio,  $\mu_t$ , needs to be determined that relates the strain in concrete to the dilation strain in the reinforcement and is comprised of an elastic and non-elastic portion. The elastic tangent Poisson's ratio,  $\mu_e$ , was recommended to be 0.2 by Hose et al. (2001) and necessary to include until the unconfined compressive strength of concrete is reached. To calculate the non-elastic term,  $\mu_m$ , the difference between the confined and unconfined stress,  $\sigma'$  (See Figure 4-5); the confining pressure,  $f_l$ ; and the  $\Sigma$  term must be found for the previous concrete strain. The values of  $\eta$  and  $J$ , constants in the  $\Sigma$  term, need to be altered to correctly depict the last portion of the concrete stress-strain curve.  $\eta$  and  $J$  values of 20 and 1/3, respectively, were recommended and used by Hose et al. (2001). Upon determining the change in dilation strain,  $\Delta\varepsilon_d$ , the new transverse hoop strain,  $\varepsilon_{d,new}$ , can be generated along with the corresponding new hoop stress,  $\sigma_h$ . The remaining equations in the model presented by Mander et al. (1988b) may then be used.

Figure 4-6 depicts the unconfined concrete curve along with the variations between the curve presented by Mander et al. (1988b) and Hose et al. (2001). VSAT uses a modified version of changes proposed by Hose et al. to generate the third confined curve on this figure. In their work, it was assumed that the horizontal stress-strain material behavior was elastic until reaching yield and then perfectly plastic. This was extended in VSAT to include the strain hardening effects of A706 mild steel reinforcement. Because the stress of the transverse reinforcement is directly calculated from the dilation strain, it's logical to include the effects of strain hardening of the steel to better reflect the concrete stress-strain behavior (See Figure 4-6).



**Figure 4-5: Incremental Step for Determining the Stress-Strain Behavior of Concrete by Hose et al. (2001)**



**Figure 4-6: Comparison of Concrete Model Proposed by Mander et al. and Hose et al.**

#### 4.2.3.4 Tensile Strength of Normal Strength Concrete

Three different methods of defining the concrete tensile strength are made available in VSAT: by specifying strain, by limiting stress, and by defining a zero tension capacity. To define the tensile strength by strain, the user may enter the maximum tensile strain of concrete. To define by stress, VSAT requires the user to enter the value  $X$  into the following equation with  $f'_c$  in psi units:

$$f'_t = X\sqrt{f'_c} \quad \text{Eq. (4.30)}$$

where  $X$  = A value greater than 0 that accurately reflects the behavior of the material

It is recommended by the American Concrete Institute (ACI) that a value ranging from 6.0 to 12.0 be used for  $X$  for normal weight concrete (ACI 318, 2008). The value of  $\varepsilon_t$  is calculated from  $f'_t$  linearly by dividing by the elastic modulus of concrete. The final option is to assume a zero tension capacity by selecting the appropriate option in VSAT. Regardless of the method used, the concrete in tension will contribute a tensile stress, tensile force and flexural moment until reaching its tensile capacity, upon which the concrete will crack and no longer contribute to the section for the remainder of the analysis.

#### 4.2.3.5 Normal Strength Maximum Concrete Strain

The maximum strain of concrete is a function of the confinement pressure within the section and the confined concrete strength used. VSAT determines a default maximum concrete strain by means of Eq. 4.31 as presented by Paulay and Priestley (1992).

$$\varepsilon_{cu} = 0.004 + 1.4 \frac{\rho_s f_{yh} \varepsilon_{su}}{f'_{cc}} \quad \text{Eq. (4.31)}$$

where  $f_{yh}$  = Yield strength of longitudinal mild steel reinforcement

$\varepsilon_{su}$  = Steel strain corresponding to the ultimate strength of longitudinal mild steel reinforcement

Since the preceding equation yields a conservative number, VSAT allows the user to enter a value of  $\varepsilon_{cu}$  that coincides with the actual maximum concrete strain in the section to be analyzed.

#### 4.2.3.6 Ultra-High Performance Concrete

Ultra-High Performance Concrete (UHPC) is available in VSAT but neglects the effects of confinement as literature is limited on this topic. The following equations, as presented by Vande Voort et al. (2008), define the stress-strain behavior of UHPC in VSAT (See Figure 4-7 for details):

For UHPC in tension:

For  $\varepsilon_t \leq f'_{te}/E_c$

$$f_{c,ten} = E_c * \varepsilon_t \quad \text{Eq. (4.32)}$$

For  $f'_{te}/E_c < \varepsilon_t \leq 0.0014$

$$f_{c,ten} = f'_{te} + \frac{(f'_{t,max} - f'_{te})(\varepsilon_t - f'_{te}/E_c)}{0.00125} \quad \text{Eq. (4.33)}$$

For  $0.0014 < \varepsilon_t \leq 0.0024$

$$f_{c,ten} = f'_{t,max} \quad \text{Eq. (4.34)}$$

For  $\varepsilon_t > 0.0024$

$$f_{c,ten} = f'_{t,max} - 0.672 * \ln(\varepsilon_t) - 4.062 \quad \text{Eq. (4.35)}$$

For UHPC in compression:

For  $\varepsilon_c \leq 0.85f'_c/E_c$

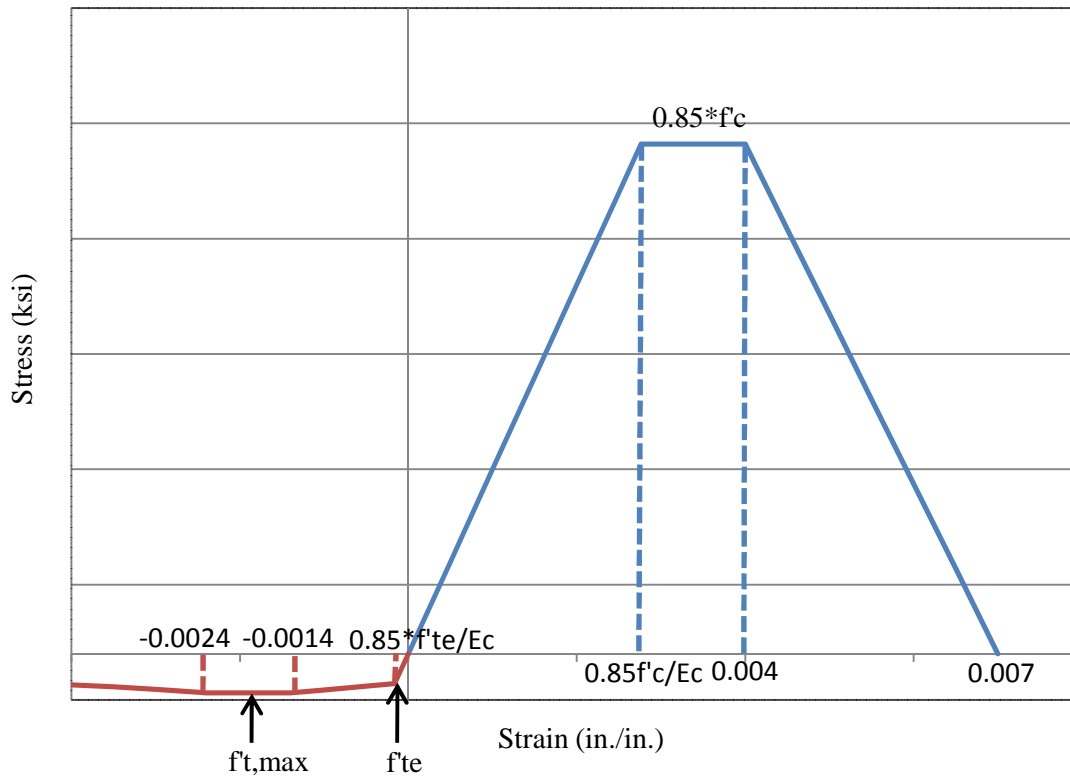
$$f_c = E_c * \varepsilon_c \quad \text{Eq. (4.36)}$$

For  $0.85f'_c/E_c < \varepsilon_c \leq 0.004$

$$f_c = 0.85f'_c \quad \text{Eq. (4.37)}$$

For  $0.004 < \varepsilon_c \leq 0.007$

$$f_c = 0.85f'_c \left(1 - \frac{\varepsilon_c - 0.004}{0.003}\right) \quad \text{Eq. (4.38)}$$

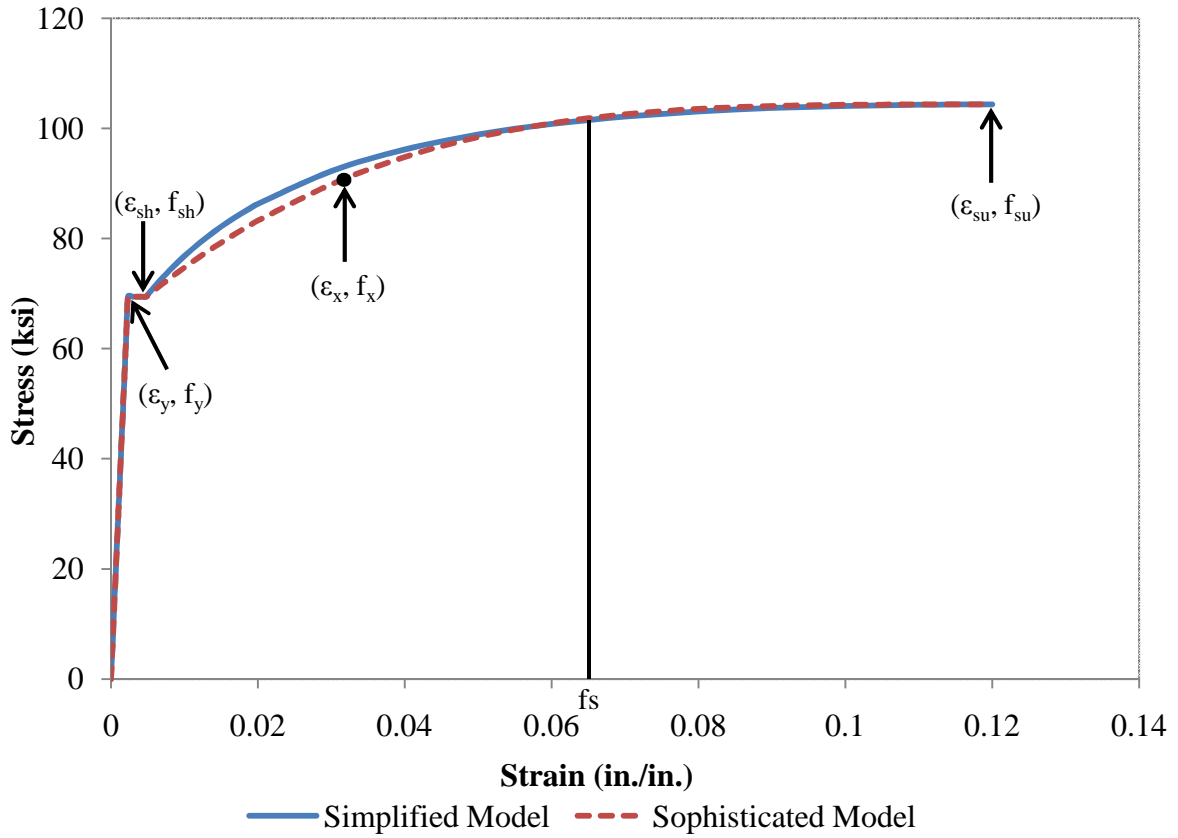


**Figure 4-7: Stress-Strain Model Used for UHPC in VSAT**

#### 4.2.4 Mild Steel Reinforcement Properties

The stress-strain behavior of longitudinal mild steel reinforcement is needed during an analysis in order to accurately balance the applied loads and correctly determine the moment capacity of the section. Strain hardening is included in VSAT to more accurately depict the location of the neutral axis and thus the strains, stresses, and moment capacity of the section at any given curvature. The following sections will present information on two stress-strain models available in VSAT: a “simplified model” and a “sophisticated model”. As shown in Figure 4-8, the two models may not correspond with one another. Consequently, it is advantageous to use the sophisticated model whenever possible, but it requires more information as detailed below.





**Figure 4-8: Stress-Strain Behavior of A706 Mild Steel Reinforcement**

#### 4.2.4.1 Simplified Model

The simplified model requires three sets of data points: the yield point  $(\varepsilon_y, f_y)$ , the point at which the strain hardening region initiates  $(\varepsilon_{sh}, f_{sh})$ , and the ultimate point  $(\varepsilon_{su}, f_{su})$ . These points allow the solid curve in Figure 4-8 to be produced in VSAT using the following equations as presented by King et al. (1986):

$$f_s = E_s \varepsilon_s \quad \text{for } \varepsilon_s \leq \varepsilon_y \quad \text{Eq. (4.39)}$$

$$f_s = f_y \quad \text{for } \varepsilon_y < \varepsilon_s \leq \varepsilon_{sh} \quad \text{Eq. (4.40)}$$

$$f_s = f_y \left[ \frac{m(\varepsilon_s - \varepsilon_{sh}) + 2}{60(\varepsilon_s - \varepsilon_{sh}) + 2} + \frac{(\varepsilon_s - \varepsilon_{sh})(60 - m)}{2(30r_s + 1)^2} \right] \quad \text{for } \varepsilon_{sh} < \varepsilon_s \leq \varepsilon_{su} \quad \text{Eq. (4.41)}$$

$$\text{where } m = \frac{\left(\frac{f_{su}}{f_y}\right)(30r_s + 1)^2 - 60r_s - 1}{15r_s^2} \quad \text{Eq. (4.42)}$$

$$r_s = (\varepsilon_{su} - \varepsilon_{sh}) \quad \text{Eq. (4.43)}$$

A default yield strength of 67.43 ksi is provided, as recommended from the testing conducted for this thesis, in VSAT but may be altered by the user. Changing this value causes the remaining parameters (i.e., yield strain, strain hardening strain, and ultimate strength) to be recalculated as described in Table 4-1. Any of these values may also be changed, if desired by the user, and any remaining parameters will be recalculated accordingly. The stress-strain curve is developed utilizing the simplified strain hardening region specified by the above equations.

**Table 4-1: Default VSAT Steel Properties**

Yield Stress $f_y$ (ksi)	As Input
Young's Modulus $E_s$ (ksi)	29,000
Yield Strain $\epsilon_s$ (in./in.)	$f_y/E_s$
Strain Hardening strain $\epsilon_{sh}$ (in./in.)	$3.24\epsilon_s$
Ultimate Strength $f_{su}$ (ksi)	$1.5f_y$
Ultimate Strain $\epsilon_{su}$ (in./in.)	0.12

#### 4.2.4.2 Sophisticated Model

The sophisticated model included in VSAT is based on that proposed by Dodd and Restrepo-Posada (1995) and requires four sets of data points: the yield point ( $\epsilon_y, f_y$ ), the point at which the strain hardening region initiates ( $\epsilon_{sh}, f_{sh}$ ), an arbitrary point along the strain hardening curve ( $\epsilon_x, f_x$ ), and the ultimate point ( $\epsilon_{su}, f_{su}$ ). These points allow the dashed curve shown in Figure 4-8 to be produced using the following equations as presented by Dodd and Restrepo-Posada (1995):

$$f_s = E_s \epsilon_s \quad \text{for } \epsilon_s \leq \epsilon_y \quad \text{Eq. (4.44)}$$

$$f_s = f_y \quad \text{for } \epsilon_y < \epsilon_s \leq \epsilon_{sh} \quad \text{Eq. (4.45)}$$

$$f_s = f_{su} + (f_y - f_{su}) \left( \frac{\epsilon_{su} - \epsilon_s}{\epsilon_{su} - \epsilon_{sh}} \right)^p \quad \text{for } \epsilon_{sh} < \epsilon_s \leq \epsilon_{su} \quad \text{Eq. (4.46)}$$

$$\text{where } p = \frac{\log\left(\frac{f_{su} - f_x}{f_{su} - f_y}\right)}{\log\left(\frac{\epsilon_{su} - \epsilon_x}{\epsilon_{su} - \epsilon_{sh}}\right)} \quad \text{Eq. (4.47)}$$

#### 4.2.4.3 Bar Sizes

VSAT uses Table 4-2 to specify the ASTM nominal diameters and areas of mild steel reinforcement bars as presented in the ACI Building Code (ACI 318, 2008). If desired, the user may define a bar diameter to represent the use of different bar sizes in a section and VSAT will calculate the corresponding area assuming a circular cross section for the bar.

**Table 4-2: ASTM Standard Bar Information**

Bar Size	Nominal Diameter (in.)	Nominal Area (in. <sup>2</sup> )
#3	0.375	0.11
#4	0.500	0.20
#5	0.625	0.31
#6	0.750	0.44
#7	0.875	0.60
#8	1.000	0.79
#9	1.128	1.00
#10	1.270	1.27
#11	1.410	1.56
#14	1.693	2.25
#18	2.257	4.00
User Defined	As Input (D)	$\pi D^2/4$

where D = Diameter of the reinforcing bar

#### 4.2.5 Prestressing Steel Properties

The following sections present information on two prestressing steel models incorporated into VSAT, following the recommendations of Menegotto and Pinto (1973) and Devalapura and Tadros (1992). Both models consist of two linear sections with a curved transition to define the stress-strain curve.

#### 4.2.5.1 Menegotto and Pinto Model

The Menegotto and Pinto model, as presented by Naaman (1985), is defined by Eq. 4.48 to characterize the stress-strain behavior of prestressing steel using three coefficients: K, N, and Q.

$$f_p = E_p \varepsilon_{ps} \left[ Q + \frac{1-Q}{\left[ 1 + \left( \frac{E_p \varepsilon_{ps}}{K f_{py}} \right)^N \right]^{\frac{1}{N}}} \right] \quad \text{Eq. (4.48)}$$

$$\text{where } Q = \frac{f_{pu} - K f_{py}}{E_p \varepsilon_{pu} - K f_{py}} \quad \text{Eq. (4.49)}$$

$K$  = Coefficient determined as a fraction of  $f_{py}$

$N$  = Coefficient determined by trial and error until the prestressing steel equation equals  $f_{py}$  for  $\varepsilon_{py}$

$f_{py}$  = Yield strength of prestressing steel

$\varepsilon_{py}$  = Yield strain corresponding to  $f_{py}$

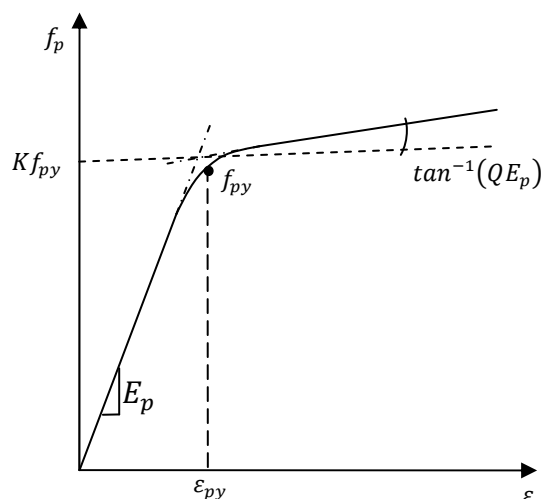
$E_p$  = Young's modulus of elasticity for prestressing steel

$f_{pu}$  = Ultimate tensile strength of prestressing steel

$\varepsilon_{pu}$  = Ultimate strain corresponding to  $f_{pu}$

$\varepsilon_{ps}$  = Prestressing steel strain

The value of  $E_p$  can be determined from the slope of the first linear portion of the curve as shown in Figure 4-9. The coefficient K can be defined by the intersection of the second linear portion of the curve, rotated by an angle of  $\tan^{-1}(QE_p)$ , and the  $f_p$ -axis. The value Q may be determined from Eq. 4.49. Finally, N is determined using trial and error until  $f_{py}$  is calculated for the strain  $\varepsilon_{py}$ . Changing the value of N adjusts the length of the curved transition and thus adjusts the  $f_{py}$  value. For example, lowering  $f_{py}$  will increase the curved transition.



**Figure 4-9: Menegotto and Pinto Model for Defining the Stress-Strain Curve of Prestressing Steel**

In addition, Naaman (1985) provides recommended coefficients that may be used for the actual stress-strain behavior of specific prestressing steels to define their stress-strain behavior as per the Menegotto and Pinto model (see Table 4-3). VSAT provides these coefficients through an option menu as described in Section B.10 of the user manual and provides an option for the user to manually define approximate values for the coefficients K, N, and Q.

**Table 4-3: Coefficients Recommended for Defining the Stress-Strain Behavior of Prestressing Steel by Naaman (1985)**

Steel Type	$E_{ps}$ (ksi)	$f_{py}$ (ksi)	$f_{pu}$ (ksi)	$\epsilon_{pu}$	K	N	Q
270 ksi strand	27890	243.5	278	0.069	1.0618	7.344	0.01174
235 ksi wire	29300	222.4	244	0.087	1.0325	6.060	0.00625
160 ksi bar	28790	141.8	160	0.041	1.0041	7.100	0.01750

#### 4.2.5.2 Devalapura and Tadros Model

The prestressing steel model, as presented by Devalapura and Tadros (1992), is defined by Eq. 4.50 and using four coefficients: A, B, C and D.

$$f_p = \varepsilon_{ps} \left[ A + \frac{B}{[1+(C\varepsilon_{ps})^D]^{1/D}} \right] \leq f_{pu} \quad \text{Eq. (4.50)}$$

$$\text{where } A = E_{ps} \left[ \frac{f_{pu} - f_{so}}{E_{ps}\varepsilon_{pu} - f_{so}} \right] \quad \text{Eq. (4.51)}$$

$$B = (E_{ps} - A) \quad \text{Eq. (4.52)}$$

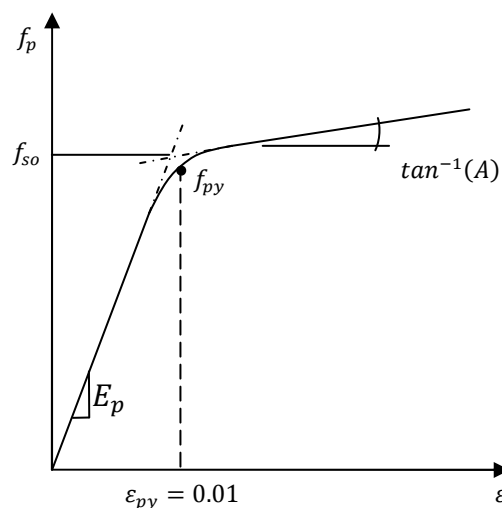
$$C = \frac{E_{ps}}{f_{so}} \quad \text{Eq. (4.53)}$$

$D$  = Coefficient determined by trial and error until the prestressing steel equation equals  $f_{py}$  for  $\varepsilon_{py}$

$f_{so}$  = The stress at the intersection of the two linear portions of the prestressing steel curve

As before, the value of  $E_p$  can be determined from the slope of the first linear portion of the curve (See Figure 4-10), in which  $f_{so}$  is the stress defined by the intersection of the two linear portions of the curve. The coefficient  $D$  is determined by trial and error until  $f_{py}$  lies on the curve using a yield strain of 0.01 in./in. Changing the value of  $D$  adjusts the length of the curved transition and thus adjusts the  $f_{py}$  value. For example, lowering  $f_{py}$  will increase the curved transition.

In addition, the Devalapura and Tadros provided recommended coefficients that may be used for specific prestressing steels in conjunction with Eq. 4.50 and to meet the ASTM specifications (see Table 4-4). VSAT provides these coefficients through an option menu as described in Section B.10 of the user manual and provides an option for the user to manually define approximate values for the coefficients  $A$ ,  $B$ ,  $C$ , and  $D$ .



**Figure 4-10: Devalapura and Tadros Model for Defining the Stress-Strain Curve of Prestressing Steel**

**Table 4-4: Coefficients Recommended for Defining the Stress-Strain Behavior of Prestressing Steel by Devalapura and Tadros (1992)**

Steel Type	$f_{py}/f_{pu}$ *	A	B	C	D
270 ksi strand	0.90**	887	27613	112.4	7.360
	0.85	756	27244	117.3	6.598
250 ksi strand	0.90	384	27616	119.7	6.430
	0.85	689	17311	126.7	5.305
250 ksi wire	0.90	435	28565	125.1	6.351
	0.85	734	28266	132.5	5.256
235 ksi wire	0.90	403	28597	133.1	5.463
	0.85	682	28318	141.0	4.612
150 ksi bar	0.85	467	28533	225.2	4.991
	0.80	629	28371	239.3	4.224

\* ASTM minimum specification

\*\* Proposed curve by Devalapura and Tadros;  $E_s = 28,500$  ksi, otherwise  $E_s = 29,000$  ksi for strands and wires and  $E_s = 28,000$  ksi for bars

#### 4.2.5.3 Prestressing Steel Properties

Due to most prestressing steel reinforcement lacking a regular cross-sectional shape and area, VSAT requires that the user to choose between various prestressing steel reinforcement types as provided by the PCI Design Handbook as detailed in Table 4-5 and Table 4-6 (PCI, 2004).

**Table 4-5: Strand Prestressing Steel Properties**

Prestressing Type	Nominal Diameter (in.)	Area (in. <sup>2</sup> )
Seven-Wire Strand, $f_{pu} = 270$ ksi	3/8	0.085
	7/16	0.115
	1/2	0.153
	1/2 special*	0.167
	9/16	0.192
	0.600	0.217
Seven-Wire Strand, $f_{pu} = 250$ ksi	1/4	0.036
	5/16	0.058
	3/8	0.080
	7/16	0.108
	1/2	0.144
	0.600	0.216
Four-Wire Strand, $f_{pu} = 250$ ksi	7/16	0.106
Three-Wire Strand, $f_{pu} = 250$ ksi	1/4	0.036
	5/16	0.058
	3/8	0.075
	7/16	0.106

\*The 1/2 in special has a larger actual diameter than the 1/2 in regular strand. This is taken into account in VSAT.



**Table 4-6: Wire and Bar Prestressing Steel Properties**

Prestressing Type	Nominal Diameter (in.)	Area (In. <sup>2</sup> )
Prestressing Wire, $f_{pu} = 279$ ksi $f_{pu} = 273$ ksi $f_{pu} = 268$ ksi $f_{pu} = 263$ ksi $f_{pu} = 259$ ksi $f_{pu} = 255$ ksi $f_{pu} = 250$ ksi $f_{pu} = 250$ ksi $f_{pu} = 240$ ksi $f_{pu} = 235$ ksi	0.105	0.0087
	0.120	0.0114
	0.135	0.0143
	0.148	0.0173
	0.162	0.0206
	0.177	0.0246
	0.192	0.0289
	0.196	0.0302
	0.250	0.0491
	0.176	0.0598
Bars, $f_{pu} = 145$ ksi	3/4	0.442
	7/8	0.601
	1	0.785
	1 1/8	0.994
	1 1/4	1.227
	1 3/8	1.485
Bars, $f_{pu} = 160$ ksi	3/4	0.442
	7/8	0.601
	1	0.785
	1 1/8	0.994
	1 1/4	1.227
	1 3/8	1.485
Deformed Bars, $f_{pu} = 157$ ksi $f_{pu} = 150$ ksi $f_{pu} = 160$ ksi $f_{pu} = 150$ ksi $f_{pu} = 160$ ksi $f_{pu} = 150$ ksi	5/8	0.28
	1	0.85
	1	0.85
	1 1/4	1.25
	1 1/4	1.25
	1 3/8	1.58

#### 4.2.6 Soil Effects

The following section provides the necessary information to alter the confined concrete curves provided in Section 4.2.3 to accommodate the effects of soil confining pressure.

Effects on both cover and core concrete are examined.

If a column is extended beneath the ground level as a foundation shaft and exposed to a lateral displacement, the soil will exert a confining pressure upon the compression side of the shaft. This can be translated into an additional confining pressure,  $f_{l,soil}$ , that is applied as an effective soil confining pressure,  $f'_{l,soil}$ . The calculation of  $f_{l,soil}$  is currently being defined by a confining pressure and an effectiveness coefficient,  $K_{e,soil}$ . Using the aforementioned guidelines in conjunction with the equations presented in Section 4.2.3, a soil-confined model can be defined that takes into consideration the modifications presented below.

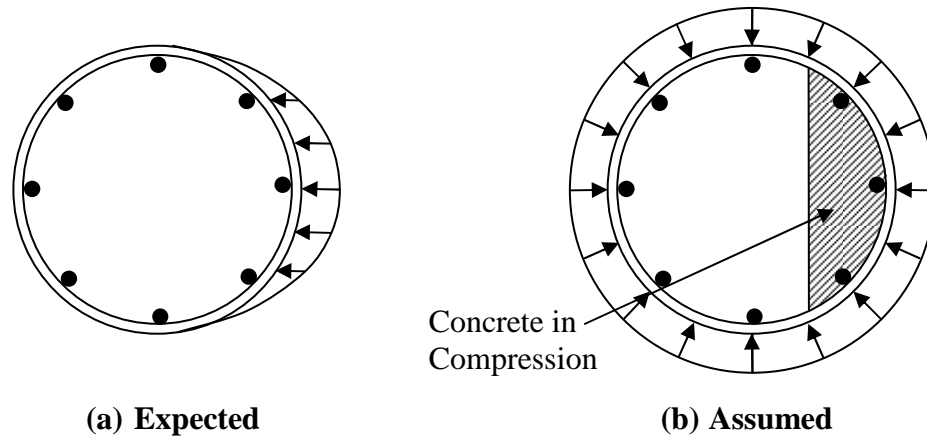
##### 4.2.6.1 Confined Core Concrete

The presence of soil pressure provides a secondary confinement to the concrete section below ground as shown in Figure 4-11; this requires another equation for the calculation of  $f'_l$  for the core concrete. Consequently, Eq. 4.2 for confined concrete is replaced with the following equation for soil-confined core concrete section. The secondary confinement is an estimate of the actual soil pressure applied specifically to the concrete region in compression, which is where the stress-strain behavior of concrete is affected in the analysis.

$$f'_{l,core} = 0.5k_e\rho_s f_{yh} + k_{e,soil}f_{l,soil} \quad \text{Eq. (4.54)}$$

where  $k_{e,soil}$  = Soil effectiveness coefficient

The default soil effectiveness coefficient,  $k_{e,soil}$ , used by VSAT is 0.95 because it was assumed this feature be used mainly for circular sections. This coefficient may be altered by the user as deemed necessary.



**Figure 4-11: Comparison between Expected and Assumed Soil Confining Pressure used in VSAT**

#### 4.2.6.2 Confined Cover Concrete

The presence of soil pressure also provides confinement to the cover concrete. For this reason it is assumed in VSAT that the external soil confinement inhibits the spalling of cover concrete. The cover concrete, which will no longer spall from the section upon reaching the spalling strain, will now continue to contribute to the axial and flexural resistances. It was assumed this confined concrete behavior will follow the equations presented in Section 4.2.3 with the effective confining pressure of Eq. 4.2 replaced by:

$$f'_{l,cover} = k_{e,soil} f_{l,soil} \quad \text{Eq. (4.55)}$$

The soil effectiveness coefficient,  $k_{e,soil}$ , used by VSAT may be altered by the user as deemed necessary.

#### 4.2.7 Steel Shell Effects

The following section provides the necessary information to alter the confined concrete curves provided in Section 4.2.3 to accommodate the effects of an exterior steel shell. Effects on both cover and core concrete will be discussed. These assumptions should be validated with experimental data before used in design.

It is a common practice to encase the column with a steel outer shell especially for circular sections. In such cases, the shell provides an additional confining pressure,  $f_{l,shell}$ , and is applied with an effective confining pressure,  $f_{l,shell}^l$ , while also increasing  $\rho_l$  and  $\rho_s$  of the section. The contribution of the shell to longitudinal/transverse reinforcement is assumed to be 50/50 for VSAT but may be altered by the user as deemed necessary. All equations from Section 4.2.3 for confined concrete are applicable to a shell-confined section except for those mentioned in Sections 4.2.7.1 and 4.2.7.2. If both soil pressure and a steel shell exist, the total confinement pressures may be taken as the sum of the two pressures.

#### 4.2.7.1 Confined Cover Concrete

The presence of a steel shell provides confinement to the “cover” concrete which will no longer spall from the section. Instead, it will follow the confined concrete behavior equations with the following alterations (see Figure 4-12):

$$f_{l,shell} = \frac{2A_{shell,trans} * f_{yh}}{d_t * s} \quad \text{Eq. (4.59)}$$

$$\rho_{s,cover} = \frac{4(A_{sh} * \pi * ds + A_{shell,trans})}{\pi * s * d_t^2} \quad \text{Eq. (4.60)}$$

$$\rho_{cc,cover} = \frac{4(A_s + A_{shell,long})}{\pi * d_t^2} \quad \text{Eq. (4.61)}$$

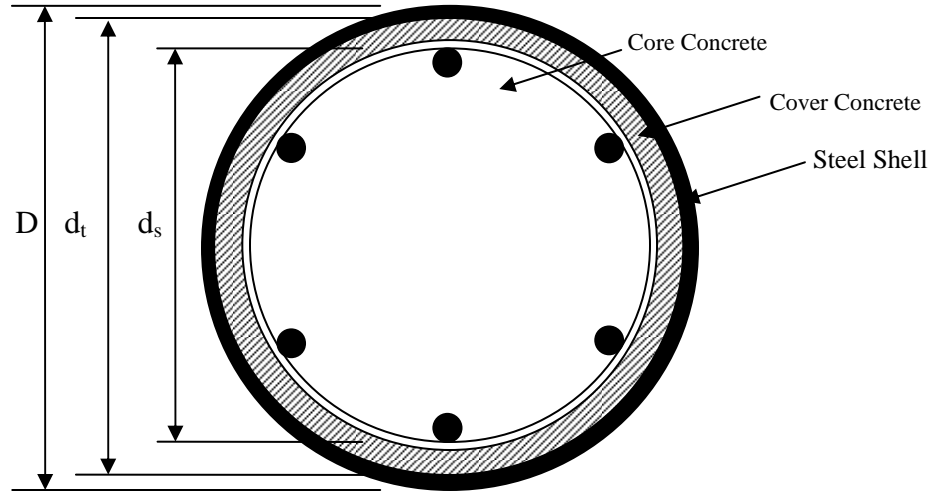
$$A_{shell,long} = \frac{\pi}{4} (D^2 - d_t^2) X_{long} \quad \text{Eq. (4.62)}$$

$$A_{shell,trans} = A_{shell} - A_{shell,long} \quad \text{Eq. (4.63)}$$

where  $X_{long}$  = Percent of total steel shell area contributing to flexural action

$D$  = Gross section diameter

$d_t$  = Diameter of concrete for a circular section with a steel shell



**Figure 4-12: Dimensions of a Circular Section with an Exterior Steel Shell**

#### 4.2.7.2 Confined Core Concrete

The addition of a steel shell also provides a secondary confinement to the concrete section; this requires the alteration of Eqs. 4.2, 4.12 and 4.13 as follows (see Figure 4-12):

$$f'_{l,core} = 0.5k_e\rho_s f_{yh} + k_{e,shell}f_{l,shell} \quad \text{Eq. (4.56)}$$

$$\rho_{s,core} = \frac{4A_{sh}}{sd_s} \quad \text{Eq. (4.57)}$$

$$\rho_{cc,core} = \frac{4A_s}{\pi d_s^2} \quad \text{Eq. (4.58)}$$

where  $k_{e,shell} = 1.0$

The shell effectiveness of 1.0 was chosen because the section is surrounded by a solid steel shell, implying full effectiveness. The effectiveness coefficient,  $k_e$ , for the core concrete follows Eqs. 4.10 and 4.11.

#### 4.2.8 Temperature Effects

Colder temperatures change the behavior of the concrete, mild steel, prestressing steel, and soil. As a result, the moment-curvature response of a concrete section will also change.

The following subsections explain the changes to material properties and models in VSAT when temperatures fall from 20<sup>0</sup>C to as low as -40<sup>0</sup>C so that the moment-curvature analysis can be performed at different temperatures. The temperature changes to these materials are adjusted based upon the available temperature data and the desired analysis temperature.

#### 4.2.8.1 Concrete

The main component attributing to the change in behavior of concrete is the presence and percentage of water. Above 0<sup>0</sup>C, concrete experiences small changes in its behavior because the water has not yet frozen. After the temperature of concrete drops below 0<sup>0</sup>C, the freezing water alters the Young's Modulus ( $E_c$ ), ultimate tensile strength ( $f_t'$ ), ultimate compressive strength ( $f_c$ ), and Poisson's Ratio ( $\nu$ ) of concrete. The modifications to material properties, taken into account by VSAT, are based upon the information provided by Lee et al. (1988) and Van Der Veen and Reinhardt (1989).

The Young's Modulus of concrete varies differently for high strength and normal strength concrete. Both concrete types generally exhibit a linear increase in modulus as the temperature decreases but to different magnitudes. VSAT is designed to address normal strength concrete, but both equations have been provided for further expansion of the program and are as follows:

For high strength concrete:

$$E_{c,cold} = E_c \left( -\frac{t}{415.110} + 1.049 \right) \quad \text{Eq. (4.64)}$$

where  $t$  = temperature in <sup>0</sup>C

For normal strength concrete:

$$E_{c,cold} = E_c \left( -\frac{t}{228.102} + 1.088 \right) \quad \text{Eq. (4.65)}$$

In addition, the maximum compressive strength of concrete increases as the temperature falls below 0<sup>0</sup>C. In 1982, Wiedemann's experimentation showed that the increase in  $f_c'$  is greater in concrete with higher moisture content. He established this conclusion from the observation that  $f_c'$  is not affected by lowering temperatures until the water within the section

begins to freeze (Van Der Veen and Reinhardt, 1989). This proves that the increase in  $f'_c$  is only affected by the increase in strength from the frozen water. VSAT uses the following equations to describe the value of  $f'_c$  for various temperatures based on a linear trendline of the equation presented by Rostasy presented in Figure 2-5 (Van Der Veen and Reinhardt, 1989).

$$f'_{c,cold} = f'_c \quad \text{for } t \geq 0^\circ\text{C} \quad \text{Eq. (4.66)}$$

$$f'_{c,cold} = f'_c - 17.72t\omega \quad \text{for } t < 0^\circ\text{C} \quad \text{Eq. (4.67)}$$

where  $\omega$  = moisture content % (by weight)

Wiedemann also found that an increase in  $f'_t$  also occurs upon lowering the temperature. This increase, however, can still be captured using Eq. 4.30 for  $f'_t$  with the recommended value of  $X$  being the same.

#### 4.2.8.2 Mild Steel Reinforcement

As previously stated in Chapter 3, Young's Modulus and the ultimate tensile strain of A706 mild steel reinforcing are unaffected by a temperature change from 20°C to as low as -40°C. The yield strength,  $f_y$ , increased quadratically by 5.1 percent and thus the yield strain,  $\epsilon_y$ , increases by the same percentage. The ultimate strength,  $f_{su}$ , increased quadratically by 6.3 percent. In order to use the sophisticated model, another data point along the strain hardening curve is needed. As discussed in Chapter 3, this value can be attained from the yield and ultimate increases at a strain of 0.03 in./in. The representation of all three of these strength increases due to temperature, as accounted in VSAT, is as follows:

$$\%Increase_{f_y} = 0.0009(T)^2 - 0.0674(T) + 0.9880 \quad \text{Eq. (4.68)}$$

$$\%Increase_{f_{su}} = 0.0007(T)^2 - 0.0912(T) + 1.5440 \quad \text{Eq. (4.69)}$$

$$\%Increase_{0.03 \text{ in/in}} = (\%Increase_{f_y} + \%Increase_{f_{su}}) / 3 \quad \text{Eq. (4.70)}$$

When creating sections with a mild steel reinforcement type other than Grade 60 and still wishing to use the temperature effects of concrete, the process of defining the material properties needs to be altered. First, a new stress-strain model of the desired material for the given temperature must be determined experimentally. Second, the desired temperature and the analysis temperature should be set to the same value. Finally, set the concrete temperature to room temperature, or the available temperature at which data is known. This process forces the user to enter their own steel properties following Section 4.2.4 that does not allow for temperature alterations. If this is not done, VSAT will alter the steel properties provided by the user in accordance with Grade 60.

#### ***4.2.8.3 Prestressing Steel***

Due to lack of available data in the literature, this feature is currently unavailable.

#### ***4.2.8.4 Soil***

Due to lack of available data in the literature, this feature is currently unavailable. Research is currently being conducted in conjunction with Iowa State University.

#### ***4.2.9 Analysis***

VSAT is designed to perform a uniaxial flexural analysis of concrete sections with or without an external axial load. The uniaxial flexural action indicates that the neutral axis of the section is always parallel to the axis of rotation. Furthermore, the program uses transformed properties for all calculations of stresses, forces and moments and assumes that the external applied axial load acts at the center of the section. The following sections provide information on how the moment-curvature response is constructed within VSAT by addressing section segmentation, the calculation of forces and moments for each material, the location of the neutral axis, the creation of the moment-curvature response, and the limit states used in the analysis.



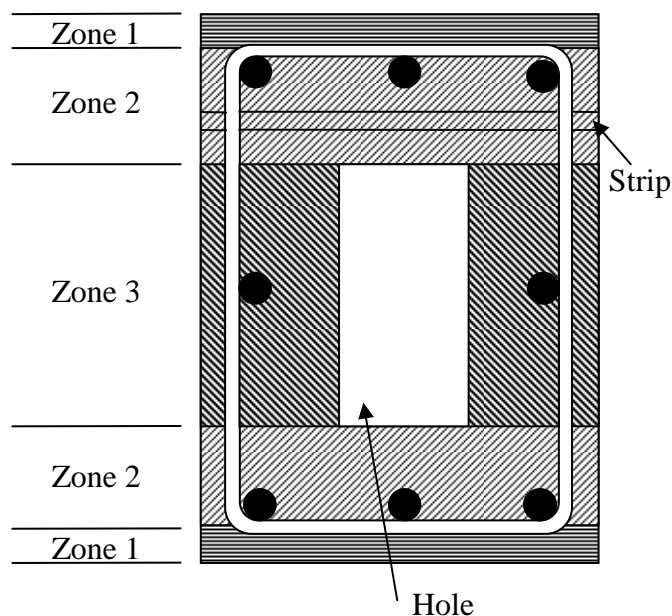
#### **4.2.9.1 Section Segmentation**

In order to conduct an analysis, VSAT must define the amount concrete, steel and prestressing steel located within the section and in such a manner that the stress-strain models of each material can be applied. Thus, the section must be divided three times: first by zone, then by strip, and finally by material (see Figure 4-13).

The first division into zones allow for important locations of different sections, such as the beginning of a core, to later be defined by a series of strips. Each zone, as shown in Figure 4-13, is comprised of different parts based upon what materials are present within the section (e.g., confined concrete, unconfined concrete, hole, mild steel, and prestressing steel). Zone 1, as shown in these figures, only contains cover concrete while Zone 2 contains cover concrete, core concrete, mild steel, and prestressing steel. Similarly, Zone 3 contains all of the materials of Zone 2 with the addition of a “hole area”. If the section is not hollow, Zone 3 does not exist. In the case of the H-Shaped section, where no core is present, Zone 2 does not exist.

After dividing the section into zones, each zone is further segmented into an even number of strips that are approximately 0.25 inch in width initially. The widths of each strip can be altered to satisfy user expectations of accuracy (more strips yields a more accurate answer). This is especially important for circular sections where each strip is modeled as a quadrilateral. This inaccuracy can be minimized by increasing the number of strips used within the section.

Each strip is divided based upon what materials are present within that strip. This division of material is needed to apply the appropriate stress-strain model to its corresponding material area. The stresses are then calculated for each material based upon the strain at the strip’s centerline with the assumption that the strain is constant over each material area for that strip.



**Figure 4-13: Example of Zone, Strip, and Material Segmentation**

#### 4.2.9.2 Forces in Concrete

To calculate the concrete force induced by each strip, the strain and concrete stresses at the centerline of that strip are determined as described in Section 2.3. The strain in each strip is calculated by the following equations (see Figure 4-14):

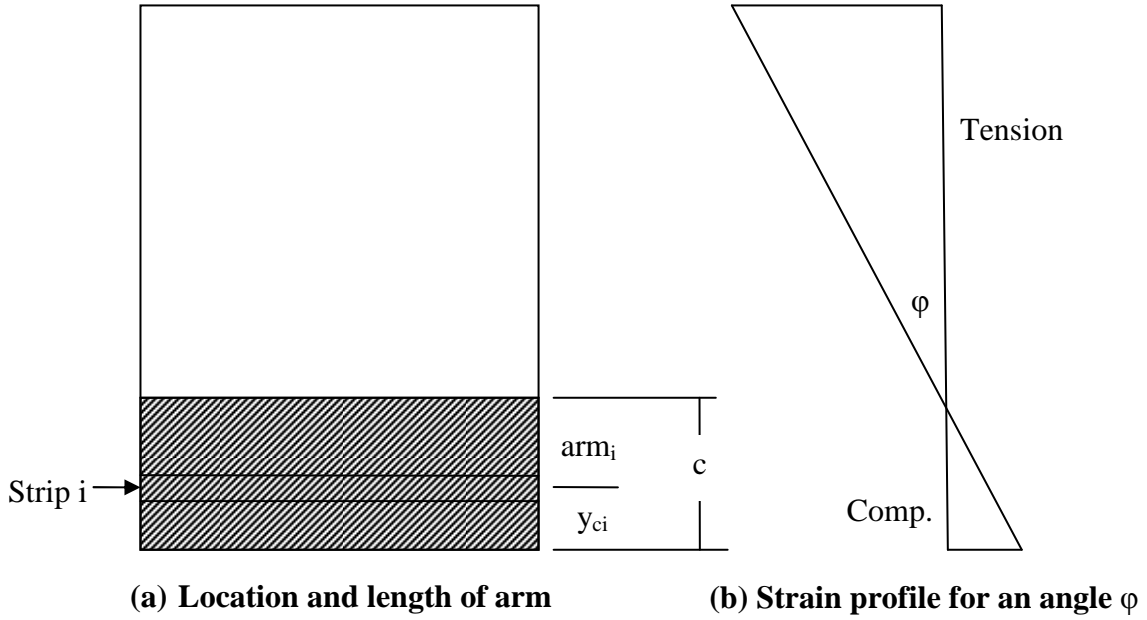
$$\varepsilon_i = arm_i * \tan(\varphi) \quad \text{Eq. (4.71)}$$

$$\text{where } arm_i = c - y_{ci} \quad \text{Eq. (4.72)}$$

$\varphi$  = Strain angle of rotation (i.e., curvature)

$c$  = Neutral axis depth

$y_{ci}$  = Distance from compressive strip  $i$  to the center of the section



**Figure 4-14: Determining the Strain for Strip i and a Given Curvature**

Upon calculating the stresses for each concrete area, the resultant tension and compression concrete forces are determined by multiplying each concrete area by its corresponding stress and using the Eqs. 4.73 and 4.74 for finding  $C_c$  and  $T_c$ , respectively.

$$C_c = \sum A_{cor,compi} * f_{cor,compi} + A_{cov,compi} * f_{cov,compi} \quad \text{Eq. (4.73)}$$

$$T_c = \sum A_{cor,teni} * f_{cor,teni} + A_{cov,teni} * f_{cov,teni} \quad \text{Eq. (4.74)}$$

where  $A_{cor,compi}$  = Area of core concrete in compression zone for strip i

$A_{cov,compi}$  = Area of cover concrete in compression zone for strip i

$A_{cor,teni}$  = Area of core concrete in tension zone for strip i

$A_{cov,teni}$  = Area of cover concrete in tension zone for strip i

$f_{cor,compi}$  = Stress of core concrete in compression zone for strip i

$f_{cov,compi}$  = Stress of cover concrete in compression zone for strip i

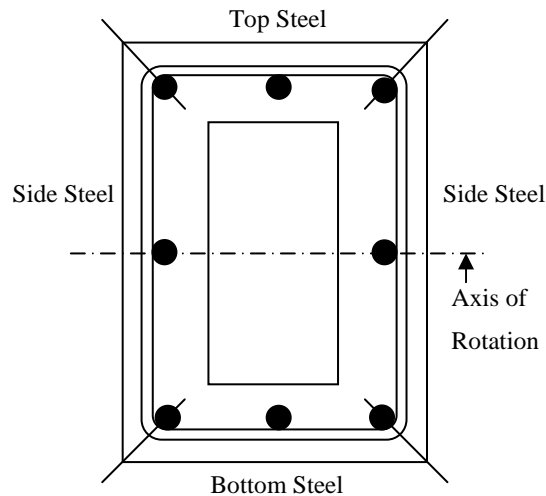
$f_{cor,teni}$  = Stress of core concrete in tension zone for strip i

$f_{cov,teni}$  = Stress of cover concrete in tension zone for strip i

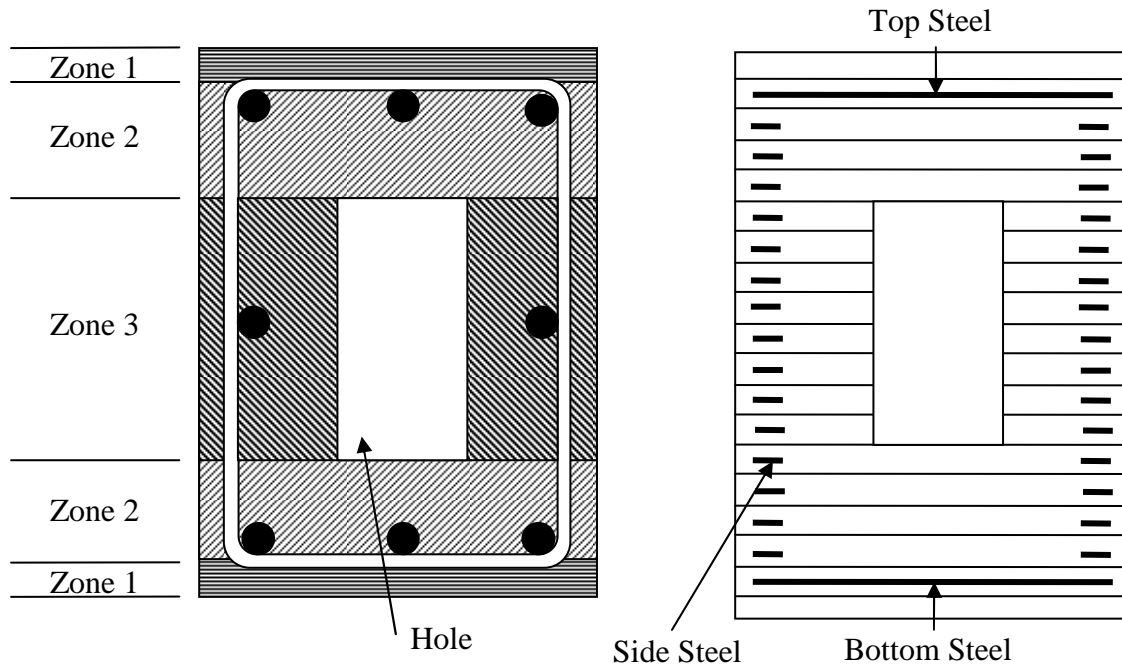
If the neutral axis depth,  $c$ , is located within a strip, the partial areas of that strip contributing to  $C_c$  and  $T_c$  are defined by the portion of the strip that lies within the compression and tension zones. New centerlines for these partial strips are then defined and the process described above is repeated.

#### 4.2.9.3 Reinforcing Steel in Rectangular Sections

Using the division method shown in Figure 4-15, the longitudinal reinforcing steel is split into top, bottom and total side steel. Using the steel distributions, the area per location is smeared along the perimeter of the section at the centerline of the reinforcing bars as shown in the Figure 4-16. The top steel and bottom steel are smeared along the strip located closest to the actual placement of the bars' centroid. The remainder of the steel area is distributed to the strips containing confined concrete (Zones 2 and/or 3) in proportion to the strip width and is assumed to act at the strip centerline. After this distribution has been made, the strains and stresses for the steel may be calculated using the appropriate stress-strain curves. Note that the analysis can only be performed about the axis of rotation, as shown in Figure 4-15, for the rectangular section.



**Figure 4-15: Steel Distribution for Rectangular Sections**



**Figure 4-16: Segmentation of a Rectangular Section and Smearing of Longitudinal Steel Reinforcement**

#### 4.2.9.4 Circular Section Reinforcing Steel

The total area of longitudinal reinforcing steel for circular sections is smeared along the centerline of the reinforcement similar to the rectangular section as shown in Figure 4-16. The steel is then distributed into each strip containing confined concrete (Zones 2 and/or 3) based on the arc length at the steel centerline. As described by King et al. (1986), the proportion of the arc length within each strip, located around the centroid of the rebar configuration, determines the proportion of the total steel area to be placed within that strip. The angle  $\theta_i$  aids in the determination of this arc length and is defined as in Figure 4-17. Each  $\theta_i$  can be calculated as follows:

$$\theta_i = 2 * \cos^{-1} \left( 1 - \frac{y_i - \text{cover} - 0.5d_b}{r} \right) \quad \text{Eq. (4.75)}$$

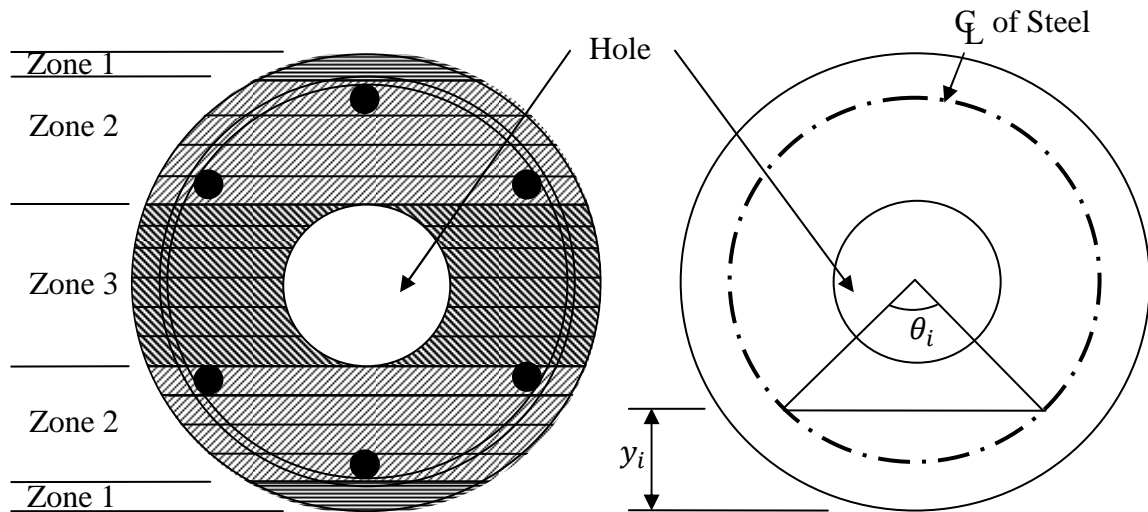
where  $r$  = Radius to the steel centerline from the center of the section

$d_b$  = Diameter of longitudinal reinforcing bar

Therefore, the area of steel within each strip is:

$$A_{s,stripi} = \frac{(\theta_i - \theta_{i-1})}{2\pi} * A_s \quad \text{Eq. (4.76)}$$

As with the rectangular section, the steel areas are assumed to be located at the centerline of each strip for the determination of strains and stresses.

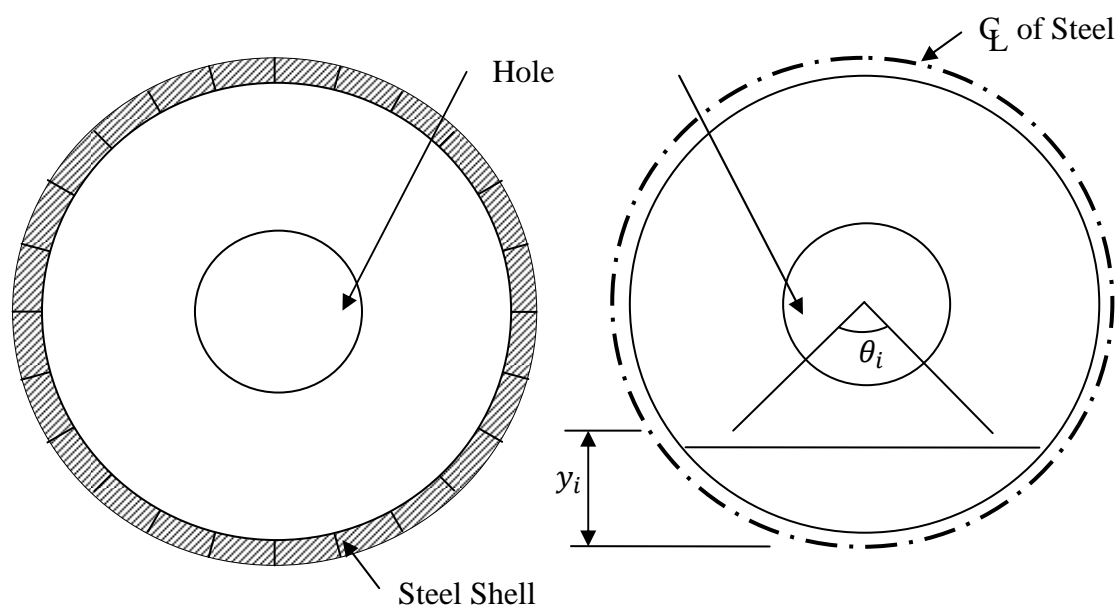


**Figure 4-17: Segmentation of a Circular Section and Smearing of Longitudinal Steel Reinforcement**

If a steel shell exists, the longitudinal portion of the steel is distributed and placed in a radial manner as shown in Figure 4-18. This reduces the amount of calculation and runtime necessary to analyze the section because each “shell strip” contains the same amount of steel from the outer shell. VSAT defines the shell strip’s arc lengths as the average of the strip widths for Zones 1, 2 and 3 as defined in Section 4.2.9.1 while also keeping an even number of strips. The area for each shell strip can then be calculated from:

$$A_{s,shelli} = \frac{Arc_i}{2\pi r} * A_{shell,long} \quad \text{Eq. (4.77)}$$

After these distributions have been made, the strains and stresses for the longitudinal steel may be calculated.



**Figure 4-18: Circular Steel Shell Segmentation and Location**

#### **4.2.9.5 Rectangular Section with Circular Reinforcing Steel**

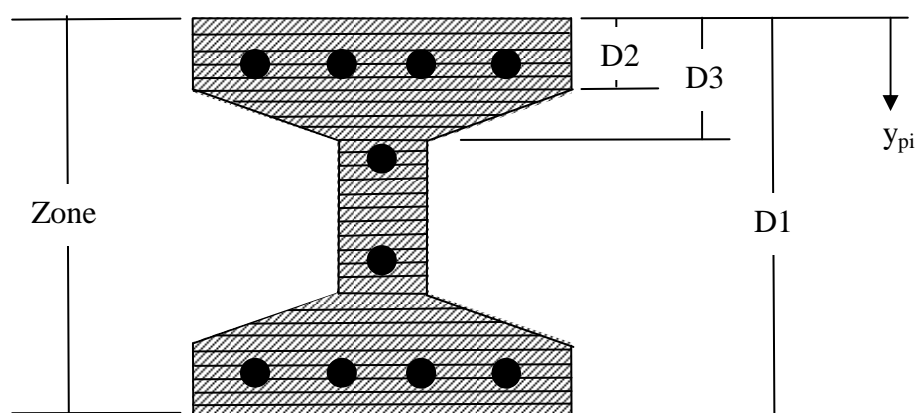
The segmentation of Zones 1, 2 and 3 for a rectangular cross section with a circular longitudinal reinforcement shape follows the segmentation provided in Figure 4-16 and explained in Section 2.9.3 while the smearing of steel follows that provided in Figure 4-17 for a circular section and explained in Section 2.9.4. This method of segmentation was used as to better replicate the behavior of the section, which should be similar to that of a circular section. This approach can be justified by the realization that the cover concrete spalls off early in the analysis leaving only a circular core for the remainder of the response.

#### **4.2.9.6 Octagonal Section with Circular Reinforcing Steel**

Similar to the rectangular section with a circular longitudinal reinforcement shape, the octagonal section is segmented by zones as described in Section 2.9.3 and the steel smeared as provided in Section 2.9.4. This can be justified by the realization that the cover concrete spalls off early in the analysis leaving only a circular core for the remainder of the response.

#### 4.2.9.7 H-Shaped Section

VSAT limits the user to only use UHPC and prestressing steel for the H-shaped section as this section was introduced to assist with ongoing research as ISU. This is due to the absence of a core and the practicality of the section. The H-shaped section is segmented with an even number of strips that is closest to 0.1 in. initially. The user may change this value to ensure that the edges of a strip fall at depths  $D2$  and  $D3$  as shown in Figure 4-19 to ensure that the correct cross-sectional area is calculated. The prestressing steel is located by a value  $y_{pi}$  measured from the top of the section down to the center of the strand. The area of each prestressing strand is subtracted from the concrete area, force and moment to ensure an accurate representation of the section. The strains are calculated at the centerline of the strips for the concrete and at the center of bars for the prestressing steel. After these distributions are made, the strains and stresses for the steel may be calculated.



**Figure 4-19: Section Segmentation of a H-Shape Section and Defining the Location of Prestressing Steel and Cross Section Width Changes**

#### 4.2.9.8 Forces in Mild Steel Reinforcement

To calculate the resultant tensile and compression forces in the mild steel reinforcement of the section, the strain at the centerline of each strip is calculated similar to Section 4.2.9.2 with stresses determined as described in Section 4.2.3. Upon calculating the stresses for each mild steel area, the resultant tension and compression steel forces are determined by



multiplying each mild steel area by its corresponding stress and using the equations for finding the resultant  $C_s$  and  $T_s$  as provided below.

$$C_s = \sum A_{s,compi} * f_{s,compi} \quad \text{Eq. (4.78)}$$

$$T_s = \sum A_{s,teni} * f_{s,teni} \quad \text{Eq. (4.79)}$$

where  $A_{s,compi}$  = Area of mild steel reinforcement in  
compression zone for strip i

$A_{s,teni}$  = Area of mild steel reinforcement in tensile  
zone for strip i

$f_{s,compi}$  = Stress of mild steel reinforcement in  
compression zone for strip i

$f_{s,teni}$  = Stress of mild steel reinforcement in tension  
zone for strip i

If the neutral axis lies within a strip, the strip is divided into a compression and tension zone and the area of mild steel is separated proportional to the new strip areas prior to determining the  $C_s$  and  $T_s$ . The new mild steel areas are then assumed to act at the center of these new partial strips.

#### 4.2.9.9 Forces in Prestressing Steel

To calculate the resultant tensile and compression forces of the prestressing steel, the strain at the centerline of each strip is calculated similar to concrete and mild steel reinforcement with stresses determined as described in Section 4.2.4. These strains include the initial jacking strains of the prestressing strands as well as the decompression strains by requiring the user to enter both the jacking stress and the loss associated with releasing. Upon calculating the stresses for each prestressing steel area, the resultant tension and compression steel forces are determined by multiplying each prestressing steel area by its corresponding stress and using the equations for  $C_p$  and  $T_p$  as provided below.

$$C_p = \sum A_{p,compi} * f_{p,compi} \quad \text{Eq. (4.80)}$$

$$T_p = \sum A_{p,teni} * f_{p,teni} \quad \text{Eq. (4.81)}$$

where  $A_{p,compi}$  = Area of prestressing steel in compression zone for strip i

$A_{p,teni}$  = Area of prestressing steel in tensile zone for strip i

$f_{p,compi}$  = Stress of prestressing steel in compression zone for strip i

$f_{p,teni}$  = Stress of prestressing steel in tension zone for strip i

If the neutral axis lies within a strip, the strip is divided into a compression and tension zone and the area of prestressing steel is separated proportional to the new strip areas before determining the  $C_s$  and  $T_s$ . The new prestressing steel areas are then assumed to act at the center of these new partial strips.

#### 4.2.9.10 Determination of the Neutral Axis Depth

The main challenge when defining the moment-curvature response by hand is finding the neutral axis depth for a given curvature such that the section satisfies force equilibrium and strain compatibility. In other words, the resultant internal axial force,  $P$ , equals the applied axial load,  $P_{applied}$ . If this is not true, every strain, stress, and force for each strip must be recalculated for a different neutral axis depth. This process can become tedious and also can provide a means for human error to occur in the many calculations required for this iterative process. In general, the section equilibrium has been reached for a given curvature when the following equation is satisfied:

$$C_C + C_s + C_p + T_c + T_s + T_p = P = P_{applied} \quad \text{Eq. (4.82)}$$

where  $C_C$  = Resultant concrete compressive force

$C_s$  = Resultant mild steel compressive force

$C_p$  = Resultant prestress compressive force

$T_c$  = Resultant concrete tensile force

$$\begin{aligned}
T_s &= \text{Resultant mild steel tensile force} \\
T_p &= \text{Resultant prestress tensile force} \\
P &= \text{Resultant internal force} \\
P_{applied} &= \text{Applied axial load}
\end{aligned}$$

If equilibrium is not satisfied, VSAT uses an iterative process to determine the correct neutral axis depth. Each new neutral axis depth is based upon the previous two and their corresponding axial loads by the following equation:

$$c = c_2 + \frac{(P_{applied} - P_2)(c_2 - c_1)}{P_2 - P_1} \quad \text{Eq. (4.83)}$$

where  $c_1$ ,  $c_2$ ,  $P_1$ , and  $P_2$  are the neutral axis and axial load values for the two previous iterations

In order to reduce runtime, if both axial loads are higher or lower than the applied axial load, the first neutral axis depth becomes the second and the second depth is determined as a fraction of the first. Upon reaching a set of neutral axis depths, where one internal axial load lies on either side of the applied axial load, the previous iteration method (Eq. 4.83) is adopted. The iteration process of each neutral axis depth for a given curvature is stopped when the internal axial load is within acceptable limits of the applied axial load. This acceptable limit is given as a percentage of the applied axial load which is provided by the user and expressed in Eq. 4.84.

$$|P_{1 \text{ or } 2} - P_{applied}| \leq X * |P_{applied}| \quad \text{Eq. (4.84)}$$

where  $X$  = Coefficient defining iteration accuracy

The default value used for  $X$  in VSAT is 0.01% of the applied axial load.

#### 4.2.9.11 Calculation of Moment Capacity

Upon determining each correct neutral axis depth, the moment capacity of the section is calculated by determining the internal moment resistance. The moment is determined from summing all applied forces times their moment arms about the centerline of the section parallel to the axis of rotation and is expressed numerically by Eq. 4.85.

$$\begin{aligned}
 M = & \sum f_{cor,compi} * A_{cor,compi} y_{ci} + \sum f_{cov,compi} * A_{cov,compi} y_{ci} + \\
 & \sum f_{cor,teni} * A_{cor,teni} y_{ti} + \sum f_{cov,teni} * A_{cov,teni} y_{ti} + \\
 & \sum f_{s,compi} * A_{s,compi} y_{ci} + \sum f_{s,teni} * A_{s,teni} y_{ti} + \\
 & \sum f_{p,compi} * A_{p,compi} y_{ci} + \sum f_{p,teni} * A_{p,teni} y_{ti}
 \end{aligned}
 \tag{4.85}$$

where  $y_i$  = Distance from strip I to the center of section

Summing the moment about the center of the section, rather than the neutral axis, allows the moment capacity to be determined without inducing a moment from the applied external axial load.

#### 4.2.9.12 Calculation of Moment-Curvature Response

VSAT iterates on the neutral axis depth for every chosen curvature value with the exception of the first three predefined points: the cracking, first yield, and ultimate curvatures; see Figure 4-20. The preceding three curvatures are defined by particular strains and then iterated using Eq. 4.86. Two initial curvature values are taken, the corresponding neutral axes are calculated to ensure the target strain is attained, and then the corresponding internal axial loads are determined. From the two previous axial load and curvature values, a new curvature (if needed) can be determined as follows:

$$\phi = \phi_2 + \frac{(P_{applied} - P_2)(\phi_2 - \phi_1)}{(P_2 - P_1)}
 \tag{4.86}$$

where  $\phi_1$ ,  $\phi_2$ ,  $P_1$ , and  $P_2$  are the neutral axis depths and axial loads for the two previous iterations

The cracking curvature (i.e., the curvature at which the section first cracks) occurs when the extreme concrete strain reaches the cracking strain or the ultimate tensile strain,  $\epsilon_t$ , as defined by the user. The first yield curvature is defined as the lowest curvature at which either the steel strain,  $\epsilon_s$ , reaches 0.004 in./in. or the concrete strain reaches  $\epsilon'_{co}$ . The ultimate curvature is the lowest curvature at which the steel reaches the maximum tension strain of  $\epsilon_{stu}$ , the steel reaches the maximum compressive strain of  $\epsilon_{scu}$ , or the compression concrete strain reaches  $\epsilon_{cu}$ . Each curvature is said to have been reached when the above conditions occur and equilibrium is satisfied.

Once these three curvatures and their corresponding parameters are defined, intermediate curvature values are evenly spaced in portions 1 and 2 of the moment-curvature curve, which are defined in Figure 4-20. Portion one of the graph is the distance between the lower of the first yield and the cracking curvature and five times the larger of the two. Portion two of the graph is the distance between five times the larger of the first yield and cracking curvature and the ultimate curvature.

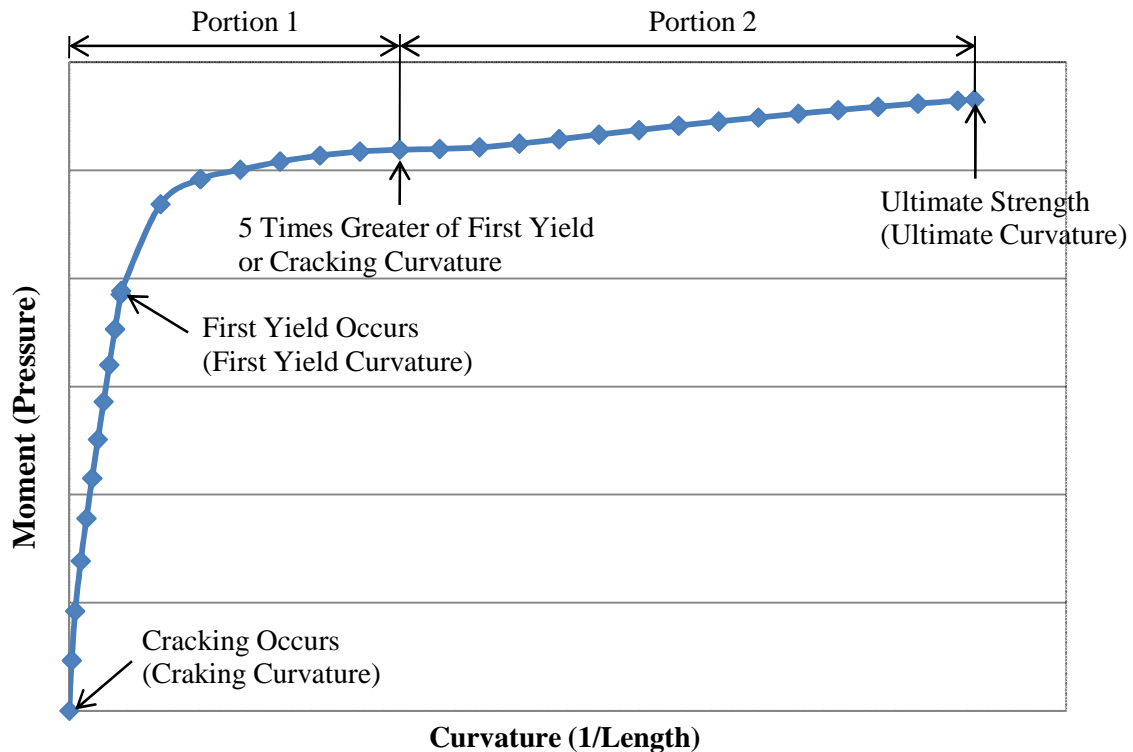


Figure 4-20: Moment-Curvature Response Segmentation and Conditions

#### 4.2.9.13 Conditions for Stopping Analysis

VSAT has six conditions which will stop the analysis. This ensures that the analysis will not get into a continuous loop or that the program will produce data beyond reaching the ultimate curvature. These conditions are as follows:

- No solution can be found with over 1000 iterations not determining a solution
- The entire section exceeds the maximum compressive strain,  $\varepsilon_{cu}$ , under the initial axial load
- The concrete strain exceeds  $\varepsilon_{cu}$  (Eq. 4.31)
- The tensile steel strain exceeds  $\varepsilon_{stu}$
- The compressive steel strain exceeds  $\varepsilon_{scu}$
- The user defined maximum curvature has been reached

If the analysis is stopped for any of these reasons, the ultimate curvature is defined as the curvature previous to that which terminated the analysis and, thus, the moment-curvature curve in Figure 4-20 can be created.

## Chapter 5: EXAMPLE PROBLEMS AND VALIDATION

### 5.1 Introduction

This chapter presents examples of different VSAT analyses and provides validation of VSAT where possible. The example problems also demonstrate accurate execution of VSAT. The section's details, including reinforcement configuration, and moment-curvature response graph are provided. Also, where applicable, moment-curvature responses were created using other means to validate the analysis results of VSAT and appropriate comments are made on the similarities and dissimilarities of the results from different analysis programs.

### 5.2 Circular Concrete Section

The example circular concrete section, seen in Figure 5-1, is comprised of a 60 in. concrete diameter with 30 #11 longitudinal bars. The concrete model used was that presented in Section 4.2.3.1 with  $f'_c = 5$  ksi and the simplified mild steel reinforcement model with  $f_y = 66$ ksi as described Section 2.4.

#### 5.2.1 Comparison of VSAT to King's Program

Since this section is based upon essentially the same concrete and steel models as that used by King's Program, only small little differences in the moment-curvature response should be found. As shown by Figure 5-2, the moment-curvature responses of VSAT and King's Program are almost identical. Although not visible, slight variation in the moment at each curvature is found due to minor alterations in the concrete model from the one used in King's Program. A difference in the curvature capacity of the section is observed and justified because the ultimate concrete strain in King's Program and VSAT are also defined differently, with VSAT using that proposed by Paulay and Priestley (1992). If VSAT's ultimate concrete strain is altered to match that used in King's Program, the difference in curvature capacity dissipates.

**External Axial Load:**      **Long. Reinforcement:**

$P_n = 700$  kip

$A_s = 30 - \#11s$  (46.80 in<sup>2</sup>)

**Concrete:**

$f'_c = 5$  ksi

$f_y = 66$  ksi

Simplified Model

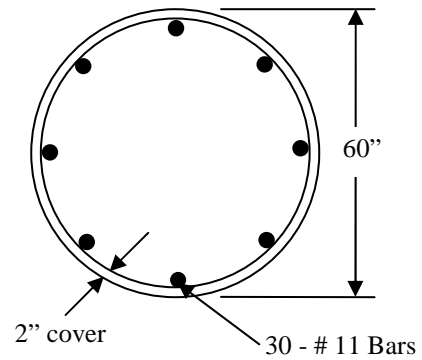
No Tension Capacity

**Trans. Reinforcement:**

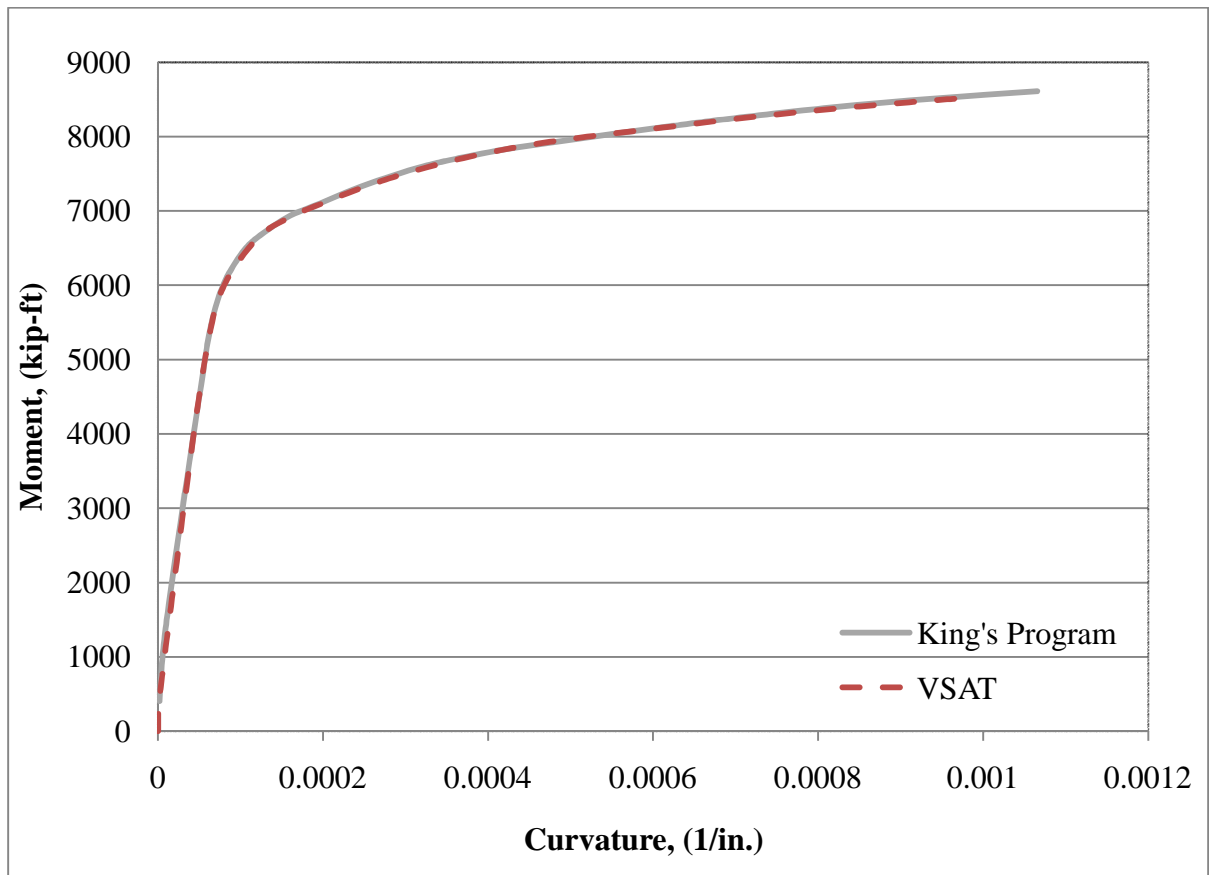
$A_{sh} = \#5 @ 4$  in. spacing

Spirals

$f_{yh} = 60$  ksi



**Figure 5-1: Details of the Circular Section Example**



**Figure 5-2: Moment-Curvature Comparison for the Example Circular Section in Figure 5-1**



### 5.3 Rectangular Concrete Section

The example rectangular section, seen in Figure 5-3, is comprised of a 36x36 in. concrete configuration with 20 #14 longitudinal bars. The concrete and mild steel reinforcement models used were similar to the circular section with  $f'_c = 5$  ksi and  $f_y = 66$ ksi.

#### 5.3.1 Comparison of VSAT to King's Program

Similar to the circular concrete section, essentially the same concrete and steel models as those in King's Program were used, only small little differences in the moment-curvature response should be found. As shown by Figure 5-4, the moment-curvature responses of VSAT and King's Program are almost identical. Although not visible, slight variation in the moment at each curvature is found due to minor alterations in the concrete model from the one used in King's Program. As with the circular concrete section, a difference in the curvature capacity of the section is observed and justified because the ultimate concrete strain in King's Program and VSAT are also defined differently, with VSAT using that proposed by Paulay and Priestley (1992). If VSAT's ultimate concrete strain is altered to match that used in King's Program, the difference in curvature capacity dissipates.

#### External Axial Load: Long. Reinforcement:

$$P_n = 525 \text{ kip}$$

$$A_{s,ten} = 6 - \#14s (13.50 \text{ in}^2)$$

#### Concrete:

$$f'_c = 6 \text{ ksi}$$

No Tension Capacity

$$A_{s,side} = 8 - \#14s (18.00 \text{ in}^2)$$

$$A_{s,comp} = 6 - \#14s (13.50 \text{ in}^2)$$

$$f_y = 66 \text{ ksi}$$

Simplified Model

#### Trans. Reinforcement:

$$A_{sh} = \#5 @ 3 \text{ in. spacing}$$

Rectangular Ties (4 x- and y-  
Direction Legs)

$$f_{yh} = 60 \text{ ksi}$$

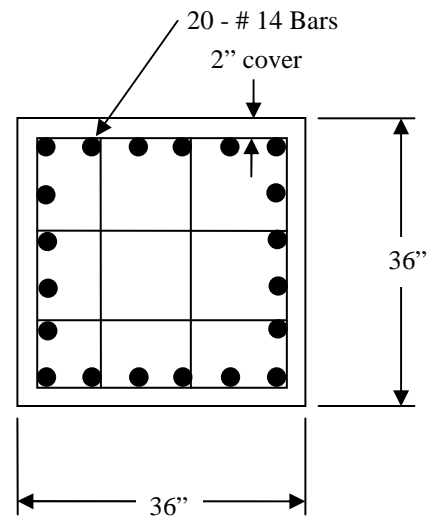
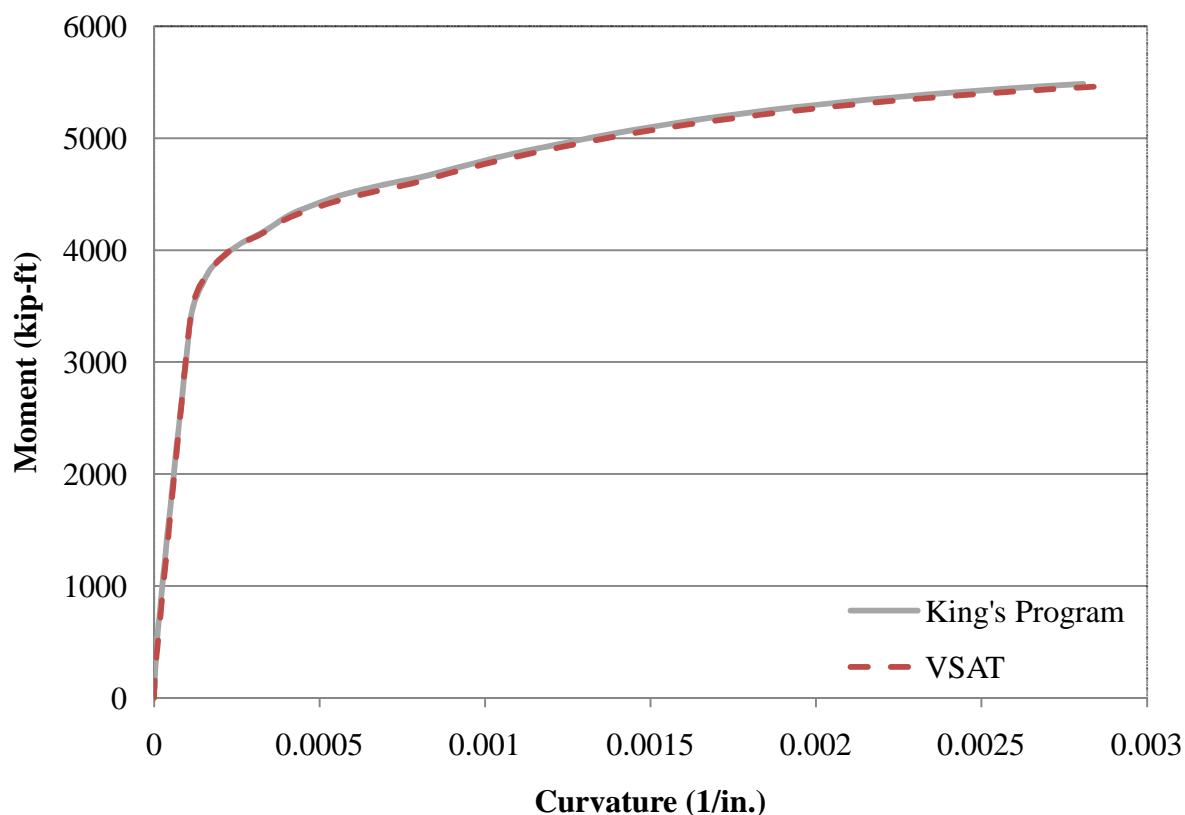


Figure 5-3: Details of the Rectangular Section Example



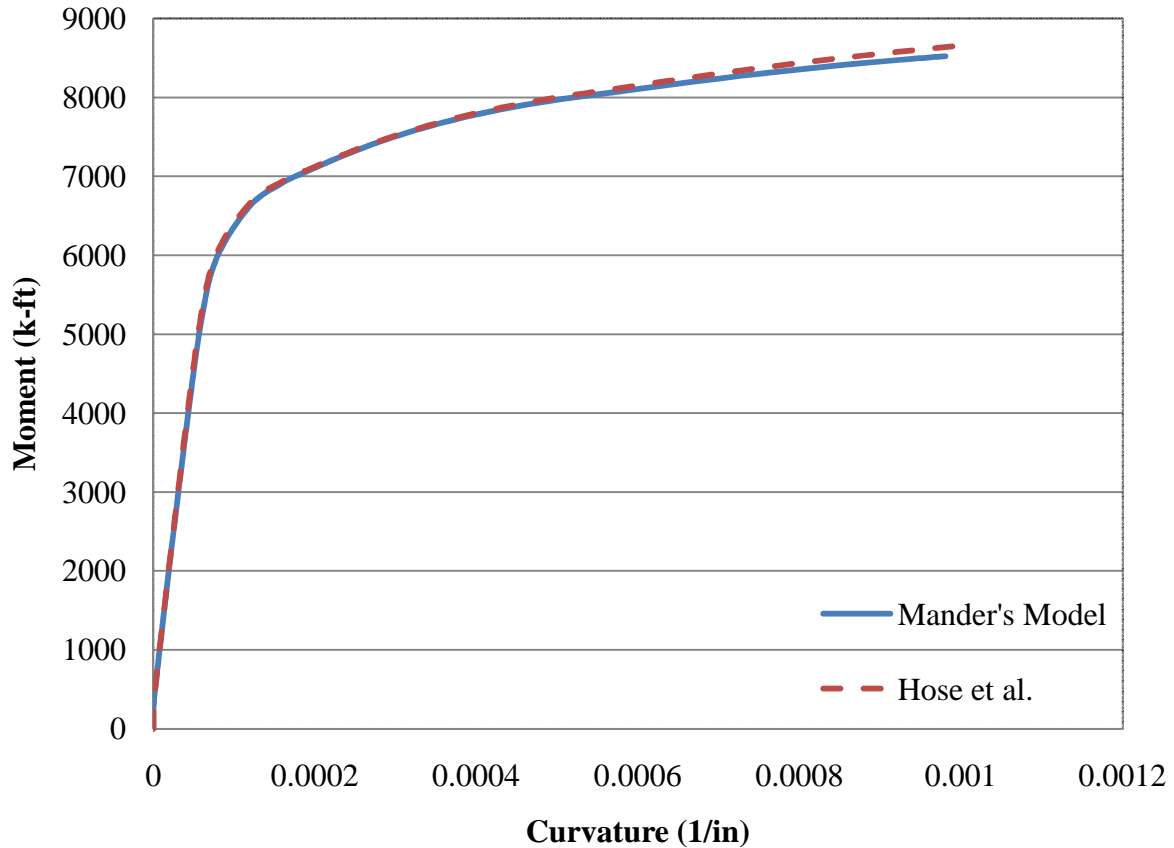
**Figure 5-4: Moment-Curvature Comparison for the Rectangular Section Example in Figure 5-3**

#### 5.4 Circular Section with Different Concrete Models

As stated in previous chapters, two models were provided in VSAT for the definition of confined and unconfined concrete. With the same input as the circular section found in Section 5.2, the effects of utilizing Hose et al.'s modified from Mander et al.'s over the original model proposed by Mander et al. will be examined. The additional information required is as follows:  $\eta = 20$ ,  $J = 1/3$ ,  $f_{yh} = 66\text{ksi}$ , and no yield plateau occurs in transverse reinforcement stress-strain graph.

As shown in Figure 5-5, slight changes occur in the moment curvature analysis. A 0.43% reduction in the cracking curvature, a 1.89% reduction in the first yield curvature, and a 2.85% increase in the ultimate curvature occurred when using Hose et al.'s concrete model over the model proposed by Mander et al. The moments corresponding to the curvatures

mentioned also increased by 0.17%, 0.30%, and 1.65% respectively. It is important to note that these results, though important, tend to greatly increase the analysis run time. This is due to the nature of how the stress-strain graph need be developed, incrementally stepping to each desired strain.



**Figure 5-5: Moment-Curvature Comparison of Different VSAT Concrete Models**

### 5.5 H-Shaped UHPC Section

The UHPC H-shaped section, as shown in Figure 5-6, consists of a 10x10 in. imprint with a total prestressing area of 1.53 in.<sup>2</sup>. The UHPC model was based upon that presented in Section 4.2.3.6 and the prestressing model was based upon that presented in Section 2.5 with the parameters set to create as close to a bi-linear curve as possible to reflect Vande Voort et al.'s work. This particular example was chosen because the stopping condition of the moment dropping below 80% of the maximum moment was needed.

5.5.1 Comparison of VSAT to Vande Voort et al. (2008)

As shown in Figure 5-7, the moment-curvature response produced by VSAT and Vande Voort et al. overlap identically, as expected. Note that the VSAT graph continues slightly after the 80% of the maximum moment mark, as it is impractical to calculate this value directly. This value was manually found in an excel program by Vande Voort et al.

**External Axial Load:    Prestressing:**

$P_n = 370 \text{ kip}$

$A_p = 1.53 \text{ in.}^2$

**UHPC:**

$f_{pi} = 202.5 \text{ ksi}$

$f'_c = 26 \text{ ksi}$

$E_p = 28,000 \text{ ksi}$

$E_c = 8,000 \text{ ksi}$

$\epsilon_{pu} = 0.05 \text{ in./in.}$

$f'_{te} = 1.30 \text{ ksi}$

Close to bi-linear curve

$f'_{t,max} = 1.70 \text{ ksi}$

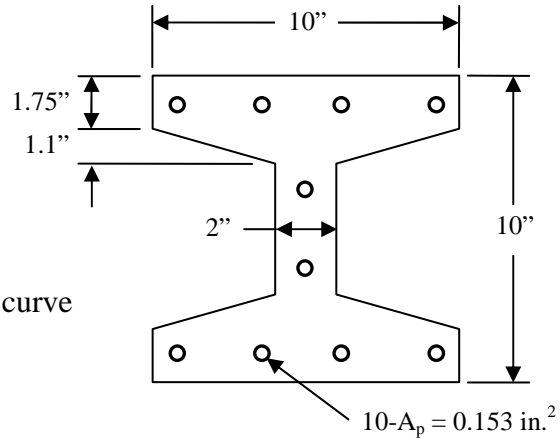


Figure 5-6: Example H-Shape Section Details

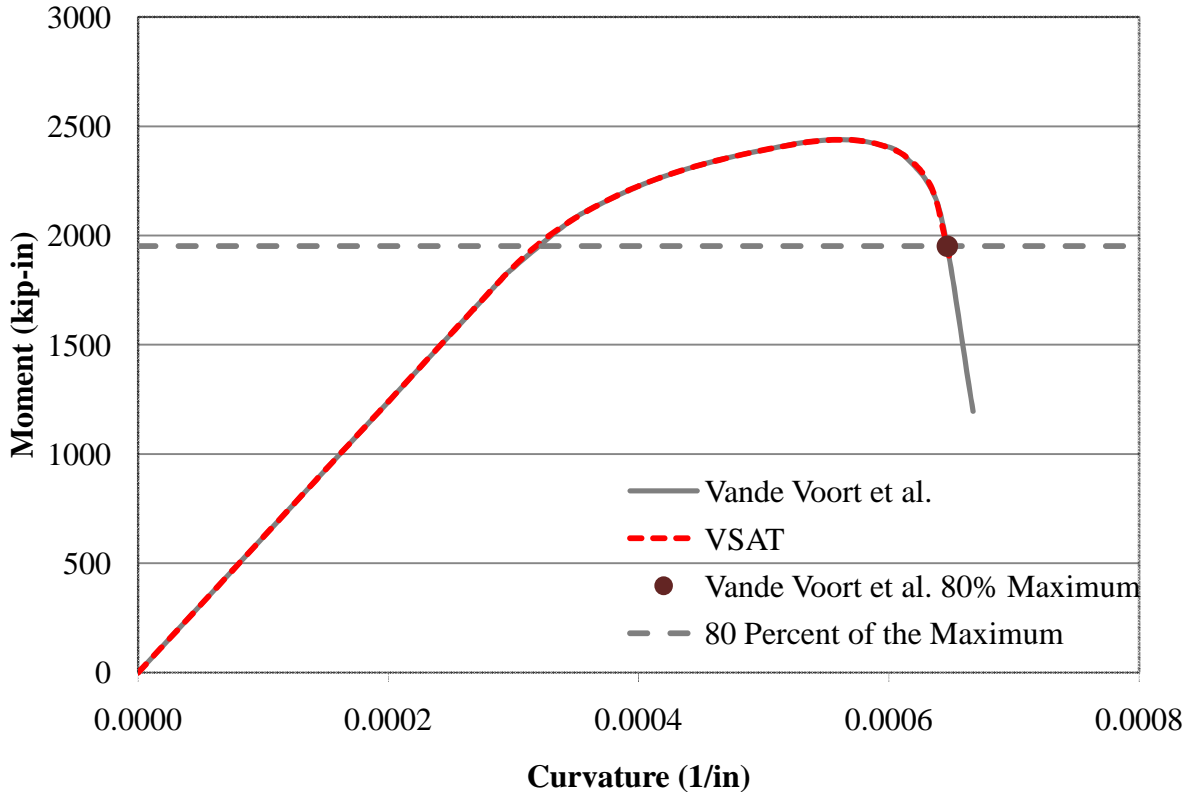


Figure 5-7: Moment-Curvature Comparison of Example H-Shaped Section

## 5.6 Rectangular Concrete Section with Circular Prestressing Steel Configuration

As shown in Figure 5-8, the section is comprised of a 14in square cross section with a circular core. The five ½ in strands follow the Menegotto and Pinto model with the provided values to mimic that used in another program.

### 5.6.1 Comparison of VSAT to Vande Voort et al. (2008)

Figure 5-9 shows a few comparisons to OpenSees. First, the section was analyzed with VSAT using the same prestressing information as OpenSees but with the computer-generated concrete model was as described in Section 4.2.3 as shown in Figure 5-9. As shown, even with smearing the prestressing steel and the concrete model proposed by Mander et al. (1988b), the moment-curvature response contour is comparable to OpenSees. The discrepancy is believed to be due to the assumption in VSAT, used to ease the user's input while insuring the moment resistance, that the reinforcement is smeared along its centerline. It is unclear the exact placement of the 5 prestressing strands in OpenSees which can greatly alter the moment-curvature response. Further investigation into the development of VSAT need be conducted to ensure this is indeed the cause of the moment-curvature response discrepancy.

The second analysis required the adjustment of the concrete stress-strain curve to fit that defined in OpenSees. This required the values of  $K_e$  and  $\epsilon'_{co}$  in VSAT to be changed to 0.63 and 0.0025, respectively. As shown in the figure, a decrease in the confined concrete strength of concrete by 2ksi can have a significant impact on the sections performance. Again, further investigation into the development of VSAT need be conducted to ensure this is indeed the cause of the moment-curvature response discrepancy.

**External Axial Load: Long. Reinforcement:**

$P_n = 490 \text{ kip}$

$A_p = 5 - \frac{1}{2} 270 \text{ ksi } (0.153 \text{ in.}^2)$

**Concrete:**

$E = 29,000 \text{ ksi}$

$f'_c = 10 \text{ ksi}$

$f_{pu} = 266 \text{ ksi}$

No Tension Capacity

$\epsilon_{pu} = 0.04$

**Trans. Reinforcement:**

$f_{py} = 245 \text{ ksi}$

$A_{sh} = \#3 @ 0.8076 \text{ in.}$

$\epsilon_y = 0.010$

spacing

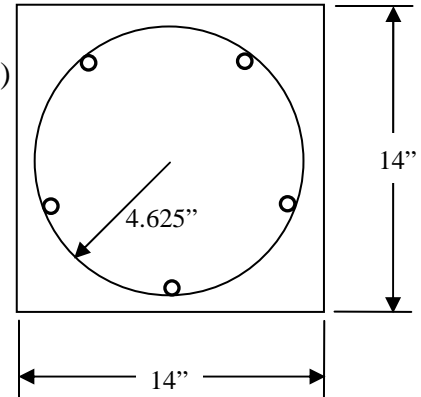
Menegotto and Pinto

Spirals

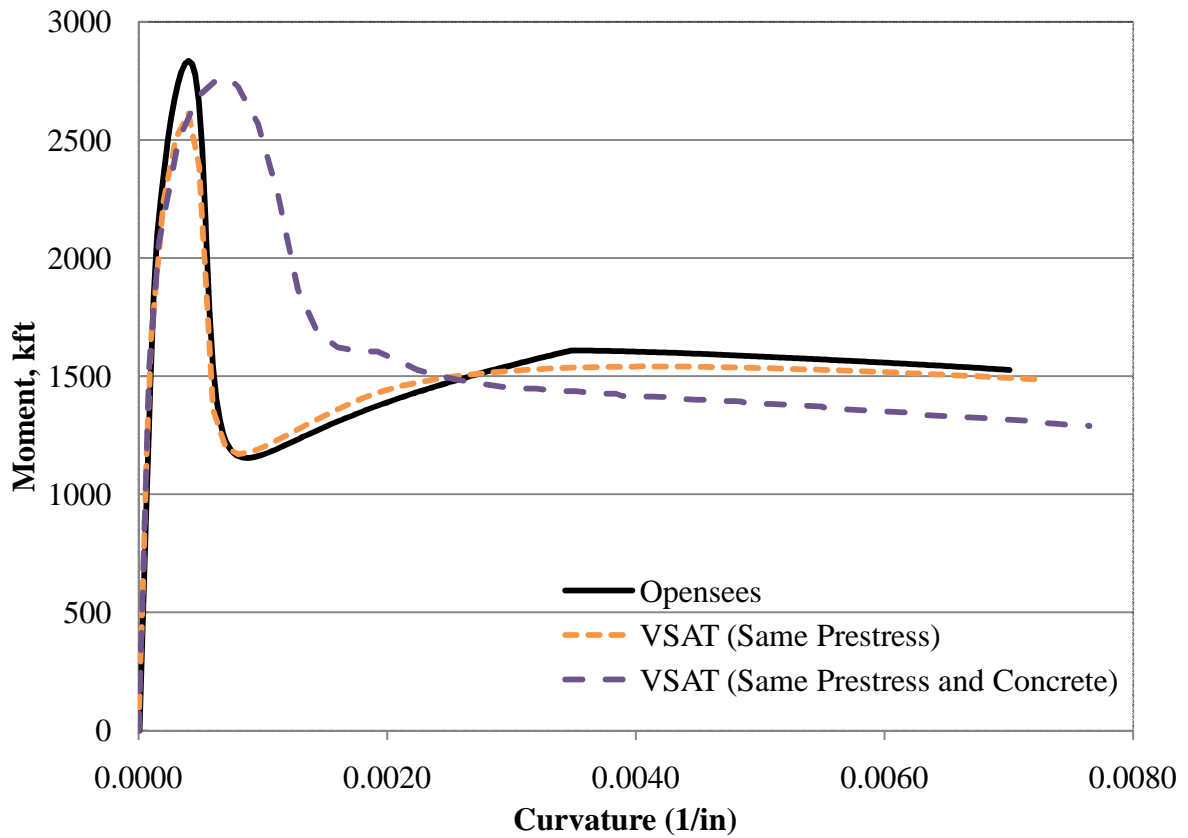
$N = 400, K = 1, Q = 0.022951$

$f_{yh} = 60 \text{ ksi}$

Transfer Stress = 30.5877 ksi



**Figure 5-8: Example Prestressed Section Details**

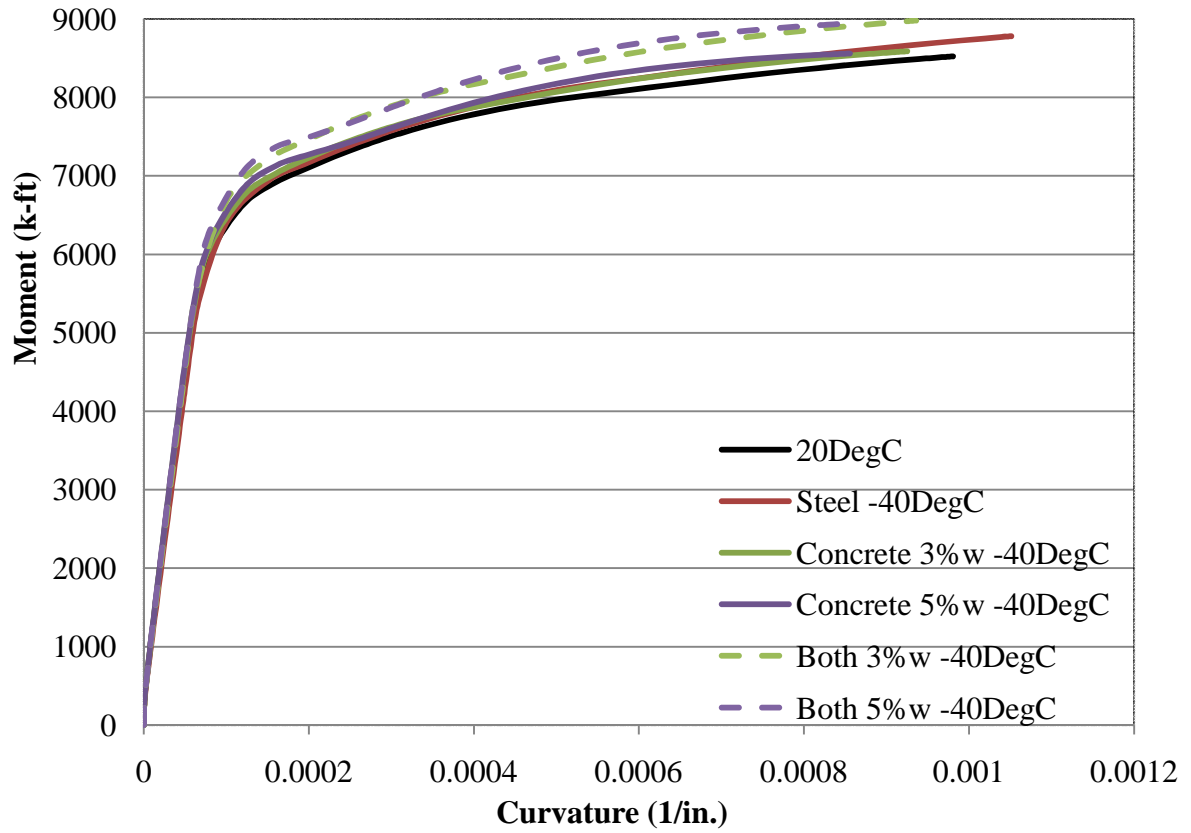


**Figure 5-9: Moment-Curvature Comparison to OpenSees**

## 5.7 Effects of Temperature

The effects of temperature on the behavior of mild steel reinforcement, but not that for concrete, has been completed for this project. To better understand the effects of temperature on the moment-curvature response, and due to the uncompleted testing of concrete at low temperatures, separate comparisons for adding the effects of temperature on mild steel reinforcement, on concrete with different water contents, and on both materials are provided in Figure 5-10. The examples used to develop this comparison follow that provided in Section 5.2 with material temperature effects modified as necessary. These examples were checked internally in VSAT to ensure no error occurred during defining the stress-strain behavioral changes due to temperature.

As shown in Figure 5-10, changing the behavior of only mild steel in accordance with Chapter 3 causes a slight increase in moment capacity and curvature ductility of this particular section. The figure also shows that changing the behavior of only concrete causes a slight increase in moment capacity with a reduction in curvature. Note that the impact on the moment-curvature response is dependent upon the concrete's water content. When combining the effects of temperature on mild steel and concrete, this particular section shows an overall increase in moment capacity with a reduction in curvature ductility. Note that this may not be the case with all possible sections; a general assumption must not be made.



**Figure 5-10: Temperature Effects on Moment-Curvature Response**



## Chapter 6: SUMMARY, CONCLUSIONS AND RECOMMENDATIONS

### 6.1 Introduction

The following chapter summarizes the information provided in this document. In addition, the conclusions made from the research presented in this report are provided followed by recommendations for future research and the expansion of VSAT.

### 6.2 Summary

Currently established moment-curvature analysis programs lack features that are beneficial or crucial to the structural design of concrete sections under seismic loading. The effects of temperature, inclusion of soil pressure confinement, versatility in stress-strain definition, and standard reinforcement sizes and areas to aid the user in design are among some of these shortcomings. A moment-curvature program, VSAT, was developed that provided these features in order to attain the better moment-curvature responses of concrete cross sections.

As part of this project, the effects of temperature on various types of steel previously tested were found. From this research, no trend could be adopted to define the stress-strain behavioral changes of ASTM A706 mild steel reinforcement. This was due to the difference in material, challenges during testing, and the exclusion of the effects of temperature on the strain hardening region of the stress-strain graph. To attain the desired information, testing was conducted on two different milled bar sizes at temperatures varying from 20°C to -40°C.

The development of VSAT is a conglomeration of several different material models for concrete, mild steel, UHPC, and prestressing steel. This was deemed necessary to develop a versatile section analysis tool capable of performing different concrete sections, as well as, standard pile and foundation cross sections. Additional information on default bar sizes, areas, and model constants were utilized in VSAT to aid the user in analyzing a section with ease regardless of how limited their knowledge of the material behaviors are.

To provide example problems and verify that VSAT was functioning properly, comparisons were made to results obtained using other established programs. Due to VSAT being a pioneer in including the effects of temperature, the stress-strain behavioral changes of

mild steel reinforcement were verified by hand calculations. Hand calculations were also performed for the other equations used in VSAT to ensure no calculation error occurred during an analysis.

### **6.2.1 VSAT**

The additional features deemed necessary for VSAT provided several observations. These features, observations and the methodology as to why they are necessary are discussed below.

The inclusion of tensile concrete strength, though a minor contribution, does have an effect on the cracking curvature of the section. Defining this strength by strain or stress was added to allow the user to define the cracking condition of the section.

The user has the option of including prestressing steel behavior in compression. It may also be assumed that the steel contributes no force or moment to the section upon reaching a compressive strain. A strand by itself exhibits little resistance in compression but one surrounded by concrete does have a compressive resistance. This is possible by the inclusion of transverse reinforcement and concrete that help prevent buckling of the material. The inclusion of this compressive stress will alter the location of the neutral axis and, therefore, the moment-curvature response.

The accuracy of the moment-curvature response can be increased or decreased by altering the strip width or the number of points generated for the graph. The decreasing of strip width or increasing of data points can have a significant impact on the run-time for the section being analyzed.

Dropping below 80% of the maximum moment was made optional because it is an ultimate condition in VSAT. If chosen, the ultimate condition is found when the section is finished or the section reaches 80% of the maximum moment resistance, whichever occurs first. If a moment is calculated below 80% of the maximum, VSAT iterates to get as close to this value as possible as indicated by the H-Shaped section example in Chapter 5.

Sometimes a section has no particular solution for the specific curvature being analyzed. This is common when large concrete strips of the section are on the verge of

crushing. If this occurs, the neutral axis depth becomes very sensitive and may cause an endless loop iteration. A cap has been put on the number of iterations to be performed before skipping to the next point to reduce run-time and avoid a computer error. This may be avoided by decreasing the strip width.

VSAT directly calculates cracking, first yield and ultimate curvature values. This saves the user from using interpolation or extrapolation in the analysis. A more accurate representation for the ductility of the section can also be developed for sections due to this feature.

### 6.3 Conclusions

From the work conducted for this thesis, several conclusions can be drawn. The following conclusions are reflective of the work mentioned previously in this document for the effects of temperature and the development of VSAT.

#### 6.3.1 *Temperature Effects on A706 Mild Steel*

This thesis has presented an investigation on the effects of cold temperature from 20°C to -40°C and strain rate variation from 0.003 in./in./min. to 0.3 in./in./min. on the behavioral changes of A706 mild steel reinforcement for the purposes of designing structures that undergo seasonal freezing. The following conclusions were made of A706 mild steel:

- The material behavior of A706 mild steel reinforcement is altered even before reaching -32°F (0°C). This is complimentary to previous research on other materials but dissimilar to the assumption made by NCSU for the material. Behavioral changes were experienced at 5°C and may occur at even warmer temperatures, though less significant in magnitude. This observation is consistent with the trend observed for the material behavior in the temperature range between 20°C and -40°C.
- There is a discrepancy between the cross-sectional area of the actual reinforcing bar and the ASTM nominal that varies with bar size. It was found that the unmilled area of the experimental rebar was 4.3 percent smaller than the ASTM area for the #8 rebar and 2.3 percent smaller for the #6 rebar.

- The modulus of elasticity is insignificantly affected by temperature and strain rate and should, therefore, assumed to be a constant value.
- The yield and ultimate strength increases of A706 mild steel reinforcement vary quadratically instead of linearly as suggested by Filiatrault and Holleran for CSA G30.16 reinforcing steel.
- An increase in the yield and ultimate strengths of 5.1 and 6.3 percent were experienced for A706 mild steel reinforcement, respectively, when lowering the temperature from 20°C to -40°C.
- The magnitude of temperature increases for the yield and ultimate strengths of A706 mild steel are generally lower than those suggested in previous research on other materials, particularly the 8 percent increase in yield strength and 12 percent increase in ultimate strength at -30°C as shown by Sloan (2005) for A706 mild steel reinforcement.
- The impact of temperature on the ultimate strength of A706 mild steel reinforcement, with an overall increase of 3 percent, is greater than that on the yield strength, 1.67 percent, and is opposite to previous research conducted on other materials.
- Although a complete conclusion on the effects of bar size could not be made, it is apparent that bar size may affect the magnitudes at which the increase in yield and ultimate strength occur.
- The yield plateau generally dissipates as the strain rate increases and it was found to diminish upon reaching a strain rate of 0.3 in./in./min.

### 6.3.2 VSAT

The following conclusions were made when comparing VSAT output with established section analysis tools and determining the effects of temperature and external soil pressure.

- It is apparent from Chapter 5 that VSAT is capable of providing accurate output for circular, rectangular, and prestressed H-shaped sections. This is shown by the close relationship of the moment-curvature response between VSAT and previous models and/or programs.

- The moment-curvature responses of prestressed sections that utilize normal concrete do not match those given by OpenSees, but are similar in contour. When changing the concrete parameters in VSAT to better fit OpenSees, the relationship deviates. Further investigation is needed to determine why this occurred.
- The temperature effects used in this program are directly representative of the testing performed for this thesis or have been assumed until ongoing research at Iowa State University can be completed. The moment-curvature response of a section can be significantly altered at temperatures as warm as 0°C.
- The moment-curvature response of a section can be significantly altered with external soil pressures as low as 10 psi.

## 6.4 Recommendations

Due to time constraints and the scope of this project, several items could not be researched that deserve attention. The following section provides information and/or concerns that may need to be further researched.

### 6.4.1 Temperature Effects

After the completion of the testing for this project, it was found that the stress-strain behavior of mild steel and the strength increases associated with temperature may be dependent on the bar size. Although this influence appears small, this topic should be fully researched for validation. It is recommended that additional testing be conducted similar to that described in Chapter 3. Choose one bar size the same as the testing conducted for this thesis and one or two additional sizes such as #11, #14, or #4 reinforcing bars. This will provide a range of bar sizes, rather than two as used for this project, to determine if indeed the bar size affects both the stress-strain behavior and the strength increases associated with temperature.

In addition, cyclic testing on the material should be conducted to verify that the stress-strain behavior utilized for VSAT is applicable under seismic loading. One can determine whether the stress-strain behavior varies differently in the elastic, plastic, and strain hardening region as it was seen in this project that the yield plateau tends to decrease as the

strain rate increases. Cyclic testing should be conducted at various rates, to reflect the effects of different seismic activity. This also provides a range of information to be used at a later date when more knowledge of seismic activity is known and a representative strain rate can be chosen for the region of the country in interest.

The effects of temperature on the behavior of soil and prestressing steel should also be considered. As shown in Chapter 5, the effects of just one component within the section can have a drastic increase in the moment-curvature response of the section. For this reason, and to provide completeness, this should also be done for all materials likely to be within the section of interest.

Due to the lack of research conducted on circular columns with exterior steel shells likely to be used in colder regions of the U.S. (e.g., Alaska), a test matrix need be designed that incorporates both the core and cover concrete. This should include the effects on the stress-strain behavior of both concrete types. Note that careful attention to the effects on core concrete with varying inner transverse reinforcement, such as a spiral, need be addressed. This information should then replace those equations initially used in VSAT and provided in Chapter 4.

#### **6.4.2 Additional Material Properties**

Aside from the effects of temperature, the behavior of soil and its effects on concrete performance needs to be correctly quantified. The behavior of soil, both cohesionless and cohesive, need be examined. The behavior of the soil undergoing displacement should first be captured. Then, tests to determine the effects upon both confined and unconfined concrete sections should be analyzed. This will allow VSAT to be altered to better reflect the effects of soil rather than assuming the same effects as transverse steel on the performance of confined or core concrete.

As shown by OpenSees and VSAT with the Mander's Concrete Model, there is a discrepancy between the confined strength and behavior of concrete. Further investigation is needed to determine a more accurate stress-strain relationship for the behavior of concrete or if a modification of an older model is necessary. Research should be conducted on high- and

low-strength concrete separately to determine if these concrete types may be expressed with a single model or needs to utilize multiple models.

Due to the advantages of using hollow sections, such as weight and price reduction, a test matrix needs to be developed to analyze the behavior of concrete of circular and rectangular hollow sections. The strength of the inner surface of the section, depending on if one or two layers of transverse reinforcement are used, should be examined.

### **6.4.3 VSAT**

As with any analysis program, there is room for improvement and expansion. It is recommended that VSAT be updated as the previously mentioned information is gathered to better reflect field performance of sections. Due to time constraints the following features were not added to VSAT that should, eventually, be included: external moment, hollow sections, steel shell validation, temperature effects of soil and prestressing steel, an arbitrary section option, and the ability to define reinforcement locations in a section rather than steel smearing (similar to the H-Shaped section).

## REFERENCES

- AASHTO Guide Specifications for LRFD Seismic Bridge Design. (2009). *1st Edition*, 8-1 to 8-36. Washington DC: American Association of State Highway and Transportation Officials.
- AASHTO LRFD Bridge Design Specifications. (2007). *4th Edition*. Washington DC: American Association of State Highway and Transportation Officials.
- ACI 318. (2008). Building Code Requirements for Structural Concrete (ACI 319-08) and Commentary. *ACI 18-05*, 266, 407. Farmington Hills, MI.
- ACI. (2008). Building Code Requirements for Structural Concrete (ACE 318-08) and Commentary. American Concrete Institute.
- ASTM Standard A615. (2009). Standard Specification for Deformed and Plain Carbon-Steel Bars for Concrete Reinforcement. West Conshohocken, PA: ASTM International.
- ASTM Standard E8. (2004 (2006)). Standard Test Methods for Tension Testing of Metallic Materials. West Conshohocken, PA: ASTM International.
- Bridge*. (2009, May 28). Retrieved May 28, 2009, from Wikipedia: The Free Encyclopedia: <http://en.wikipedia.org/wiki/Bridge>.
- Bruneau, M., Uang, C.-M., & Whittaker, A. (1997). *Ductile Design of Steel Structures*. New York: McGraw-Hill.
- Budek, A. M., Priestley, M. J., & Benzoni, G. (2004). The Effect of External Confinement on Flexural Hinging in Drilled Pile Shafts. *Earthquake Spectra* , 20 (1), 1-24.
- Collins, M., & Mitchell, D. (1997). *Prestressed Concrete Structures*. Canada: Response Publications.
- Concrete Reinforcing Steel Institute. (1990). *ASTM A706 REINFORCING BARS TECHNICAL INFORMATION WITH COMMENTARY ON USAGE AND AVAILABILITY*. Schaumburg, IL.
- Devalapura, R., & Tadros, P. P. (1992). Stress-Strain Modeling of 270 ksi Low-Relaxation Prestressing Strands. *PCI Journal* , 37 (2), 100-106.
- Dodd, L. L., & Restrepo-Posada, J. I. (1995). Model for Predicting Cyclic Behaviour of Reinforcing Steel. *Journal of Structural Engineering* , 121 (3), 433-445.



- Ensoft, Inc. (2005, February 9). *LPILE Plus 5.0 for Windows*. Retrieved August 24, 2009, from Ensoft, Inc.: Computer-based solutions of complex geotechnical and structural engineering challenges: <http://www.ensoftinc.com/>.
- Filiatrault, A., & Holleran, M. (2002). Characteristics of Reinforced Concrete Bridge Components Under Seismic Strain Rates and Low Temperatures. In D. Sanders (Ed.), *Proceedings of the 18th US-Japan Bridge Engineering Workshop*, (pp. 49-63). Reno.
- Filiatrault, A., & Holleran, M. (2001). Stress-strain behavior of reinforcing steel and concrete under seismic strain rates and low temperatures. *Materials and Structures*, 34, 235-239.
- Gustafson, D. (2007, January). *Revisiting Low-Alloy Steel Reinforcing Bars*. Retrieved May 5, 2009, from BNET: [http://findarticles.com/p/articles/mi\\_qa5363/is\\_200701/ai\\_n21290713/?tag=content;coll](http://findarticles.com/p/articles/mi_qa5363/is_200701/ai_n21290713/?tag=content;coll).
- Hose, Y., Brestel, D., Seible, F., & Dowell, R. (2001). *Assessment of Hoop Strains in the Flexural Plastic Hinge Region of Typical Bridge Columns*. University of California at San Diego.
- Jha, G., Singh, A., Bandyopadhyay, N., & Mohanty, O. (2001). Seismic Resistant Reinforcing Bars. *Journal of Failure Analysis and Prevention*, 53-56.
- King, D. J., Priestley, M. J., & Park, R. (1986). *Computer Programs For Concrete Column Design*. University of Canterbury, Department of Civil Engineering, Christchurch, New Zealand.
- Lee, G. C., Shih, T. S., & Chang, K. C. (1988). Mechanical Properties of High-Strength Concrete at Low Temperatures. *Journal of Cold Regions Engineering*, 2 (4), 169-178.
- Mander, J. B., Priestley, J. N., & Park, R. (1988). Observed Stress-Strain Behavior of Confined Concrete. *Journal of Structural Engineering*, 114 (8), 1827-1849.
- Mander, J. B., Priestley, J. N., & Park, R. (1988). Theoretical Stress-Strain Model for Confined Concrete. *Journal of Structural Engineering*, 114 (8), 1804-1826.
- Mazzoni, S., McKenna, F., Scott, M. H., & Fenves, G. L. (2009, May). *OpenSees Features*. Retrieved August 24, 2009, from OpenSees: <http://opensees.berkeley.edu/index.php>.
- Montejo, L. A., Kowalsky, M. J., & Hassan, T. (2008). *Seismic Behavior of Reinforced Concrete Bridge Columns at Sub-Freezing Temperatures*. North Carolina State University, Constructed Facilities Laboratory. Raleigh: Alaska Department of Transportation.

- Naaman, A. (1985). Partially Prestressed Concrete: Review and Recommendations. *PCI Journal* , 30 (6), 32-71.
- Naaman, A., & Harajli, M. (1985). Evaluation of the Ultimate Steel Stress in Partially Prestressed Flexural Members. *PCI Journal* , 30 (5), 54-76.
- Paulay, T., & Priestley, M. (1992). *Seismic Design of Reinforced Concrete and Masonry Buildings*. New York: John Wiley & Sons, Inc.
- PCI, I. H. (2004). *PCI Design Handbook. 6th Edition*, 11-30/31. (P. L. Martin, & S. P. Perry, Eds.) Chicago, Illinois: Precast/Prestressed Concrete Institute.
- Priestley, M. J., Seible, F., & Calvi, G. M. (1996). *Seismic Design and Retrofit of Bridges*. New York: John Wiley & Sons, Inc.
- Sehna, Kronen, & Marshall. (1983). Factors Influencing the Low Temperature Strength of Concrete. *Second International conference on Cryogenic Concrete*. Amsterdam, Netherlands: London: Concrete Society.
- Sloan, J. E. (2005). *The Seismic Behavior of Reinforced Concrete Members at Low Temperatures*. MS Thesis, North Carolina State University, Civil, Construction, and Environmental Engineering, Raleigh.
- Sritharan, S., & Shelman, A. (2008). An Assessment of Broad Impact of Seasonally Frozen Soil on Seismic Response of Bridges in the U.S. and Japan. *Proceedings of the 24th US-Japan Bridge Engineering Workshop*.
- Sritharan, S., Suleiman, M. T., & White, D. J. (2007). Effects of Seasonal Freezing on Bridge Column-Foundation-Soil Interaction and Their Implications. *Earthquake Spectra* , Volume 23 (1), 199-222.
- Stover, & Coffman. (2009, January 30). *New Madrid Earthquakes 1811-1812*. Retrieved May 28, 2009, from USGS: Science for a Changing World: <http://earthquake.usgs.gov/regional/states/events/1811-1812.php>.
- Suleiman, M. T., Sritharan, S., & White, D. (2006). Cyclic Lateral Load Response of Bridge Column-Foundation-Soil Systems in Freezing Conditions. *Journal of Structural Engineering*, 132 (11).
- TRC/Imbsen Software Systems. (2009). *IAI Xtract*. Retrieved August 23, 2009, from IAI Software: <http://www.imbsen.com/xtract.htm>.

U.S. Geological Survey. (2009, 6 26). *Historic United States Earthquakes*. Retrieved 8 1, 2009, from USGS: Science for a Changing World:  
<http://earthquake.usgs.gov/regional/states/historical.php>.

Van Der Veen, C., & Reinhardt, H. W. (1989). Bond Strength in Reinforced Concrete at Low Temperatures. *Proceedings of the Eighth International Conference on Offshore Mechanics and Arctic Engineering*. 3, pp. 573-582. New York: The American Society of Mechanical Engineers.

Vande Voort, T. L., Suleiman, M. T., & Sritharan, S. (2008). *Design and Performance Verification of UHPC Piles for Deep Foundations*. Iowa State University, Structural Engineering. Ames: Center for Transportation Research and Education.

Wiedemann. (1982). *Zum Einfluss tiefer Temperaturen auf Festigkeit und Verformung von Beton*. Dissertation Technische Universität Braunschweig.

## APPENDIX A: A706 MILD STEEL ADDITIONAL GRAPHS

The following section provides additional information on the results of testing A706 mild steel reinforcement as discussed in Chapter 3. The effects of temperature on the elastic modulus, yield plateau length, and ultimate strain are discussed along with the effects of strain rate on the elastic modulus and ultimate strain. The last portion of this section provides a comparison between the recommended strength increases discussed in Chapter 3 and the experimental data.

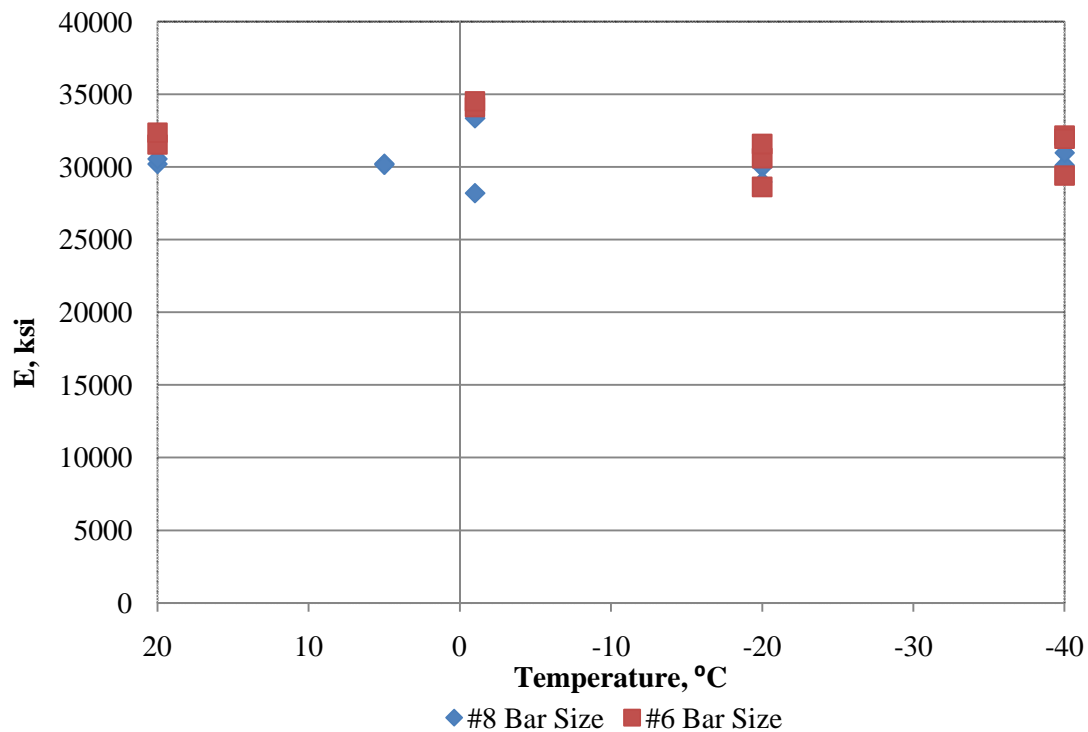


Figure A-1: Modulus of Elasticity vs. Temperature at 0.001896 in./in./min.

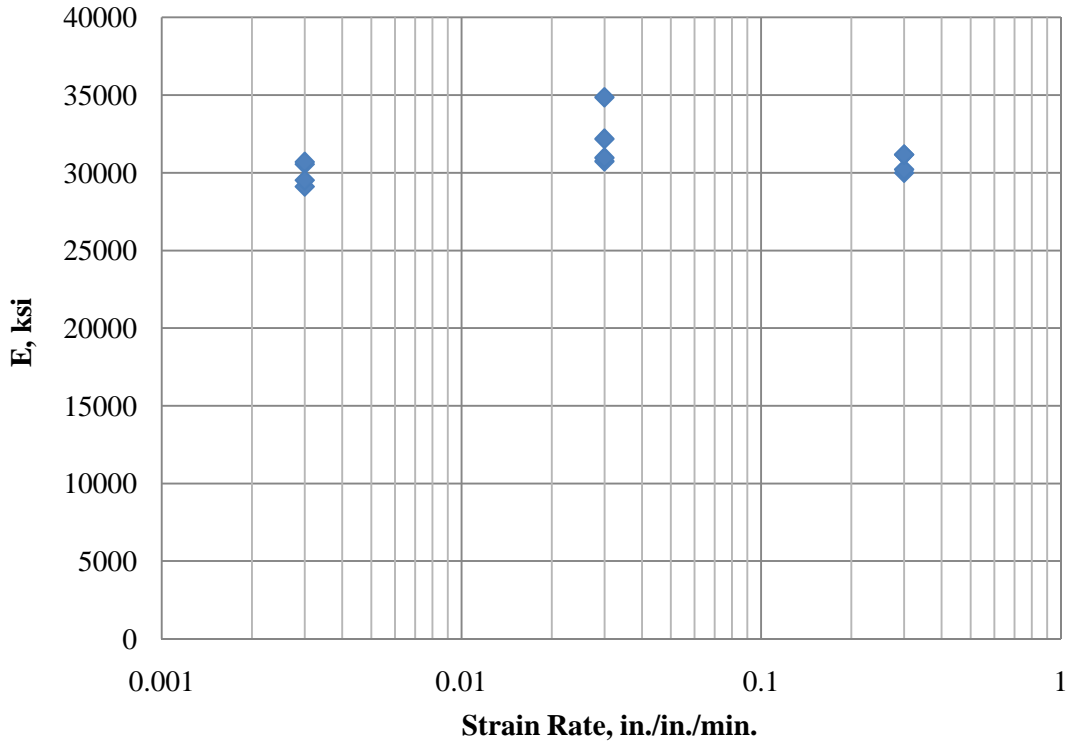


Figure A-2: Modulus of Elasticity vs. Strain Rate

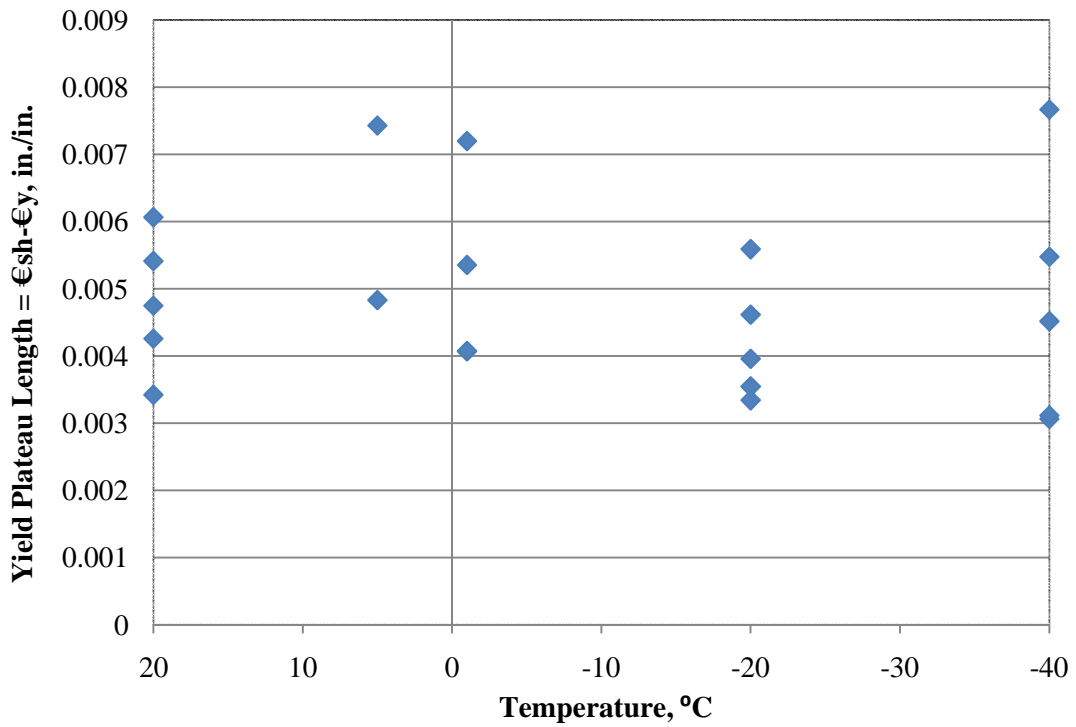


Figure A-3: Yield Plateau Length vs. Temperature at 0.001897 in./in./min.

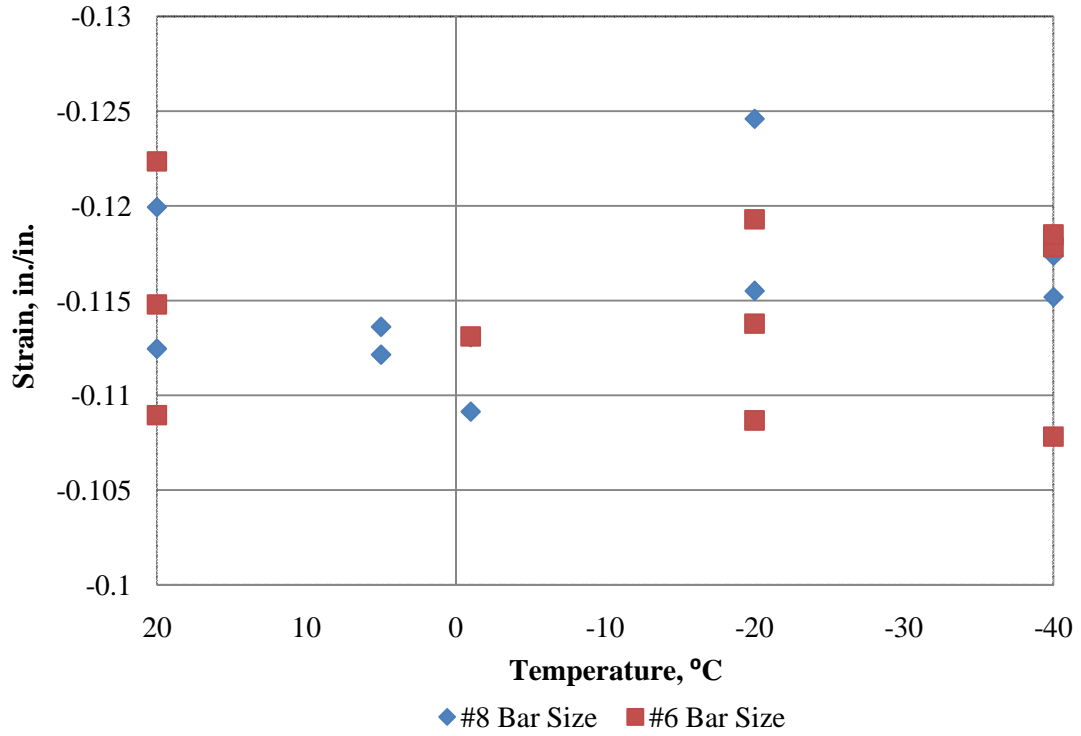


Figure A-4: Ultimate Strain vs. Temperature at 0.275 in./in./min.

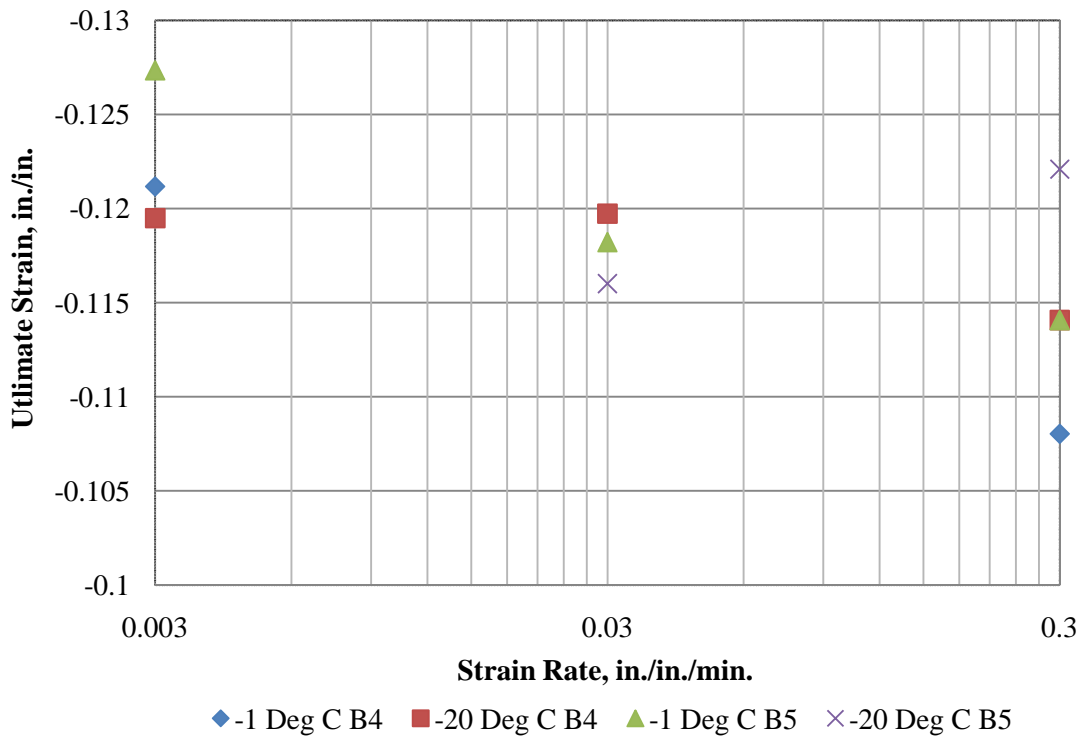


Figure A-5: Ultimate Strain vs. Strain Rate

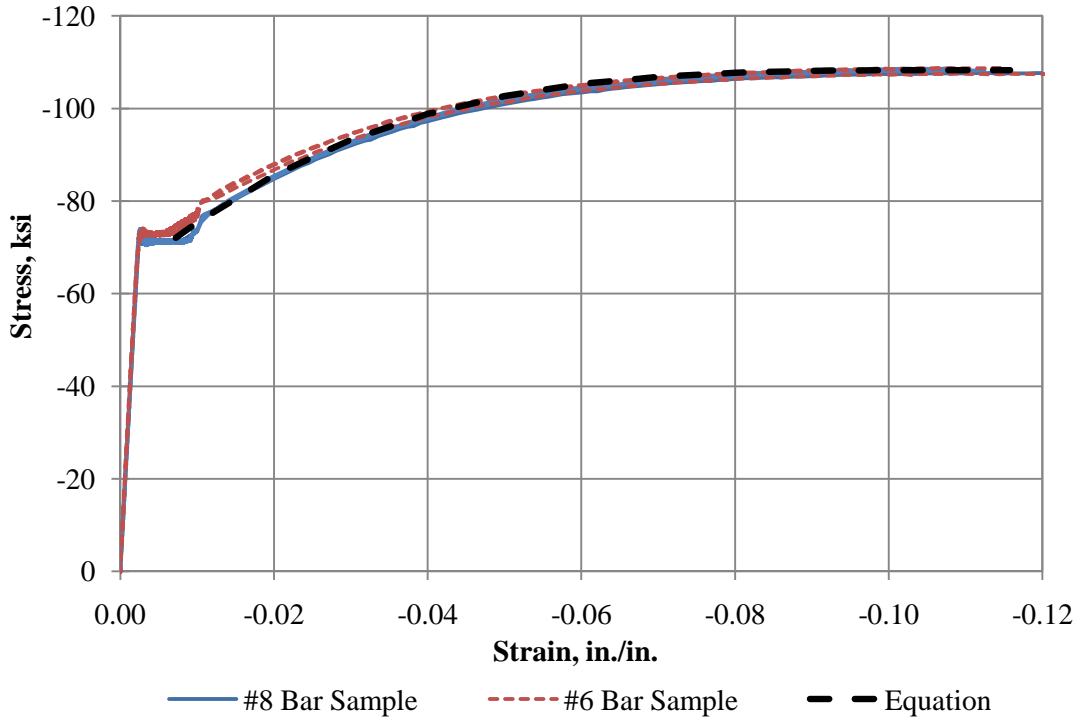


Figure A-6: Strain-Hardening Equation Validation at 20°C

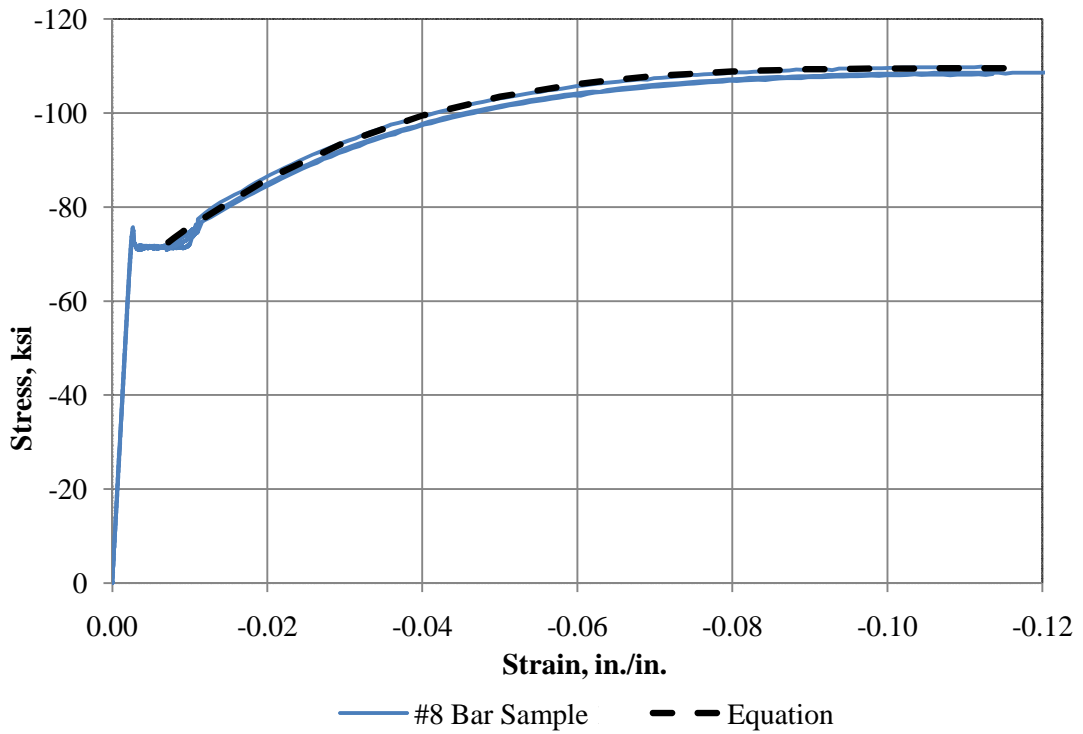
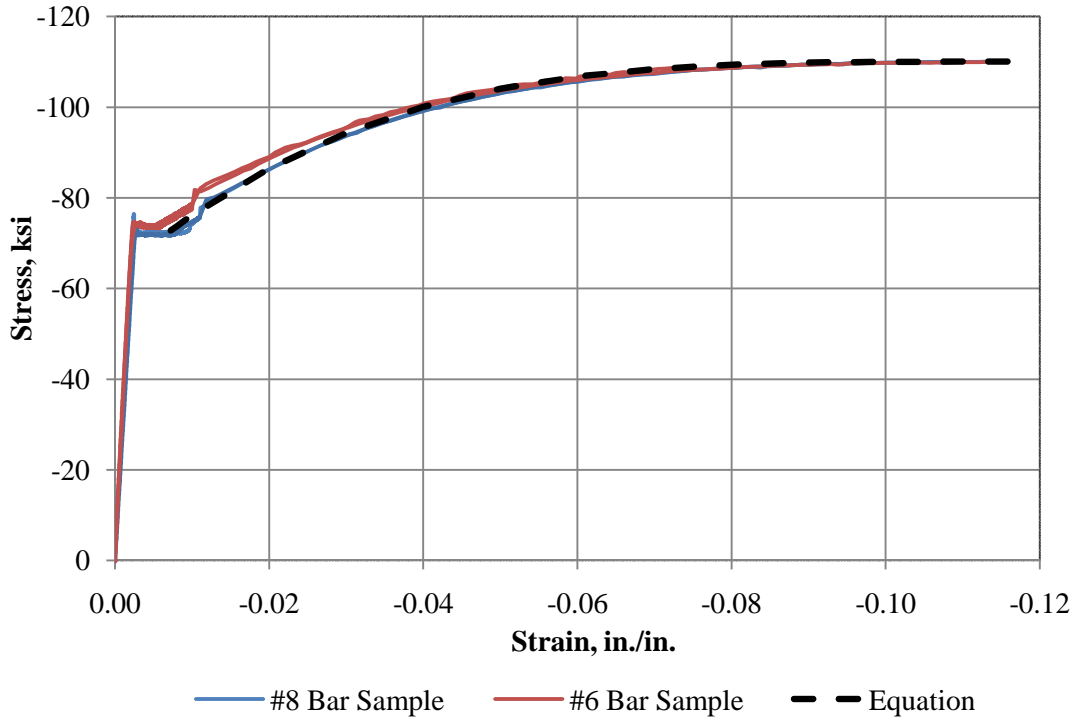
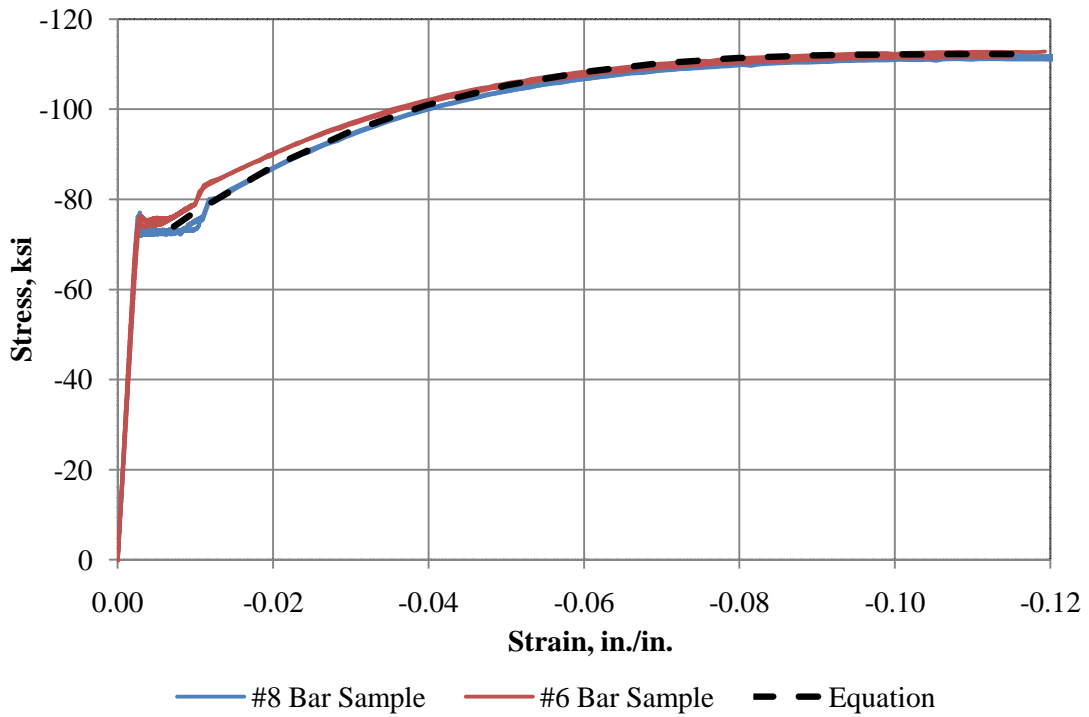


Figure A-7: Strain-Hardening Equation Validation at 5°C

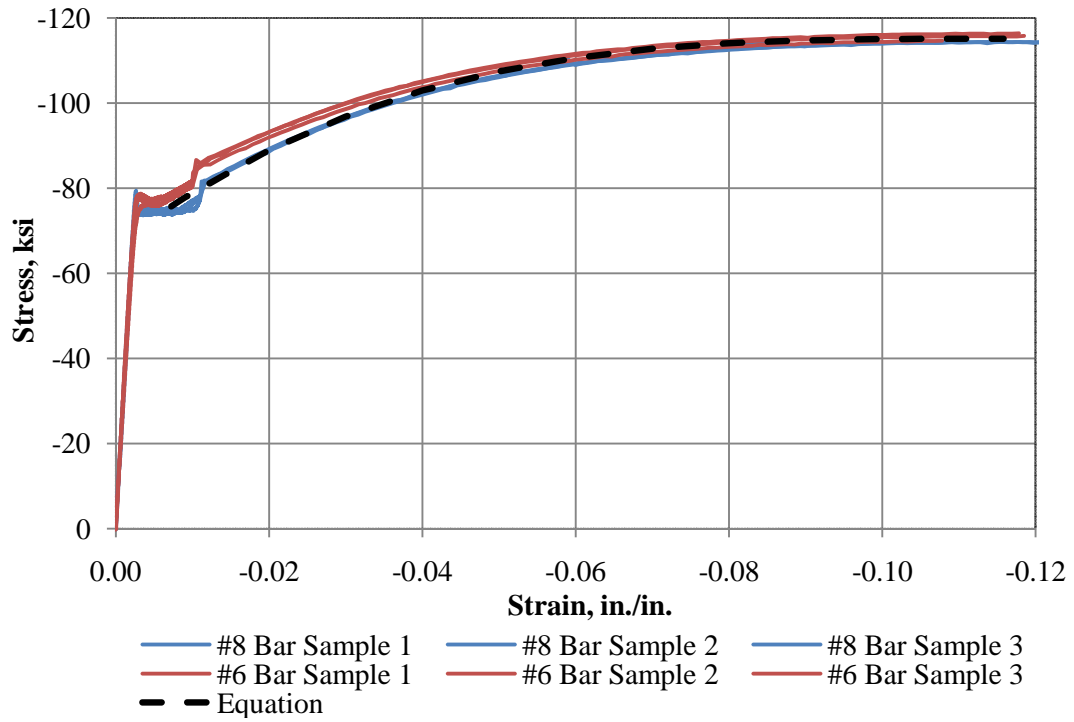


**Figure A-8: Strain-Hardening Equation Validation at -1°C**



**Figure A-9: Strain-Hardening Equation Validation at -20°C**





**Figure A-10: Strain-Hardening Equation Validation at -40°C**

## APPENDIX B: VSAT USER MANUAL

### B.1 Introduction

This user's manual was created to aid in the understanding of how to execute a section analysis in VSAT through a visual reference. The following sections will help define all necessary input information that needs to be entered prior to running an analysis. If technical information is required on any output or methods of determining output of the analysis, refer to the theoretical procedures provided in Chapter 4 of this thesis. Note that a hollow section is not available for this version of VSAT. Thus, the steps pertaining to these options should be ignored.

## B.2 Title Page and Section Type

The steps provided in this section are those for the first page that the user will encounter upon loading VSAT (see Figure B-1). This page is intended to collect user information, such as a project title, and also requires the user to select the basic concrete section type (i.e., rectangular, circular, or circular with an outer shell). As shown in Figure B-1, the required information is labeled with the expected input, and the associated choices, are discussed below for this page as well as for all other pages of VSAT.

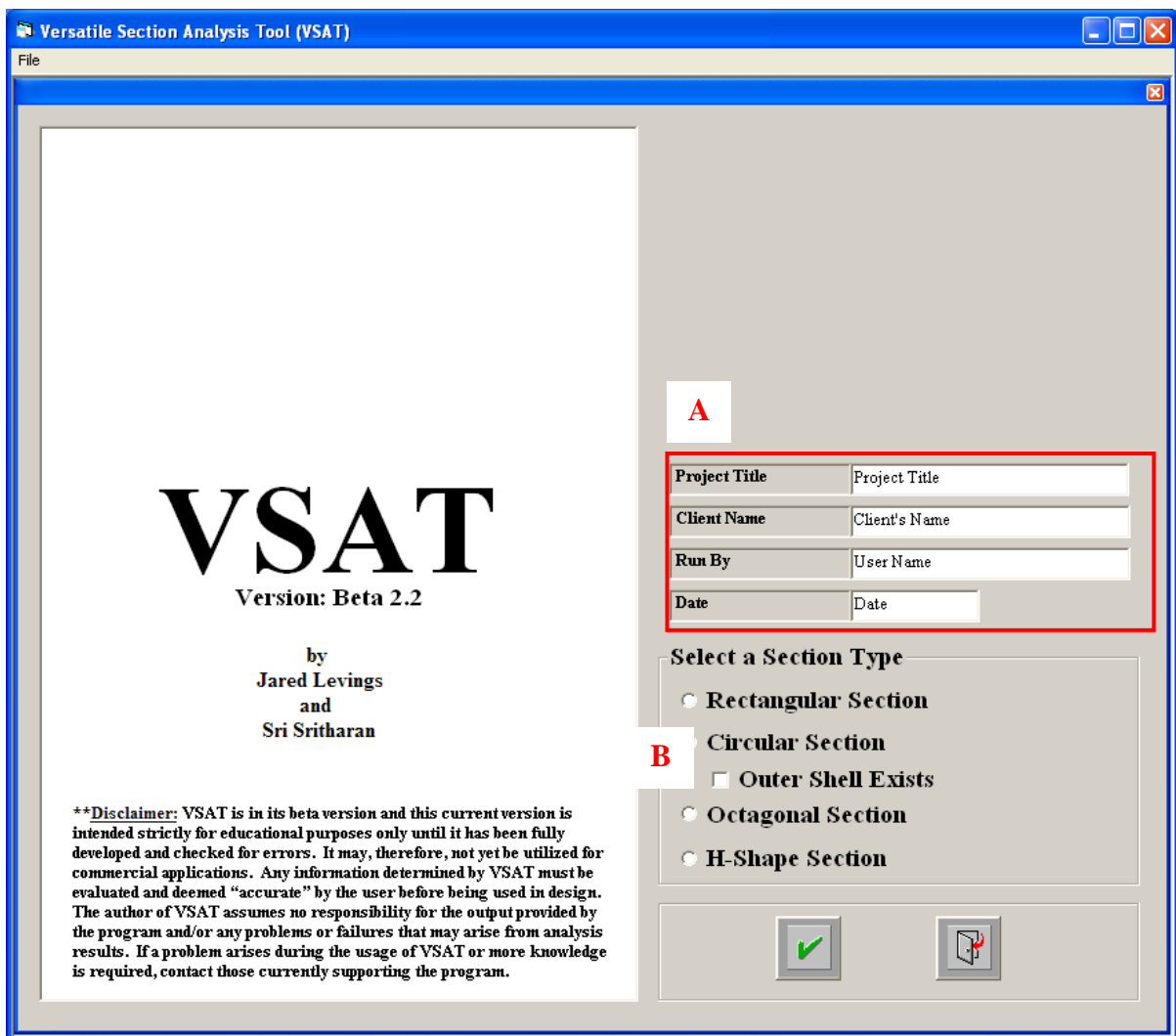


Figure B-1: Definition of User Information in VSAT

A: Enter in user information as desired.

B: Select the section type to be analyzed.

C: Click on  to continue.

D: Click on  to exit the program.

### B.3 Section Parameters

The section parameters page is where the user provides information such as the steel type/configuration to be used, the applied loads, and the effects of soil and/or temperature if appropriate. Note that a hollow section and prestressing steel may not be used in this version of VSAT. For this reason disregard any steps pertaining to these options. The following steps will aid in completion of the section parameters page (see Figure B-2):

**Section Type**

**A**  Solid  
 Hollow

Rectangular Hole  
 Circular Hole

**Longitudinal Steel**

**B**  Mild Steel

Steel Configuration

Rectangular  
 Circular

**C**  Prestressing Steel

**i** Strands Steel Configuration  
 Rectangular  
 Circular

**ii** Wires Steel Configuration  
 Rectangular  
 Circular

**ii** Bars Steel Configuration  
 Rectangular  
 Circular

**External Actions**

Applied Axial Force **D** Kips

**E**  Soil Pressure

**F** Temperature Effects

Analysis Temp	20	Deg C
Concrete Temp	20	Deg C
Mild Steel Temp	20	Deg C
Prestress Steel Temp	20	Deg C

**Transverse Reinforcement**

The transverse reinforcement location is based upon the:

**G**  Mild Steel Longitudinal Reinforcement  
 Prestressing Longitudinal Reinforcement  
 There is no Transverse Reinforcement

Reinforcement Style

**H**  Rectangular Ties  
 Hoops  
 Spiral

**Figure B-2: Definition of Section Parameters in VSAT**

A: Select whether the section is solid or hollow (only solid is currently available).

B: If mild steel is present in the section, check the box and specify the steel configuration.

- C: If prestressing steel is present in the section, check the box.
- C(i): If strands are present in the section, check the box and specify the steel configuration.
- C(ii): If prestressing wires are present in the section, check the box and specify the steel configuration.
- C(iii): If prestressing bars are present in the section, check the box and specify the steel configuration.
- D: Enter the external axial load applied to the section (kips).
- E: If external soil pressure provides confinement, check this option.
- F: If you wish to include temperature effects in the analysis, check the appropriate box. Then enter the temperature at which the analysis should be executed. If material properties are to be defined at different temperatures, then provide this information by altering the material temperatures from the listed analysis temperatures. The required input will be collected under the material section.
- G: Define whether the transverse reinforcement will be measured from the placement of the mild steel, prestressing steel, or that no transverse reinforcement exists. This step is necessary to accurately locate the transverse reinforcement and other steel present within the section. It is intended to reduce the necessary input required from the user.
- H: Choose the desired transverse reinforcement option.

## B.4 Circular Section Geometry

Skip to Section B.5 if the section type is not circular.

The circular section geometry page defines gross section dimensions and steel reinforcement within the section. The section's geometry facilitates with determining the effectiveness of the core as presented in Section 4.2.3.1. Figure B-3 below presents the information required to perform a moment-curvature analysis on a circular section.

The screenshot shows the VSAT Geometry window with the following sections and fields:

- Section Details:**
  - Concrete Outside Diameter: **A** Inches
  - Cover Thickness to Main Reinf.: **B** Inches
  - Outer Steel Shell Thickness: **C** Inches
  - Shell Long/Trans Contribution: **D** 50 Percent
- Hole Dimensions:**
  - Concrete Inside Diameter: **E** Inches
- Longitudinal Mild Steel:**
  - Total Steel: **F** No. Of Bars, **G** Bar Size, Area Per Bar (Sq. in)
- Transverse (Tie) Reinforcement:**
  - Transverse Bar Size: **H**
  - Transverse Bar Style: **M**
  - Bar Spacing (on centers): **I** Inches
  - Yield Strength: **J** Ksi, With Temp. Effects 60 Ksi
  - Yield Strength of Outer Shell: **K** Ksi, With Temp. Effects 60 Ksi
  - Ultimate Strain: **L**, With Temp. Effects 0.12
- Prestressing Steel Reinforcement:**
  - Strands: Type **N**, Size **O**, Area, Sq. In.
  - Bars: Type, Size, Area, Sq. In.
  - Wires: Size, Area, Sq. In.
  - Quantity: Strands **P** n, Bars, Wires
- Concrete Layout:**
  - Diagram showing Outside Diameter, Cover, Hole, and Outer Steel Shell.
  - Diagram showing Tie Spacing.
  - User Defined Ke Value: **Q** Outer Ke = 0, Ke = 0, **R** Apply

Figure B-3: Defining Details of a Circular Section in VSAT

- A: Enter the section diameter in inches.
- B: Enter the cover thickness, measured from the outer edge of the main (longitudinal) reinforcement to the outer edge of the section, in inches.

- C: If an outer steel shell exists, enter the shell thickness in inches. The default thickness is 2 inches. If no shell exists, this option will not be available.
- D: If an outer steel shell exists, enter the steel shell's longitudinal contribution in percent. The default value is 50 percent, and the other contribution is automatically calculated to provide the steel shell's transverse contribution. If no shell exists, this option will not be available.
- E: If the section is hollow, enter the diameter of the hole at the center of the section in inches.
- F: Enter in the number of longitudinal mild steel reinforcing bars.
- G: Select the mild steel deformed reinforcing bar size by selecting a size from the drop down menu.
- H: Select the bar size of the transverse reinforcement by choosing a size from the drop down menu.
- I: Enter the transverse reinforcement spacing measured from center to center in inches.
- J: Enter the yield strength of the transverse reinforcement in kips per square inch (ksi).
- K: Enter the yield strength to be used of the outer steel shell in kips per square inch (ksi).
- L: Enter the ultimate strain of the transverse reinforcement.
- M: If temperature effects are chosen to be included, these boxes will reveal the adjustments made to the yield strength and ultimate strain of the mild steel reinforcement from that entered in steps G and I.
- If prestressing steel does not exist, continue to step Q; otherwise,
- N: Select the type(s) of prestressing steel to be used.
- O: Select the size(s) of prestressing steel to be used.
- P: Enter in the number of prestressing strands, bars and wires.
- Q: If a user defined section effectiveness,  $K_e$ , is desired, check this box and enter the appropriate value. Note: for a steel shell, the effectiveness of the exterior portion of the section is also required.
- R: Click  to calculate the  $K_e$  value(s) of the section or to update the user defined  $K_e$  value in the program.



S: Click on  to continue. If you need to start over, click on . If you need to go back to a previous page, click on .

If external soil pressure provides confinement on the section, skip to Section B.9 If not, skip to Section B.10

## B.5 Rectangular Section Geometry and Circular Core

**Skip to Section B.6 if the section type is not rectangular with circular reinforcement.**

The rectangular section geometry page defines gross section dimensions and steel reinforcement within the section. The section's geometry facilitates with determining the effectiveness of the core as presented in Section 4.2.3.1. Figure B-4 below presents the information required to perform a moment-curvature analysis on a rectangular section with a circular core.

**Section Details**

Depth	<b>A</b>	Inches	Concrete Inside Diameter	<b>D</b>	Inches
Width	<b>B</b>	Inches			
Dist. Center to Outside of Reinf.	<b>C</b>	Inches			

**Longitudinal Mild Steel**

No. of Bars	<b>E</b>	Bar Size	<b>F</b>	Area per Bar (Sq. in.)	0.11
-------------	----------	----------	----------	------------------------	------

**Transverse (Tie) Reinforcement**

Transverse Bar Size	<b>G</b>		0	
Transverse Bar Style		Spirals	<b>K</b>	
Bar Spacing (on centers)	<b>H</b>	Inches		
Yield Strength	<b>I</b>	Ksi	60	Ksi
Ultimate Strain	<b>J</b>		0.12	

**Prestressing Steel Reinforcement**

	Type	Size	Area	
Strands	<b>L</b>	<b>M</b>	0	Sq. In.
Bars			0	Sq. In.
Wires			0	Sq. In.

**Quantity**

Strands	<b>N</b>	0
Bars		
Wires		

**Concrete Layout**

Diagram showing a rectangular section with a circular core. Dimensions: Width, Depth, Hole. Reinforcement: Reinf. Dist., Moment Applied.

**User Defined Ke Value**

Ke = 0 **P** Apply

Note: If Ke is 0, the concrete section is unconfined

**Figure B-4: Defining Details of a Rectangular Section and Circular Core**

A: Enter the section depth (i.e. dimension orthogonal to the moment axis) in inches.

B: Enter the section width (i.e. dimension parallel to the moment axis) in inches.

- C: Enter the distance measured from the outer edge of the main (longitudinal) reinforcement to the center of the section in inches.
- D: If the section is hollow, enter the diameter of the hole at the center of the section in inches.
- E: Enter in the number of longitudinal mild steel reinforcing bars.
- F: Select the mild steel deformed reinforcing bar size from the drop down menu.
- G: Select the bar size of the transverse reinforcement from the drop down menu.
- H: Enter the transverse reinforcement spacing measured from center to center in inches.
- I: Enter the yield strength of the transverse reinforcement (ksi).
- J: Enter the ultimate strain of the transverse reinforcement.
- K: If temperature effects are chosen to be included, these boxes will reveal the adjustments made to the yield strength and ultimate strain of the mild steel reinforcement from that entered in steps G and I.


If prestressing steel does not exist, continue to step O; otherwise,


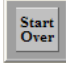

L: Select the type(s) of prestressing steel to be used.

M: Select the size(s) of prestressing steel to be used.

N: Enter in the number of prestressing strands, bars and wires.

O: If a user defined section effectiveness,  $K_e$ , is desired, check this box and enter the appropriate value.

P: Click  to calculate the  $K_e$  value of the section or to update the value of  $K_e$  within the program for a user defined value.

Q: Click on  to continue. If you need to start over, click on . If you need to go back to a previous page, click on .

If external soil pressure provides confinement on the section, skip to Section B.9 If not, skip to Section B.10

## B.6 Rectangular Section Geometry and Rectangular Core

Skip to Section B.7 if the section is not rectangular with rectangular reinforcement.

The rectangular section geometry page defines gross section dimensions and steel reinforcement within the section. The section's geometry facilitates with determining the effectiveness of the core as presented in Section 4.2.3.1. Figure B-5 below presents the information required to perform a moment-curvature analysis on a rectangular section with a rectangular core.

**Section Details**

Depth	<b>A</b>	Inches	Concrete Inside Depth	<b>D</b>	Inches
Width	<b>B</b>	Inches	Concrete Inside Width	<b>E</b>	Inches
Cover Thickness to Main Reinf.	<b>C</b>	Inches			

**Longitudinal Mild Steel**

	No. of Bars	Bar Size	Area per Bar (Sq. in.)
Tension	<b>F</b>	<b>G</b>	0.11
Side	<b>H</b>	#3	0.11
Compression	<b>I</b>	#3	0.11

**Transverse (Tie) Reinforcement**

Transverse Bar Size	<b>J</b>	0
Transverse Bar Style	Rectangular	<b>N</b>
Bar Spacing (on centers)	<b>K</b>	Inches
Yield Strength	<b>L</b>	Ksi
Ultimate Strain	<b>M</b>	
No. of Steel X-Direction Legs	<b>O</b>	
No. of Steel Y-Direction Legs	<b>P</b>	

**With Temp. Effects**

With Temp. Effects	60	Ksi
With Temp. Effects	0.12	

**Prestressing Steel Reinforcement**

	Type	Size	Area	Sq. In.
Strands	<b>Q</b>	<b>R</b>	0	Sq. In.
Bars	<b>Q</b>	<b>R</b>	0	Sq. In.
Wires	<b>Q</b>	<b>R</b>	0	Sq. In.

**Quantity**

	Tens.	Side	Comp.	Total
Strands	<b>S</b>	<b>T</b>	<b>U</b>	0
Bars	<b>S</b>	<b>T</b>	<b>U</b>	0
Wires	<b>S</b>	<b>T</b>	<b>U</b>	0

**Concrete Layout**





Width, Depth, Transverse Legs, Moment Applied, Cover, Hole, Tension Steel, Side Steel, Comp. Steel, Tie Spacing, User Defined Ke Value, Ke = 0, W Apply

Note: If Ke is 0, the concrete section is unconfined

**Figure B-5: Defining Details of a Rectangular Section and Rectangular Core**

A: Enter the section depth (i.e. dimension orthogonal to the moment axis shown) in inches.

B: Enter the section width (i.e. dimension parallel to the moment axis shown) in inches.

- C: Enter the cover thickness measured from the outer edge of the main (longitudinal) reinforcement to the outer edge of the section in inches.
- D: If the section is hollow, enter the depth of the hole at the center in inches.
- E: If the section is hollow, enter the width of the hole in inches.
- F: Enter in the number of longitudinal mild steel reinforcing bars in the steel tension zone.
- G: Select the mild steel deformed reinforcing bar size from the drop down menu.
- H: Enter in the number of longitudinal mild steel reinforcing bars in the side steel zone.
- I: Enter in the number of longitudinal mild steel reinforcing bars in compression steel zone.
- J: Select the bar size of the transverse reinforcement from the drop down menu.
- K: Enter the transverse reinforcement spacing measured from center to center in inches.
- L: Enter the yield strength of the transverse reinforcement (ksi).
- M: Enter the ultimate strain of the transverse reinforcement.
- N: If temperature effects are chosen to be included, these boxes will reveal the adjustments made to the yield strength and ultimate strain of the mild steel reinforcement.
- O: Enter the total number of legs in the horizontal direction, parallel to the width.
- P: Enter the total number of legs in the vertical direction, parallel to the depth.
- If prestressing steel does not exist, continue to step V; otherwise,
- Q: Select the type(s) of prestressing steel to be used.
- R: Select the size(s) of prestressing steel to be used.
- S: Enter in the number of prestressing strands, bars and wires in the tension zone.
- T: Enter in the number of prestressing strands, bars and wires in the side steel zone.
- U: Enter in the number of prestressing strands, bars and wires in the compression zone.
- V: If a user defined section effectiveness,  $K_e$ , is desired, check this box and enter the value.
- W: Click  to calculate the  $K_e$  value of the section or to update the value of  $K_e$  within the program for a user defined value.
- X: Click on  to continue. If you need to start over, click on . If you need to go back to a previous page, click on .

If external soil pressure provides confinement on the section, skip to Section B.9 If not, skip to Section B.10

## B.7 Octagonal Section Geometry

Skip to Section B.8 if the section is not octagonal.

The octagonal section geometry page defines gross section dimensions and steel reinforcement within the section. The section's geometry facilitates with determining the effectiveness of the core as presented in Section 4.2.3.1. Figure B-6 below presents the information required to perform a moment-curvature analysis on an octagonal section.

**Section Details**

Width	<b>A</b>	Inches
Depth	30	Inches
Dist. Center to Outside of Reinf.	<b>B</b>	Inches

**Hole Dimensions**

Concrete Inside Diameter	<b>C</b>	Inches
--------------------------	----------	--------

**Longitudinal Mild Steel**

	No. Of Bars	Bar Size	Area Per Bar (Sq. in.)
Mild Steel	<b>D</b>	<b>E</b>	

**Tie Reinforcement**

Tie Bar Size	<b>F</b>	
Transverse Bar Style		
Tie Bar Spacing (on centers)	<b>G</b>	Inches
Tie Bar Yield Strength	<b>H</b>	Ksi
Ultimate Strain	<b>I</b>	

With Temp. Effects	60	Ksi
With Temp. Effects	0.12	

**Prestressing Steel Reinforcement**

	Type	Size	Area	Sq. In.
Strands	<b>K</b>	<b>L</b>	0	Sq. In.
Bars			0	Sq. In.
Wires			0	Sq. In.

	Quantity
Strands	<b>M</b>
Bars	
Wires	

**Concrete Layout**

Diagram showing an octagonal cross-section with dimensions: Width, Depth, and Reinf. Dist. A moment is applied to the section.

**User Defined Ke Value**

Ke = 0 **O** Apply

Figure B-6: Defining Details of an Octagonal Section

A: Enter the section width in inches.

B: Enter the distance measured from the outer edge of the main (longitudinal) reinforcement to the center of the section in inches.

- C: If the section is hollow, enter the diameter of the hole at the center of the section in inches.
- D: Enter in the number of longitudinal mild steel reinforcing bars.
- E: Select the mild steel deformed reinforcing bar size by selecting a size from the drop down menu.
- F: Select the bar size of the transverse reinforcement by choosing a size from the drop down menu.
- G: Enter the transverse reinforcement spacing measured from center to center in inches.
- H: Enter the yield strength of the transverse reinforcement in kips per square inch (ksi).
- I: Enter the ultimate strain of the transverse reinforcement.
- J: If temperature effects are chosen to be included, these boxes will reveal the adjustments made to the yield strength and ultimate strain of the mild steel reinforcement from that entered in steps G and I.

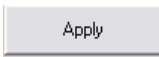
If prestressing steel does not exist, continue to step N; otherwise,

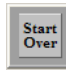
K: Select the type(s) of prestressing steel to be used.

L: Select the size(s) of prestressing steel to be used.

M: Enter in the number of prestressing strands, bars and wires.

N: If a user defined section effectiveness,  $K_e$ , is desired, check this box and enter the appropriate value.

O: Click  to calculate the  $K_e$  value(s) of the section or to update the user defined  $K_e$  value in the program.

P: Click on  to continue. If you need to start over, click on . If you need to go back to a previous page, click on .

If external soil pressure provides confinement on the section, skip to Section B.9 If not, skip to Section B.10

## B.8 H-Shaped Section Geometry

The H-shaped section geometry page defines gross section dimensions and steel reinforcement within the section. Figure B-7 below presents the information required to perform a moment-curvature analysis on a H-shaped section.

**Section Details**

Depth	<b>A</b>	Inches	Width	<b>D</b>	Inches
D1	<b>B</b>	Inches	W1	<b>E</b>	Inches
D2	<b>C</b>	Inches			

**Prestressing Steel Reinforcement**

Total Quantity of Prestressing Layers: **F**

Rein. Layer	Y (in)	Strand Quantity	Bar Quantity	Wire Quantity
<b>G</b>	<b>H</b>	<b>I</b>		
4	8	4	0	0

**J** Add

Layer #	Y (in.)	# Strands	# Bars	# Wires
1	2	4	0	0
2	0	0	0	0
3	0	0	0	0
4	8	4	0	0

**K**

Strands	Type <b>L</b>	Size <b>M</b>	Area	0	Sq. In.
Bars	Type	Size	Area	0	Sq. In.
Wires	Type	Size	Area	0	Sq. In.

**Concrete Layout**

Diagram showing the H-shaped section geometry with dimensions: Width, W1, Depth, D1, D2, and Moment Applied.

**Figure B-7: Defining Details of a H-Shape Section**

- A: Enter the section overall depth in inches.
- B: Enter the first flange depth D1 in inches as shown in the figure.
- C: Enter the second flange depth D2 in inches as shown in the figure.
- D: Enter the section overall width in inches.
- E: Enter the width of the concrete web, W1, in inches as shown in the figure.




F: Enter the total number of layers of prestress reinforcement present within the section.

Steps G through K should be repeated until all layers of prestress reinforcement have been defined.

G: Enter the layer number to be defined.

H: Enter the distance measured from the top of the section to the centerline of the prestressing reinforcement in inches.




I: Enter in the number of prestressing strands, bars and wires.

J: Click  to finish defining that layer of reinforcement or update a previously defined layer.

K: Check to see if the reinforcement layer has been successfully added and is correct. If more layers of reinforcement need be defined, go back to step G. Otherwise, continue to step L.

L: Select the type(s) of prestressing steel to be used.

M: Select the size(s) of prestressing steel to be used.

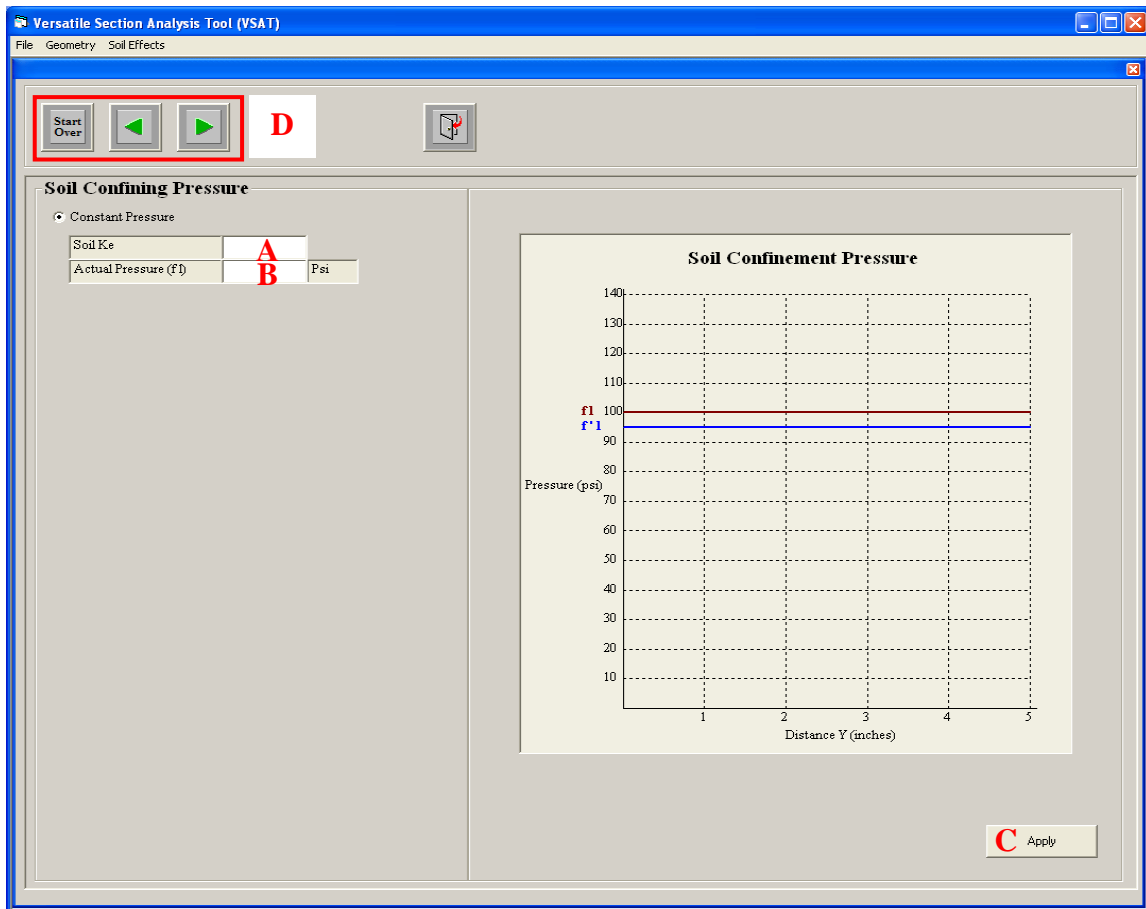
N: Click on  to continue. If you need to start over, click on . If you need to go back to a previous page, click on .

[Skip to Section B.10](#)

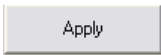
## B.9 External Soil Pressure

Continue to the next page if external soil pressure is not present.

The external soil pressure option allows the user to enter a constant soil confinement pressure for the section and define how effectively the pressure confines the section in the analysis. Note that only a constant pressure is available in this version of VSAT. Figure B-8 below presents the expected information for a rectangular section with a rectangular core.



**Figure B-8: Defining an External Soil Pressure for Confinement of a Section**

- A: Enter the effectiveness to which the soil pressure confines the section.
- B: Enter the soil pressure acting on the section in pounds per square inch (psi).
- C: Click  to add or update the soil parameters to the section.
- D: Click on the icons as needed.

## B.10 Defining Properties of Concrete

The concrete material section allows the user to specify unconfined concrete properties for normal concrete, a transverse reinforcement stress-strain graph for variable confining normal concrete, and properties for ultra-high performance concrete (UHPC). The stress-strain curves created for normal concrete without temperature effects (see Figure B-9), normal concrete with temperature effects (see Figure B-10), variably confined normal concrete (see Figures B-11 and B-12), and UHPC (see Figure B-13) are formulated in Sections 4.2.3, 4.2.8.1, 4.2.3.3 and 4.2.3.6, respectively. The following sections present the expected input for defining the properties of normal concrete or UHPC.

### B.8.1 Properties of Concrete without Temperature Effects

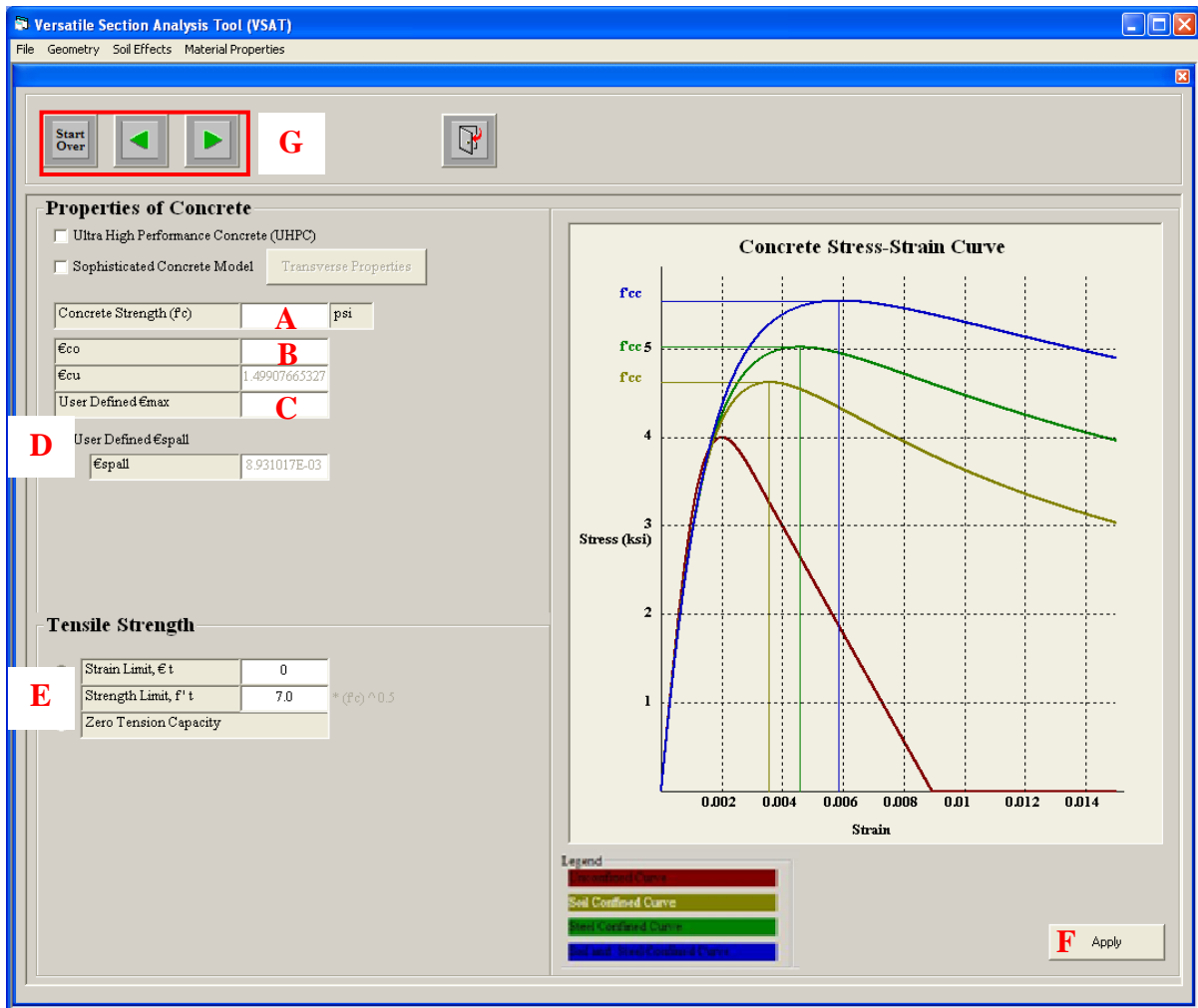





Figure B-9: Defining Material Properties of Concrete without Temperature Effects

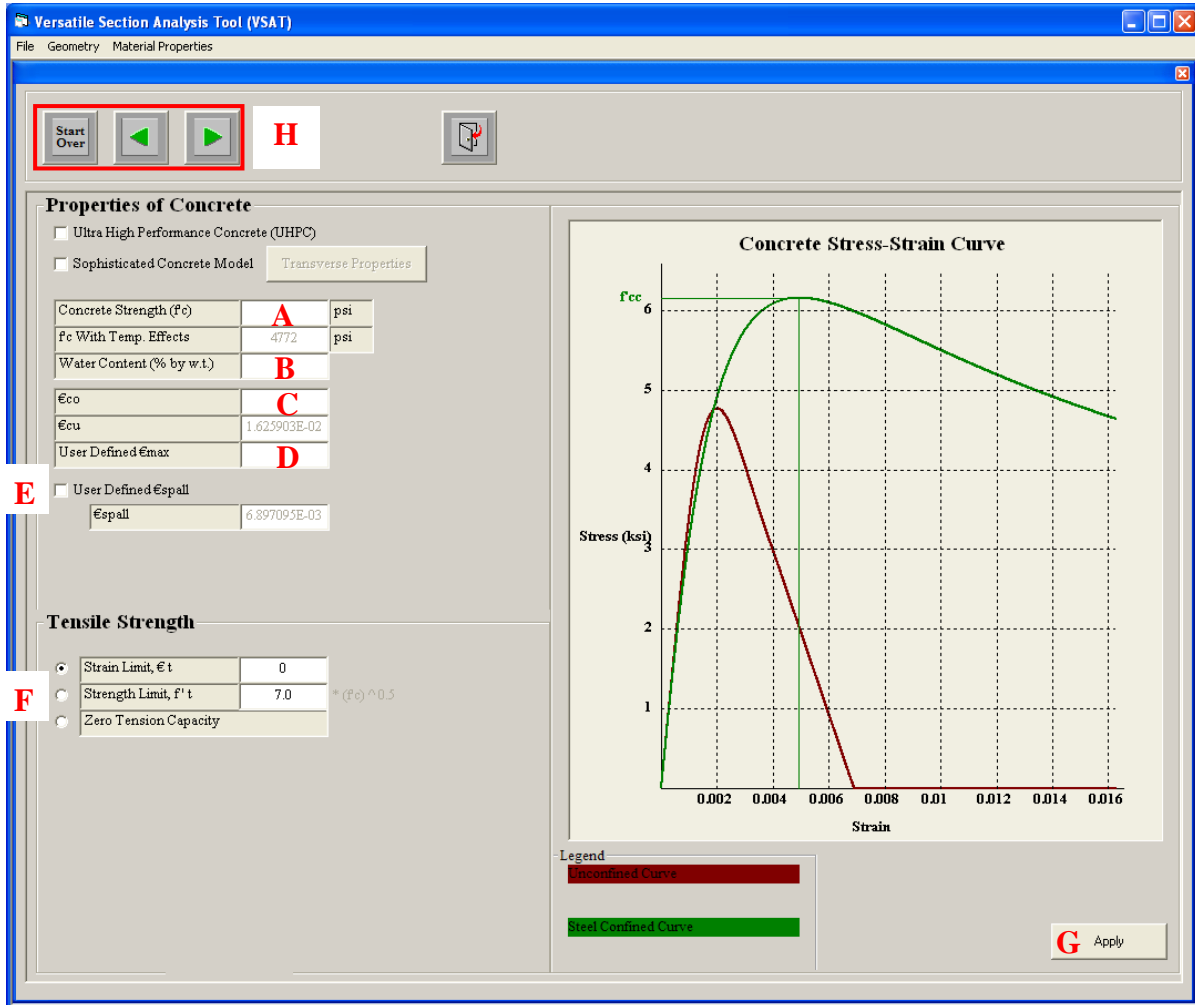
- A: Enter the unconfined compressive strength of concrete in psi.
- B: Enter the strain at which the unconfined concrete strength,  $f'_c$ , is reached (in./in.).
- C: The strain limit of confined concrete as per Paulay and Priestley (1992), or Section 4.2.3.5, is displayed. Alter this value if desired. Beyond this strain limit, the concrete stress contribution is assumed to be zero.
- D: If a user defined spalling concrete strain is desired, check the appropriate option and enter a desired, but realistic, strain value (in./in.).
- E: Define the concrete strength by selecting the “Strain Limit”, “Stress Limit”, or “Zero Tension Capacity” option. If the strain limit is selected, enter the appropriate value. If the strength limit is chosen, define the tensile strength in terms of  $\sqrt{f'_c}$  (e.g., a value of 6 is interpreted as  $6\sqrt{f'_c}$  (psi)).

F: Click  to update the graph in the display window.

G: Click on  to continue. If you need to start over, click on . If you need to go back to a previous page, click on .

**If mild steel is present in the section skip to Section B.11 otherwise skip to Section B.12**


### B.8.2 Properties of Concrete with Temperature Effects

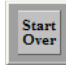



**Figure B-10: Defining the Properties of Concrete with Temperature Effects**

- A: Enter the unconfined compressive strength of concrete in psi.
- B: Enter the percentage of water content by weight.
- C: Enter the strain at which the unconfined concrete strength,  $f'_c$ , is reached (in/in).
- D: The strain limit of confined concrete as per Paulay and Priestley (1992), or 4.2.3.5, is displayed. Alter this value if desired. Beyond this strain limit, the concrete stress contribution is assumed to be zero.
- E: If a user defined spalling concrete strain is desired, check the appropriate option and enter a desired, but realistic, strain value (in/in).
- F: Define the concrete strength by selecting the “Strain Limit”, “Stress Limit”, or “Zero Tension Capacity” option. If the strain limit is selected, enter the appropriate value. If

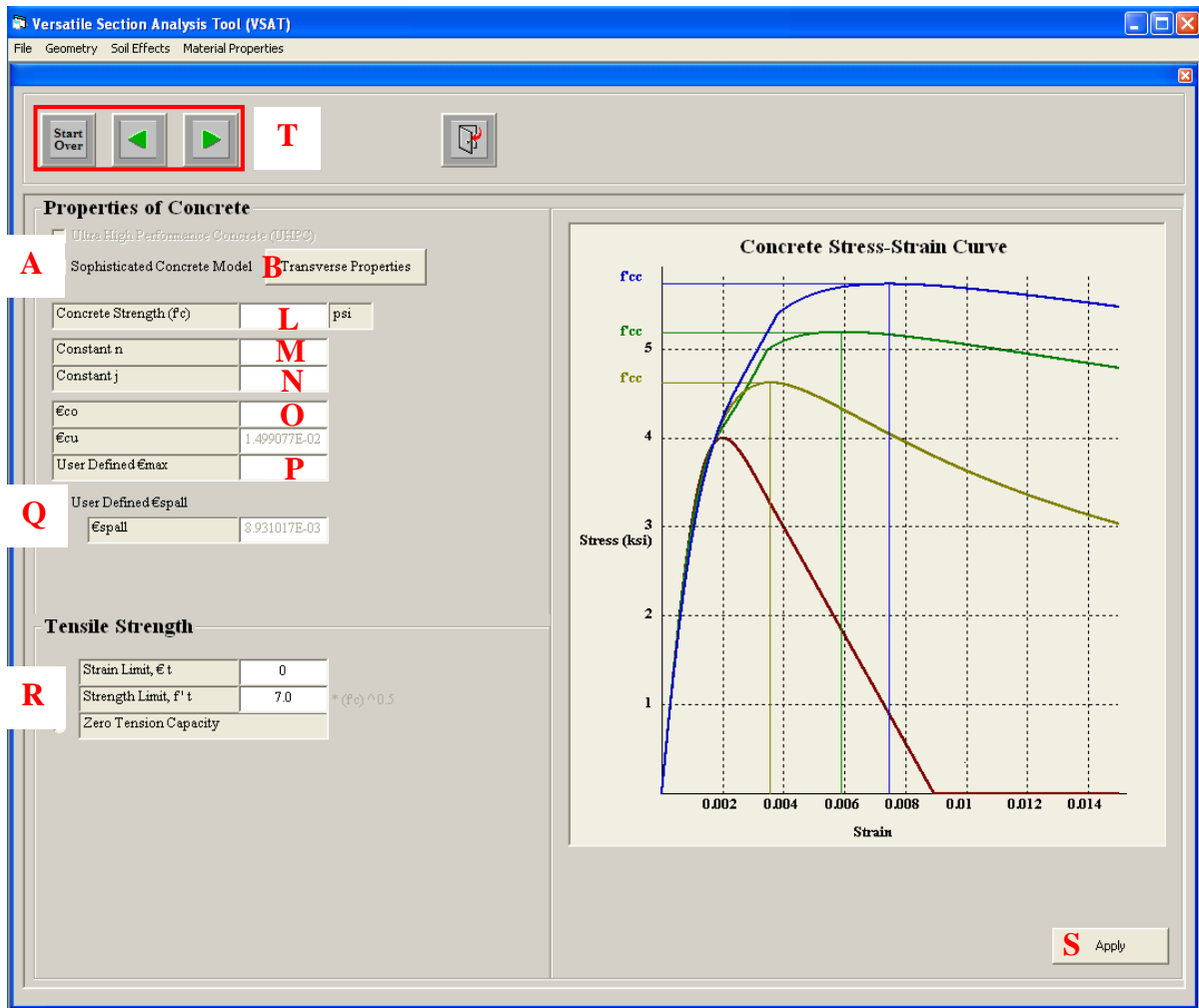
the strength limit is chosen, define the tensile strength in terms of  $\sqrt{f'_c}$  (e.g., a value of 6 is interpreted as  $6\sqrt{f'_c}$  (psi)).

G: Click  to update the graph in the display window.

H: Click on  to continue. If you need to start over, click on . If you need to go back to a previous page, click on .

If mild steel is present in the section skip to Section B.11 otherwise skip to Section B.12

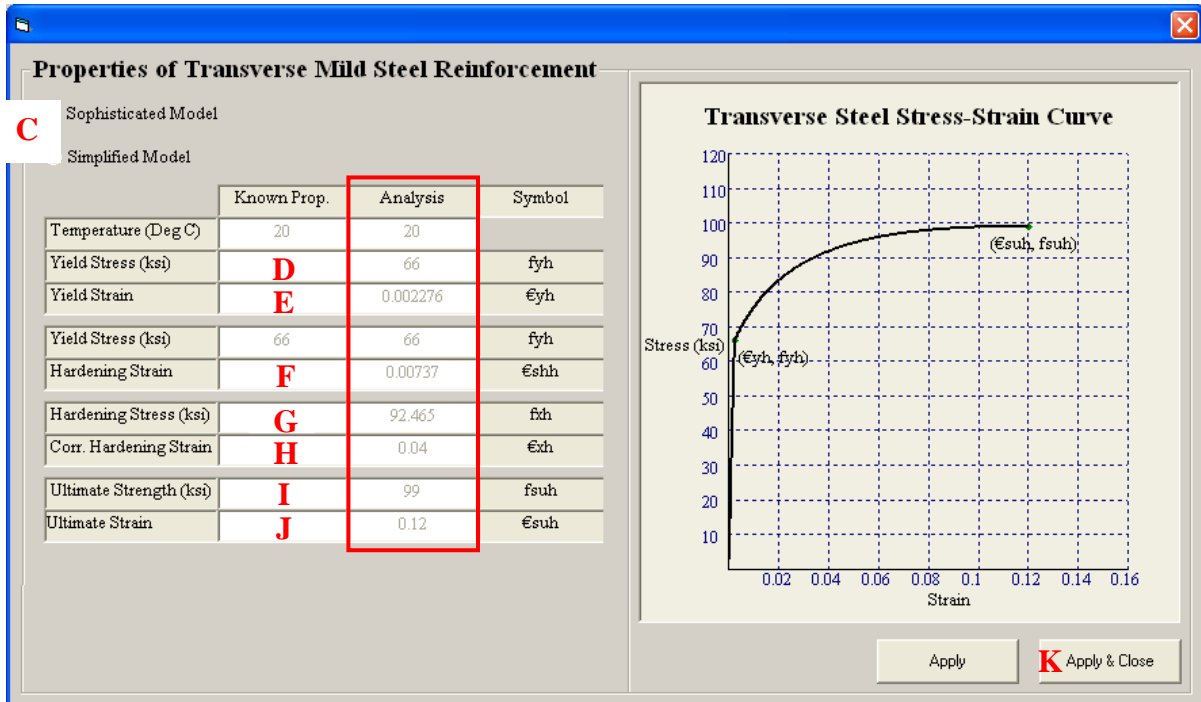
### B.8.3 Properties of Concrete with Variable Confinement



The screenshot shows the 'Versatile Section Analysis Tool (VSAT)' interface. The window title is 'Versatile Section Analysis Tool (VSAT)' and the menu bar includes 'File', 'Geometry', 'Soil Effects', and 'Material Properties'. The interface is divided into several sections:

- Navigation:** Includes 'Start Over', 'Previous', 'Next', and 'T' buttons.
- Properties of Concrete:**
  - Model: Ultra High Performance Concrete (UHPC)
  - Model Type: Sophisticated Concrete Model (A)
  - Transverse Properties (B)
  - Concrete Strength ( $f'_c$ ): L (psi)
  - Constant n: M
  - Constant j: N
  - $\epsilon_{co}$ : O
  - $\epsilon_{cu}$ : 1.499077E-02
  - User Defined  $\epsilon_{max}$ : P
  - User Defined  $\epsilon_{spall}$ : Q
  - $\epsilon_{spall}$ : 8.931017E-03
- Tensile Strength:**
  - Strain Limit,  $\epsilon_t$ : 0
  - Strength Limit,  $f_t$ : 7.0 \* ( $f'_c$ )<sup>0.5</sup> (R)
  - Zero Tension Capacity
- Concrete Stress-Strain Curve:** A graph showing Stress (ksi) on the y-axis (ranging from 0 to 6) and Strain on the x-axis (ranging from 0 to 0.014). The curve shows a peak stress  $f_{cc}$  at a strain of approximately 0.008. The peak stress  $f_{cc}$  is indicated by a horizontal line at approximately 5.5 ksi. The curve is labeled 'Concrete Stress-Strain Curve'.
- Apply Button:** A red 'S' button labeled 'Apply' is located at the bottom right of the interface.

Figure B-11: Defining the Properties of Concrete with Variable Confinement



**Figure B-12: Defining the Transverse Mild Steel Reinforcement Properties for Concrete with Variable Confinement**

A: Check the “Sophisticated Concrete Model” box.

B: Click  to define the stress-strain behavior of the transverse reinforcement.

C: Choose between the “Sophisticated Model” and “Simplified Model” options. The sophisticated model may be chosen only if all required values, as shown in the display section of Figure B-12, are known; otherwise choose the simplified model. Note that if temperature effects are used, the known properties of the steel reinforcement shall be entered under the “Known Prop.” column of Figure B-12. The “Analysis” column, as indicated by the red box in Figure B-12 will automatically be updated.


If “Sophisticated Model” was chosen, provide the following parameters:

D: Specify the yield strength,  $f_y$ , in ksi.


E: Specify the strain corresponding to the yield strength specified in B,  $\epsilon_y$ , (in/in).

F: Specify the hardening strain,  $\epsilon_{sh}$ , (in/in).

G: Specify an arbitrary stress on the hardening portion of the curve,  $f_x$ , in ksi.

- H: Specify the strain corresponding to the arbitrary stress specified in E,  $\epsilon_x$ , (in/in).
- I: Specify the ultimate strength,  $f_{su}$ , in ksi.
- J: Specify the strain corresponding to the ultimate strength specified in G,  $\epsilon_{su}$ , (in/in).
- K: Click  to update the graph in the display window. Continue to step L.

If “Simplified Model” was chosen, provide the following parameters:

- D: Specify the yield strength,  $f_y$ , in ksi.
- E: A default yield strain,  $\epsilon_y$ , is calculated assuming  $E = 29,000$  ksi. Specify a more appropriate value if desired (in/in).
- F: A default hardening strain,  $\epsilon_{sh}$ , of  $3.24 \cdot \epsilon_y$  is used. Specify a more appropriate value if desired (in/in).
- G: Not Used for this model.
- H: Not Used for this model.
- I: A default ultimate strength,  $f_{su}$ , of  $1.5 \cdot f_y$  is used. Specify a more appropriate value if desired in ksi.
- J: A default strain ultimate strain,  $\epsilon_{su}$ , of 0.12 in/in is used. Specify a more appropriate value if desired (in/in).
- K: Click  to update the graph in the display window. Continue to step L.

L: Enter the unconfined compressive strength of concrete in psi.

M: Enter the parameter  $\eta$ , a default value of 20 has been used as recommended by Hose et al. (2001).

N: Enter the parameter  $J$ , a default value of 1/3 has been used as recommended by Hose et al. (2001).


O: Enter the strain at which the unconfined concrete strength,  $f'_c$ , is reached (in/in).

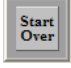
P: The strain limit of confined concrete as per Paulay and Priestley (1992), or 4.2.3.5, is displayed. Alter this value if desired. Beyond this strain limit, the concrete stress contribution is assumed to be zero.



Q: If a user defined spalling concrete strain is desired, check the appropriate option and enter a desired, but realistic, strain value (in/in).

R: Define the concrete strength by selecting the “Strain Limit”, “Stress Limit”, or “Zero Tension Capacity” option. If the strain limit is selected, enter the appropriate value. If the strength limit is chosen, define the tensile strength in terms of  $\sqrt{f'_c}$  (e.g., a value of 6 is interpreted as  $6\sqrt{f'_c}$  (psi)).

S: Click  to update the graph in the display window.

T: Click on  to continue. If you need to start over, click on . If you need to go back to a previous page, click on .

If mild steel is present in the section skip to Section B.11 otherwise skip to Section B.12

### B.8.4 Properties of UHPC

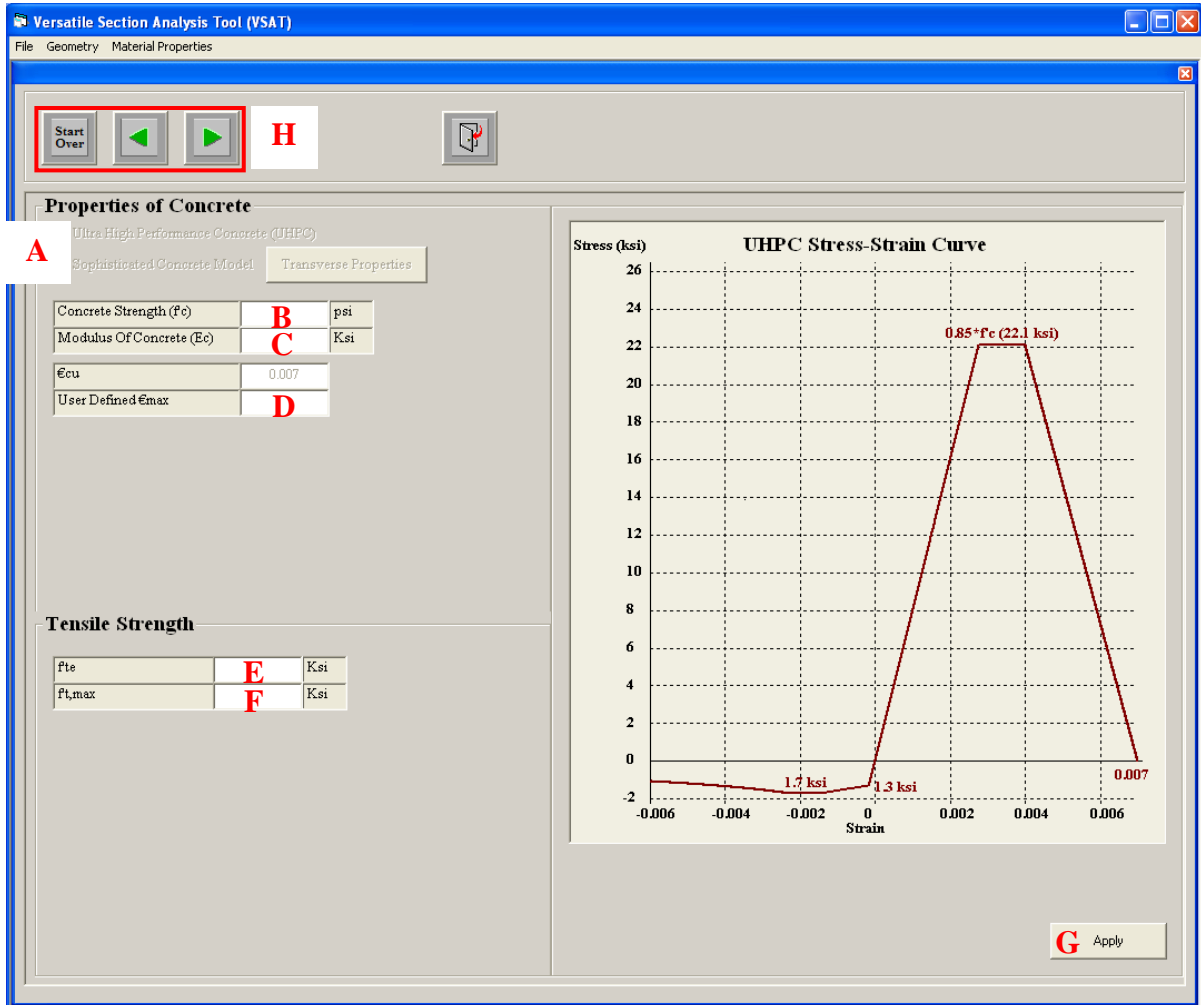


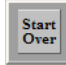



Figure B-13: Defining the Properties of UHPC

- A: Check the “Ultra-High Performance Concrete” box if it has not already been done so for you.
- B: Enter the unconfined compressive strength of UHPC in psi.
- C: Enter the elastic modulus of UHPC in ksi.
- D: The strain limit of UHPC is displayed. Specify a reasonable value if desired. Beyond this strain limit, the UHPC stress is assumed to be zero.
- E: Enter the cracking stress,  $f'_{te}$ , of UHPC in ksi.
- F: Enter the maximum tensile stress,  $f'_{t,max}$ , of UHPC in ksi.

G: Click  to update the graph in the display window.

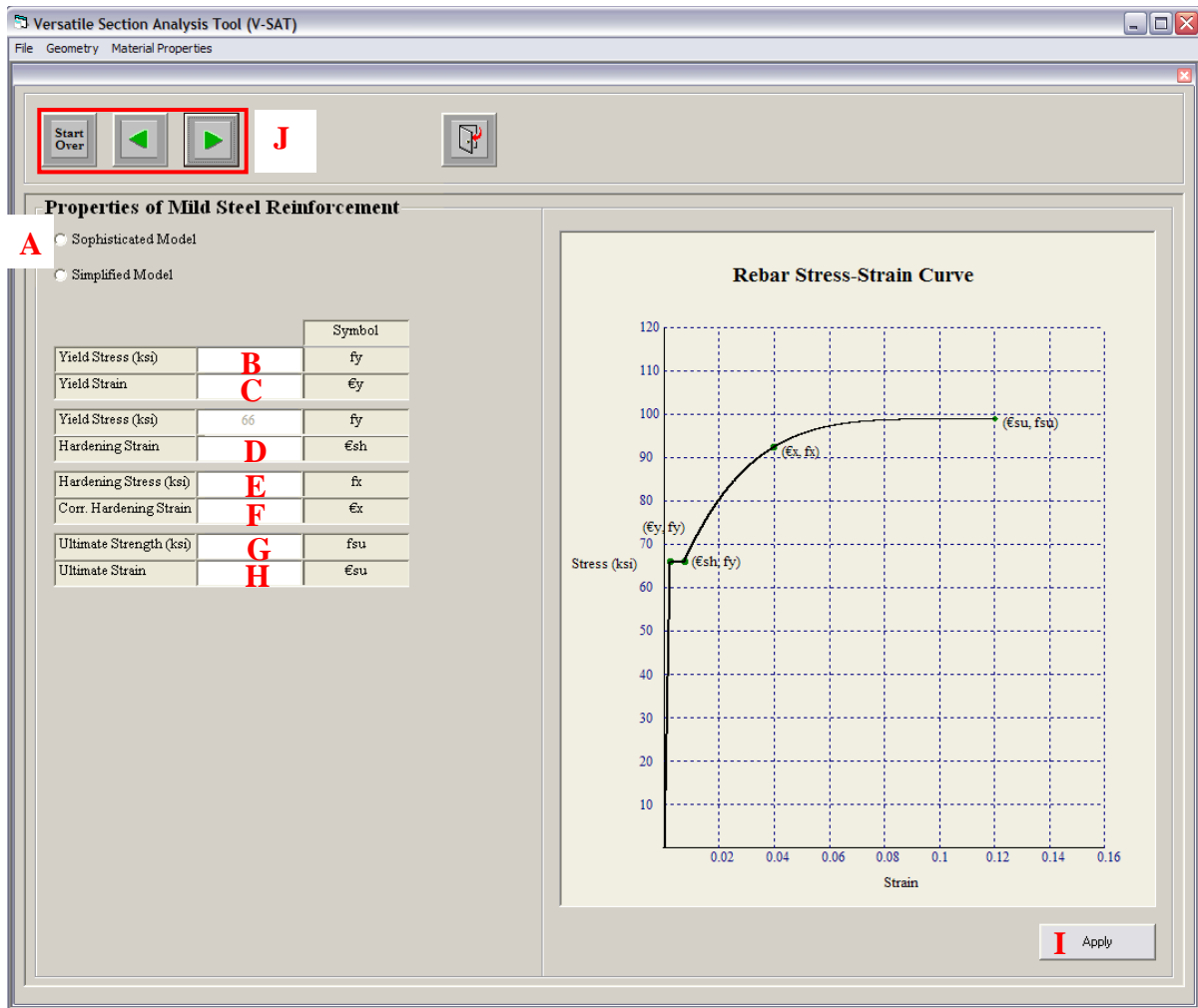
H: Click on  to continue. If you need to start over, click on . If you need to go back to a previous page, click on .

If mild steel is present in the section, continue to the next page; otherwise, skip to Section B.12

## B.11 Defining Properties of Mild Steel Reinforcement

The properties of a mild steel reinforced section allow the user to specify a suitable stress-strain behavior. The steps provided in Section 4.2.4 will aid in the defining the mild steel reinforcement properties without accounting for any temperature effects (see Figure B-14) while Section 4.2.8.2 defines the properties with temperature effects (see Figure B-15). The following information presents the expected information for defining the properties of mild steel reinforcement.

### B.9.1 Properties of Mild Steel Reinforcement without Temperature Effects



**Figure B-14: Defining Mild Steel Reinforcement Properties without Temperature Effects**

A: Choose between the “Sophisticated Model” and “Simplified Model” options. The sophisticated model may be chosen only if all required values, as shown in the display section of Figure B-14, are known; otherwise choose the simplified model.

If “Sophisticated Model” was chosen, provide the following parameters:

B: Specify the yield strength,  $f_y$ , in ksi.

C: Specify the strain corresponding to the yield strength specified in B,  $\epsilon_y$ , (in/in).


D: Specify the hardening strain,  $\epsilon_{sh}$ , (in/in).




E: Specify an arbitrary stress on the hardening portion of the curve,  $f_x$ , in ksi.

F: Specify the strain corresponding to the arbitrary stress specified in E,  $\epsilon_x$ , (in/in).

G: Specify the ultimate strength,  $f_{su}$ , in ksi.

H: Specify the strain corresponding to the ultimate strength specified in G,  $\epsilon_{su}$ , (in/in).

I: Click  to update the graph in the display window.

J: Click on  to continue. If you need to start over, click on . If you need to go back to a previous page, click on .

**Skip to Section B.12 if prestressing is provided; otherwise skip to Section B.13**

If “Simplified Model” was chosen, provide the following parameters:

B: Specify the yield strength,  $f_y$ , in ksi.

C: A default yield strain,  $\epsilon_y$ , is calculated assuming  $E = 29,000$  ksi. Specify a more appropriate value if desired (in/in).





D: A default hardening strain,  $\epsilon_{sh}$ , of  $3.24 \cdot \epsilon_y$  is used. Specify a more appropriate value if desired (in/in).

E: Not Used in this model.

F: Not Used in this model.

G: A default ultimate strength,  $f_{su}$ , of  $1.5 \cdot f_y$  is used. Specify a more appropriate value if desired in ksi.

H: A default strain ultimate strain,  $\epsilon_{su}$ , of 0.12 in/in is used. Specify a more appropriate value if desired (in/in).

- I: Click  to update the graph in the display window.
- J: Click on  to continue. If you need to start over, click on . If you need to go back to a previous page, click on .

Skip to Section B.12 if prestressing is provided; otherwise skip to Section B.13

### B.9.2 Properties of Mild Steel Reinforcement with Temperature Effects

The known properties of the steel reinforcement shall be entered under the “Known Prop.” column of Figure B-15 and have been provided with default values based upon the testing described in Chapter 3 of this thesis. The “Analysis” column, as indicated by the red box in Figure B-15, will automatically show the temperature adjusted parameters.

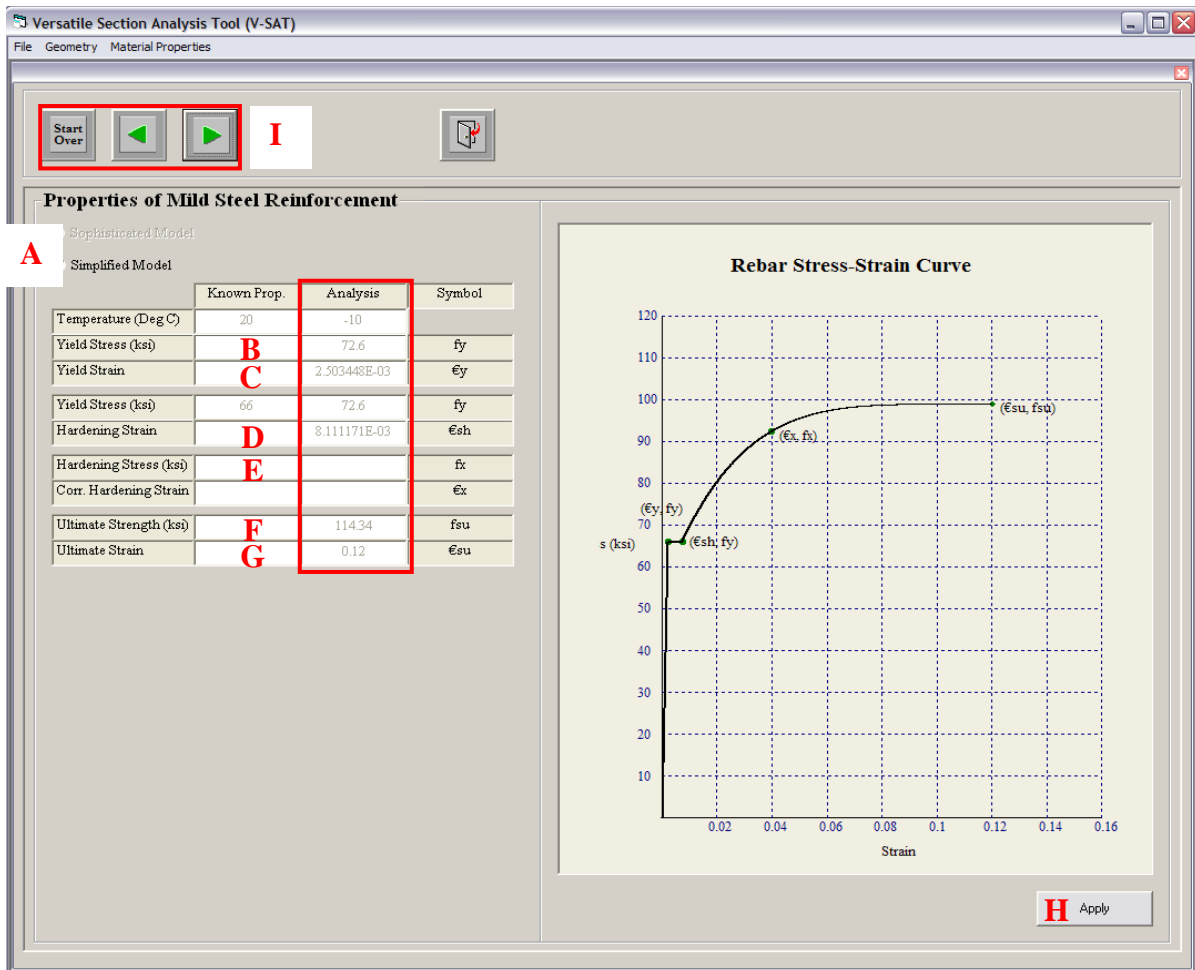


Figure B-15: Defining Mild Steel Reinforcement Properties with Temperature Effects

A: Choose between the “Sophisticated Model” and “Simplified Model” options. The sophisticated model may be chosen only if all required values, as shown in the display section of Figure B-15, are known; otherwise choose the simplified model.

If “Sophisticated Model” was chosen, provide the following parameters:

B: Specify the yield strength,  $f_y$ , in ksi. Only grade 60 mild steel with temperature effects is supported in VSAT and thus any specified steel properties shall reflect the A706 Grade 60 temperature property changes. If another grade of reinforcement is used, the known temperature and analysis temperatures must be the same value. Go back to Section B.3 if needed.


C: Specify the yield strain,  $\epsilon_y$ , (in./in.). Specify a more appropriate value at the chosen temperature if desired.


D: Specify the hardening strain,  $\epsilon_{sh}$ , (in./in.). Specify a more appropriate value at the chosen temperature if desired.

E: Specify the arbitrary strain,  $f_x$ , in ksi. Due to the effects of temperature being used, the stress at a strain of 0.03 in./in. has been provided. Specify a more appropriate value at the chosen temperature for 0.03 in./in. strain if desired.

F: Specify the ultimate strength,  $f_{su}$ , in ksi. Specify a more appropriate value at the chosen temperature if desired.



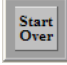

G: Specify the ultimate strain,  $\epsilon_{su}$ , (in./in.). Specify a more appropriate value at the chosen temperature if desired.

H: Click  to update the graph in the display window.

I: Click on  to continue. If you need to start over, click on . If you need to go back to a previous page, click on .

**Continue to Section B.12 if prestressing is provided; otherwise skip to Section B.13**

If “Simplified Model” was chosen, specify the following parameters:

- B: Yield strength,  $f_y$ , in ksi. Only grade 60 mild steel with temperature effects is supported in VSAT and thus any specified steel properties shall reflect the A706 Grade 60 temperature property changes. If another grade of reinforcement is used, the known temperature and analysis temperatures must be the same value. Go back to Section B.3 if needed.
- C: A default yield strain,  $\epsilon_y$ , is calculated assuming  $E = 29,000$  ksi. Specify a more appropriate value at the chosen temperature if desired (in/in).
- D: A default hardening strain,  $\epsilon_{sh}$ , of  $3.24 \cdot \epsilon_y$  is used. Specify a more appropriate value at the chosen temperature if desired (in/in).
- E: Note used in this model.
- F: A default ultimate strength,  $f_{su}$ , of  $1.5 \cdot f_y$  is used. Specify a more appropriate value at the chosen temperature if desired in ksi.
- G: A default strain ultimate strain,  $\epsilon_{su}$ , of 0.12 in/in is used. Specify a more appropriate value at the chosen temperature if desired (in/in).
- H: Click  to update the graph in the display window.
- I: Click on  to continue. If you need to start over, click on . If you need to go back to a previous page, click on .

**Continue to Section B.12 if prestressing is provided; otherwise skip to Section B.13**



## B.12 Defining Properties of Prestressing Steel Reinforcement

The prestressing steel material properties page allows the user to specify the key parameters for defining the stress-strain behavior of prestressing strands, bars and wires in Sections B.12.1, B.12.2, and B.12.3, respectively. Note that any prestressing loss should be accounted for when defining the initial prestress. The following steps will aid in completion of the prestressing steel properties page (see Figure B-16, Figure B-21 and Figure B-26). For technical details about the chosen prestressing steel material models, refer to Section 4.2.5.

### B.12.1 Prestressing Strands

Skip to Section B.12.2 if prestressing strands are not present within the section.

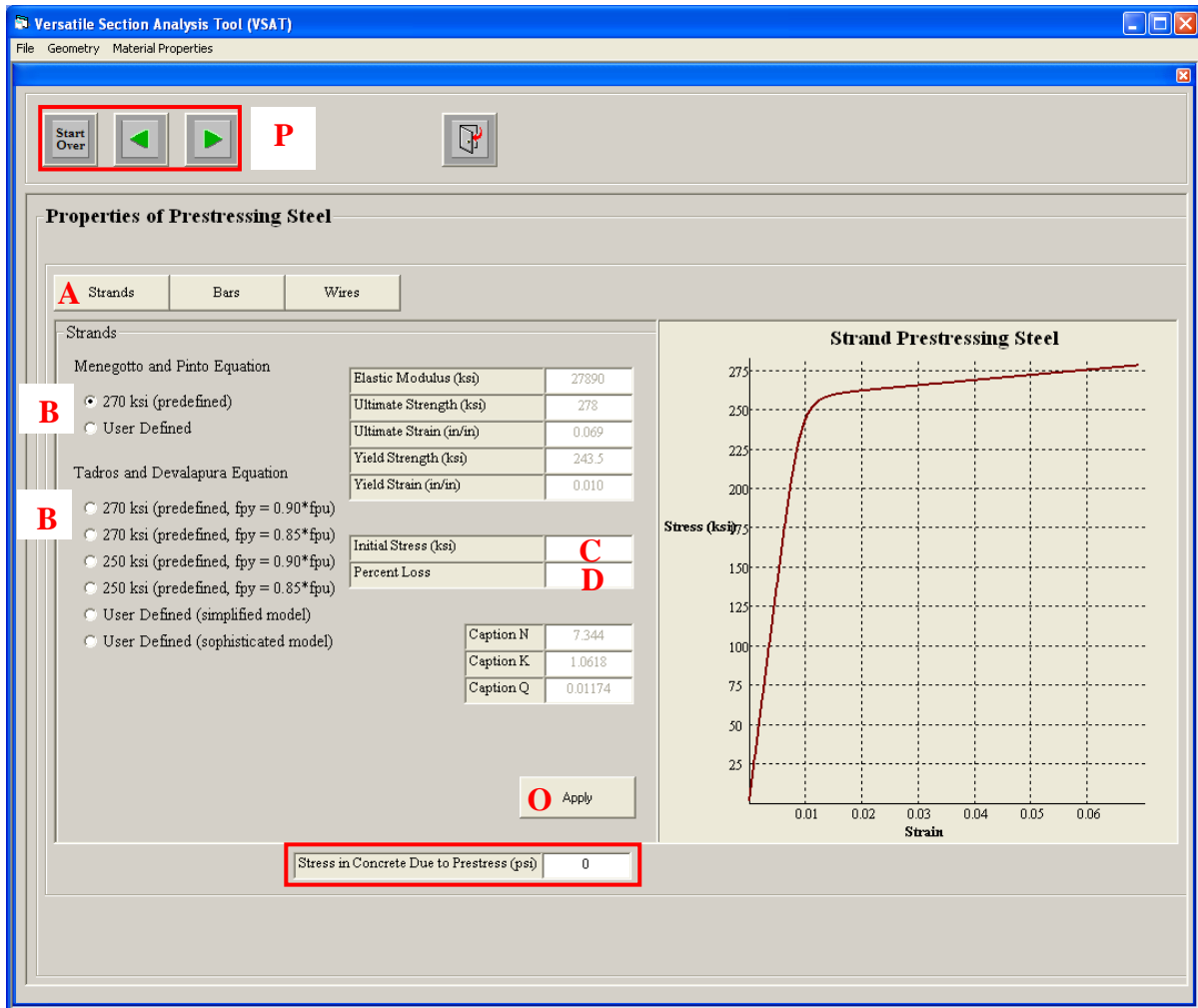


Figure B-16: Defining Prestressing Strand Properties

A: Click on **Strands** to show the prestressing strand information window.

B: Choose a suitable stress-strain model.

If you chose a “predefined” option, follow the steps below and use Figure B-17 as a guide. As shown in the figure, only two values are not predefined. Either a model presented by Menegotto and Pinto (1973) or Devalapura and Tadros (1992) may be used.

Elastic Modulus (ksi)	27890
Ultimate Strength (ksi)	278
Ultimate Strain (in/in)	0.069
Yield Strength (ksi)	243.5
Yield Strain (in/in)	0.010
Initial Stress (ksi)	<b>C</b>
Percent Loss	<b>D</b>

Caption N	7.344
Caption K	1.0618
Caption Q	0.01174

OR

Caption A	887
Caption B	27613
Caption C	112.4
Caption D	7.360

**Figure B-17: Defining the Stress-Strain Model for Prestressing Strands**

C: Specify the initial prestressing strand stress in ksi.

D: Specify the percent loss of prestressing at after transfer. If the entered stress in step C includes losses, leave this value as 0. Continue with step O at the end of this section.

If you chose “User Defined” under Menegotto and Pinto (1973), follow the steps below and use Figure B-18 as a guide. All input labeled C through L may be altered (see Section 4.2.5.1 for more information) and they are defined below.

Elastic Modulus (ksi)	<b>C</b>
Ultimate Strength (ksi)	<b>D</b>
Ultimate Strain (in/in)	<b>E</b>
Yield Strength (ksi)	<b>F</b>
Yield Strain (in/in)	<b>G</b>
Initial Stress (ksi)	<b>H</b>
Percent Loss	<b>I</b>

Caption N	<b>J</b>
Caption K	<b>K</b>
Caption Q	<b>L</b>

**Figure B-18: Defining the Menegotto and Pinto (1973) Stress-Strain Model for Prestressing Strands**

- C: Specify the elastic modulus in ksi.
- D: Specify the ultimate strength in ksi.
- E: Specify the strain corresponding to the ultimate strength defined in step D (in/in).
- F: Specify the yield strength (ksi) at the appropriate strain offset.
- G: Specify the strain corresponding to the yield strength defined in step F (in/in).
- H: Specify the initial prestress in the strands in ksi.
- I: Specify the percent loss of prestressing at after transfer. If the entered stress in step H includes losses, leave this value as 0. Continue with step O at the end of this section.
- J: Specify the model constant N.
- K: Specify the model constant K.
- L: Specify the model constant Q. Continue with step O at the end of this section.

If you chose “User Defined (simplified model)” under Devalapura and Tadros (1992), follow the steps below and use Figure B-19 as a guide. All input labeled C through N may be altered (see Section 4.2.5.2 for more information) and they are defined below.

Elastic Modulus (ksi)	<b>C</b>
Ultimate Strength (ksi)	<b>D</b>
Ultimate Strain (in/in)	<b>E</b>
Yield Strength (ksi)	<b>F</b>
Yield Strain (in/in)	<b>G</b>
f <sub>so</sub> (default 1.04 * f <sub>py</sub> )	<b>H</b>
Initial Stress (ksi)	<b>I</b>
Percent Loss	<b>J</b>

Caption A	<b>K</b>
Caption B	<b>L</b>
Caption C	<b>M</b>
Caption D	<b>N</b>

**Figure B-19: Defining the Simplified Devalapura and Tadros (1992) Model for Prestressing Strands**

- C: Specify the elastic modulus in ksi.
- D: Specify the ultimate strength in ksi.
- E: Specify the strain corresponding to the ultimate strength in step D (in/in).
- F: Yield strength (ksi) at the appropriate strain offset. The default yield strength, f<sub>py</sub>, is 0.9 \* f<sub>pu</sub>. If desired, enter appropriate yield strength in ksi.
- G: Specify the strain corresponding to the yield strength in step F (in/in).
- H: The stress corresponding to the point of intersection of the two linear portions of the stress-strain curve, f<sub>so</sub>, where the default value is 1.04 \* f<sub>py</sub>. If desired, enter an appropriate f<sub>so</sub> value.
- I: Specify the initial prestress in the strands in ksi.
- J: Specify the percent loss of prestressing at after transfer. If the entered stress in step I includes losses, leave this value as 0.
- K: If desired, alter the model constant A.
- L: If desired, alter the model constant B.
- M: If desired, alter the model constant C.
- N: If desired, alter the model constant D. Continue with step O at the end of this section.

If you chose “User Defined (sophisticated model)” under Devalapura and Tadros (1992), follow the steps below and use Figure B-20 as a guide. All input labeled C through M may be altered (see Section 4.2.5.2 for more information) and they are defined below.

Elastic Modulus (ksi)	<b>C</b>
Ultimate Strength (ksi)	<b>D</b>
Ultimate Strain (in/in)	<b>E</b>
Yield Strength (ksi)	<b>F</b>
Yield Strain (in/in)	<b>G</b>
Initial Stress (ksi)	<b>H</b>
Percent Loss	<b>I</b>

Caption A	<b>J</b>
Caption B	<b>K</b>
Caption C	<b>L</b>
Caption D	<b>M</b>

**Figure B-20: Defining the Sophisticated Devalapura and Tadros Model for Prestressing Strands**

C: Specify the elastic modulus in ksi.

D: Specify the ultimate strength in ksi.

E: Specify the strain corresponding to the ultimate strength in step D (in/in).

F: Specify the yield strength (ksi) at the appropriate strain offset.

G: Specify the strain corresponding to the yield strength in step F (in/in).

H: Specify the initial prestress in the strands in ksi.


I: Specify the percent loss of prestressing at after transfer. If the entered stress in step H includes losses, leave this value as 0.


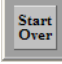

J: Specify the model constant A.

K: Specify the model constant B.

L: Specify the model constant C.

M: Specify the model constant D. Continue with step O at the end of this section.

O: Click  to update the graph in the display window. The stress in concrete due to prestress is updated for all prestressing types that exist.

P: Click on  to continue. If you need to start over, click on . If you need to go back to a previous page, click on .

### B.12.2 Prestressing Bars

Skip to Section 3.12.3 if prestressing bars are not present within the section.

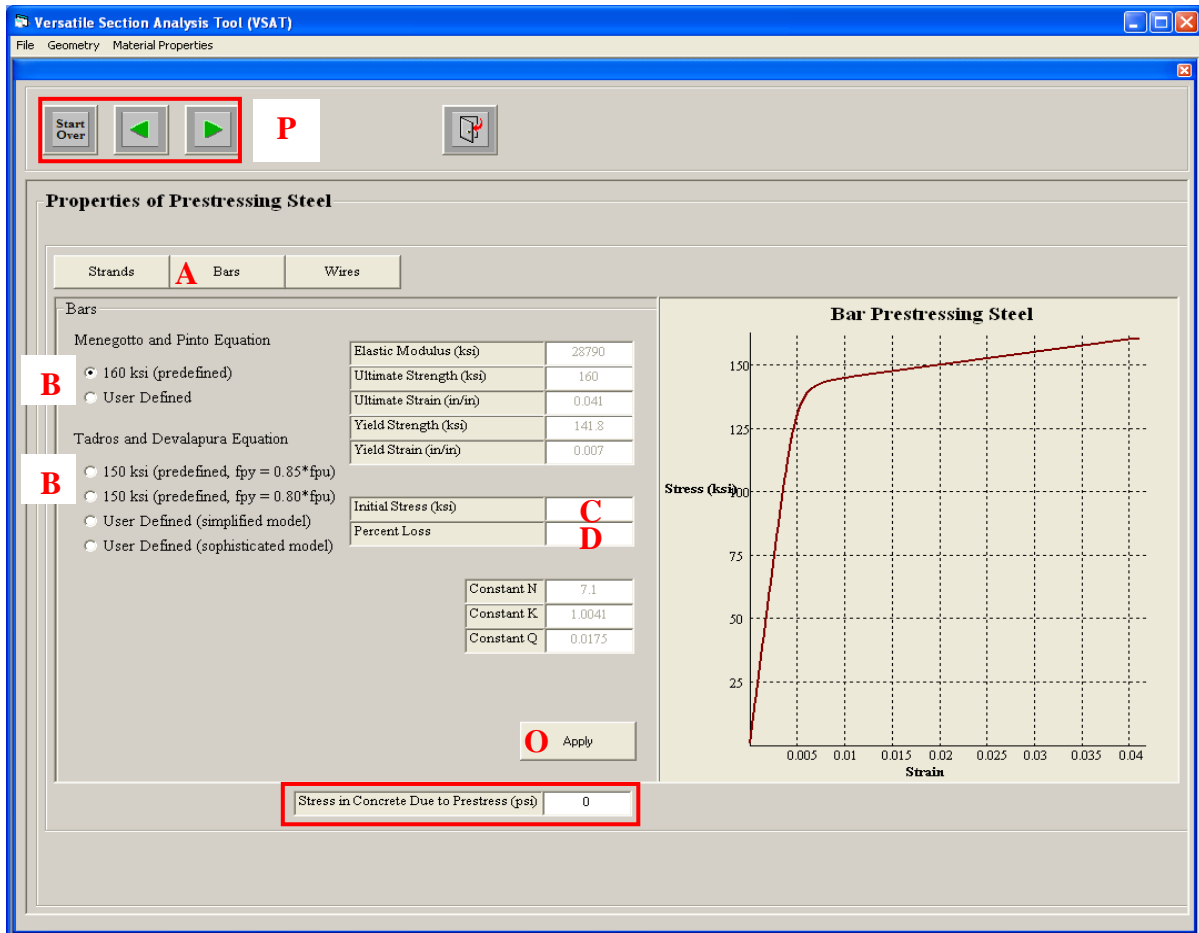
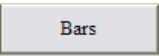


Figure B-21: Defining Prestressing Bar Properties

- A: Click on  to show the prestressing bar information in display the window.
- B: Choose a suitable stress-strain model.

If you chose a “predefined” option, follow the steps below and use Figure B-22 as a guide. As shown in the figure, only two values are not predefined. Either a model presented by Menegotto and Pinto (1973) or Devalapura and Tadros (1992) may be used.

Elastic Modulus (ksi)	27890
Ultimate Strength (ksi)	278
Ultimate Strain (in/in)	0.069
Yield Strength (ksi)	243.5
Yield Strain (in/in)	0.010
Initial Stress (ksi)	<b>C</b>
Percent Loss	<b>D</b>

Menegotto and Pinto

Caption N	7.344
Caption K	1.0618
Caption Q	0.01174

OR

Tadros and Devalapura

Caption A	887
Caption B	27613
Caption C	112.4
Caption D	7.360

**Figure B-22: Defining the Stress-Strain Model for Prestressing Bars**

C: Enter the initial prestressing bar stress in ksi.

D: Enter the percent loss of prestressing at after transfer. If the entered stress in step C includes losses, leave this value as 0. Continue with step O at the end of this section.

If you chose “User Defined” under Menegotto and Pinto (1973), follow the steps below and use Figure B-23 as a guide. All input labeled C through L may be altered (see Section 4.2.5.1 for more information) and they are defined below.

Elastic Modulus (ksi)	<b>C</b>
Ultimate Strength (ksi)	<b>D</b>
Ultimate Strain (in/in)	<b>E</b>
Yield Strength (ksi)	<b>F</b>
Yield Strain (in/in)	<b>G</b>
Initial Stress (ksi)	<b>H</b>
Percent Loss	<b>I</b>

Caption N	<b>J</b>
Caption K	<b>K</b>
Caption Q	<b>L</b>

**Figure B-23: Defining the Menegotto and Pinto Stress-Strain Model for Prestressing Bars**

C: Specify the elastic modulus in ksi.

D: Specify the ultimate strength in ksi.

E: Specify the strain corresponding to the ultimate strength defined in step D (in/in).

- F: Specify the yield strength (ksi) at the appropriate strain offset.
- G: Specify the strain corresponding to the yield strength defined in step F (in/in).
- H: Specify the initial prestress in the bars in ksi.
- I: Specify the percent loss of prestressing at after transfer. If the entered stress in step H includes losses, leave this value as 0. Continue with step O at the end of this section.
- I: Specify the model constant N.
- J: Specify the model constant K.
- K: Specify the model constant Q. Continue with step O at the end of this section.

If you chose “User Defined (simplified model)” under Devalapura and Tadros (1992), follow the steps below and use Figure B-24 as a guide. All input labeled C through N may be altered (see Section 4.2.5.2 for more information) and they are defined below.

Elastic Modulus (ksi)	<b>C</b>
Ultimate Strength (ksi)	<b>D</b>
Ultimate Strain (in/in)	<b>E</b>
Yield Strength (ksi)	<b>F</b>
Yield Strain (in/in)	<b>G</b>
f <sub>so</sub> (default 1.04 * f <sub>py</sub> )	<b>H</b>
Initial Stress (ksi)	<b>I</b>
Percent Loss	<b>J</b>

Caption A	<b>K</b>
Caption B	<b>L</b>
Caption C	<b>M</b>
Caption D	<b>N</b>

**Figure B-24: Defining the Simplified Devalapura and Tadros Model for Prestressing Bars**

- C: Specify the elastic modulus in ksi.
- D: Specify the ultimate strength in ksi.
- E: Specify the strain corresponding to the ultimate strength in step D (in/in).
- F: Yield strength (ksi) at the appropriate strain offset. The default yield strength, f<sub>py</sub>, is 0.9 \* f<sub>pu</sub>. If desired, enter appropriate yield strength in ksi.
- G: Specify the strain corresponding to the yield strength in step F (in/in).



- H: Stress corresponding to the point of intersection of the two linear portions of the stress-strain curve,  $f_{so}$ , where the default value is  $1.04 * f_{py}$ . If desired, enter an appropriate  $f_{so}$  value in ksi.
- I: Specify the initial prestress in the bars in ksi.
- J: Specify the percent loss of prestressing at after transfer. If the entered stress in step I includes losses, leave this value as 0.
- K: If desired, alter model constant A.
- L: If desired, alter model constant B.
- M: If desired, alter model constant C.
- N: If desired, alter model constant D. Continue with step O at the end of this section.

If you chose “User Defined (sophisticated model)” under Devalapura and Tadros (1992), follow the steps below and use Figure B-25 as a guide. All input labeled C through M may be altered (see Section 4.2.5.2 for more information) and they are defined below.

Elastic Modulus (ksi)	<b>C</b>
Ultimate Strength (ksi)	<b>D</b>
Ultimate Strain (in/in)	<b>E</b>
Yield Strength (ksi)	<b>F</b>
Yield Strain (in/in)	<b>G</b>
Initial Stress (ksi)	<b>H</b>
Percent Loss	<b>I</b>

Caption A	<b>J</b>
Caption B	<b>K</b>
Caption C	<b>L</b>
Caption D	<b>M</b>

**Figure B-25: Defining the Sophisticated Devalapura and Tadros Model for Prestressing Bars**

- C: Specify the elastic modulus in ksi.
- D: Specify the ultimate strength in ksi.
- E: Specify the strain corresponding to the ultimate strength in step D (in/in).
- F: Specify the yield strength (ksi) at the appropriate strain offset.
- G: Specify the strain corresponding to the yield strength in step F (in/in).

H: Specify the initial prestress in the bars in ksi.


I: Specify the percent loss of prestressing at after transfer. If the entered stress in step H includes losses, leave this value as 0.

J: Specify the model constant A.

K: Specify the model constant B.

L: Specify the model constant C.

M: Specify the model constant D. Continue with step O at the end of this section.

O: Click  to update the graph in the display window. The stress in concrete due to prestress is updated for all prestressing types that exist.

P: Click on  to continue. If you need to start over, click on . If you need to go back to a previous page, click on .

### B.12.3 Prestressing Wires

Skip to Section 3.13 if prestressing wires are not present within the section.

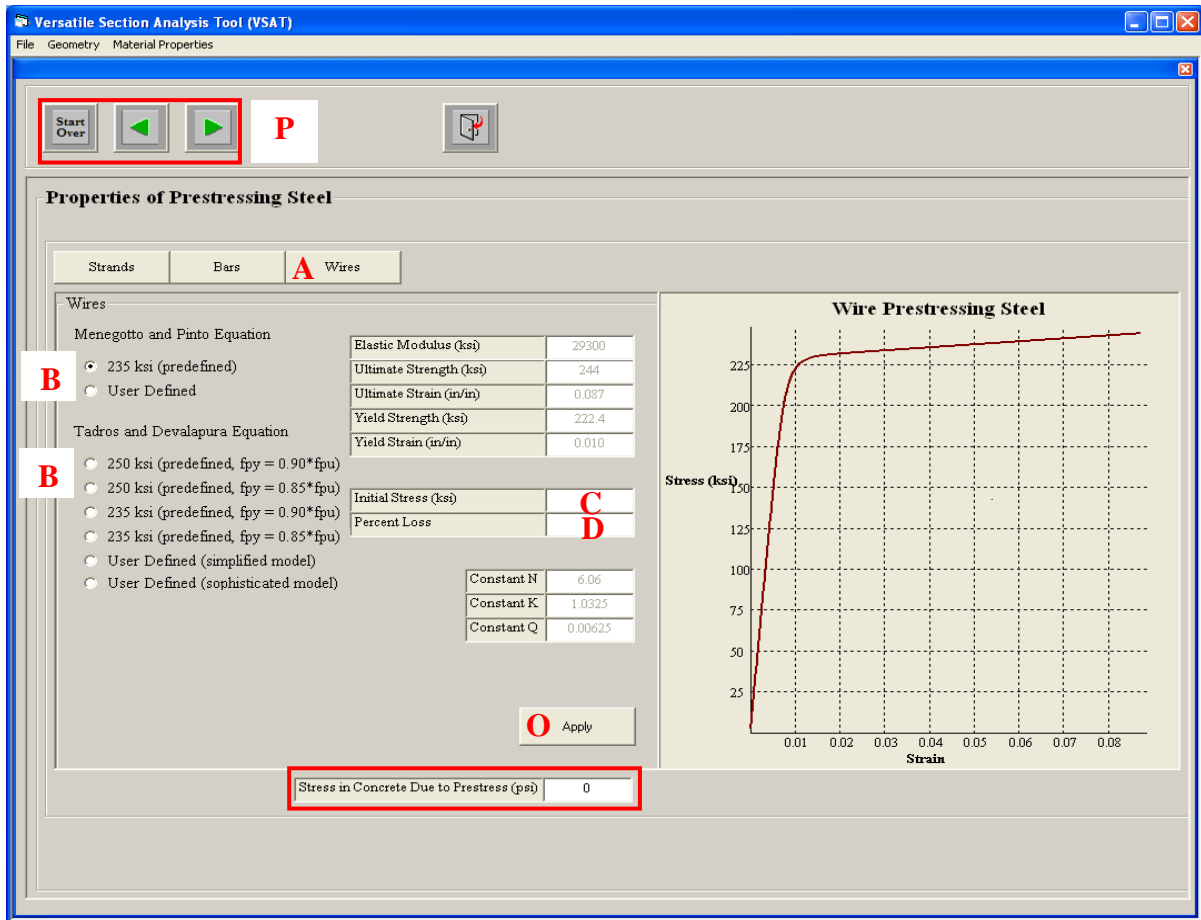


Figure B-26: Defining Prestressing Wire Properties

- A: Click on **Wires** to show the prestressing wire information in display the window.
- B: Choose a suitable stress-strain model.

If you chose a “predefined” option, follow the steps below and use Figure B-27 as a guide. As shown in the figure, only two values are not predefined. Either a model presented by Menegotto and Pinto (1973) or Devalapura and Tadros (1992) may be used.

Elastic Modulus (ksi)	27890
Ultimate Strength (ksi)	278
Ultimate Strain (in/in)	0.069
Yield Strength (ksi)	243.5
Yield Strain (in/in)	0.010
Initial Stress (ksi)	<b>C</b>
Percent Loss	<b>D</b>

Menegotto and Pinto	
Caption N	7.344
Caption K	1.0618
Caption Q	0.01174

OR

Tadros and Devalapura	
Caption A	887
Caption B	27613
Caption C	112.4
Caption D	7.360

**Figure B-27: Defining the Stress-Strain Model for Prestressing Wires**

C: Enter the initial prestressing wire stress in ksi.

D: Enter the percent loss of prestressing at after transfer. If the entered stress in step C includes losses, leave this value as 0. Continue with step O at the end of this section.

If you chose “User Defined” under Menegotto and Pinto (1973), follow the steps below and use Figure B-28 as a guide. All input labeled C through L may be altered (see Section 4.2.5.1 for more information) and they are defined below.

Elastic Modulus (ksi)	<b>C</b>
Ultimate Strength (ksi)	<b>D</b>
Ultimate Strain (in/in)	<b>E</b>
Yield Strength (ksi)	<b>F</b>
Yield Strain (in/in)	<b>G</b>
Initial Stress (ksi)	<b>H</b>
Percent Loss	<b>I</b>

Caption N	<b>J</b>
Caption K	<b>K</b>
Caption Q	<b>L</b>

**Figure B-28: Defining the Menegotto and Pinto Stress-Strain Model for Prestressing Wires**

C: Specify the elastic modulus in ksi.

D: Specify the ultimate strength in ksi.

E: Specify the strain corresponding to the ultimate strength defined in step D (in/in).

- F: Specify the yield strength (ksi) at the appropriate strain offset.
- G: Specify the strain corresponding to the yield strength defined in step F (in/in).
- H: Specify the initial prestress in the wires in ksi.
- I: Specify the percent loss of prestressing at after transfer. If the entered stress in step H includes losses, leave this value as 0. Continue with step O at the end of this section.
- J: Specify the model constant N.
- K: Specify the model constant K. Continue with step O at the end of this section.

If you chose “User Defined (simplified model)” under Devalapura and Tadros (1992), follow the steps below and use Figure B-29 as a guide. All input labeled C through N may be altered (see Section 4.2.5.2 for more information) and they are defined below.

Elastic Modulus (ksi)	<b>C</b>
Ultimate Strength (ksi)	<b>D</b>
Ultimate Strain (in/in)	<b>E</b>
Yield Strength (ksi)	<b>F</b>
Yield Strain (in/in)	<b>G</b>
f <sub>so</sub> (default 1.04 * f <sub>py</sub> )	<b>H</b>
Initial Stress (ksi)	<b>I</b>
Percent Loss	<b>J</b>

Caption A	<b>K</b>
Caption B	<b>L</b>
Caption C	<b>M</b>
Caption D	<b>N</b>

**Figure B-29: Defining the Simplified Devalapura and Tadros Model for Prestressing Wires**

- C: Specify the elastic modulus in ksi.
- D: Specify the ultimate strength in ksi.
- E: Specify the strain corresponding to the ultimate strength in step D (in/in).
- F: Yield strength (ksi) at the appropriate strain offset. The default yield strength, f<sub>py</sub>, is 0.9 \* f<sub>pu</sub>. If desired, enter appropriate yield strength in ksi
- G: Specify the strain corresponding to the yield strength in step F (in/in).

- H: Stress corresponding to the point of intersection of the two linear portions of the stress-strain curve,  $f_{so}$ , where the default value is  $1.04 * f_{py}$ . If desired, enter an appropriate  $f_{so}$  value in ksi.
- I: Specify the initial prestress in the wires in ksi.
- J: Specify the percent loss of prestressing at after transfer. If the entered stress in step I includes losses, leave this value as 0.
- K: If desired, alter model constant A.
- L: If desired, alter model constant B.
- M: If desired, alter model constant C.
- N: If desired, alter model constant D. Continue with step O at the end of this section.

If you chose “User Defined (sophisticated model)” under Devalapura and Tadros (1992), follow the steps below and use Figure B-30 as a guide. All input labeled C through M may be altered (see Section 4.2.5.2 for more information) and they are defined below.

Elastic Modulus (ksi)	<b>C</b>
Ultimate Strength (ksi)	<b>D</b>
Ultimate Strain (in/in)	<b>E</b>
Yield Strength (ksi)	<b>F</b>
Yield Strain (in/in)	<b>G</b>
Initial Stress (ksi)	<b>H</b>
Percent Loss	<b>I</b>

Caption A	<b>J</b>
Caption B	<b>K</b>
Caption C	<b>L</b>
Caption D	<b>M</b>

**Figure B-30: Defining the Sophisticated Devalapura and Tadros Model for Prestressing Wires**

- C: Specify the elastic modulus in ksi
- D: Specify the ultimate strength in ksi.
- E: Specify the strain corresponding to the ultimate strength in step D (in/in).
- F: Specify the yield strength (ksi) at the appropriate strain offset.
- G: Specify the strain corresponding to the yield strength in step F (in/in).

H: Specify the initial prestress in the wires in ksi.


I: Specify the percent loss of prestressing at after transfer. If the entered stress in step H includes losses, leave this value as 0.

J: Specify the model constant A.

K: Specify the model constant B.

L: Specify the model constant C.

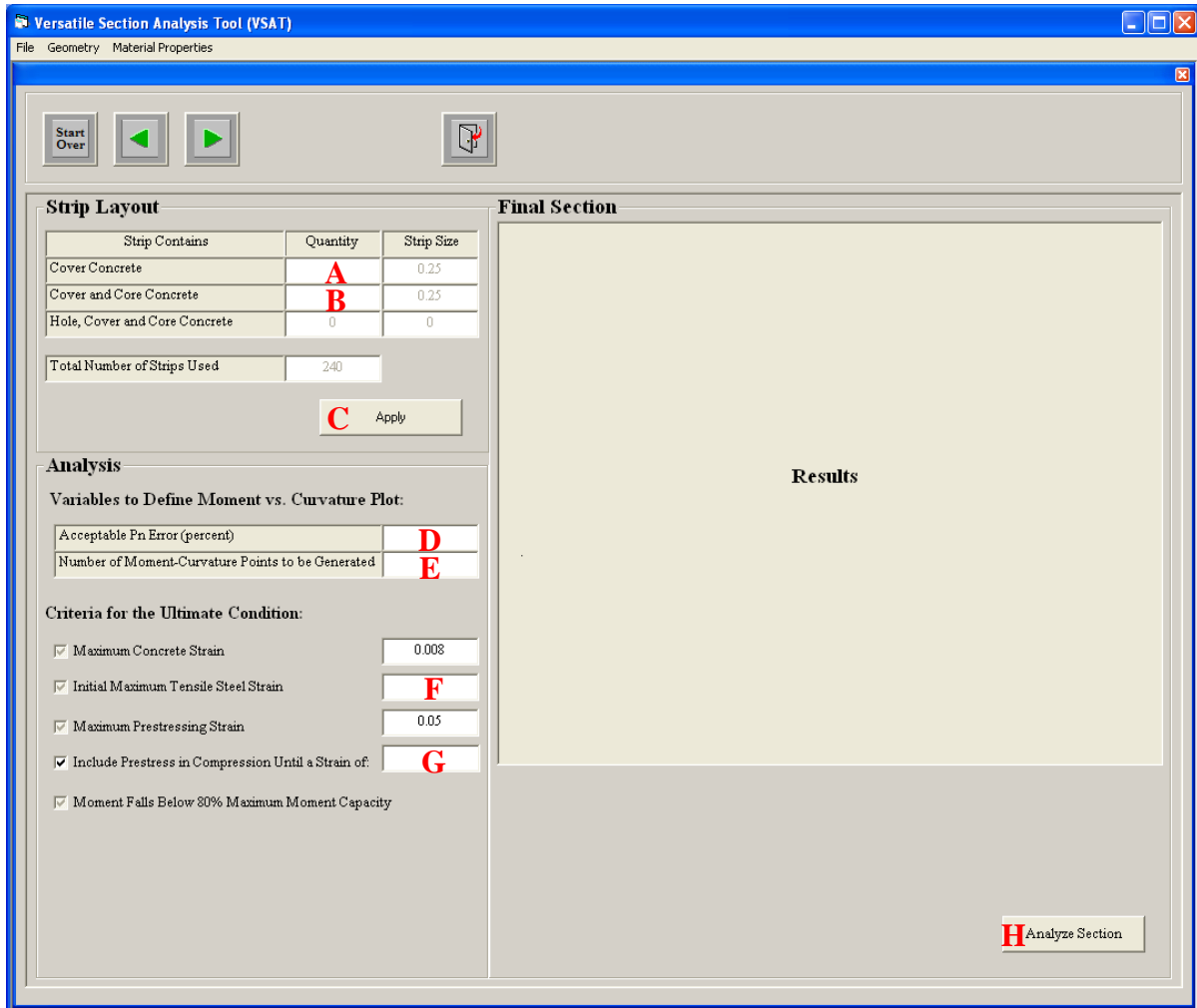
M: Specify the model constant D. Continue with step O at the end of this section.

O: Click  to update the graph in the display window. The stress in concrete due to prestress is updated for all prestressing types that exist.

P: Click on  to continue. If you need to start over, click on . If you need to go back to a previous page, click on .

### B.13 Analysis Parameters

The analysis parameters page allows the user to specify different parameters that may improve the analysis results. Although the steps provided will aid in the completion of the analysis parameters (see Figure B-31), the default parameters are expected to provide satisfactory results.



**Figure B-31: Defining the Analysis Parameters in VSAT**

A: Enter an even number of strips that will adequately discretize the cover concrete. The default value assumes the closest even number of strips that allows a strip width of 0.25 in. (0.10 in. for H-Shaped section) in the direction parallel to the analysis axis.



B: Enter an even number of strips that will adequately discretize the core of the section.

These strips will consist of both cover and core concrete, which will be separated in the analysis. The default value assumes the closest even number of strips that allows a strip width of 0.25 in. (0.10 in. for H-Shaped section) in the direction parallel to the analysis axis.

C: If boxes A or B were changed, click  to recalculate the strip sizes.

D: Enter an acceptable percent of error for the external axial load applied to the section. The default value is 0.1 percent.

E: Enter the required number of moment-curvature ( $M, \varphi$ ) data points to be calculated from  $\varphi = 0$  to  $\varphi_u$ , where  $\varphi_u$  is the ultimate section curvature.

Note that the concrete and prestressing ultimate conditions need not be defined because it has been defined in Section B.10 and B.12, respectively.

F: Enter the initial permissible tensile strain of mild steel reinforcement, if present. The maximum compressive mild steel reinforcement strain will be the difference between the ultimate strain and the maximum permissible tensile strain (e.g., a maximum tensile strain of 0.07 and an ultimate strain of 0.12 yields a maximum compressive strain of  $0.12 - 0.07 = 0.05$ ).

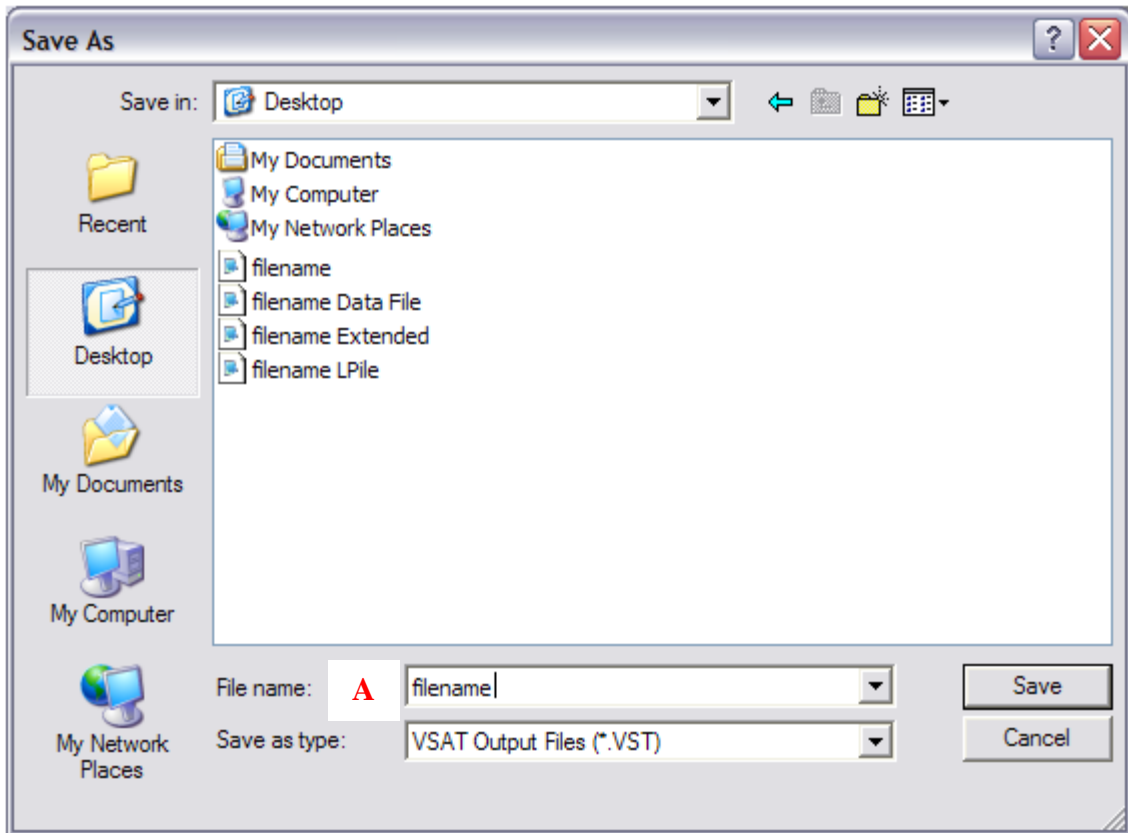
G: Alter the maximum permissible compressive strain of prestressing steel, if applicable.

H: Click  to run and finish the analysis.

Upon the completion of the analysis, the moment-curvature response will be displayed on the screen where “Results” was previously located. The user may then choose to continue working and analyze a different section or exit VSAT.

## B.14 Saving and Viewing Output

During an analysis, VSAT requires the user to input a filename for saving the analysis results. The following instructions describe how to save VSAT analysis output files on a computer operating with Windows, Windows XP, or Windows Vista (see Figure B-32).

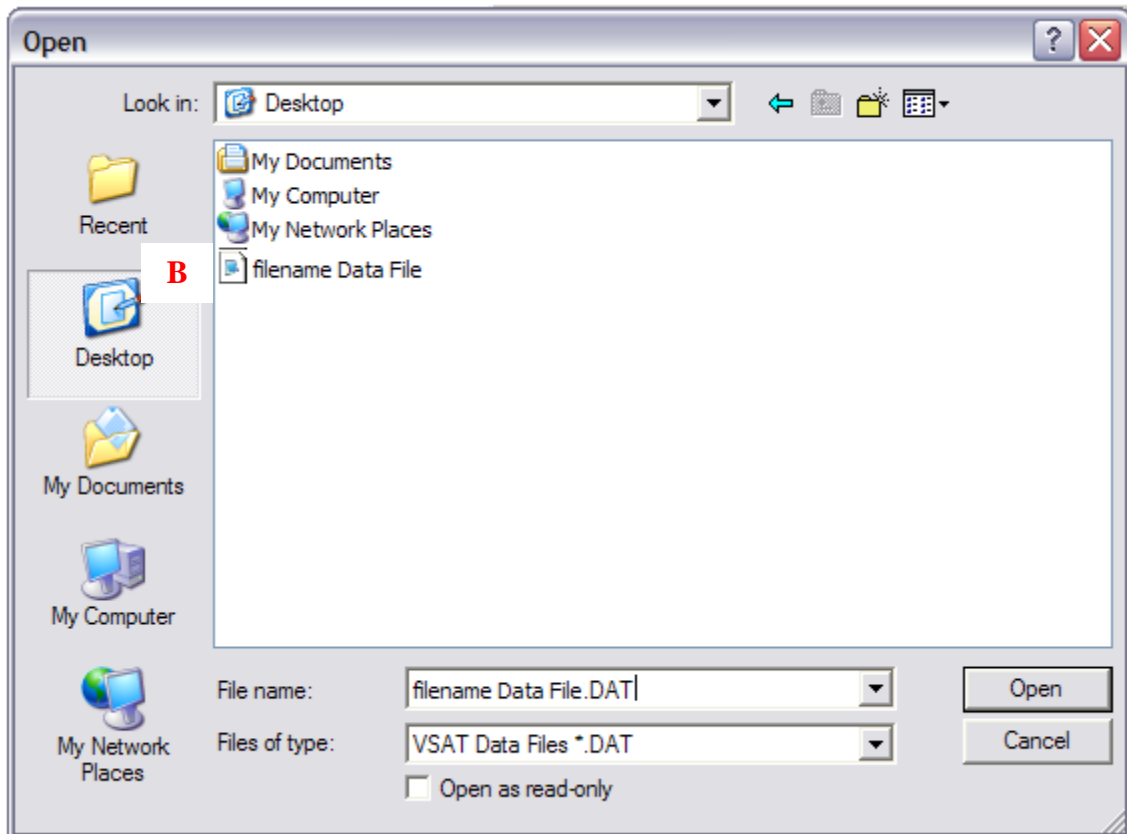


**Figure B-32: Saving VSAT Analysis Results**

- A: Select the location and filename of the output files to be created. Use the default extension (.VST) on the filename; **DO NOT** add your own extension.
- B: Choose if you wish to exit VSAT or “continue working” (e.g. analyze a similar section without closing VSAT to save time).
- C: To view the output files, open the document(s) with notepad or a similar document program. For each analysis, VSAT will write four different files: a basic output file, an extended output file, an L-Pile output file, and a data file. It is highly recommended that no change be made to the data file as this file is used to reopen a saved section.

### B.15 Opening a Saved Input File

During an analysis, VSAT requires the user to input a filename for saving the analysis results. The following instructions describe how to open a VSAT analysis that has been previously run or saved with Windows, Windows XP, or Windows Vista (see Figure B-33). The purpose of this option is to lessen the amount of input required from the user.



**Figure B-33: Opening a Saved VSAT Input File**

- A: From the Title Page menu, select “Open” or type Ctrl O.
- B: Select the location and filename of the file you wish to open. Use ONLY a .DAT file that has been created by VSAT. Any other type of file will not be recognized by VSAT.
- C: Follow the user manual, making changes as desired. Be sure to “apply” all information that is new since opening the existing file. Save the information as another file name upon running the analysis to create the modified file. Note that if the same filename is used when resaving, the previous files will be lost.